BOND BEHAVIOR OF PRESTRESSED REINFORCEMENT IN BEAMS

CONSTRUCTED WITH SELF-CONSOLIDATING CONCRETE

Except where reference is made to the work of others, the work described in this thesis is my own or was done in collaboration with my advisory committee. This thesis does not include proprietary or classified information.

_____

Kelly Rebecca Levy

Certificate of Approval:

Anton K. Schindler Gottlieb Assistant Professor Civil Engineering	Robert W. Barnes, Chair Associate Professor Civil Engineering
Mary L. Hughes Assistant Professor Civil Engineering	George T. Flowers Interim Dean Graduate School

BOND BEHAVIOR OF PRESTRESSED REINFORCEMENT IN BEAMS CONSTRUCTED WITH SELF-CONSOLIDATING CONCRETE

Kelly Rebecca Levy

A Thesis

Submitted to

the Graduate Faculty of

Auburn University

in Partial Fulfillment of the

Requirements for the

Degree of

Master of Science

Auburn, Alabama
May 10, 2007

BOND BEHAVIOR OF PRESTRESSED REINFORCEMENT IN BEAMS

CONSTRUCTED WITH SELF-CONSOLIDATING CONCRETE

Kelly Rebecca Levy

_____

Signature of Author

_____

Date of Graduation

VITA

Kelly Rebecca Levy, daughter of George Edward Levy and Emily (McNeil) Levy, was born February 11, 1983, in Tampa, Florida. She graduated high school with honors as Valedictorian from Chamberlain High School in Tampa, Florida, in 2001. She attended Auburn University on an academic scholarship and graduated magna cum laude with a Bachelor of Civil Engineering degree in 2005. She entered the Graduate School at Auburn University in August, 2005 to seek the degree of Master of Science in Civil Engineering (Structures). After graduate school, she began work as a graduate engineer for Walter P. Moore and Associates, Inc. in Atlanta, Georgia.

THESIS ABSTRACT

BOND BEHAVIOR OF PRESTRESSED REINFORCEMENT IN BEAMS

CONSTRUCTED WITH SELF-CONSOLIDATING CONCRETE

Kelly Rebecca Levy

Master of Science, May 10, 2007
(B.C.E., Auburn University, 2005)

277 Typed Pages

Directed by Robert W. Barnes

Accurate behavioral characteristics of self-consolidating concrete (SCC) should be established prior to its widespread implementation in prestressed members. This thesis describes an investigation of bond behavior of prestressed reinforcement in SCC flexural members. Sixteen eccentrically prestressed T-beams were subjected to transfer and development length testing. One conventional mixture and three SCC mixtures were used to construct the beams. The conventional mixture was a moderate-strength mixture with a compressive strength at prestress transfer of 5,000 psi. The three SCC mixtures included two moderate-strength mixtures with compressive strengths at prestress transfer of approximately 5,500 psi and one high-strength mixture with compressive strength at transfer of 9,900 psi.

SCC transfer bond behavior only differed significantly from that of the standard mixture at flame-cut ends of the moderate-strength SCC mixture with a 50% replacement of GGBF slag. On average, specimens constructed with higher compressive strengths at transfer had shorter transfer lengths than specimens that were constructed with lower concrete strengths at transfer. The average decrease in transfer length with increasing concrete strength could be accurately estimated by assuming the transfer length is inversely proportional to the square root of the concrete strength at transfer. Current design provisions for transfer length that do not include concrete strength as a parameter, including equations suggested by ACI 318 and AASHTO, do not adequately predict transfer length for specimens cast with SCC or conventional concrete.

The development length test program was characterized by flexural tests of all specimens. Results indicated that SCC mixture proportioning did not have an adverse effect on the overall flexural bond performance—either with respect to current design procedures or with respect to the comparable conventionally consolidated mixture. The flexural bond length predicted by the ACI 318 and AASHTO expressions proved to be conservative for all SCC specimens.

ACKNOWLEDGEMENTS

I would like to thank Dr. Robert Barnes for his invaluable wisdom and guidance throughout the years; it is greatly appreciated and will never be forgotten. I would also like to thank Dr. Anton Schindler for his assistance throughout this project. Graduate Research Assistants Kurtis Boehm, Mustafa Gurbuz, Jason Meadows, Jiangong Xu, and the concrete lab technician Billy Wilson contributed a lot of time and effort to this investigation. Countless more Graduate and Undergraduate Research Assistants also contributed numerous hours towards this project as well. Their hard work is greatly appreciated.

Financial support provided by the Alabama Department of Transportation is greatly appreciated. Assistance with the mixture process from Charles Bell of Twin City Concrete in Auburn, Alabama and the help provided with the experimental design and prestressing strand from Dwain Hamby of Sherman Prestress in Pelham, Alabama are greatly appreciated. I would also like to thank Degussa and Cresset Chemical Company for their generous donations to this study.

I would like to thank God, without Him, nothing would be possible. I would also like to thank my parents, sisters, and family for their unwavering support and love. Finally, I would like to thank Jamie Roberts for his steadfast encouragement, advice, and support.

Style manual used Kate L. Turabian A Manual for Writers of Term Papers, Theses, and Dissertations. 6th ed.

Computer software used Microsoft Word, Microsoft Excel

TABLE OF CONTENTS

LIST OF TABLES

LIST OF FIGURES

CHAPTER 1

INTRODUCTION

1.1 BACKGROUND

Prestressed concrete construction has proven to be an efficient means of providing structural systems for a variety of applications. Precast, prestressed concrete elements are typically used in highway bridges, parking garages, floor systems, and several other building applications. Historically, concrete mixtures utilizing conventional vibration techniques to ensure proper consolidation have been used for this type of construction. Achieving proper consolidation using conventional methods has left much room for improvement. The vibration procedures can be costly, time consuming, and potentially hazardous. However, due to the recent advent of self-consolidating concrete (SCC) and its apparent success in reinforced concrete applications, research ventures by the precast, prestressed concrete industry have been undertaken to investigate the possible use of this material for prestressed applications. If approved for use in prestressed concrete applications, SCC could increase productivity and worker safety, lower labor costs, and provide innumerable design possibilities for the prestressed concrete industry.

SCC was first developed in Japan in the early 1980's by Hajime Okamura, a professor at Kocki University of Technology, as a result of the lack of sufficiently skilled workers able to ensure proper consolidation of conventional concrete in everyday

concreting applications (Okamura and Ouchi 1999). SCC allows concrete to be placed without the need for internal vibration or consolidation. It is a highly flowable concrete that is able to deform under its own weight and completely encapsulate any reinforcement without exhibiting segregation or bleeding (Khayat 1999). The highly desirable workability and fluidity of SCC are obtained by using less coarse aggregate, more chemical admixtures, and more cementitious materials than are used in conventional concrete.

The use of SCC for construction is increasing rapidly as contractors realize the economic benefits of reduced labor costs associated with casting and finishing operations. Workers would no longer be needed to vibrate concrete to ensure proper consolidation. Ongoing research indicates that optimum SCC mixtures can include supplementary cementing materials (SCM) that replace up to 50 percent of the cement content in the concrete. SCMs include industrial waste products such as fly ash and ground-granulated blast-furnace slag. Thus, implementation of SCC offers the dual benefit of reducing the energy demands and environmental hazards associated with cement production, while offering a safe use for waste materials that would otherwise occupy valuable space in landfills. Finally, SCC offers aesthetic benefits such as smoother finishes.

The prestressed concrete industry is pressing transportation agencies for permission to use SCC for construction of prestressed bridge members. Because the performance and design of prestressed concrete is heavily influenced by the behavior of the constituent materials, it is crucial that accurate behavioral characteristics of SCC be established prior to its widespread implementation in prestressed bridge construction. One of the most important issues that must be investigated prior to the acceptance of SCC for use in the

prestressing industry is the effect that this material has on the bond behavior of the prestressed reinforcement. This issue is a suspected cause for concern due to the increased fine aggregate content and a lack of vibration inherent within SCC mixtures.

1.2 RESEARCH OBJECTIVES

The Alabama Department of Transportation (ALDOT) has sponsored an investigation by the Auburn University Highway Research Center into the use of SCC in precast, prestressed concrete bridge girders. The primary objectives of the sponsored investigation are to evaluate the long-term performance of SCC when used in prestressed concrete girders and to develop recommendations for ALDOT for the use of SCC in prestressed concrete girder applications. The study presented in this thesis is a portion of the aforementioned project. The primary objective of this study was to evaluate the bond behavior of prestressed reinforcement in beams constructed with SCC.

In order to evaluate bond behavior, beams constructed with SCC underwent transfer and development length testing. All specimens in this study were pretensioned with 0.5-in. "oversized" prestressing strand, which is the most frequently specified strand size in ALDOT prestressed girders. Limited test data is available concerning the bond interaction of this strand with conventional concrete or SCC.

1.3 RESEARCH SCOPE

This study consisted of an investigation into the bond behavior of the prestressed reinforcement in a total of sixteen beams with a T-shaped cross section. Twelve of these T-beams were constructed with SCC. The remaining four beams were constructed with a concrete mixture commonly used in precast, prestressed ALDOT girders in which proper consolidation is obtained using internal vibration. Initial and four-day transfer length

measurements were performed on all sixteen specimens. All specimens were tested to investigate their response to flexural loading up to ultimate strength. Strand embedment lengths were varied to assess the bonded length necessary to ensure a desirable flexural failure type. The mixing, fabrication, measurement, and flexural testing were performed in the Structural Engineering Laboratory of the Auburn University Department of Civil Engineering.

One conventional mixture and three SCC mixtures were used to construct the beams. For each mixture, four beams of varying lengths were constructed. The conventional, or standard, mixture was a moderate-strength mixture with a compressive strength at prestress transfer of 5,000 psi. Three SCC mixtures were utilized to construct the remaining twelve beams, including two moderate-strength mixtures and one high-strength mixture. The first moderate-strength SCC mixture utilized Class C fly ash as an SCM and had a compressive strength at transfer of 5,500 psi. The next moderate-strength SCC mixture utilized ground-granulated blast-furnace (GGBF) slag as an SCM and had a compressive strength at transfer of 5,300 psi. The high-strength SCC mixture utilized GGBF slag as an SCM and had a compressive strength at transfer of 9,900 psi.

1.4 ORGANIZATION OF THESIS

Chapter 2 provides a description of key terms relating to prestressing bond, a discussion of transfer bond theory, a review of the current code provisions that address anchorage design, and an overview of previous studies relating to the bond behavior of SCC in prestressing applications. This chapter provides a discussion of current code provisions relating to transfer and development length as stated in the American Concrete Institute's (ACI) *Standard Building Code Requirements for Reinforced Concrete* (ACI 318-05) and

the American Association of State Highway and Transportation Officials' (AASHTO) *Standard Specifications for Highway Bridges* (2002) and *LRFD Bridge Design Specifications* (2006).

Chapter 3 provides a thorough discussion of the design and fabrication of the prestressed specimens. The selection of the mixtures, mixture proportions, fresh property testing and hardened property testing are discussed in this chapter

Chapter 4 provides an overview of the details and results of the transfer length testing program. The procedures for specimen preparation and measurement of concrete surface strains are presented in this chapter. In a previous phase of this project, extensive transfer length testing was conducted on thirty-six concentrically prestressed specimens. A comparison of the transfer lengths of the concentrically prestressed specimens and T-beams is presented in this chapter.

Chapter 5 provides details on the configuration, instrumentation, procedure, and results of the development length testing program. The results of the sixteen development length tests performed for this study are presented in this chapter.

Chapter 6 summarizes the thesis and offers conclusions and recommendations based on the work documented in this thesis. Recommendations for further research are also provided within this chapter.

1.5 NOTATION

The notation commonly used in the United States for the design of prestressed concrete bridge elements follows the specifications outlined in the *AASHTO LRFD Bridge Design Specifications* (2006). Therefore, this notation is utilized throughout this thesis. A list of the notation used throughout this thesis is presented in Appendix A.

CHAPTER 2

BOND BEHAVIOR IN PRETENSIONED MEMBERS

2.1 INTRODUCTION

Bond behavior between prestressing tendons and the concrete is a very important topic related to the design of pretensioned members. Inadequate bond between the steel and concrete will compromise the structural integrity of the member and can result in decreased flexural, shear, and torsional resistance. Anchorage of prestressing steel must be determined to be adequate in the design phase of all prestressed members. In pretensioned concrete members such as precast/prestressed concrete bridge girders, anchorage of prestressed reinforcement is usually achieved through bond between the steel and the surrounding concrete. There are currently provisions in both ACI building code requirements and AASHTO bridge design codes to check for anchorage adequacy.

This chapter provides a description of key terms relating to prestressing bond, a discussion of transfer bond theory, a review of the current code provisions that address anchorage design, and a background on previous studies relating to the bond behavior of SCC in prestressing applications.

2.2 DEFINITIONS

This section introduces a few basic definitions required to begin the discussion of bond behavior.

2.2.1 TRANSFER LENGTH

Transfer length, l_t, can be defined as the bonded length of a tendon required to fully develop the effective prestress, f_{pe}, in a strand by bond to the concrete (ACI-318 R12.9 2005). Since the prestressing force in the tendon is constantly changing due to losses, it is important to note that the effective prestress force corresponds to the prestress level after losses.

2.2.2 FLEXURAL BOND LENGTH

The flexural bond length, l_{fb}, is the additional distance beyond the transfer length in which the prestressing strand must be bonded to the concrete to develop the full resistance of the tendons, f_{ps}, required to achieve the nominal flexural strength of the member (ACI318 R12.9 2005, Barnes et. al 1999).

2.2.3 DEVELOPMENT LENGTH

The development length, l_d, is the sum of the transfer length and the flexural bond length (ACI 318 2005). Figure 2-1 illustrates this concept by showing the development of steel stress along the length of a member. It is the complete bonded length required to develop the full steel stress required at the nominal strength of the member. For prestressed tendons, the development length is the bonded tendon length required to develop the full resistance of the tendons, f_{ps}, at the nominal strength of the member. Development length is also referred to as anchorage length in European practice.

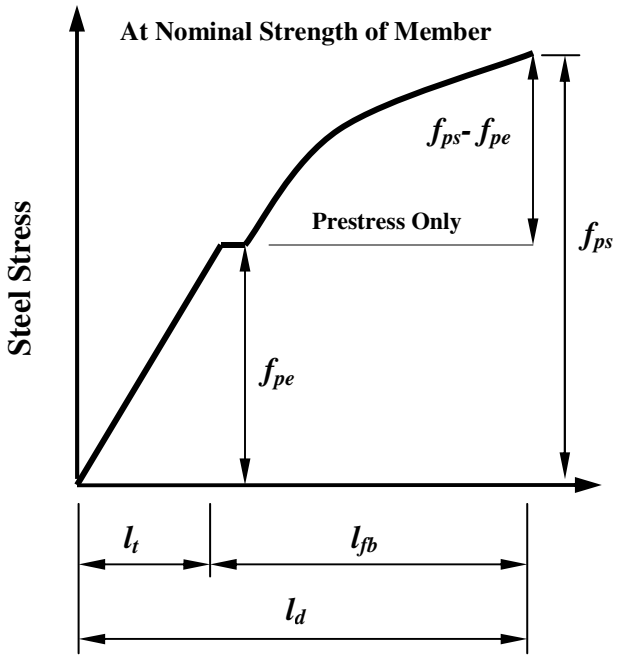

Figure 2-1: Variation of Steel Stress in a Pretensioned Member

(Adapted from Barnes et. al 1999)

2.2.4 EMBEDMENT LENGTH

Embedment length, l_e, can be defined as the bonded length of tendon from the beginning of bond of the tendon to the cross section for which strength capacity is being assessed. The critical section of the member is usually taken as the cross section closest to the beginning of bond at which the member needs to develop its full flexural resistance. If the embedment length at a cross section is shorter than the development length, a bond failure will occur before the section can develop its full flexural capacity. Design of such cross sections should reflect the reduced strand stress achievable prior to bond failure.

2.3 CODE PROVISIONS

This section discusses the current code provisions relating to bond of prestressed reinforcement as stated in ACI's *Standard Building Code Requirements for Reinforced Concrete* (ACI 318-05) and AASHTO's *Standard Specifications for Highway Bridges* (2002) and *LRFD Bridge Design Specifications* (2006). The background research that contributed to these code provisions is also discussed.

2.3.1 CURRENT ACI DESIGN PROVISIONS

Provisions for the development and transfer length of prestressing strand can be found in Section 12.9 of the ACI *Standard Building Code Requirements for Reinforced Concrete* (ACI 318-05). The existing expression for development length was first incorporated into the ACI code in 1963 (Tabatabai and Dickson 1993). The notation used throughout this thesis is not the same notation used by ACI, but rather corresponds to the notation used by AASHTO due to the Federal Highway Administration's (FHWA) acceptance of the AASHTO LRFD Specification.

Section 12.9.1 of ACI 318-05 reads as follows:

> Seven-wire strand shall be bonded beyond the critical section, a distance not less than
>
> $$l_d = \left(\frac{f_{pe}}{3000}\right) d_b + \left(\frac{f_{ps} - f_{pe}}{1000}\right) d_b$$ ***Equation 2-1***
>
> where, d_b = nominal strand diameter (in.)
>
> f_{pe} and f_{ps} are in psi

This expression can be broken into two distinct parts. The first term represents the transfer length and the second term represents the flexural bond length. This results in the following expression for transfer length:

$$l_t = \left(\frac{f_{pe}}{3000} \right) d_b \qquad \textit{Equation 2-2}$$

In addition to the equations suggested above, the following equation for transfer length, Equation 2-3, can be inferred from the ACI 318-05 shear design provisions. Sections 11.4.4 and 11.4.5 of ACI 318-05 state that the transfer length may be assumed to be 50 diameters for strand when computing the web-shear cracking capacity of prestressed concrete members.

$$l_t = 50 d_b \qquad \textit{Equation 2-3}$$

As discussed previously, Figure 2-1 shows the generally assumed development of the steel stress along the length of the beam. This figure illustrates the two terms represented in Equation 2-1. Along the transfer length, the steel stress varies linearly with distance. However, beyond the transfer length, the slope of the steel stress decreases steadily along the remaining portion of the development length. The ACI Commentary of Section 12.9.1.1 attributes the development of Equation 2-1 to findings presented by Hanson and Kaar (1959) and Kaar, LaFraugh, and Mass (1963).

2.3.2 Background Research for Current ACI Design Provisions

As stated in the preceding section, the current ACI code provisions for transfer and flexural bond are based on papers published by Hanson and Kaar (1959) and Kaar, LaFraugh, and Mass (1963). These studies were conducted in the Research and Development Laboratories of the Portland Cement Association (PCA).

2.3.2.1 Hanson and Kaar (1959)

The work presented in this paper was conducted at the Research and Development Laboratories of the Portland Cement Association from 1955-57. At the time of this study, no generally accepted method existed to predict the bond performance of prestressing strand. In this study, 47 pretensioned beams with varying strand diameters of ¼, ⅜ , and ½ in, were tested to evaluate flexural bond. All beams were simply supported and loaded to failure. The primary variables investigated in this study were strand diameter and embedment length. Secondary variables included reinforcement percentage, concrete strength, strand surface condition and the effect of end embedded anchorages on pretensioned strand.

Hanson and Kaar concluded that there is a critical embedment length for each strand diameter. They discovered that the average bond stress that occurs immediately before general bond slip decreases with increasing embedment length. Hanson and Kaar developed charts to predict required embedment lengths for varying strand diameters based on determined values of average bond stress at general bond slip. They also discovered that percentage of steel, concrete strength, and embedment length are interrelated variables in flexural design. Finally, they discovered that, unlike smooth individual wires, seven-wire strand can develop additional bond strength after general bond slip has occurred.

2.3.2.2 Mattock (1962)

In *The History of the Prestressing Strand Development Length Equation*, Tabatabai and Dickson (1995) give an overview of how the results of Hanson and Kaar's findings

turned into the current expression for development length (Equation 2-1) in ACI 318. Alan H. Mattock, working in conjunction with ACI-ASCE Committee 323, now ACI Committee 423, determined Hanson and Kaar's value of average transfer bond stress to be 400 psi and then used his value to determine an equation for transfer length based on the following equilibrium equation (Tabatabai and Dickson 1995):

$$U_t \Sigma o l_t = A_{ps} f_{pe} \qquad \textbf{\textit{Equation 2-4}}$$

where;

	U_t	=	Average transfer bond stress
	Σo	=	Bonded perimeter of prestressing strand
	l_t	=	Transfer length
	A_{ps}	=	Area of prestressing strand
	f_{pe}	=	Effective prestress

Solving for transfer length, the resulting equation is (Tabatabai and Dickson 1995):

$$l_t \approx (1/3)\, f_{pe}\, d_b \qquad \textbf{\textit{Equation 2-5}}$$

Except for a switch from ksi to psi units for strand stress, this equation is functionally equivalent to Equation 2-2. The full committee then incorporated Mattock's equation into the overall expression for development length (Tabatabai and Dickson 1995). This development length equation was first published in the 1963 ACI Building Code and is functionally equivalent to the current equation presented previously as Equation 2-1.

Tabatabai and Dickson (1995) also discuss how Mattock arrived at an expression for development length using Hanson and Kaar's results. Hanson and Kaar ascribed to Janney's (1954) hypothesis that high bond stresses progress as a wave from the original cracks toward the beam ends leaving a bond stress behind the wave which is always

much lower than the maximum stress. They, like Janney (1954), concluded that if the wave were to reach the prestress transfer zone, the increase in steel stress reduces the strand diameter and thus frictional resistance and ultimately precipitates bond slip.

In 1962, Mattock proposed a redraft to the code concerning bond based on a "reappraisal" of measurements of anchorage bond behavior at ultimate by Hanson and Kaar. Mattock first proposed Equation 2-6 to the committee (Tabatabai and Dickson 1995).

$$l_d \approx (1.11\, f_{ps} - 0.77\, f_{pe})\, d_b \qquad \textbf{\textit{Equation 2-6}}$$

Mattock evaluated Hanson and Kaar's results and developed a linear relationship to model their data. In order to develop this relationship, Mattock subtracted the transfer length from the embedment length to determine the flexural bond length. To determine the increase in strand stress due to flexure at general bond slip, he subtracted the effective prestress from the stress in the strand at the time of bond slip. Similarly, to determine the increase in strand stress due to flexure at ultimate, he subtracted the effective prestress from the stress in the strand at ultimate. However, he suggested that "the avoidance of bond slip should be the criterion for design". The linear relationship he derived from this procedure is presented as Equation 2-7 (Tabatabai and Dickson 1995).

$$f_{ps} \le f_{pe} + 0.9\left(\frac{l_e - l_t}{d_b}\right) \qquad \textbf{\textit{Equation 2-7}}$$

However, before its introduction into the code, ACI-ASCE Committee 323, now ACI Committee 423, changed the previous equation to Equation 2-8.

$$f_{ps} \le f_{pe} + \left(\frac{l_e - l_t}{d_b}\right) \qquad \textbf{\textit{Equation 2-8}}$$

Solving for flexural bond length, the equation becomes Equation 2-9.

$$l_{fb} = \left(f_{ps} - f_{pe}\right)d_b \qquad \textit{Equation 2-9}$$

Combining this equation with the equation for transfer length, the result is Equation 2-10, which is still present in the code today .

$$l_d = \left(f_{ps} - \frac{2}{3} f_{pe}\right)d_b \qquad \textit{Equation 2-10}$$

2.3.2.3 Kaar, LaFraugh, and Mass (1963)

The work presented by Kaar, LaFraugh, and Mass focused on the influence of concrete strength on transfer length. In this study, 36 small, pretensioned prisms of various sizes with varying concrete strengths ranging from 1660 to 5000 psi and varying strand diameters of ¼, ⅜ , ½, and 0.6 in. were tested in series of tests to evaluate transfer length. Mechanical strain gauges were employed to determine transfer lengths at ten ages spanning a period from transfer to one year after transfer. All specimens were cast from the same mixture; concrete strength at transfer was varied by varying the concrete age at prestress transfer.

It was concluded that for strand diameters up to 0.6 in., concrete strength had no influence on transfer length. However, for the 0.6 in. strands, transfer length decreased with increasing concrete strength (Barnes et. al 1999). It was also concluded that variances in transfer length were proportional to strand diameter and that transfer lengths at the ends of the specimens adjacent to strand cutting appeared to be twenty to thirty percent higher than those observed at the dead ends. Finally, their results showed that transfer length increased an average of six percent over a period of one year.

2.3.3 CURRENT AASHTO DESIGN PROVISIONS

Provisions for the development and transfer length of prestressing strand can also be found in Section 9.28 of the AASHTO *Standard Specifications for Highway Bridges* (2002), and in Article 5.11.4 of the AASHTO *LRFD Bridge Design Specifications* (2006). Section 9.28 of the AASHTO *Standard Specifications for Highway Bridges* also suggests Equation 2-2 for predicting transfer length (AASHTO 2002).

The current provisions for transfer and development length are slightly different in the AASHTO *LRFD Bridge Design Specifications* (2006) than the previously mentioned ACI code provisions. AASHTO LRFD suggests the following equation for transfer length:

$$l_t = 60 d_b \qquad \textbf{\textit{Equation 2-11}}$$

In Section 5.11.4 AASHTO LRFD suggests the following equation for development length:

$$l_d \geq \kappa \left(f_{ps} - \frac{2}{3} f_{pe} \right) d_b \qquad \textbf{\textit{Equation 2-12}}$$

where, $\kappa = 1.0$ for pretensioned panels, pilings, and other pretensioned members with a depth less than or equal to 24.0 in.

$\kappa = 1.6$ for pretensioned members with a depth greater than 24.0 in.

In the Commentary C5.11.4.2 of AASHTO LRFD, the specification states that Equation 2-12 is conservative, but is meant to reflect worst-case scenarios of strands shipped prior to 1997. Except for the addition of the κ multiplier, this equation is functionally equivalent to the ACI 318-05 equation for development length.

2.3.4 Background Research for Current AASHTO Design Provisions

The current AASHTO provisions for transfer and flexural bond are very similar to those in ACI and are therefore also based on papers published by Hanson and Kaar (1959) and Kaar, LaFraugh, and Mass (1963). However, the current AASHTO LRFD equation has an additional κ multiplier. Although not explicitly stated in the Commentary of the AASHTO LRFD specifications, the evolution of the addition of the κ multiplier was added to the specification based on recommendations published by Cousins, Johnston, and Zia (1986), the FHWA (1988), and Shahawy (2001).

2.3.4.1 Cousins, Johnston, and Zia (1990)

This study was conducted at North Carolina State University in the mid 1980's to investigate the development length of epoxy-coated strands. In this study, sixteen rectangular prestressed prisms beams were tested to failure. The beams were prestressed with a single prestressing strand with a variable diameter. Strands surfaces were either left uncoated or were coated with epoxy.

Although the focus of this study was to investigate the performance of epoxy-coated strands, the results of the behavior of the uncoated strands seemed to be of more immediate significance. The authors reported that the current AASHTO provisions at that time underpredicted the development length for these beams with uncoated strands by as much as 30 percent in some cases.

2.3.4.2 FHWA (1988)

In response to the findings made by Cousins et al., on October 26, 1988 the FHWA distributed a memorandum which suggested that several changes be made to the current

AASHTO provisions for the development length of prestressing strands. The current provisions at that time reflected what was earlier presented as Equation 2-1. The memorandum stated that for strands with diameters less than or equal to 9/16 in. the predicted development length for all members should be multiplied by a factor of 1.6. They also suggested changes for center to center spacing, special provisions for unbonded strands, and imposed a moratorium on the use of 0.6 in. diameter strand for prestressing applications. However, the moratorium on 0.6 in. diameter strand has since been lifted.

2.3.4.3 Shahawy (2001)

The recommendations suggested by Shahawy in this paper are the result of an extensive testing program on transfer and development length of strands in prestressed members. The study was conducted at the Florida Department of Transportation (FDOT) Structures Research Center (FRSC) over a period of ten years. The objectives of the study were to compare the results of the study with current code provisions and the results of past studies as well as to present a rational method for calculating development length. This study included testing of prestressed concrete slabs, precast piles, and AASHTO girders. Seven solid and voided prestressed slabs were tested to determine the minimum development length of fully bonded ½ in. strands. The effect of pile embedment on the development length of ½ in. prestressing strands was tested on precast, prestressed piles with varying cross sections, pan lengths, and shear spans. Finally, several AASHTO Type II girders were investigated to determine transfer and development length of the prestressing strand, as well as flexural, shear, and fatigue behavior.

Shahawy recommends the following equations for the determination of development length:

For members with depth equal to or less than 24 in.:

$$l_d = \left(\frac{f_{pe}}{3}\right)d_b + \left(\frac{\left(f_{ps} - f_{pe}\right)}{1.2}\right)d_b \qquad \textbf{\textit{Equation 2-13}}$$

where, f_{pe} and f_{ps} are in ksi

For members with depth greater than 24 in.:

$$l_d = \left(\frac{f_{pe}}{3}\right)d_b + \left(\frac{\left(f_{ps} - f_{pe}\right)}{1.2}\right)d_b + 1.47h \qquad \textbf{\textit{Equation 2-14}}$$

where, h = depth of member (in.)

The author concluded that shear-flexural interaction has a definite effect on the development length of prestressing strands and should be accounted for in any design specifications. Therefore, he concluded that for members with a depth less than 24 in., the current AASHTO equation (Equation 2-1) and Equation 2-13 yield appropriate predictions and the use of a multiplier is not warranted. He also concluded that for prestressed concrete members with a depth greater than 24 in., Equation 2-14 yielded the best results and Equation 2-1 with the addition of a 1.6 multiplier yielded conservative results.

2.4 BOND THEORY

The bond of concrete to prestressing strand is generally subdivided into two types of bond: transfer bond and flexural bond. Descriptions of flexural and transfer bond as well as the various mechanisms and factors which affect bond are presented in this section.

2.4.1 BOND MECHANISMS

The three factors that contribute to bond between the concrete and steel are adhesion, friction, and mechanical resistance (Hanson and Kaar 1959). These three mechanisms will be discussed in this section.

2.4.1.1 Adhesion

Adhesion is the chemical bond between the strand and the concrete. It serves to resist slip between the strand and the concrete. However, this chemical bond layer is very thin which results in a rigid-brittle relationship between the bond stress and slip behavior (Russell and Burns 1993). Upon detensioning of the strand, immediate relative movement (slip) between the strand and the concrete occurs within the transfer zone. This immediate movement accompanies an immediate brittle failure of the chemical bond. Therefore, adhesion plays a very minimal role in bond performance, as it is only effective within the flexural bond length.

2.4.1.2 Friction

Friction plays a significant role in the transfer of stress from the strand to the concrete. Radial compressive stresses are required for frictional resistance to occur. These radial stresses are created due to the Hoyer Effect (Barnes et. al 1999). Figure 2-2 is a representation of this effect.

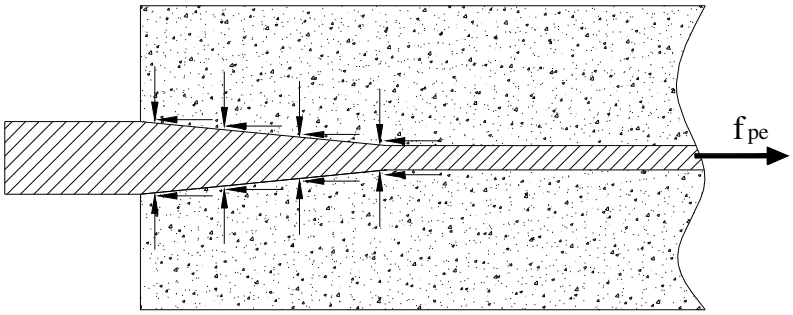

Figure 2-2: Hoyer Effect (Adapted from Haq 2005)

When a strand is pretensioned the strand diameter contracts. At the time of transfer, this contraction is partially recovered and the strand attempts to swell to its original diameter as the strand shortens elastically. However, the hardened concrete surrounding the strand prevents this expansion, creating radial stresses around the strand as equilibrium is achieved. As a result, frictional resistance between the concrete and the strand is created and a portion of the longitudinal stress in the strand is transferred to the concrete through friction. The Hoyer Effect exists primarily near the free end of the strand where the strand undergoes the largest strain change at transfer (Barnes et. al 1999).

2.4.1.3 Mechanical Resistance

Mechanical resistance or mechanical interlock is the result of axial bearing stresses created between the concrete and the strand. Prestressing strands are made of six wires wound into a helical shape around a straight center wire. When concrete is cast, the paste fills the resulting helical grooves around the strand and then hardens in these grooves. The hardened concrete around the strand forms a unique shape (Figure 2-3) which restrains sliding of the strand within the concrete, particularly if unwinding of the strand is restrained near the free ends. The forces on the concrete from the strand due to this

mechanism have longitudinal and radial components which contribute to bond strength. Once the concrete is cracked, mechanical resistance is the most important mechanism affecting bond behavior. Therefore, this mechanism is critical within the flexural bond length.

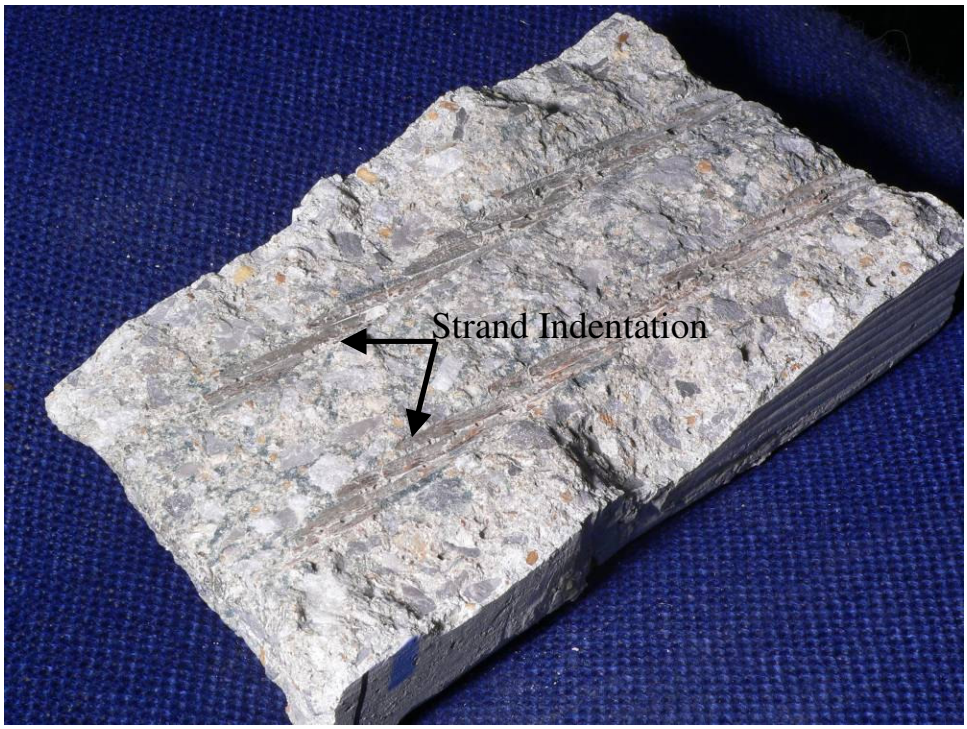

Figure 2-3: Hardened Concrete Displaying the Unique Cast around Prestressing Strand

2.4.2 TRANSFER BOND

Transfer bond exists within the transfer length, which, as stated previously, is the bonded length of a tendon required to fully develop the effective prestress, f_{pe}, in a strand by bond to the concrete. When the pretensioned tendons are detensioned at either end, the following reactions occur: the tendons shorten longitudinally, expand radially, and slip relative to the concrete along a finite length called the transfer length, bond stresses develop along the transfer length, and a buildup of concrete compressive stress results

along the transfer length parallel to the axis of the tendon (Barnes et al. 1999). The release of prestress ultimately results in zero axial stress at the free end of the strand and a constant value of prestress, f_{pe}, at the other end of the transfer length.

2.4.3 FLEXURAL BOND

Flexural bond develops as a result of flexure and plays an important role in the overall bond behavior after cracking has occurred. When the concrete cracks, slip of the tendon takes place near the cracks, as the bond stress immediately adjacent to the cracks quickly reaches the bond stress capacity (Hanson and Kaar 1959). This phenomenon is best illustrated by Figure 2-4.

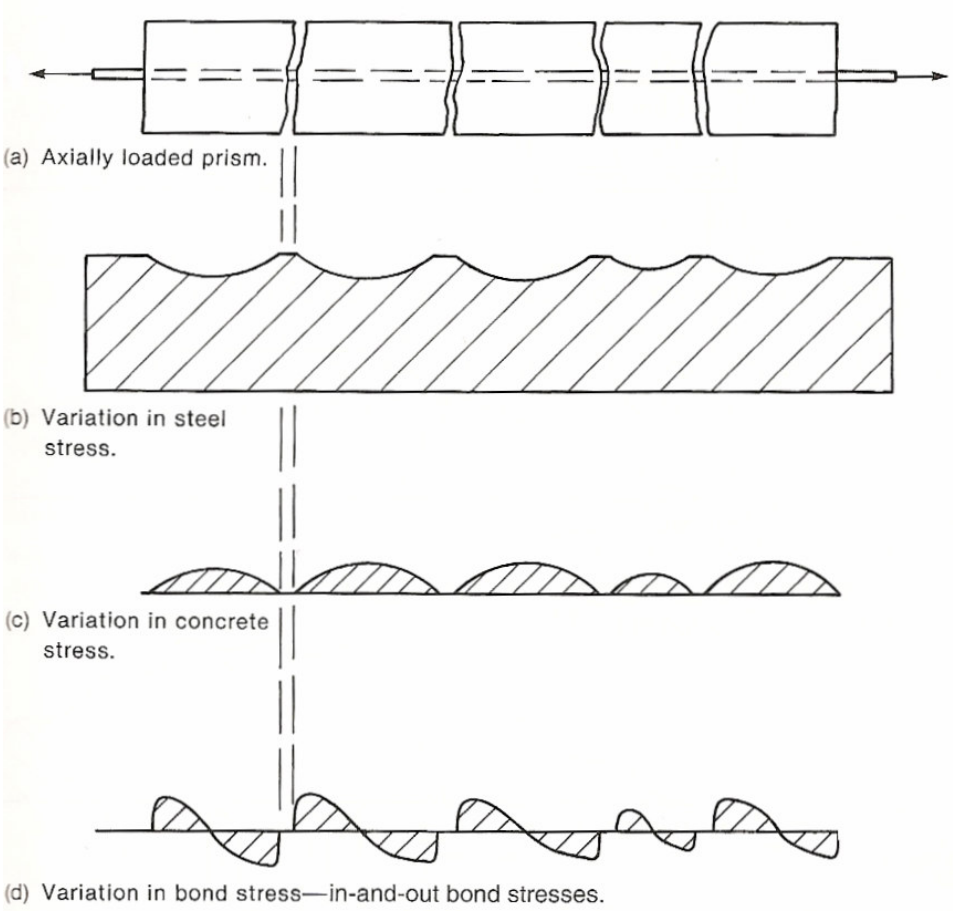

Figure 2-4: Steel, Concrete and Bond Stresses (MacGregor and Wight 2005)

The above figure shows that near the cracks, the concrete stress decreases due to a loss of bond. As a result, the reinforcing steel or prestressing tendon must carry the tensile force at the cracks, resulting in increased steel stress at the cracks.

The bond stresses shown that result from cracking are known as "true bond stresses" or "in and out bond stresses" because they transfer stress into the tendon and back out again (MacGregor and Wight 2005). These flexural bond stresses can be described as a "wave" that progresses from the original cracks toward the end of the beam (Hanson and Kaar 1959). If this wave progresses into the transfer zone, the increase in steel stress resulting from the bond slip decreases the strand diameter, reduces friction, and will propagate bond slip (Hanson and Kaar 1959). Thus, due to the Poisson effect, if cracking is present in the transfer zone, Hoyer's effect will be minimized, and the primary bond mechanism in the transfer zone, friction, will be severely compromised. It is therefore vital that cracking not influence the bond in transfer zone.

2.4.4 Factors Affecting Transfer and Flexural Bond

Although there are several known factors which affect transfer bond in prestressed members, the factors which affect flexural bond are somewhat unclear and still being researched. The factors which affect transfer bond are concrete strength, time-dependent deformations, strand size, strand surface condition, method of release, level of prestressing, member size, and concrete quality and placement. Factors which are thought to affect flexural bond include concrete strength, strand size, and member size. These factors will be discussed in detail in this section.

2.4.4.1 Concrete Strength

The effect that concrete strength has on transfer bond has been studied and debated for quite some time. In 1954, Janney conducted a study on bond in the transfer regions of smooth wires. He concluded that the transfer length was made up of an elastic and inelastic zone. The inelastic zone exists throughout the majority of the transfer length due to high radial pressures and tension stresses resulting from the expansion of the strand. He also stated that "one might anticipate some improvement in bonding quality of higher strength concretes" (Janney 1954). However, as mentioned previously, Kaar, LaFraugh, and Mass concluded that concrete strength had no effect on transfer length. The results of this study contrasted Janney's original hypothesis and spurred several research studies on the topic.

Several research studies found results which conflicted with those of Kaar, LaFraugh and Mass. In 1978, Zia and Mostafa conducted tests on concrete members with strengths ranging from 2000 to 8000 psi. They found that concrete strength was inversely proportional to transfer length (Zia and Mostafa 1978). Russell and Burns (1993) also concluded that higher concrete strengths led to shorter transfer lengths. In 1998, Lane published similar findings that increased concrete strengths resulted in smaller transfer lengths.

While it is now generally accepted that higher concrete strengths result in lower transfer lengths, the exact relationship between the two properties is still under debate. Micro-cracking of the concrete in the inelastic zone creates a softened response resulting in the stiffness of the concrete being dependent on the tensile strength and modulus of elasticity of the concrete (Barnes et al. 1999). Since the tensile strength and modulus are

usually estimated as being proportional to the square root of the compressive strength of the concrete in ACI practice and bond stress is inversely proportional to the transfer length, the transfer length should be inversely proportional to the square root of the concrete's compressive strength (Barnes et al. 1999). Research by Mitchell et al. (1993) and Barnes et al. (2003) show that relating the transfer length to the inverse of the square root of the concrete's compressive strength yields accurate models of transfer length over a broad range of concrete strengths.

2.4.4.2 Time Effects

The time-dependent effects on transfer length have not been studied in detail; however, several research studies have concluded that transfer length increases over time. As mentioned previously, Kaar, LaFraugh, and Mass (1963) report an average increase in transfer length of 6 percent over a period of one year. Lane (1998) reports an increase in transfer length of 30 percent over the first twenty-eight days after release with an additional increase of 7 percent over the next six months. In a review of various research studies, Zia and Mostafa (1977) report studying findings which showed overall increases in transfer length of 100 percent. Barnes et al. (2003) reported average increases in transfer lengths between 10–20 percent over the first 28 days after transfer with little increase thereafter.

Although the stress in a prestressed tendon decreases over time due to continually accumulating prestress losses from creep, shrinkage, and relaxation, the inelastic behavior of the surrounding concrete prevents the recovery of these stresses within most of the transfer zone. This inelasticity is caused by softening of the concrete surrounding

the tendon due to micro-cracking at prestress transfer. As a result, the length required to transfer the prestress force increases over time until crack growth and creep stabilize. Likewise, the transfer length does not decrease significantly as prestress losses accumulate because the concrete cannot respond elastically to decreases in tendon stress.

2.4.4.3 Strand Size

By examining the current development and transfer length equations, it is evident that strand diameter is an important factor relating to transfer bond. It is also a factor that has received a lot of attention by researchers over the years. Although the current equations suggest that increases in diameter will be linearly proportional to increases in transfer length, this theory has been debated for some time. As stated in a preceding section, in 1988, the FHWA placed a ban on the use of 0.6 in. strand for all prestressing applications. This spawned several research projects in the 1990's to determine the effect that strand size has on transfer bond. In Buckner's (1995) evaluation of several of these research projects, he concluded that transfer length increases directly with strand diameter for diameters up to 0.6 in.

The effects of strand size cannot be completely separated from the effects of strand spacing. As is the case with nonprestressed reinforcement, bond capacity is likely to be reduced due to splitting action when the clear spacing between strands (or the clear cover) is less than a critical value. The critical center-to-center spacing between strands is function of the strand size. At the same center-to-center spacing, smaller-diameter strands benefit from a larger amount of surrounding concrete available to resist splitting forces.

2.4.4.4 Strand Surface Condition

The surface condition of the prestressing tendon is another important factor relating to transfer bond. Slightly weathered or rusted strand may improve transfer bond although there have been varying reports on the subject. Hanson (1969) reports that rusted strands showed 30 percent lower transfer lengths than clean strands. Deatherage, Burdette, and Chew (1994), investigated transfer lengths on weathered and un-weathered seven-wire strand and concluded that the weathered strands had lower transfer lengths by as much as 39 percent. However, Logan (1997) could not find any benefit from using rusted strands.

Another element of strand surface condition that is important to transfer bond is the presence of oil on the strand. Janney (1954) studied the effect of lubrication on 5/16" prestressing wire and determined that lubricated wire showed significantly increased transfer length. In prestressing applications, it is very easy for oil used on the formwork to contaminate, and thus lubricate, the strand. Lubrication of the strand will decrease bond capacity significantly.

In terms of flexural bond, Janney (1954) reports that the flexural bonding performance of strand was much better than that of clean wire. He went on to say that the bonding capacity of rusted wire was much better than clean wire.

Shahawy (2001) suggests that the wide scatter and variability in transfer and development length results is likely due to variation in strand surface condition, and recommends that quality control be implemented to ensure adequate surface condition of prestressing strands. Strand surface condition is very important to transfer bond, but it also highly variable and unpredictable.

Barnes et al. (2003) also found strand surface condition to be an important factor affecting transfer length. They reported that transfer lengths in specimens with rusted strands were shorter on average. In some specimens, rusted strand transfer lengths were 13% shorter on average than non-rusted strand transfer lengths. However, in another set of specimens, they found that rusted strand produced longer transfer lengths than non-rusted strand. Overall, they found the dispersion of transfer lengths among rusted strands to be much greater than that of non-rusted strands, and conclude that surface weathering cannot be relied upon to produce reliable results.

2.4.4.5 Method of Release

The two methods to transfer prestress are gradual release and sudden release. Gradual release is accomplished by slowly detensioning the strand. Sudden release is generally achieved by flame cutting. The latter method results in one of two conditions at either end of the specimen. The "cut or live" end refers to the end which is adjacent to the flame cutting and the "dead" end is at the opposite end of the specimen. The sudden release of prestressing strands has been found to result in transfer lengths which are longer on the "live" ends of specimens than on the "dead" ends.

Several studies have used the "sudden release" method to transfer prestress and have found results coinciding with the preceding theory. Kaar, LaFraugh, and Mass (1963) found transfer lengths to be 20 percent longer on live ends than dead ends. In 1969, Hanson reported that live ends had transfer lengths 25 percent longer than on dead ends. Similarly, Russell and Burns (1997) found the average transfer length to be 34 percent longer on live ends than dead ends.

Barnes et al. (2003) found that the method of prestress release had no effect on bright strands in specimens with concrete release strengths up to 7000 psi. However, they also found that transfer lengths were 30 to 50 percent longer in specimens using rusted strands which utilized sudden release as the method of prestress transfer.

2.4.4.6 Member Size

Although most transfer length studies have been performed on small specimens, a study conducted by Russell and Burns (1993) on a variety of cross-section shapes and sizes revealed that member size has an effect on transfer bond. Tests on a variety of different cross section shapes with varying strand patterns showed that test specimens with larger cross sections possess shorter transfer lengths than smaller specimens (Russell and Burns 1993). It is possible that larger cross sections with greater mass can absorb more energy than smaller sections, and will therefore exhibit greater transfer bond.

Member size has been reported to have an effect on flexural bond as well. Shahawy (2001) concluded that shear-flexure interaction has a definitive effect on development length. Since the most important factor in shear-flexure interaction is member depth, Shahawy (2001) concluded that member depth has an effect on flexural bond. He suggests that members with depths greater than 24 in. require a longer development length than shallower members and should be designed accordingly.

2.4.4.7 Concrete Quality and Placement

Another factor influencing transfer and flexural bond is concrete quality and placement. In order for the concrete to achieve adequate bond to the prestressing tendon, the concrete must be consolidated properly to fully surround the area encompassing the tendon.

Without proper consolidation, the mechanisms influencing bond will not function properly. Consolidation is especially important for flexural bond since it depends primarily on mechanical interaction of the strand. However, with the use of SCC, this factor may become less of a concern in the future.

2.5 PREVIOUS FINDINGS RELATED TO SCC IN PRESTRESSED GIRDERS

There have been several recent studies of the effect of SCC on the bond of prestressing strands. This first part of this section provides a description of each study and gives an overview of the parameters and testing methods of each study. The results of these studies relating to several topics including the modulus of elasticity, tensile strength, transfer length, flexural behavior, shear behavior, and bond behavior are presented in the next part of this section. Finally, the last part of this section includes a summary of these results.

2.5.1 DESCRIPTIONS OF PREVIOUS STUDIES

Recent studies which have investigated the effect of SCC on the bond of prestressing strands include those conducted by Hamilton et al. (2005) at the University of Florida, Naito at al. (2005) at Lehigh University, Zia et al. (2005, 2006) at North Carolina State University, and Burgueño and Haq (2005) at Michigan State University. The details of these studies will be discussed in this section and the results will be discussed in a subsequent section.

2.5.1.1 University of Florida

Hamilton et al. (2005) conducted a study at the Florida Department of Transportation (FDOT) Structures Research Center in conjunction with the University of Florida. Six

42-ft. AASHTO Type II girders with a depth of 42 in. were cast with a standard concrete mixture and an SCC mixture. The beams were constructed with 12 Grade 270, ½ in. diameter prestressing tendons. Both the standard concrete and SCC mixture contained similar quantities of cement, Class F fly ash, and water. SCC characteristics were achieved with the addition of a high-range water reducer (HRWR) to the SCC mixture. The mixture proportions used in this study are displayed in Table 2-1.

Table 2-1: University of Florida Study Mixture Proportions (Hamilton et al. 2005)

Mixture Constituents	**Description**	**Mixtures**	
		Control	SCC
Water (pcy)	Local	258	258
Cement (pcy)	Lehigh Type I/II	752	752
Fly Ash (pcy)	ISG Class F	0	225
Coarse agg. (pcy)	Tarmac #67	1307	1307
Fine agg. (pcy)	Florida Rock	1414	1414
AEA (oz/cy)	MBVR-S	1.80	0.80
MRWRA (oz/cy)	Pozzolith 100 XR	13.8	13.8
HRWRA (oz/cy)	Glenium 3200 HES	27.6	64.4

Three of the six beams were cast with the standard concrete mixture, and the other three were cast with the SCC mixture. All six beams were cast in a single line on one day. Transfer of prestress was achieved by torch-cutting single strands, resulting in each beam having one live end and one dead end. At the time of release, the concrete strengths for the standard concrete and SCC mixture were 3170 and 3810 psi, respectively. Transfer lengths were estimated on one conventional beam and one SCC

beam using longitudinal strain measurements from long length vibrating wire strain gauges.

The girders were load tested at ages ranging from 8 to 10 months, when the compressive strengths of the standard concrete and SCC beams were greater than 7500 and 9000 psi, respectively. Four of the beams (two SCC and two standard concrete mixture beams) were designed to be tested in flexure and shear with a 12-in. composite cap. The composite cap served to simulate the composite action of a bridge deck. Two beams (one SCC and one standard concrete mixture beam) were designed to be tested in shear without the benefit of composite action. The target 28-day compressive strength of the deck was 4,500 psi.

Three types of tests were done on the beams to achieve the following failure modes: shear, flexure, and strand-slip failures. For each beam, each end was tested separately resulting in a total of 12 beam tests. For each failure mode, 4 beam ends were tested (two SCC and two standard concrete mixture beams). Shear failure modes were accomplished using wide stirrup spacings and a unique test geometry to create a concrete strut or node crushing failure mode. Flexural failure modes were created using a unique test geometry designed to promote a flexural failure with shear cracking. Finally, strand-slip failure modes were accomplished by creating a short shear span and a short embedment length to promote strand slip.

2.5.1.2 Lehigh University

Naito et al. (2005, 2006) conducted a study at Lehigh University in conjunction with the Pennsylvania Infrastructure Technology Alliance (PITA). Four 35-ft. standard PCEF

(Mid-Atlantic States Prestressed Concrete Committee for Economic Fabrication) girders with a depth of 45 in. were constructed using 26 Grade 270, ½ in. diameter special strands. A standard girder concrete mixture design (denoted HESC) was used for two of the beams, and an SCC mixture was used for the two other beams. Both mixtures contained Grade 120 GGBF slag with replacement percentages for the standard concrete and SCC mixtures being 35 percent and 25 percent respectively. SCC characteristics were achieved with the addition of a HRWR and a viscosity-modifying admixture (VMA). The mixture proportions used in this study are displayed in Table 2-2.

Table 2-2: Lehigh University Study Mixture Proportions (Naito et al. 2005)

Table 11: Concrete proportions				
	Average of Batches		Design Proportions	
Material Type	HESC	SCC	HESC	SCC
Total Cement [lb/yd^3 (kg/m^3)]	**750(445)**	**849(504)**	752(446)	850(504)
Slag Cement [%]	**34**	25	35	25
Fine Aggregate SSD [lb/yd^3 (kg/m^3)]	**1172 (695)**	**1283(761)**	1171(695)	1287(763)
Coarse Aggregate #67 SSD [lb/yd^3 (kg/m^3)]	**1383(820)**	0	1359(806)	0
Coarse Aggregate #8 SSD [lb/yd^3 (kg/m^3)]	**552(327)**	**1651(979)**	582(345)	1650(979)
Water / Cement Ratio	0.34	0.32	0.34	0.32
High Range Water Reducer [oz/yd^3 (ml/m^3)]	60.0(2320)	136.2(5270)	60.0(2320)	136.2(5270)
Retarding Admixture [oz/yd^3 (ml/m^3)]	4.0(154)	0	4.0(154)	0
Air Entrainment Admixture (AEA) [oz/yd^3 (ml/m^3)]	2.4(93)	2.0(76)	2.4(93)	2.0(76)
Viscosity Modifying Admixture [oz/yd^3 (ml/m^3)]	0	16.0(620)	0	16.0(620)
Coarse Aggregate Volume [%]	39	34	39	34
Target Air Content [%]	NA	NA	5.0	5.0
Target Slump / Spread [in. (cm)]	NA	NA	5 ± 1 (12.7 ± 2.5)	23 ± 1 (58.4 ± 2.5)

Prestress transfer occurred by gradual release of the strands. At the time of release, the reported strand stress was 185.6 ksi and reported concrete strengths for the standard concrete and SCC beams were 6809 and 8232 psi, respectively. Transfer length was

estimated using resistance- and vibration-based strain gauges that were installed prior to concrete placement.

The girders were load tested at ages ranging from 1 to 4 months when the compressive strengths of the standard concrete and SCC beams were greater than 7000 and 8000 psi, respectively. Each beam was tested in two configurations. In the first configuration, the entire span was used and loads were applied at one development length plus the flexural depth of the beam to promote a compressive flexural failure. After the completion of the first test, the remaining undamaged section was tested in one of two configurations. The first of these used the full section of the beam with the load applied at one development length from the end of the beam to create a combined shear and flexure failure. In the other configuration, the lower 14 strands were severed to create a reduced cross section. In this setup, the load was also applied at one development length from the end, resulting in a flexural tensile mode failure. A total of 8 tests were performed in this study.

2.5.1.3 North Carolina State University

Zia et al. (2005) conducted a study at North Carolina State University in conjunction with the North Carolina DOT and the FHWA. Three 54.8-ft. AASHTO Type II girders with a depth of 45 in. were selected for this investigation. One of the girders was cast using a standard concrete mixture and the other two girders were cast using an SCC mixture. SCC characteristics were achieved by decreasing the amount of coarse aggregate and the usage of a HRWR. No supplementary cementing materials (SCM) were used in either of the mixtures. The mixture proportions used in this study are displayed in Table 2-3.

Table 2-3: North Carolina State University Study Mixture Proportions (Zia et al. 2005)

Mixture Constituents	**Description**	**Mixtures**	
		Normal Concrete	SCC
Water (pcy)	-	283.6	341.9
Cement (pcy)	Type III	680	810
Coarse agg. (pcy)	Granite	1700	1330
Fine agg. (pcy)	Manufactured Sand	1295	1300
AEA (oz/cwt)	Darex II	0.30	0.30
HRWRA (oz/cwt)	ADVA Flow*/170**	5.0*	10.0**
Retarder (oz/cwt)	Daratard 17	4.0	4.0
Corrosion Inhibitor (gal/yd)	DCIS	3.0	3.0

Prestress transfer was achieved by flame-cutting the strands. At the time of release, the strand stress was estimated to be 194 ksi and the concrete strengths of the standard concrete and SCC beams were 4700 and 5500 psi, respectively. Transfer lengths were determined using strain transducer bars which had seven pairs of electrical resistance strain gauges attached.

All of the girders were load tested at an age of 98 days when the compressive strengths of the standard concrete and SCC beams were greater than 7000 and 10,000 psi, respectively. The girders were simply supported and a concentrated load was applied at midspan. Loading was discontinued when the maximum bottom fiber stress reached 300 psi, which is slightly above the design service load. The girders remained uncracked during the entire loading process and recovered all deflection elastically at the end of the loading.

2.5.1.4 Michigan State University

Burgueño and Haq (2005) conducted a study at Michigan State University in conjunction with the Precast Prestressed Concrete Institute (PCI). Twelve 38-ft T-beams with a depth of 15 in. were cast with one standard concrete mixture and three different SCC mixtures. The beams were constructed with 2 Grade 270, ½ in. diameter strands. All of the mixtures used Type III cement without the addition of any SCMs. All of the SCC mixtures used a VMA as well. The mixture proportions used in this study are displayed in Table 2-2.

Table 2-4: Michigan State University Study Mixture Proportions (Haq 2005)

Mixture Constituents	**Mixtures**			
	Normal Concrete	SCC1	SCC2	SCC3
Water (pcy)	280	280	280	315
Type III Cement (pcy)	700	750	700	700
Coarse agg. (pcy)	1580	1380	1380	1435
Fine agg. (pcy)	1216	1628	1426	1275
AEA (oz/cwt)	3.50	1.75	1.75	3.18
Set Retardant (oz/cwt)	52.5	70.0	58.6	46.7
HRWRA (oz/cwt)	4.0	14.6	12.0	15.4
VMA (oz/cwt)	0.0	7.0	1.8	15.4

Prestress transfer was achieved by sudden release of the strand by torch-cutting at both ends of the beam simultaneously. At the time of release, the concrete strengths for the standard concrete and SCC mixtures were approximately 5000 and 6000–7000 psi, respectively. Transfer lengths were measured twice on each side of each end of each

beam using mechanical strain gauges. Transfer lengths were also estimated using strand draw-in measurements.

The T-beams were load tested at ages ranging from 4 to 5 months when the compressive strengths of the standard concrete and SCC beams were 7000 and 8000–9000 psi, respectively. The effective span length for all tests using beams made with successful mixtures (two mixtures had to be redone due to poor fresh properties) was held constant at 24 ft. The available development length was varied by varying the shear span. Three failure modes were observed during testing: shear-slip, flexural, and flexural-slip failure.

2.5.2 Findings in Previous Studies

Results of the aforementioned studies are presented in this section. Variations between standard concrete and SCC are evaluated with respect to several properties and behaviors including the modulus of elasticity, tensile strength, transfer length, flexural behavior, shear behavior and bond behavior.

2.5.2.1 Modulus of Elasticity

Variations between the modulus of elasticity of the standard concrete and the SCC were observed in the majority of these studies. Naito et al. (2005) reported that cylinder testing showed that the elastic modulus of the standard concrete was 11 percent higher than the SCC. However, camber and elastic shortening measurements indicated that the SCC had a higher in-place elastic modulus than the standard concrete (Naito et al. 2006).

Zia et al. (2005) reported that the elastic modulus based on cylinder tests for both the standard concrete and SCC was less than expected from ACI formulations. The authors

suggested that this may be due to the lack of moist curing and the use of limestone as fine aggregate. During static loading, the stiffness of all girders was the same; however, under sustained loading, the stiffness of the SCC girders appeared to decrease more than the stiffness of the normal concrete girder (Zia et al. 2005).

Hamilton et al. (2006) reported that the elastic modulus for the SCC specimens was lower than the elastic modulus of the standard concrete as well as the ACI 318 estimate. They also predicted that the deflection associated with camber and applied loads may be significantly greater in the SCC beams than originally expected because of the smaller elastic modulus (Hamilton et al. 2006).

2.5.2.2 Tensile Strength

The results concerning tensile capacity based on the splitting tensile test (ASTM 496) and the modulus of rupture test (ASTM C78) are not consistent for all of these tests. Hamilton et al. (2005) reported that the tensile strengths for SCC specimens were lower for both the splitting tensile and modulus of rupture test, despite the SCC specimens possessing higher compressive strengths.

Naito et al. (2006) concluded that the tensile capacity of the standard concrete and the SCC were comparable based on splitting tensile and modulus of rupture tests. For this study, the researchers conducted tests on 4 x 8 in. cylinders, 6 x 12 in. cylinders and modulus of rupture beams. However, they also reported that overall tensile capacities were greater than those predicted according to ACI formulations.

Zia et al. (2005) stated that they observed comparable values of the flexural modulus of rupture for the standard and SCC mixtures based on the modulus of rupture test.

However, they stated that these values were lower than expected for their respective compressive strengths. The low values were attributed to a lack of moist curing and the use of a weak fine aggregate (Zia et al. 2005).

2.5.2.3 Transfer Length

The majority of the studies concluded that the transfer lengths recommended by ACI and AASHTO were conservative. Both Naito et al. (2005) and Hamilton et al. (2005) reported that the transfer length recommended by AASHTO was conservative for all of their specimens. They also both concluded that the standard concrete and SCC beams had comparable transfer lengths. Although Zia et al. (2005) also came to the conclusion that the standard concrete and SCC beams had comparable transfer lengths, they observed average transfer lengths for their specimens to be 40 percent higher than the AASHTO transfer length.

Burgueño and Haq (2005) reported that the average transfer length of the standard concrete beams was approximately 86 percent of the transfer length suggested by AASHTO, and the average transfer lengths of beams constructed with two of the three SCC mixtures were approximately 90 percent of the AASHTO transfer lengths. However, beams made with one of the three SCC mixtures exhibited an average transfer length 2 percent higher than the AASHTO transfer length. Overall, they found that SCC mixtures had longer transfer lengths when compared to standard concrete mixtures (Haq 2005).

2.5.2.4 Flexural Behavior

Although results relating flexural behavior are consistent throughout these studies, the research results relating to the ductility of SCC in prestressed girders are rather inconclusive. In the Michigan State University study, the actual nominal moment for all flexural failures exceeded the nominal moment predicted using ACI 318 (Haq 2005).

Naito et al. (2006) stated that both standard concrete and SCC specimens exceeded the predicted cracking moment and reached 101–104 percent of the predicted moment capacity. They concluded that the standard concrete and SCC specimens exhibited comparable flexural behavior and comparable damage progression. They also reported that in all cases SCC specimens showed evidence of greater ductility than the standard concrete specimens.

Zia et al. (2005) stated that the standard concrete and SCC girders produced identical load-deflection relationships up to service loads without any cracking present. They concluded that all specimens exceeded design expectations.

Hamilton et al. (2005) reported that there was no difference in the flexural capacities between standard concrete and SCC girders. They also noted that all girders experiencing flexural failures showed similar cracking patterns and crack widths. However, the standard concrete beams had 17.1 percent more deflection at ultimate load than the SCC beams. Thus, they concluded that the standard concrete mixture exhibited better ductility than the SCC mixture.

2.5.2.5 Shear Behavior

Comparing the shear behavior of the specimens in these different studies is a much more difficult task. The Michigan State University study did not include any shear failures independent of significant bond failure (Haq 2005). Also, the North Carolina State University Study did not include failure testing of beams, thus precluding any conclusions concerning shear behavior (Zia et al. 2005).

However, Hamilton et al. (2005) experienced shear failure modes consisting of a compression failure at the top of the section near the applied load. They stated that there are no discernable differences in shear behavior between standard concrete and SCC specimens and therefore concluded that all specimens experiencing shear failures had comparable shear capacities.

Naito et al. (2006) also concluded that no difference in shear capacity existed between standard concrete and SCC girders. They also reported that shear failure specimens exhibited 106–107 percent of ACI 318 shear capacity for those specimens.

2.5.2.6 Bond Behavior

There does not seem to be a trend in terms of bond behavior among the findings of these studies. Naito et al. (2006) observed minimal or no strand slip in bonded strands. The maximum slip observed was less than 0.05 in. They concluded that there was no difference in bond behavior between SCC and standard concrete specimens.

Hamilton et al. (2005) observed one premature beam failure due to strand slip. This bond failure occurred in an SCC beam. They attributed this failure to unfavorable transfer conditions caused by the sudden release of the strand. The transfer length for this

particular beam was observed to be longer than other specimens, which may account for the premature bond failure (Hamilton et al. 2005).

In contrast, the Michigan State University researchers reported a definitive difference in transfer and flexural bond behavior between standard concrete and SCC beams. All of the SCC beams required development lengths longer than ACI and AASHTO recommendations. The standard concrete beams exhibited development lengths within design recommendations, but the three SCC mixtures exhibited development lengths 3, 17, and 42 percent longer than ACI design recommendations. The possibility of low bond-quality strand was offered as a possible reason for these findings because rusted strand was used for the conventional mixture, but not for the SCC mixtures. However, it was also concluded that the SCC mixture proportioning has a clear and different effect on bond mechanisms contributing to the development length of prestressing strands (Haq 2005).

2.5.3 Conclusions from Previous Studies

It is clear from the results presented in the previous section that there is no definite consensus related to SCC in prestressed girders. However, the conclusions reached by the researchers of the aforementioned studies are reported here so as to fully relate the results and recommendations of each study.

Naito et al. (2006) concluded that their results indicate that the mechanical characteristics of SCC outperform current recommendations. They stated that SCC is a viable construction material for prestressed bridge beam members. However, they also

offered the disclaimer that the conclusions drawn in their research are only for the specific mixtures studied in that project.

The Michigan State University study concluded that design recommendations were conservative for most of the observed transfer lengths. However, these researchers also concluded that the design recommendations for development length were unconservative for SCC members and also concluded that SCC mix proportioning has clear and different effects on bond behavior and mechanisms relating to the development length of prestressing tendons (Haq 2005).

Zia et al. (2005) concluded that SCC and standard concrete were very similar in their performance with respect to the modulus of elasticity, flexural modulus, transfer length and flexural behavior. However, they also reported that the design recommendations for transfer length are unconservative for their specimens.

Hamilton et al. (2005) concluded that, overall, no notable differences between standard concrete and SCC were observed with respect to transfer length, camber growth, flexural capacity, shear capacity, or cracking. However, they did report reduced ductility with SCC as well as one case of premature bond failure in an SCC beam.

The conclusions presented in this section reveal that a general accord for specific material properties of SCC in prestressed girders does not exist. However, in general, the performance and behavior of SCC has been found to be comparable to standard concrete in most of the studies. Nonetheless, it is clear that more research is needed to clarify the behavior and performance of SCC in prestressed members.

CHAPTER 3

DESIGN AND FABRICATION OF EXPERIMENTAL SPECIMENS

3.1 INTRODUCTION

The test specimens used in this study consisted of sixteen prestressed T-beams. One standard mixture and three SCC mixtures were used in this study. For each of the four mixtures, four T-beams of varying lengths were cast for a total of sixteen beams. The design and fabrication of these specimens are presented in this chapter.

3.2 SPECIMEN DESIGN AND IDENTIFICATION

The design and identification of the specimens fabricated for use in this study are presented in this section.

3.2.1 SPECIMEN DESIGN

Figure 3-1 shows the cross section details for all sixteen T-beams tested for this study. The specimens were prestressed with two seven-wire, low-relaxation, Grade 270 ½-in. "special" diameter strands. Four Grade 60 No. 3 reinforcing bars were provided as compression reinforcement. Transverse reinforcement was also provided in the form of No. 3 reinforcing bars. In addition, Grade 60 No. 3 reinforcing bars were also used for the shear reinforcement. The shear reinforcement consisted of custom-made U-stirrups fabricated in the Auburn University Structural Engineering Laboratory. For each beam

length, a slightly different stirrup layout was used. More information about stirrup spacing can be found in Chapter 5 of this thesis. Appendix B contains details of the shear reinforcement layout used in each of the specimens.

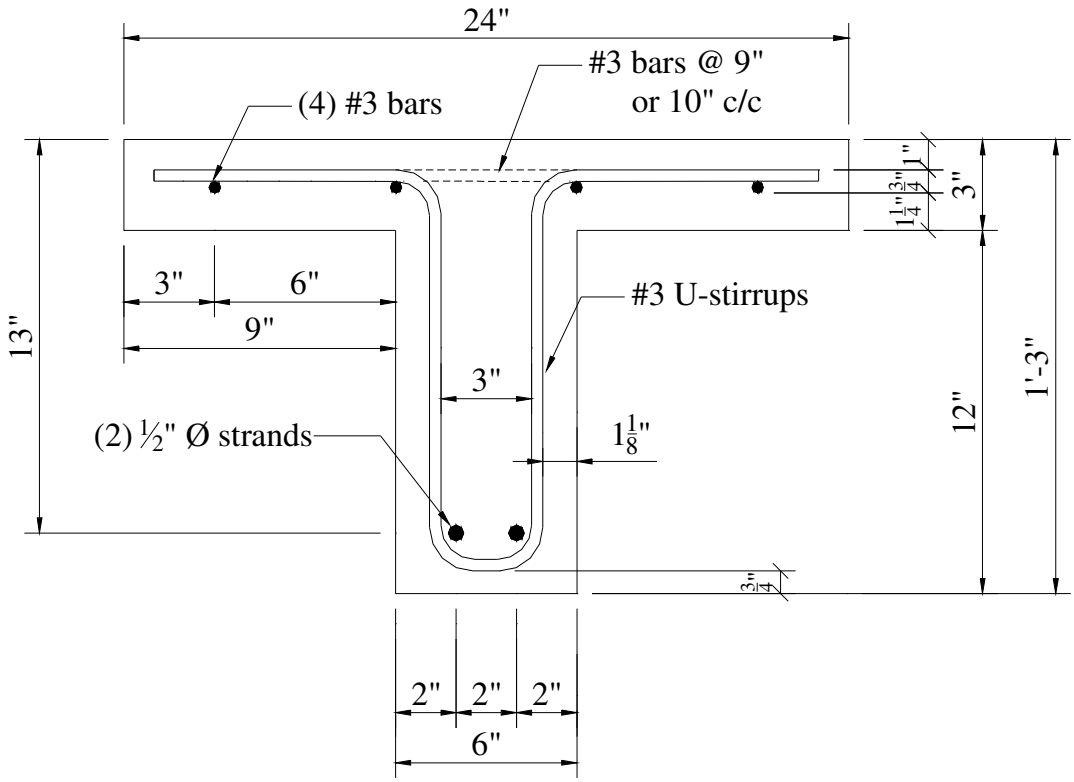

Figure 3-1: T-Beam Cross Section Detail

As mentioned previously, for each of the mixtures, a total of four T-beams with varying lengths were cast. The lengths of the beams were varied to provide different embedment lengths for the development length test program. Specimens were cast with lengths of 9'-8", 13'-0", 16'-4" and 23'-0". Details regarding the determination of specimen length will be discussed in detail in Chapter 5.

3.2.2 SPECIMEN IDENTIFICATION

The specimen identification system used throughout this thesis is summarized by Figure 3-2.

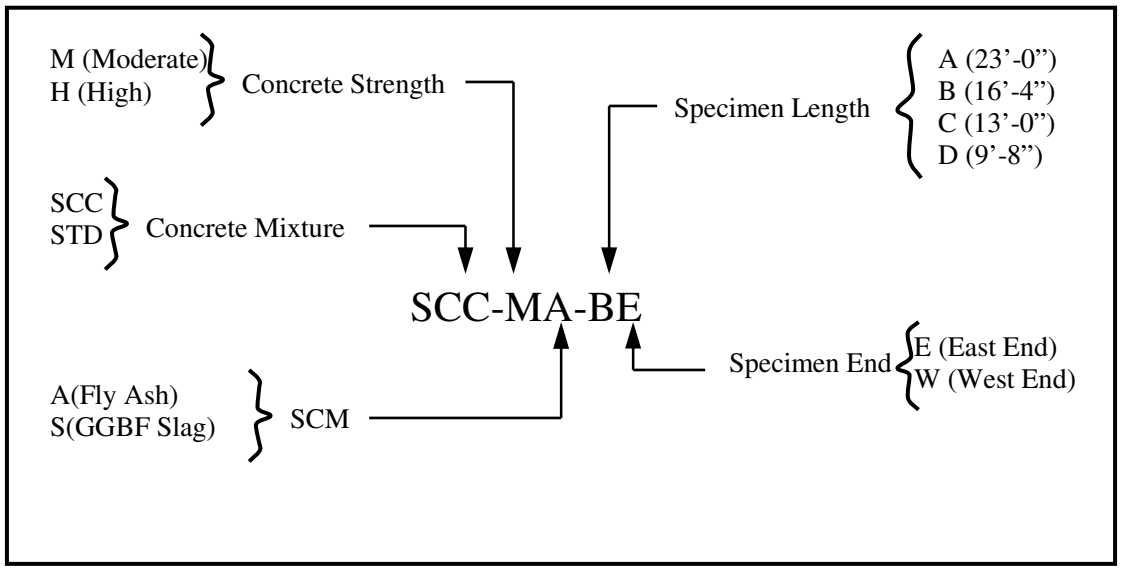

Figure 3-2: Specimen Identification System

The sixteen beam specimens were cast in groups of four using a total of four different mixtures. One moderate-strength standard mixture (denoted STD-M) as well as three SCC mixtures were used in this study. The three SCC mixtures consisted of a moderate-strength mixture using a 30% cement replacement with Class C Fly Ash (SCC-MA), a moderate-strength mixture using a 50% cement replacement with Grade 100 GGBF slag (SCC-MS), and a high-strength mixture using a 30% cement replacement with Grade 100 GGBF slag (SCC-HS).

Beam ends are specified by east or west end. The beams were cast on two different prestressing beds, with two beams on one bed and the other two beams on another bed. The beam setup configuration is shown in Figure 3-3. As can be seen by their casting

locations, Beams A and D were prestressed with the same two strands and Beams B and C were prestressed with another pair of strands. The strand cutting location is also specified in Figure 3-3. As can be seen, each beam has one live end and one dead end. An actual aerial view of the prestressing beds is depicted in Figure 3-4.

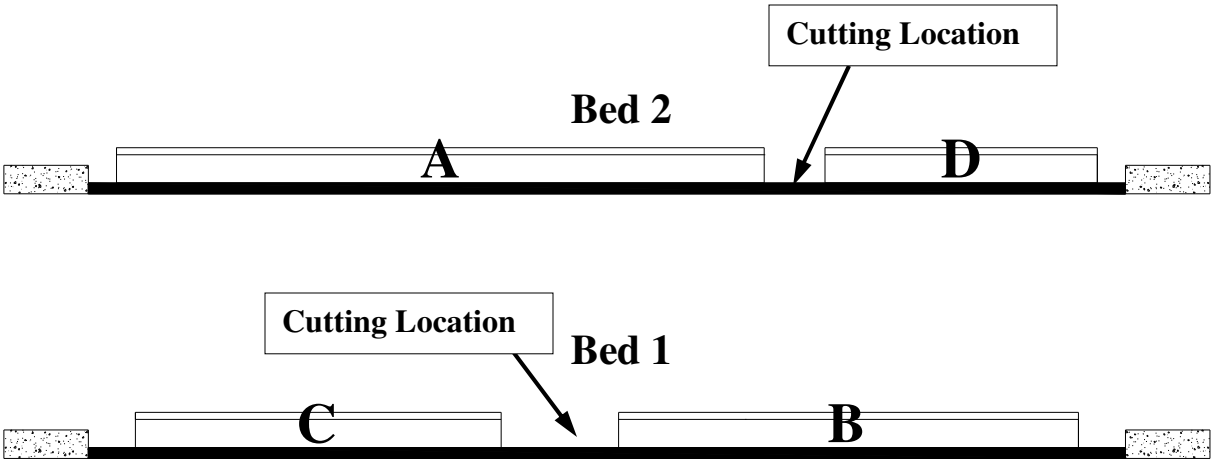

Figure 3-3: Casting Configuration

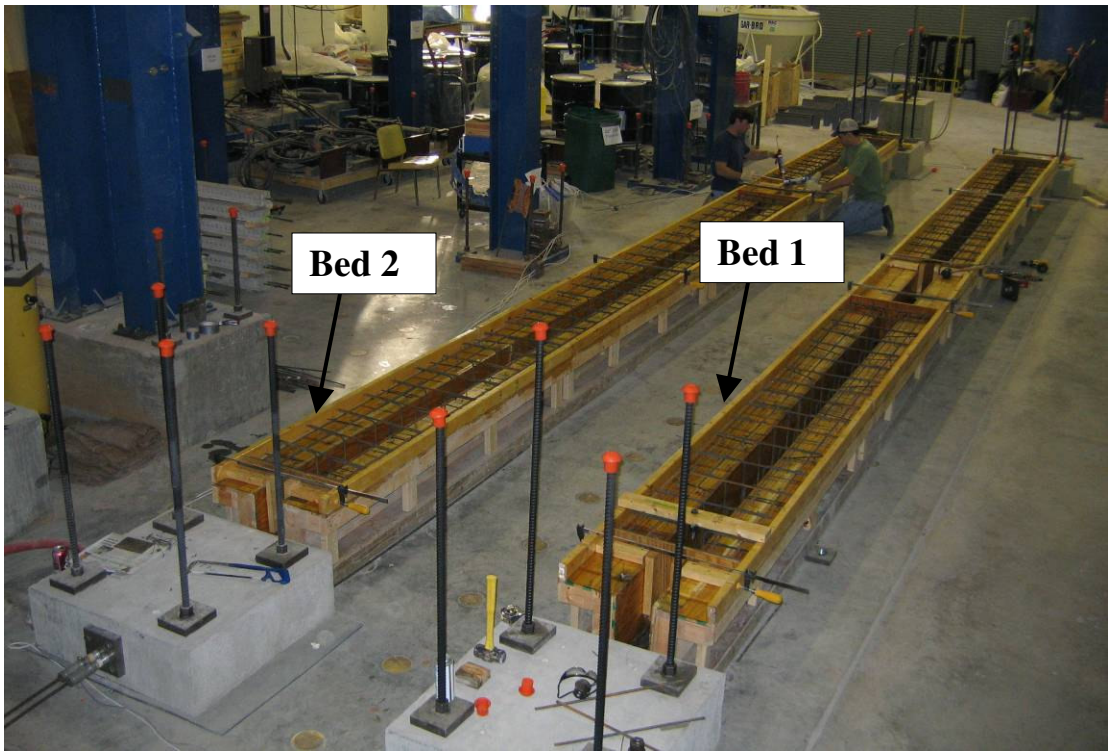

Figure 3-4: Prestressing Beds with Forms

3.3 MATERIAL PROPERTIES

The materials used in the fabrication of the beams used in this study were concrete, prestressing strand, and mild steel. These materials are discussed in this section.

3.3.1 PRESTRESSING STEEL

The prestressing steel used in this study consisted of low-relaxation, ½-in. "special", Grade 270, seven-wire prestressing strand. The cross-sectional area and elastic modulus of this strand based on the manufacturer's tests are 0.164 in^2 and 28,900 ksi, respectively. The measured diameter (across a three-wire width) of this strand is 0.515 in.

The strand used in all of the beams came from one strand pack that was manufactured by American Spring Wire Corporation in Houston, Texas. The strand had some very

slight surface weathering due to a short period of weather exposure prior to storage in the air-conditioned laboratory. However, prior to prestressing, each strand was wiped with a new cotton cloth to remove any surface debris. No pitting was present on the strands. Figure 3-5 shows the slightly weathered surface condition of the prestressing strand in place.

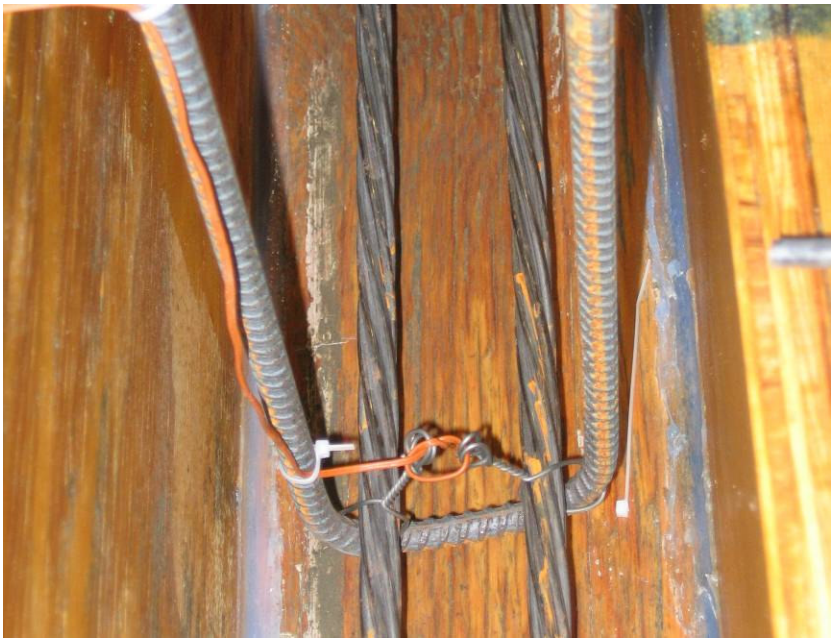

Figure 3-5: Slightly Rusted Strand Surface Condition

3.3.2 MILD REINFORCING STEEL

The mild reinforcing steel used in this study was ASTM A615 Grade 60 reinforcing bar. The longitudinal compression reinforcement, transverse flange reinforcement, and shear stirrups all consisted of No. 3 bars. The modulus of elasticity and yield stress of the bars was taken to be 29,000 ksi and 60 ksi, respectively. A detail of the reinforcement is given in Figure 3-1. Shear reinforcement details are given in Appendix B. Figure 3-6 depicts the reinforcement for the specimens in the forms before casting.

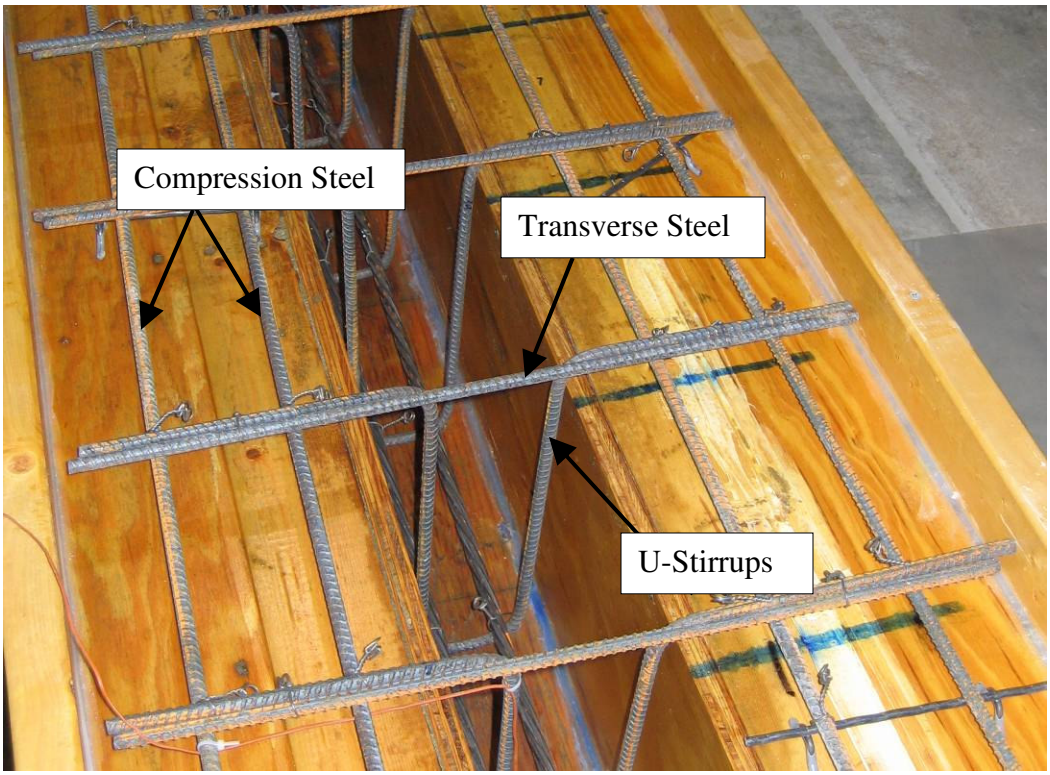

Figure 3-6: T-Beam Reinforcement

3.3.3 CONCRETE

Four concrete mixtures were used in this study including one standard and three SCC mixtures. The selection of the mixtures, mixture proportions, fresh property testing and hardened property testing are discussed in this section.

3.3.3.1 Concrete Mixtures

As mentioned previously, the study detailed in this thesis is part of a larger ongoing study at Auburn University. In an earlier phase of this study, twenty-one experimental SCC mixtures were designed and tested using the mixture matrix depicted in Table 3-1.

Table 3-1: Experimental Mixture Matrix (Swords 2005)

Powder Combination	Sand/Aggregate (by volume)	Water-to-powder ratio			
		0.28	**0.32**	**0.36**	**0.40**
Type III cement + 30% Class C fly ash	0.38	SCC-1	SCC-2	SCC-3	
	0.42	SCC-4	SCC-5	SCC-6	
	0.46	SCC-7	SCC-8	SCC-9	
Type III cement + *x*% Grade 100 GGBF Slag		*(30% Slag)*	*(40% Slag)*	*(50% Slag)*	
	0.42	SCC-10	SCC-11	SCC-12	
	0.46	SCC-13	SCC-14	SCC-15	
Type III cement + 22% Class C ash + 8% Silica Fume	0.42		SCC-16	SCC-17	SCC-18
	0.46		SCC-19	SCC-20	SCC-21

Table 3-2 shows that twenty-one SCC mixtures were created by varying the type and percentage of supplementary cementing material, the sand-aggregate ratio, and the water-to-powder ratio. Class C fly ash, Grade 100 GGBF slag, and silica fume were used to replace the Type III Portland cement in different mixtures. The coarse aggregate used in this study was a #78 dolomitic limestone; the fine aggregate was a natural river sand.

The SCC mixtures selected for this study were SCC-9, SCC-13, and SCC-15. Using the nomenclature of this thesis, SCC-9, SCC-13, and SCC-15 are SCC-MA, SCC-HS, and SCC-MS respectively. In addition to the SCC mixtures, a standard concrete mixture was also selected to be used in this study as a control. This standard mixture resembles a mixture commonly used in ALDOT prestressed concrete girders, that achieve an f'_{ci} of approximately 5,500 psi.

Thus, there were three moderate-strength mixtures: a standard concrete mixture, one SCC mixture with a 30% fly ash replacement, and another SCC mixture with a 50% Grade 100 GGBF slag replacement. In addition, one high-strength SCC mixture with a 30% Grade 100 GGBF slag replacement was chosen for this phase of the project. These mixtures were selected based on favorable performance during previous phases of this project. The research results of these phases are presented in Roberts (2005), Swords (2005), and Schindler et al. (2007).

Target values for the acceptance of SCC mixtures were developed in a series of meetings at the Alabama Department of Transportation at which representatives from ALDOT, FHWA, the chemical admixture industry, the prestressing industry, and Auburn University were present. Table 3-2 outlines the target values agreed upon at these meetings.

Table 3-2: Concrete Mixture Target Values

	Target Value
Air Content	0%–5%
Slump Flow	27 in. ± 3 in.
Moderate-Strength Concrete	$f_{ci}^{'} \approx 5000$ psi
High-Strength Concrete	$f_{ci}^{'} \approx 9000$ psi

As shown in the above table, the air content and slump flow ranges were specified to be 0%–5% and 27 in. ± 3 in., respectively. Two strength levels for f'_{ci}, moderate-strength and high-strength, were specified for the concrete mixtures. The moderate-strength level

for f'_{ci} was specified to be approximately 5000 psi and the high-strength level for f'_{ci} was specified to be approximately 9000 psi.

The actual proportions of the mixtures chosen for this phase of the project are shown in Table 3-3. The admixtures used in these mixtures include a high-range water reducing admixture (HRWR), a viscosity-modifying admixture (VMA), a mid-range water reducing admixture (WRA), and an air-entraining admixture (AEA).

Table 3-3: Concrete Mixture Proportions

Mixture Constituents	Mixtures			
	STD-M	**SCC-MA**	**SCC-MS**	**SCC-HS**
Water (pcy)	270	270	270	260
Cement (pcy)	640	525	375	650
Fly Ash (pcy)	0	225	0	0
GGBF Slag (pcy)	0	0	375	279
Coarse Agg. (pcy)	1964	1607	1613	1544
Fine Agg. (pcy)	1114	1316	1323	1265
AEA (oz/cwt)	0.33	0.00	0.00	0.00
WRA (oz/cwt)	4.0	4.0	6.0	6.0
HRWRA (oz/cwt)	3.5	4.0	4.5	5.0
VMA (oz/cwt)	0.0	2.0	2.0	2.0
w/cm	0.40	0.36	0.36	0.28
s/agg	0.46	0.46	0.46	0.46

3.3.3.2 Fresh Concrete Property Testing

The specimens were cast in the Auburn University Structural Engineering Laboratory using a concrete ready-mixture truck from Twin City Concrete to produce the 3.5 cubic

yards of concrete needed for each mixture. Fresh property testing was conducted on all mixtures prior to mixture acceptance and casting. All mixtures met the specifications for air content and slump flow with only one exception which will be discussed herein.

Fresh property testing is crucial for the acceptance of an SCC mixture. An SCC mixture must have a good balance between deformability and stability while preventing the blockage of concrete flow (Khayat 1999). Thus, an SCC concrete mixture must completely fill the formwork and flow around obstructions while maintaining homogeneity and resisting segregation. This "workability" or ability to flow under its own weight around reinforcement without creating blockages is what essentially defines SCC. Therefore, it is critical that the workability of each SCC mixture be defined according to its deformability, filling capacity, and stability. A number of tests exist to quantify these properties including the slump flow test, J-Ring test, and L-Box test.

The slump flow test was created to quantify the deformability of SCC by measuring its consistency and unrestricted flow potential. This test follows the guidelines of ASTM C 1611 (2006). Figure 3-7 shows a basic schematic of the apparatus used in this test and Figure 3-8 shows the actual apparatus used.

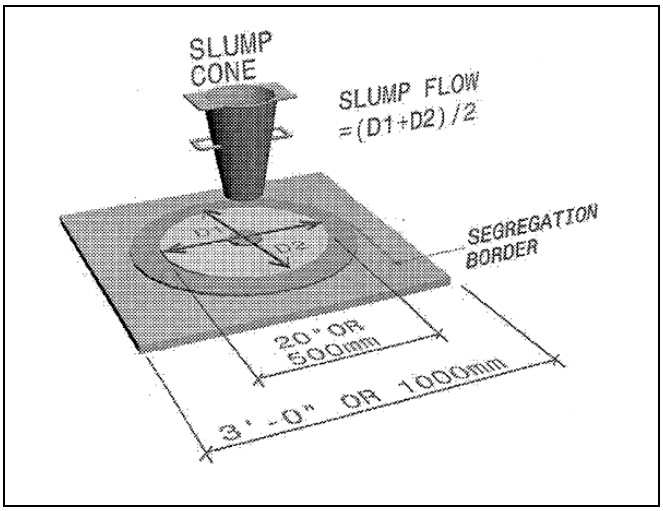

Figure 3-7: Slump Flow Apparatus Schematic (PCI 2003)

Figure 3-8: Actual Slump Flow Apparatus

In this test, a sample of fresh SCC is placed in a cone-shaped mold in one lift without any external vibration. This "slump cone" is filled on top of a non-absorptive base. After being filled, the slump cone is lifted, and the SCC is allowed to spread horizontally across the base. After the SCC stops spreading, diameters of the "slump patty" are measured in two mutually perpendicular directions. The slump flow is the mean of these two diameters. Figure 3-9 depicts an actual slump flow test being performed.

Figure 3-9: Performing the Slump Flow Test

During the slump flow test, other indicators of the flowing ability of the concrete, including the T-50 time and VSI (Visual Stability Index), can be assessed. The T-50 time is the time it takes from when the slump cone is lifted to when the edge of the slump patty reaches a diameter of 20 in. The T-50 time provides a relative measure of the unrestricted flow rate of the concrete mixture. A relatively higher T-50 time indicates a higher viscosity for similar materials. The Visual Stability Index (VSI), as its name implies, includes a visual inspection of the concrete mixture and provides a relative measure of the stability of the concrete. The ASTM guidelines for the slump flow test include the table shown as Table 3-4 to determine appropriate VSI values (ASTM C 1611 2006).

Table 3-4: Visual Stability Index Values (ASTM C 1611)

VSI Value	Criteria
0 = Highly Stable	No evidence of segregation or bleeding.
1 = Stable	No evidence of segregation and slight bleeding observed as a sheen on the concrete mass.
2 = Unstable	A slight mortar halo ≤ 0.5 in.(≤ 10 mm) and/or aggregate pile in the of the concrete mass.
3 = Highly Unstable	Clearly segregating by evidence of a large mortar halo > 0.5 in. (> 10 mm) and/or a large aggregate pile in the center of the concrete mass.

Another test used to determine the workability of fresh SCC is the J-Ring test. This test quantifies the passing ability of the concrete by comparing the spread of the concrete in the J-Ring test to the spread of the concrete in the slump flow test. This test follows the guidelines of ASTM C 1621 (2006). Figure 3-10 shows a basic schematic of the apparatus used in this test, and Figure 3-11 shows the actual apparatus used.

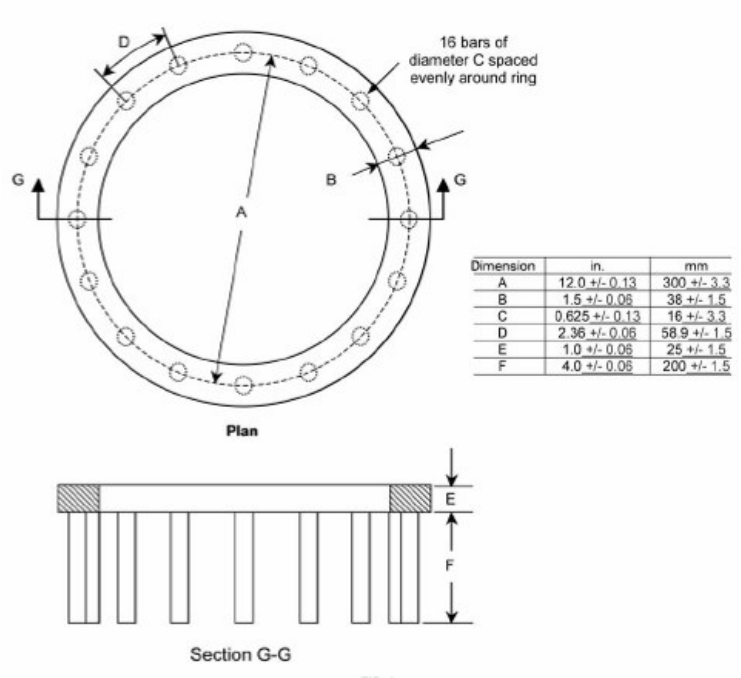

Dimension	in.	mm
A	12.0 +/- 0.13	300 +/- 3.3
B	1.5 +/- 0.06	38 +/- 1.5
C	0.625 +/- 0.13	16 +/- 3.3
D	2.36 +/- 0.06	58.9 +/- 1.5
E	1.0 +/- 0.06	25 +/- 1.5
F	4.0 +/- 0.06	200 +/- 1.5

Figure 3-10: J-Ring Apparatus Schematic (ASTM C 1621 2006)

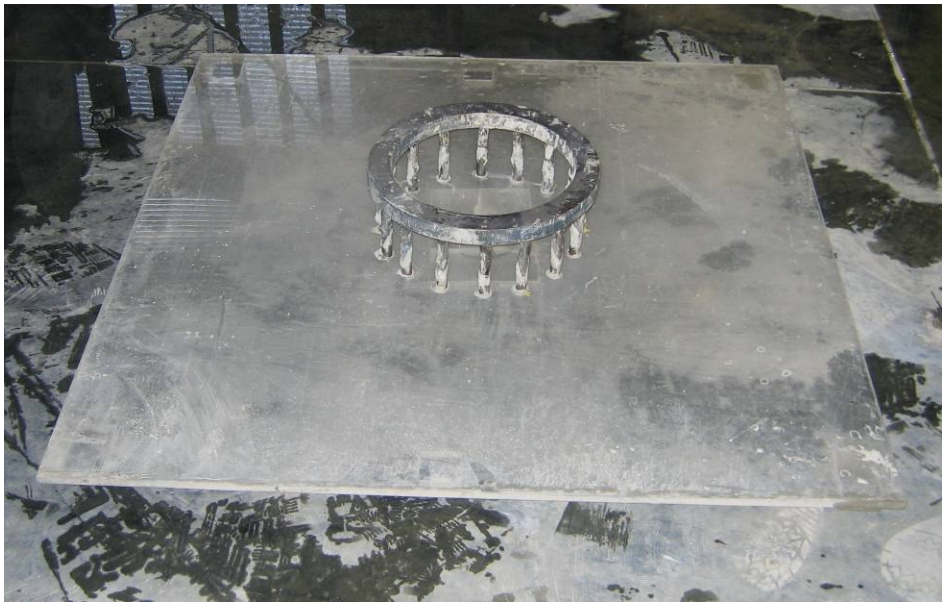

Figure 3-11: Actual J-Ring Apparatus

In the J-Ring test, a sample of fresh SCC is placed in a slump cone in the middle of the J-Ring in one lift without external vibration. After being filled, the slump cone is lifted and the SCC is allowed to spread horizontally through the J-Ring across the base. After the SCC stops spreading, two diameters of the "slump patty" are measured in perpendicular directions. The J-Ring slump flow is the mean of these two diameters. The difference between the slump flow and J-Ring flow is an indicator of the passing ability of the concrete. The ASTM guidelines offer the table shown as Table 3-5 to determine the concrete's passing ability by assessing the amount of blockage.

Table 3-5: J-Ring Blocking Assessment (ASTM C1621 2006)

Difference Between Slump Flow and J-Ring Flow	Blocking Assessment
0 to 1 in. [0 to 25 mm]	No visible blocking
>1 to 2 in. [>25 to 50 mm]	Minimal to noticeable blocking
>2 in. [>50mm]	Noticeable to extreme blocking

Yet another test for determining the workability of fresh SCC is the L-Box test. This test has not been accepted by ASTM and therefore does not follow official guidelines. This test determines the passing ability of the SCC. Figure 3-12 shows a basic schematic of the apparatus used in this test, and Figure 3-13 shows the actual apparatus used.

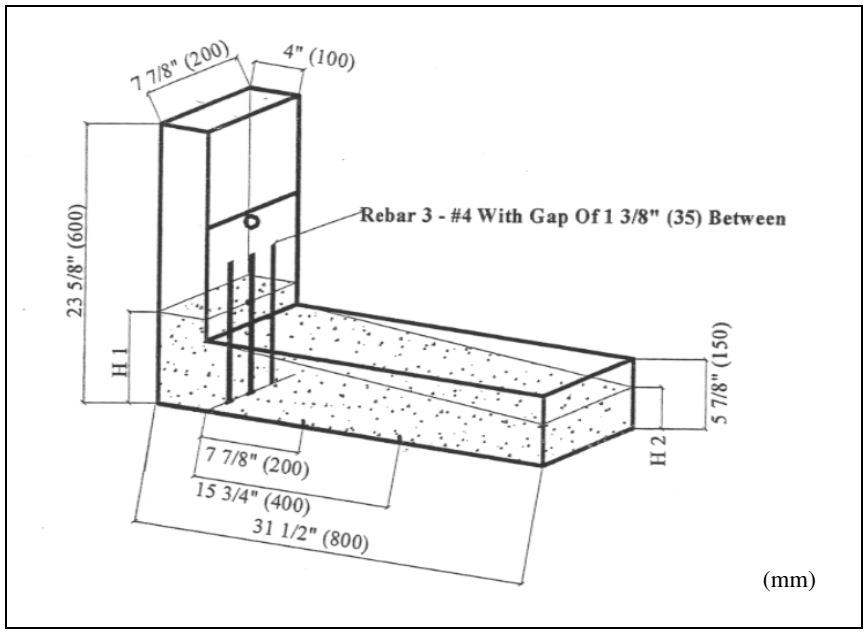

Figure 3-12: L-Box Apparatus Schematic (PCI 2003)

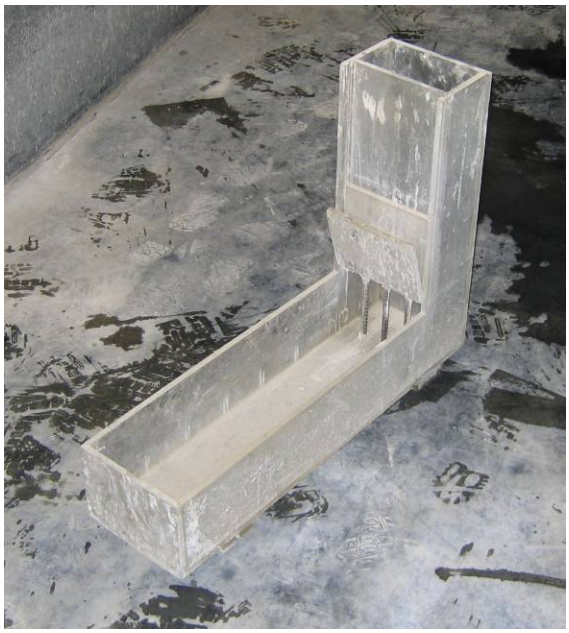

Figure 3-13: Actual L-Box Apparatus

In the L-Box test, a sample of fresh SCC is placed in the vertical portion of the L-Box apparatus in one lift without external vibration. After the vertical portion is filled and one minute has passed, the gate is lifted and the SCC is allowed to flow into the horizontal portion of the apparatus. After the SCC stops flowing, the height of the concrete at the end of the horizontal portion is measured as H_2 and the height of the concrete in the vertical portion is measured as H_1. The resulting ratio of H_2/H_1 is called the blocking ratio which is an indication of the passing ability of the concrete. Proximity to a value of 1.00 indicates a favorable passing ability (PCI 2003).

The aforementioned tests along with air content and unit weight measurements were conducted for each mixture. A standard slump test was performed on the standard concrete mixture in lieu of the slump flow, J-Ring and L-Box tests. Table 3-6 is a summary of the fresh property test results for all four mixtures.

Table 3-6: Summary of Fresh Property Test Results

FRESH PROPERTIES	MIXTURES			
	STD-M	SCC-MA	SCC-MS	SCC-HS
Slump Flow (in.)	9.5	29	28.5	26
Unit Weight (lb/ft^3)	142.2	151.8	148.4	155.2
Air (%)	11.0	2.0	5.0	3.0
VSI	-	1.0	1.0	1.0
T-50 (sec.)	-	2.47	1.54	3.75
J-Ring Difference (in.)	-	1.5	2	2.5
L-Box (H_2/H_1)	-	0.84	0.92	0.63
Placement Temperature (°F)	82	62	89	95

As can be seen in the above table, the target air content was exceeded substantially for the standard concrete mixture.

The J-Ring results represent another item of possible concern. As reported previously in Table 3-5, a difference of more than two inches between the slump flow spread and J-Ring spread usually indicates extreme blockage. However, despite the large differences, excellent passing ability was witnessed within the actual specimens. The actual T-beams did not experience any major blockage during casting.

3.3.3.3 Maturity

This study utilized the maturity method to predict when to transfer prestress as well as to estimate the strength of the concrete at transfer. Strength-maturity relationships developed in a previous phase of this project were used to estimate when to transfer prestress. Although 4 in. x 8 in. match-cured cylinders were cast with each mixture using a match-curing mold system, proper moisture could not be maintained during the curing

process for three out of four mixes. This resulted in unreliable compressive strengths for these specimens. Therefore, the concrete strength at release was estimated from strength tests on air-cured cylinders at comparable maturity levels.

During casting, thermocouples were embedded in two of the T-beams, an air-cured cylinder and a match-cured cylinder. The thermocouples were embedded at the strand depth in Beams A and C at the approximate locations shown in Figure 3-14.

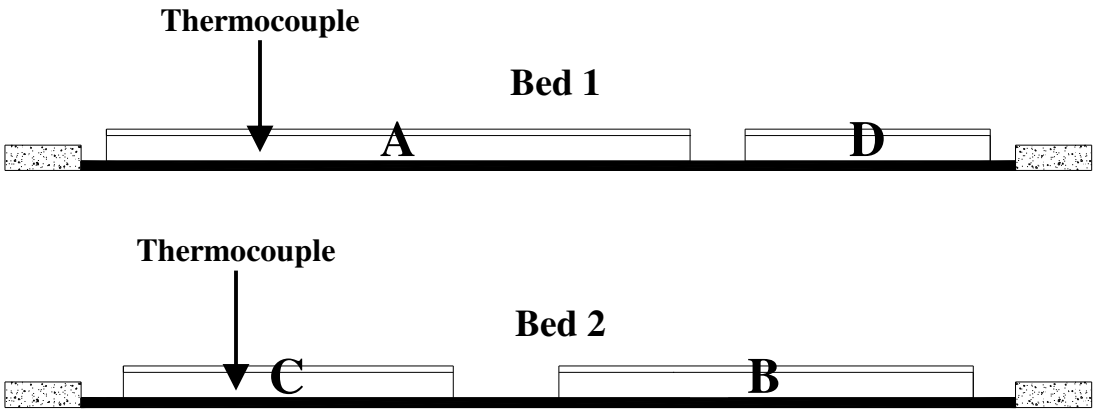

Figure 3-14: Thermocouple Locations

These thermocouples measured the temperature history, and the equivalent concrete age was calculated according to the Arrhenius Equation (Equation 3-1) by assuming an activation energy of 45,000 J/mol and a reference temperature of 23°C.

$$t_e = \sum_0^t e^{\frac{-E}{8.314}\left[\frac{1}{273+T_c}-\frac{1}{273+T_r}\right]} \cdot \Delta t$$

where; t_e = equivalent age (hours)

Δt = time interval (hours)

E = activation energy (J/mol)

T_c = average concrete temperature during time interval (°C)

T_r = reference curing temperature (°C)

Once the equivalent ages of the beams, air-cured cylinders, and match-cured cylinders were known, the strength of the concrete in each set of beams could be estimated using the strength vs. maturity relationship established from tests of the air-cured cylinders. Several air-cured cylinders were tested prior to transfer to establish a strength development curve for each concrete mixture. This curve was then compared with the strength maturity curve for the mixture developed in a previous phase of this project to estimate when to transfer prestress. The air-cured cylinders did not develop as much heat as the beams, and therefore their equivalent age lagged that of the beams. Thus, cylinder testing continued several days after transfer to determine the concrete compressive strength at transfer. Measured strength vs. maturity relationships for each mixture are depicted in Appendix D. The equivalent ages of each set of specimens, as well as the corresponding values of concrete compressive strength, are indicated.

3.3.3.4 Hardened Concrete Property Testing

Several hardened property tests were conducted on cylinders and other specimens made during casting. The hardened properties measured by these tests include concrete compressive strength (f_c), elastic modulus (E_c), splitting tensile strength (f_{ct}), and modulus

of rupture (f_r). Table 3-7 shows the hardened property tests that were performed and their corresponding AASHTO and ASTM specifications.

Table 3-7: ASTM and AASHTO Specifications for Hardened Concrete Property Tests

Property	AASHTO Specification	ASTM Specification
Concrete Compressive Strength	T22	C39
Modulus of Elasticity	-	C469
Splitting Tensile Strength	T198	C496
Modulus of Rupture	T97	C78

Three types of curing methods were used on various specimens: air curing, match curing, and AASHTO R39 (ASTM C192) curing. The air-cured cylinders were all 4 in. x 8 in. and kept in the same environment as the beams throughout their lifespan. They were stripped when they reached the same maturity at which the beams were stripped. These air-cured cylinders were used for concrete compressive strength, elastic modulus, and splitting tensile strength tests. Three 6 in. x 12 in. cylinders were also cast for each mixture and moist cured according to AASHTO R39/ASTM C192 standard curing specifications. These cylinders were used only for compressive strength tests at 28 days. Also six 6 in. x 6in. x 20 in. prisms were cast for modulus of rupture testing. Three of these specimens were cured according to AASHTO R39 (ASTM C 192) specifications, and the other three were air-cured. Table 3-8 presents a summary of the testing schedule used for hardened property testing.

Table 3-8: Hardened Property Testing Schedule

Property	Curing Method	Specimen Size	Number of Specimens					
			Transfer	Testing age (days)				
				1	3	7	28	Post-Test
f_c	Match Cure	4x8 in.	3					3
	Air Cure	4x8 in.	3	3	3	3	3	3
	AASHTO R39	6x12 in.					3	
E_c	Match Cure	4x8 in.	3					3
	Air Cure	4x8 in.	3			3	3	3
f_{ct}	Air Cure	4x8 in.					3	3
f_r	Air Cure	6x6x20 in.						3
	AASHTO R39	6x6x20 in.						3

Note: Post-Test indicates a time after development length testing

Table 3-8 shows that 3 cylinders were broken at prestress transfer for each mixture. The actual day of transfer after casting varied for each mixture. Table 3-8 also shows that several material property tests occurred at a time called "Post-Test". "Post-Test" indicates a day after all load testing was completed for all four beams cast with a certain mixture. This date also varied for each mixture. Table 3-9 shows the dates of casting, transfer, and post-test testing for each mixture.

Table 3-9: Casting , Transfer, and Post-Test Testing Dates

	MIXTURES			
	STD-M	**SCC-MA**	**SCC-MS**	**SCC-HS**
Casting Date	11/14/2005	12/13/2005	6/26/2006	8/21/2006
Transfer Date (days after casting)	11/17/2005 (3 days)	12/14/2005 (1 day)	6/29/2006 (3 days)	8/22/2006 (1 day)
Post-Test Testing Date (days after casting)	6/27/2006 (225 days)	7/28/2006 (227 days)	9/22/2006 (88 days)	10/9/2006 (49 days)

Table 3-10 is a summary of the hardened concrete property results. As can be seen in that table, the moderate-strength mixes had concrete strengths at transfer in a range from 5000–5500 psi and the high-strength mixture had a concrete strength at transfer of 9990 psi. It is also important to note that the modulus of elasticity at transfer was very consistent for the three moderate-strength mixtures. However, it is also apparent that after transfer, the two moderate-strength SCC mixtures gained much more strength than the moderate-strength standard concrete mixture. This is most likely due to the high air content of the standard concrete mixture or due to the use of SCMs in the SCC mixtures.

Table 3-10: Hardened Concrete Property Summary

PROPERTY	**MIXTURES**			
	STD-M	SCC-MA	SCC-MS	SCC-HS
f'_{ci} **(psi)**	5000	5500	5300	9990
E_{ci}**(ksi)**	4900	4900	4950	6050
$f'_{c,28(ASTM)}$ **(psi)**	5990	8840	9640	13150
$f'_{c,28(AC)}$ **(psi)**	6320	8540	9170	13380
$E_{c,28(AC)}$ **(ksi)**	5150	5400	6950	7050
$f_{ct,28(AC)}$**(psi)**	560	760	840	830

A more detailed table of all of the hardened concrete property results can be found in Appendix E of this thesis. Also contained in Appendix E are graphs of the development of concrete compressive strength and modulus of elasticity over time based on the tests of air-cured cylinders.

The elastic modulus was tested using the ASTM C469 standard method. The values collected were then compared to the AASHTO LRFD/ACI 318 formulation for the elastic modulus, given by Equation 3-2.

$$E_c = 33\, w_c^{1.5} \sqrt{f_c'}$$

Figure 3-15 compares the ratio of the measured to predicted elastic modulus versus the compressive strength. It can be seen that for lower-strength concretes, this formulation underestimates the actual elastic modulus, whereas for higher-strength concretes, the elastic modulus is overestimated. The measured modulus of elasticity was never more than 10 percent less than the predicted value. When considering only the SCC tests conducted at concrete maturities equal to or exceeding the expected maturity at prestress transfer, ratios of measured-to-predicted E_c range from 0.91 to 1.16.

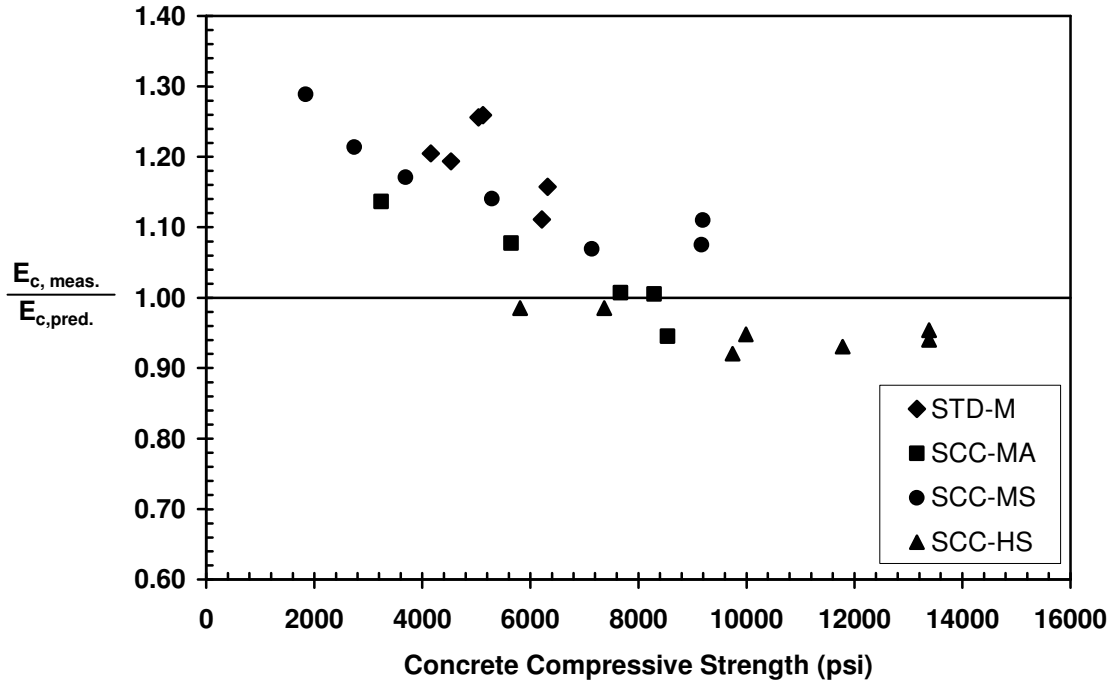

Figure 3-15: Comparison of Measured to Predicted Elastic Modulus

3.4 SPECIMEN FABRICATION

Sixteen prestressed T-beams were fabricated for this study. The fabrication procedure prior to casting and during the casting of these specimens is presented in this section.

3.4.1 OPERATIONS PRIOR TO CASTING

The section includes a description of the form construction and reinforcement preparation that occurred prior to any casting operations. Figure 3-5 shows the prestressing beds on which the beams were cast. The form surfaces were made from plywood and coated with polyurethane to ease the stripping process. After the forms were constructed, the shear reinforcement was cut and bent. Figure 3-16 shows the completed U-stirrups.

Figure 3-16: Shear Reinforcement

After all of the forms were constructed and the reinforcing bars were cut and bent, the forms were placed on the prestressing beds, and a release agent was applied to all interior surfaces. After the release agent was applied, the compression steel was placed on top of bolsters on the flange forms. The stirrups were then placed on top of the compression

steel and tied with metal bar ties at all intersections. Figure 3-17 shows the stirrups being tied to the compression reinforcement.

Figure 3-17: Tying the Stirrups to the Compression Reinforcement

After the stirrups were secured, the strands were put into position. The stirrups created a type of cradle (Figure 3-5 and Figure 3-6) for the strands which prevented any contamination from the release agent on the form surfaces. As the strands were threaded through the existing cage, they were wiped with a clean cotton rag to remove excess surface debris. Before the strands were tied to the stirrups, the strands were tensioned to a jacking stress, f_{pj}. Load transducers were placed on each end of each strand between the chuck and anchor plate and monitored during the tensioning process. Figure 3-18 depicts the load transducers, chucks, and anchor plate.

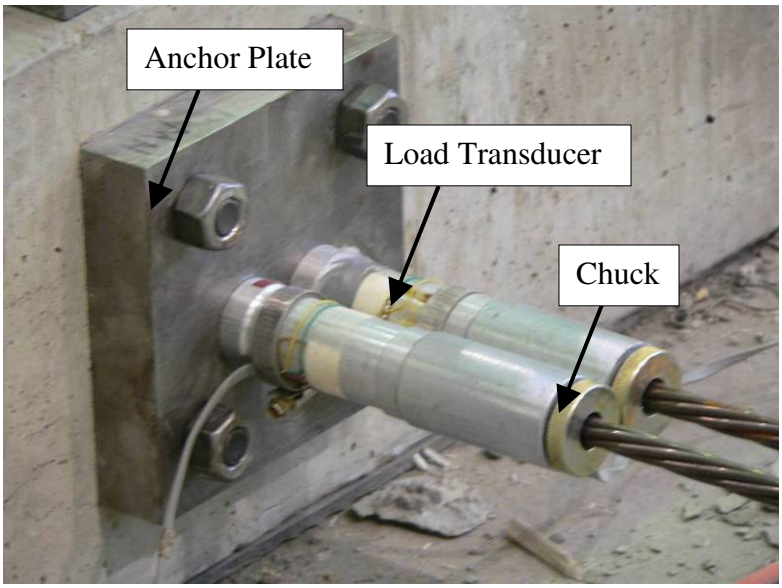

Figure 3-18: Load Transducers, Chucks, and Anchor Plate

After the strands were tensioned, the transverse flange reinforcement was placed and tied to the cage. The finished cage in the forms is shown in Figure 3-19.

Figure 3-19: Finished Reinforcement Cage

3.4.2 CASTING OPERATIONS

On the day of casting, the stress in the strand was checked to ensure the stress was at least 200 ksi. As mentioned previously, a ready-mixture concrete truck from Twin City Concrete was used to mix each 3.5-yd^3 batch. Prior to leaving the plant, the truck was loaded with coarse and fine aggregate as well as any air-entraining admixtures and 80% of the mixture water. The remaining water, cementitious material, and other admixtures were added to the truck at the Auburn University Structural Engineering Laboratory. The dry materials were batched in a 1.5-yd^3 concrete-placing bucket. The addition of these materials is depicted in Figure 3-20.

Figure 3-20: Addition of Remaining Materials

After the material was mixed sufficiently, fresh property testing began. The forms were filled using a crane-supported concrete-placing bucket. Vibration of the concrete was only used for the standard mixture. Figure 3-21 depicts one of the SCC mixtures flowing into the forms after being released from the bucket. The bucket chute is visible in the top portion of the photograph.

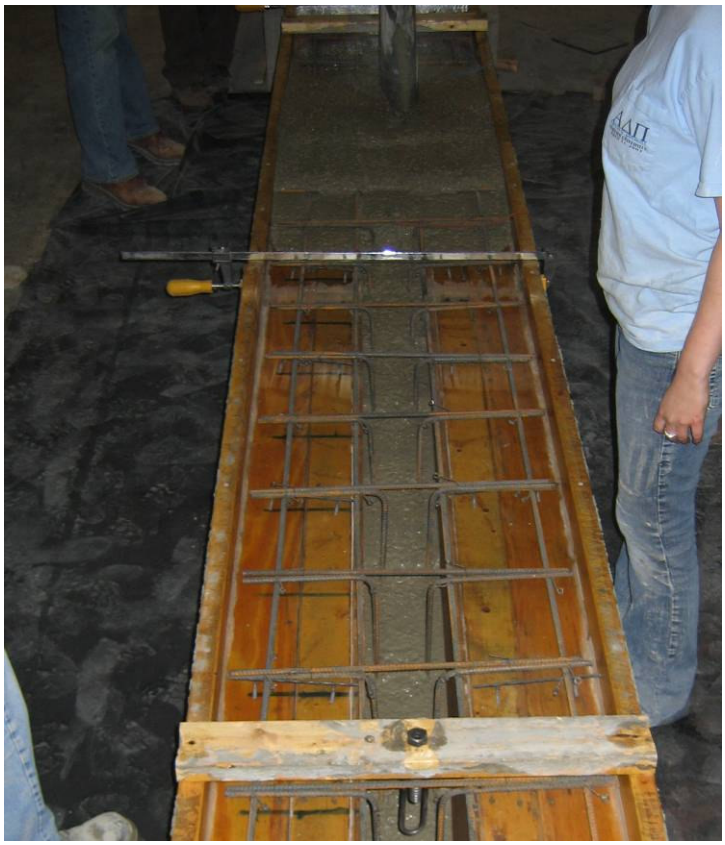

Figure 3-21: SCC Flowing into Forms

The SCC flowed into the forms very easily. Decreased casting time and greater ease of casting were experienced during the fabrication of SCC specimens compared to the fabrication of standard concrete specimens. After casting, wood 2x4s was used to screed off the excess concrete. Figure 3-22 depicts the excess concrete being screeded off the specimens.

Figure 3-22: Screeding of Excess Concrete

Along with the beams, several other specimens were cast for material testing including 4 in. x 8 in. cylinders, 6 in. x 12 in. cylinders, match-cured cylinders, and 6 in. x 6 in. x 12 in. prisms. Only specimens cast with conventional concrete were rodded and tapped according to ASTM specifications. Figure 3-23 and Figure 3-24 show the cylinders and match-cured specimens being cast.

Figure 3-23: Cylinder Casting

Figure 3-24: Match-Cured Cylinders

After the concrete was finished and allowed to achieve initial set, the specimens were covered in wet, AASHTO M182 Class 3 burlap. Drying of the burlap was prevented by a layer of polyethylene plastic as well as constant rewetting. The covered specimens are shown in Figure 3-25. The specimens made for material property testing were either capped or covered with burlap to ensure sufficient moisture retention.

Figure 3-25: Specimens Covered in Burlap and Plastic

3.5 INSTRUMENTATION INSTALLATION

After casting operations were complete, the specimens were cured until the day of prestress transfer. The burlap was rewetted as needed to prevent drying of specimens. This section presents an overview of the procedures followed on the day of prestress transfer up to actual transfer length testing.

On the day of prestress transfer, the first step was form removal. Figure 3-26 shows the forms being removed from the beams. After all of the forms were removed, each beam was prepared for transfer length testing.

Figure 3-26: Removal of Side Forms

As part of the transfer length testing program, concrete surface strains were measured using two demountable mechanical (DEMEC) strain gauges. After the removal of all side and end forms, a chalk line was marked along the surface of the beam on both sides at the height of the strands. Once this chalk line was marked, DEMEC locating discs were placed along this line at the centroid of the strand. This process is described in

detail in Chapter 4 of this thesis. After all locating discs had been placed, initial strain measurements were taken. Each measurement was read twice to improve accuracy. Figure 3-27 shows a line of locating discs being measured with a DEMEC strain gauge.

Figure 3-27: Using a DEMEC Strain Gauge

3.6 TRANSFER OF PRESTRESS FORCE

After all of the initial strain readings had been taken, the beams were prepared for the transfer operation. Several precautionary measures were taken to prevent beam damage. Hose clamps were affixed to each strand to prevent excessive unraveling of the strand and thus damage to the beam during transfer. To prevent excessive specimen movement during the transfer operation, wooden blocks were placed between the dead ends of the beam and the prestressing anchorages. Corrugated cardboard and compressible foam

were inserted between these wooden blocks and the concrete to act as shock absorbers. Figure 3-28 shows the location of these precautionary measures.

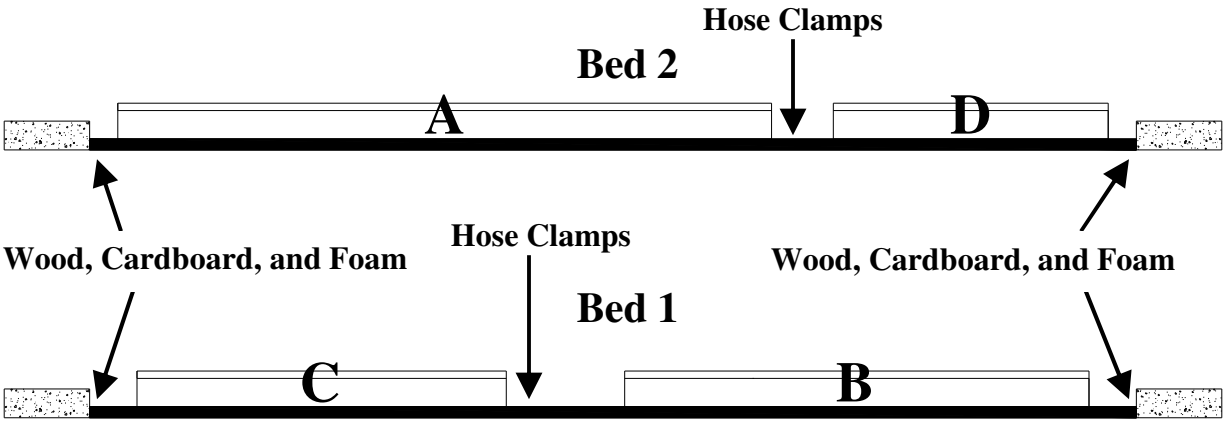

Figure 3-28: Location of Measures to Prevent Beam Damage

The transfer of prestress force was achieved by flame cutting the strands. This method of sudden release is consistent with common practice in the precast, prestressed industry. The strands were gradually heated by a low-oxygen flame moved gradually along a minimum distance of five inches of strand. As mentioned previously, both strands were cut simultaneously at one location for each bed (Figure 3-3). This resulted in each beam specimen having one cut end and one dead end. After prestress was transferred, the dead end of each strand was also cut to allow easy removal of the chuck behind the anchorage. Figure 3-29 depicts the strands about to be flame cut.

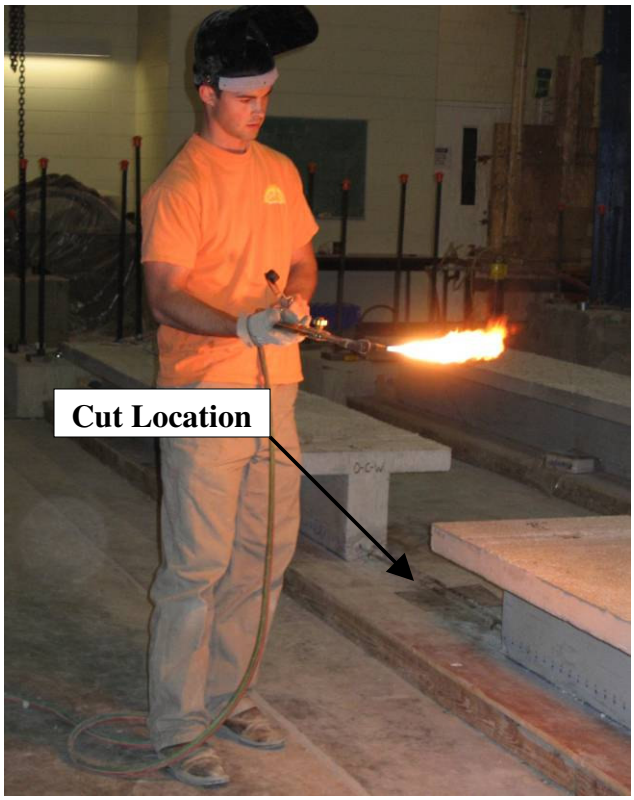

Figure 3-29: Flame-Cutting the Strand

After prestress transfer, another set of readings was taken with the DEMEC strain gauges to determine the initial transfer lengths. This process and the transfer length results are discussed in detail in Chapter 4 of this thesis.

CHAPTER 4

TRANSFER LENGTH TEST PROGRAM

4.1 INTRODUCTION

The details and results of the transfer length testing program are presented in this chapter. Transfer length testing was performed on all sixteen specimens. Each of the specimens had two transfer zones, one at each end, resulting in a total of thirty-two transfer zones. Transfer lengths were determined using a mechanical strain gauge to measure concrete surface strains. Concrete surface strains were measured immediately after transfer as well as four days after transfer to track any possible transfer length growth. The transfer length testing procedure and results are presented in this chapter.

In a previous phase of this project, extensive transfer length testing was conducted on thirty-six concentrically prestressed specimens (Swords 2005). In addition to the testing procedure and results, a comparison of the transfer lengths of the concentrically prestressed specimens and T-beams is presented in this chapter.

4.2 PREVIOUS RESEARCH ASSOCIATED WITH THIS PROJECT

As mentioned previously, the research presented in this thesis is part of a larger, ongoing project to investigate the use of SCC in prestressed bridge girders. One of the previous phases of this project focused primarily on the effect of SCC on transfer length. The results of that phase are discussed in detail by Swords (2005). Thirty-six concentrically

prestressed concrete specimens were investigated in that phase. Initial and long-term transfer length measurements were performed on all specimens in the study.

Six sets of specimens cast with five different mixtures were cast for that study. One conventional mixture and four different SCC mixtures were tested. The SCC mixtures included a high- and moderate-strength mixture for each type of SCM: Class C fly ash or ground-granulated blast-furnace (GGBF) slag. The conventional mixture and three of the SCC mixtures employed the same mixture proportions as the mixes used in this phase of the project. The additional SCC mixture, a high-strength fly ash mixture, was cast twice due to high air content in the first set of specimens and was not utilized in the T-beam phase of the project. For each mixture, a total of six concentrically prestressed specimens were cast.

For each set of specimens, three specimens were prestressed with a single strand, and three specimens were prestressed with two strands spaced at two inches on center. Figure 4-1 depicts the cross-section details of the concentrically prestressed specimens.

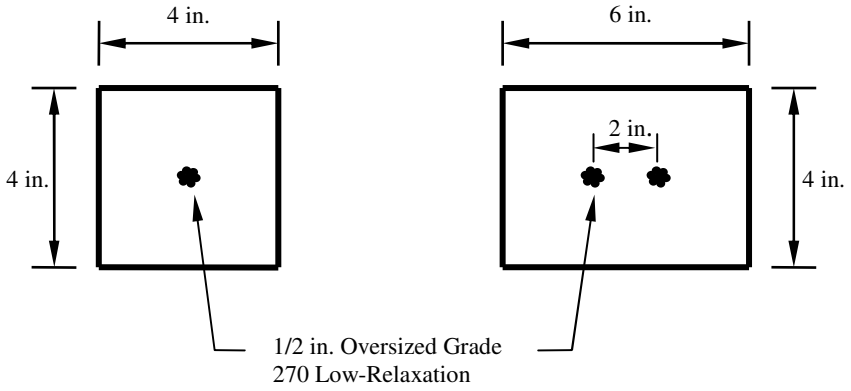

Figure 4-1: Concentrically Prestressed Single- and Double-Strand Cross Sections (Swords 2005)

A total of seventy-two transfer zones were investigated. Prestress transfer was achieved by flame-cutting, and surface strain measurements were collected with the use of mechanical strain gauges. Although these results will not be discussed in this thesis, strand draw-in measurements were also compared to the transfer lengths obtained from surface-strain measurements. The transfer length data collected by the use of mechanical stain gauges will be compared to transfer length data collected from the current study.

4.3 TEST PROCEDURE

Transfer lengths for the sixteen T-beam specimens were determined by measuring concrete surface strains and then applying the 95% Average Maximum Strain (AMS) Method. The 95% AMS Method has been used in many studies for determining transfer length, including the FHWA study upon which the AASHTO equation for transfer length (Equation 2-5) is based (Lane 1998, Russell and Burns 1993, Barnes et al. 1999). Concrete surface strains were measured using a demountable mechanical (DEMEC) strain gauge. Figure 4-2 shows the instruments used during transfer length testing. The procedures for specimen preparation and measurement of concrete surface strains are presented in this section.

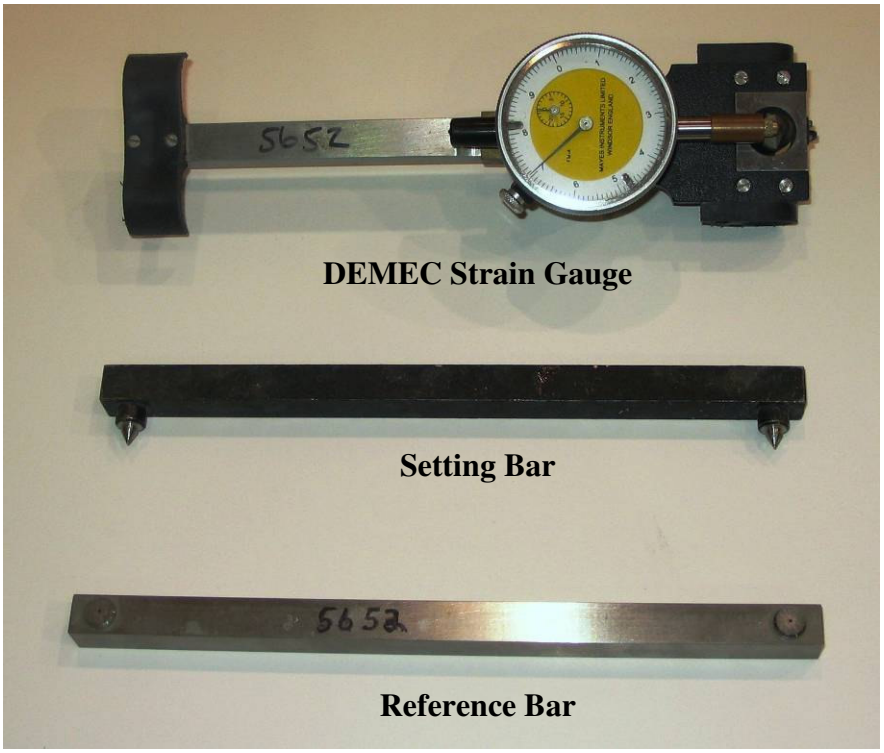

Figure 4-2: Actual DEMEC Instruments

4.3.1 SPECIMEN PREPARATION

Specimen preparation for transfer length testing began with removal of side forms. Once it was determined that the concrete had reached adequate strength, form removal procedures began. This process took about one hour to complete and occurred approximately 7 hours prior to prestress transfer. Figure 4-3 shows the specimens in the middle of the form-removal process with some beams already exposed.

Figure 4-3: T-Beams during Form Removal

After the removal of all side and end forms, a chalk line was marked along the surface of the beam on both sides level with the height of the strands. The strand height was 2 in. from the bottom of the beam for all of the specimens. Once the chalk line was placed along the beam at the height of the strands, distances of 25 mm, 75 mm, 125 mm, and 175 mm were marked along this line from each end of the beam. Locating discs for the DEMEC strain gauge were then set on each of these four locations using a five-minute epoxy.

After the first four discs were adhered to each face of each beam on each end, another set of four points were set relative to the original points using a 200-mm setting bar. Figure 4-4 depicts the application of these discs using a setting bar.

Figure 4-4: Use of Setting Bar to Place Locating Discs

This procedure was repeated until a total of 28 targets were applied for each face at each end of each beam. The first disc was placed 25 mm from the end of the beam, followed by 27 discs placed 50 mm apart. Therefore, each beam had a 53-in. zone over which concrete surface strains were measured to establish a strain profile. Eight additional discs were placed at 50-mm intervals across midspan of each beam as well. If observed to be rough or uneven, the surface of the beam was ground until smooth to ensure adequate adhesion of the discs. The task of placing these discs took about four hours to complete.

4.3.2 Concrete Surface Strain Measurements

After all locating discs had been placed, initial strain measurements were taken for all beams before prestress transfer. Before any set of readings, a reference reading was taken using an Invar reference bar (Figure 4-2). As mentioned previously in Section

3.5.1, measurements were taken using a DEMEC strain gauge (Figure 4-2) with a 7.87-in. (200-mm) gauge length. Since the discs were placed 1.97 in. (50 mm) apart, overlapping measurements for every interval were taken. Each measurement was read twice to ensure that the readings were within 0.02 mm of each other. If the readings were within 0.02 mm of each other, then the next set of points could be read. If a set of points could not be read due to poor positioning, the faulty disc was identified and replaced. Figure 4-5 shows the collection of concrete surface deformation measurements using a DEMEC strain gauge.

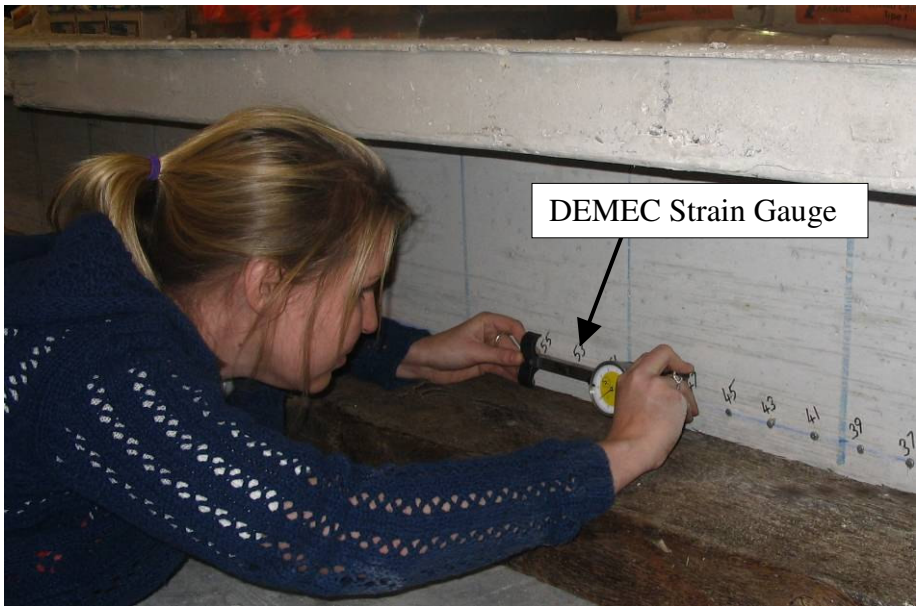

Figure 4-5: Collecting Concrete Surface Strain Measurements

After the initial readings were complete, prestress was transferred in Specimens B and C located on Bed 1. After prestress was transferred in Bed 1, strain measurements were taken for specimens on that bed immediately. After those readings were completed, prestress was transferred in Specimens A and D located on Bed 2. Strain measurements were then taken immediately for these specimens. This procedure minimized the amount of time between prestress transfer and strain measurement completion for all specimens.

Strain measurements were completed within an hour of prestress release. Table 4-1 shows the resulting live (adjacent to flame cut) and dead ends for each specimen.

Table 4-1: Location of Live and Dead Ends for Prestressed Specimens

SPECIMEN	LIVE END	DEAD END
A	West	East
B	East	West
C	West	East
D	East	West

Another set of concrete surface strain measurements was taken four days after the transfer of prestress for all specimens. This additional set of measurements was used to determine any possible transfer length growth over time.

4.4 TRANSFER LENGTH DETERMINATION

The process to determine initial and four–day transfer lengths based on DEMEC gauge readings is presented in this section. This process includes the construction of the surface compressive strain profile and the determination of the average maximum strain.

4.4.1 CONSTRUCTION OF SURFACE COMPRESSIVE STRAIN PROFILE

To begin the process of quantifying initial and four day transfer lengths, a surface compressive strain profile was first constructed. The first step in determining the measured strain for each interval was calculating the difference between the DEMEC gauge reading of the interval at the time in question and the initial DEMEC gauge reading for the interval. This difference was then multiplied by the DEMEC gauge factor.

As mentioned previously, overlapping readings were taken for each gauge length. Therefore at any one disc location, three overlapping readings were taken over that location. These three readings were averaged to determine the strain value for that location. Figure 4-6 depicts the procedure for which strain values are assigned to individual locations. Once strain values were assigned individual disc locations, corresponding disc locations on opposite faces of the beam were averaged to construct one smoothed strain profile for each transfer zone.

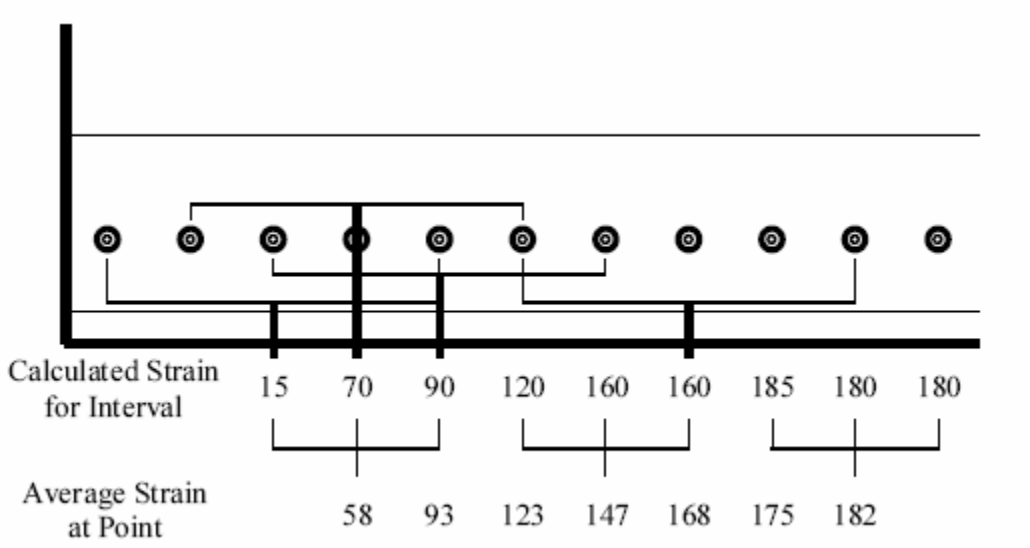

Figure 4-6: Assigning Strain Values to Disc Locations (Barnes et al. 1999)

The next step in this process was to correct the resulting strain profiles to discount the variable flexural strain attributable to the self-weight of the beam. Due to the eccentricity of the prestressing in these beams, the specimens cambered off the beds and the weight of the beam was transferred to the supported ends. The self-weight induces a curvature into the beam which creates a tensile strain opposing the compressive strain of the prestress force. Once calculated, the tensile strain must be deducted from the measured surface strain to more accurately determine the strain due to prestressing only.

This tensile strain can be calculated for each location along the beam using engineering beam theory, represented here as Equation 4-1.

$$\varepsilon_{weight} = \frac{My_{DEMEC}}{E_c I_{tr}} \qquad \textit{Equation 4-1}$$

where, ε_{weight} = tensile strain component due to self-weight

M = moment due to self-weight

y_{DEMEC} = vertical distance from locating disc to centroid of transformed section

I_{tr} = moment of inertia of transformed section

E_c = modulus of elasticity of concrete

It is important to note that the moment due to self-weight increases as the distance from the end of the beam increases, resulting in larger tensile strains toward the middle of the beam. Therefore, the tensile strain due to the self weight has a greater impact on the shape of the stain profile as the distance from the end of the beam increases.

This adjustment was also made for the four-day compressive strain profiles. However, for the four-day adjustments, additional creep strains due to self-weight were also considered. Creep strains were estimated using creep coefficients experimentally determined for each mixture in the previous phase of this project.

4.4.2 Determination of Average Maximum Strain (AMS)

The next step in the process to determine transfer length was the determination of the average maximum strain (AMS) for each specimen. As defined in Chapter 2, transfer length is the bonded length of a tendon required to fully develop the effective prestress in a strand by bond to the concrete. On a surface compressive strain profile, when the stain

reaches a plateau, the effective prestress force has been developed in the strand. AMS is determined by identifying a plateau on the surface compressive strain profile and then averaging the strains within this plateau. Figure 4-7 illustrates the AMS for a typical surface compressive strain profile for two strain measurement events.

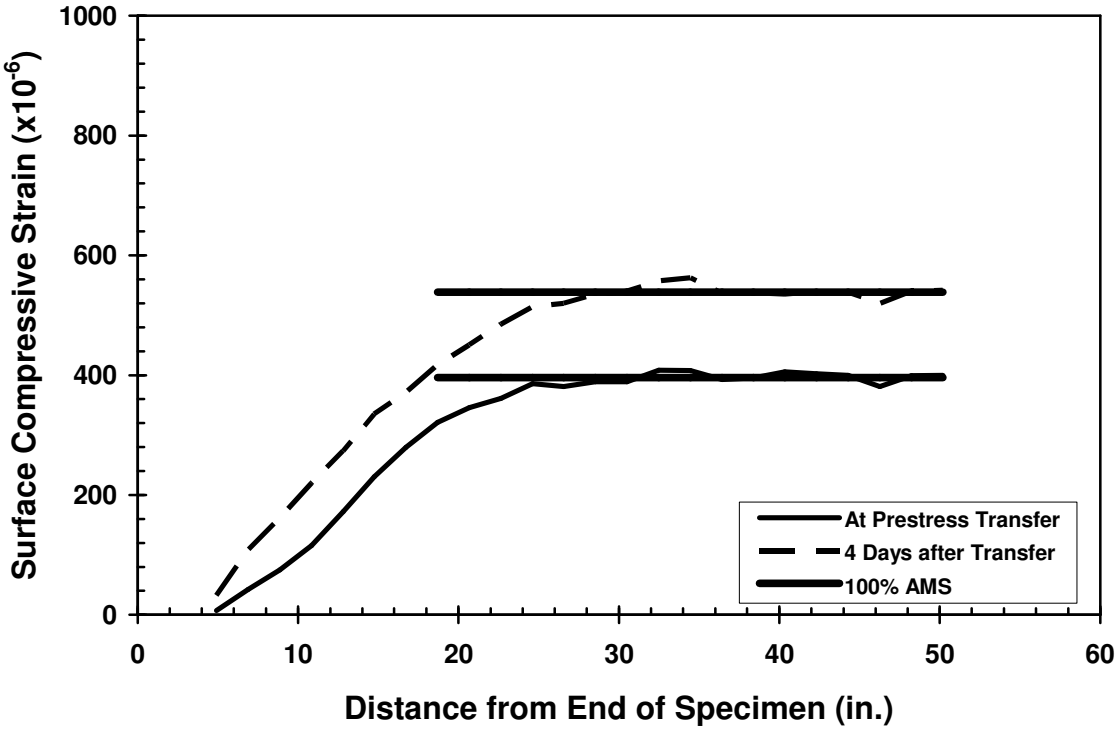

Figure 4-7: Location of Average Maximum Strain Values for Specimen STD-M-B-E

4.4.3 DETERMINATION OF 95% AMS

The 95% AMS method was used in this study to establish transfer lengths from surface compressive strain profiles. According to this method, for a particular strain measurement event, the transfer length is bounded by the intersection of a horizontal line representing 95% of the average maximum strain and the surface compressive strain profile. The determination of initial and four day transfer lengths are presented in this

section. Figure 4-8 illustrates the 95% AMS for a typical surface compressive strain profile for two strain measurement events.

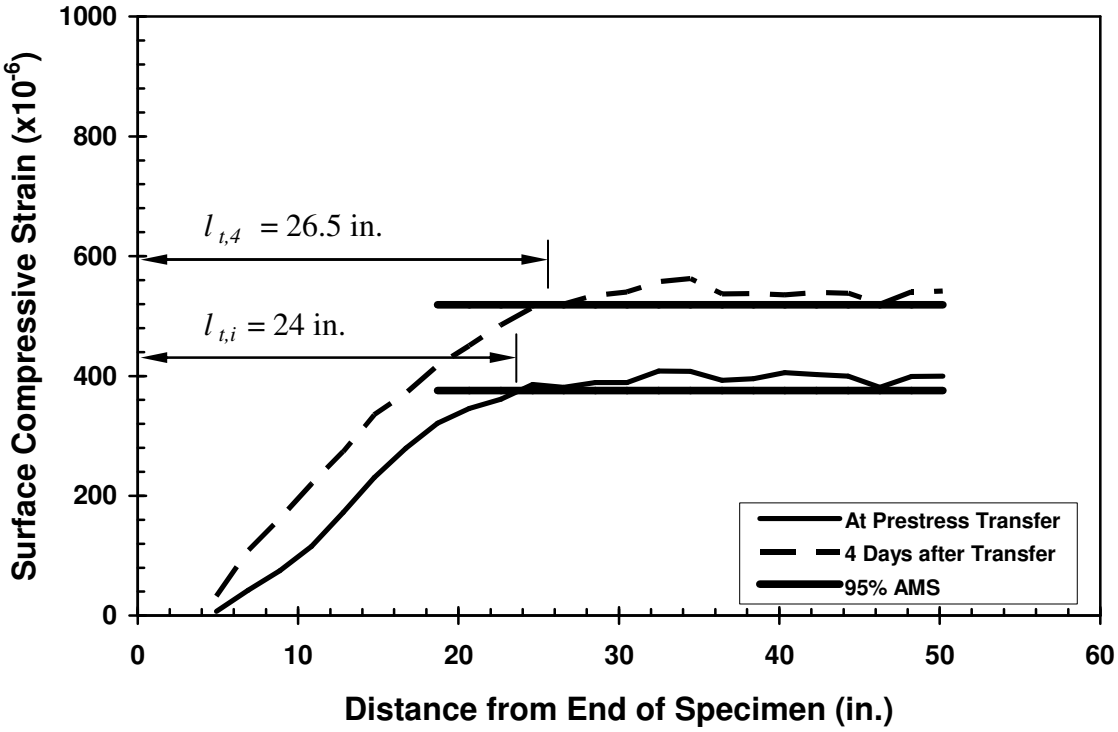

Figure 4-8: Location of Average Maximum Strain Values for Specimen STD-M-B-E

4.4.3.2 Initial Transfer Lengths

Using the 95% AMS method, determination of the initial transfer length was very simple to achieve. The average maximum strain was multiplied by 0.95 to obtain the 95% AMS value for each strain profile.

4.4.3.3 Four-day Transfer Lengths

Determining the four day transfer lengths for each specimen end is a more complicated process than the process used for calculating initial transfer lengths. The four day strain profiles represent elastic strains due to prestress transfer as well as strains due to time-dependent deformations. In order to accurately determine four day transfer lengths, time-

dependent deformations due to creep and shrinkage must be accounted for when calculating 95% AMS for four day strain profiles.

The time-dependent deformations due to creep and shrinkage affect the strain profile in two different ways. Because creep deformations are proportional to elastic deformations, creep causes an *amplification* of the strain profile, which results in an increase in the slope of the strain profile and an increased plateau strain value. The rate of increase of the slope of the non-plateau strain and plateau strain are identical. Therefore, multiplying the average maximum strain by a factor of 0.95 will continue to yield consistent results over time when considering creep deformations.

Shrinkage strains, however, do not affect the strain profile in the same way. Shrinkage strains cause an upward *translation* of the entire strain profile. In this case, the average maximum *strain* increases, but the *slope* of the non-plateau portion of the profile does not. If strain growth is entirely due to shrinkage, a five-percent reduction of the average maximum strain for the later-age values results in calculated transfer lengths that incorrectly appear to decrease over time even if the actual transfer length remains constant (Barnes et al. 2003).

Since the individual portions of time-dependent strain attributable to creep and shrinkage were unknown, another approach was used to account for the effect of shrinkage strains. Instead of multiplying the four-day AMS by 0.95, the AMS at four days was reduced by five percent of the initial AMS. Consequently, the same strain offset was used for both initial and four-day measurements. While this choice is not theoretically ideal, the error is small, and the resulting calculated transfer length is on the "safe" side.

4.4.4 PRECISION OF RESULTS

There were several factors which affected the accuracy of the transfer length results. First, the spacing of the DEMEC discs was 1.97 in.; therefore, any precision less than this value relies on smoothing and interpolation. In addition, researchers were subjected to awkward positions while collecting surface strain measurements. Although creep strains were estimated using a previously determined creep coefficient, transfer length values are not sensitive to the creep coefficient chosen. Considering these factors, a precision of 0.5 in. was adopted for all reported transfer length results.

4.5 RESULTS AND DISCUSSION

A total of thirty-two transfer zones were evaluated in this study. The results of the transfer length testing are presented in this section. Also contained in this section are comparisons to results from a previous phase of this project.

4.5.1 TRANSFER LENGTH RESULTS

Thirty-two transfer lengths were determined for the flexural specimens in this study. The surface compressive strain profile and corresponding transfer lengths for each beam end are presented in Appendix F of this thesis. The transfer lengths for all specimens are summarized in Table 4-2. In addition to the transfer length, the concrete compressive strength at transfer (f'_{ci}) is reported, as well as the stress in the strand immediately before transfer (f_{pbt}), the stress in the strand immediately after transfer (f_{pt}), and the effective prestress four days after transfer ($f_{pe,4}$). The effective prestress four days after transfer was determined by subtracting the product of the modulus of the steel and the peak strain measured at four days from strain gauge readings from the stress in the strand at transfer.

Graphical depictions of the relative transfer lengths for all mixtures can be found in Appendix G of this thesis.

Table 4-2: Summary of Specimen Material Properties and Transfer Lengths

Specimen	f'_{ci} (psi)	f_{pbt} (ksi)	f_{pt} (ksi)	$f_{pe,4}$ (ksi)	Transfer Length (in.)			
					Live End		Dead End	
					Initial	4-day	Initial	4-day
STD-M-A	5000	209	197	193	34.0	32.0	22.0	22.0
STD-M-B		202	190	186	24.0	26.5	27.0	27.5
STD-M-C		202	191	188	21.0	24.0	24.0	24.5
STD-M-D		209	197	192	32.0	32.5	19.0	23.5
SCC-MA-A	5500	200	189	184	21.0	25.5	19.0	22.0
SCC-MA-B		196	184	178	27.5	28.5	21.5	22.0
SCC-MA-C		196	186	180	23.5	26.0	21.0	26.0
SCC-MA-D		200	189	183	23.5	26.0	20.0	26.0
SCC-MS-A	5300	211	200	196	31.0	31.0	20.0	20.5
SCC-MS-B		207	196	192	40[a]	44[a]	20.5	22.0
SCC-MS-C		207	195	191	43.5	44.5	25.0	24.0
SCC-MS-D		211	199	194	37.5	40.0	16.5	17.0
SCC-HS-A	9990	210	201	197	18.0	20.5	14.0	18.0
SCC-HS-B		210	200	197	20.0	19.0	12.0	14.0
SCC-HS-C		210	201	197	20.5	22.0	11.0	14.0
SCC-HS-D		210	200	196	25.0	25.5	16.0	19.5

NOTE: [a] Value estimated using maximum strain on opposite end of specimen.

As indicated in the note below the preceding table, a strain plateau could not be clearly identified at the live end of specimen SCC-MS-B. Therefore, the 95% AMS value for the opposite (dead) end of the same beam was taken as the 95% AMS value for the live end. The transfer length value for the live end of SCC-MS-B was then

determined from the location where the live-end strain profile exceeded this 95% AMS value.

4.5.2 Effects of Concrete Strength

As discussed in Section 2.4.4.1, the effect of concrete strength on transfer length has been debated for some time. It has been generally accepted that transfer length decreases with increasing concrete compressive strength. Figure 4-9 depicts the relationship between initial transfer lengths and the concrete compressive strength at transfer. Figure 4-9 indicates that the transfer lengths measured in this phase confirm this relationship. Overall, transfer lengths measured for concrete with lower strengths are larger. However, the exact relationship between the two is still not clear. As mentioned in Chapter 2, some have suggested that transfer length is inversely proportional to the square root of the concrete compressive strength. This hypothesis will be explored and discussed for the remainder of this section.

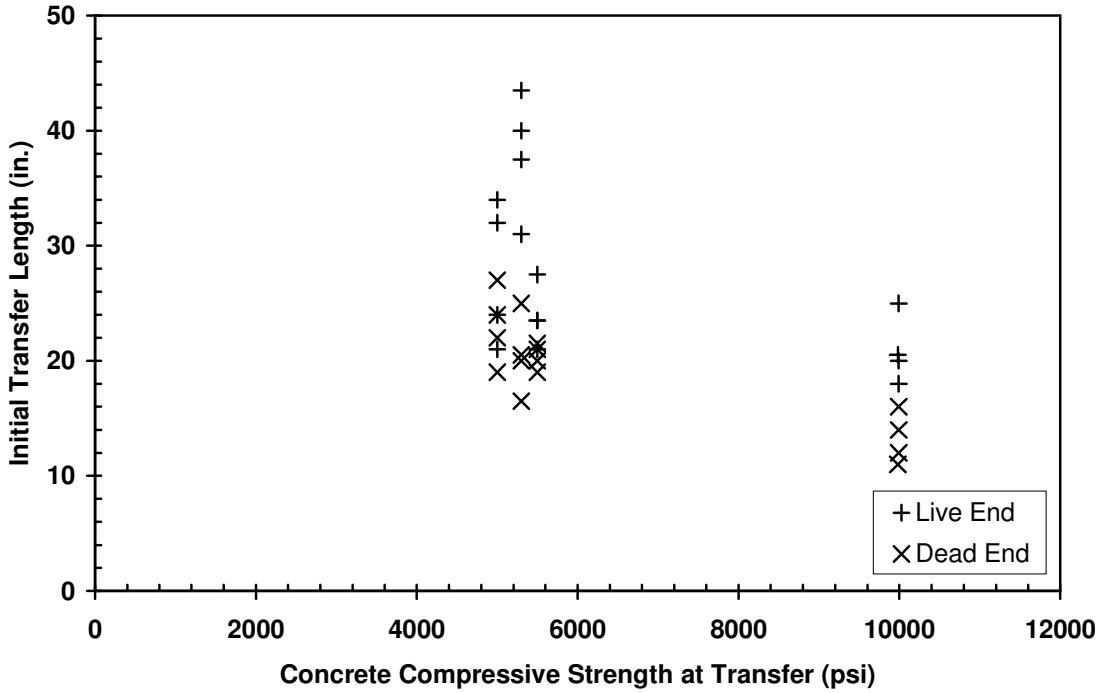

Figure 4-9: Initial Transfer Length versus Concrete Compressive Strength at Transfer

In Section 2.3.2.2, Equation 2-3 was presented to demonstrate the equilibrium forces that Mattock identified to formulate a transfer length equation (Tabatabai and Dickson 1993). These forces indicate that initial transfer length, $l_{t,i}$, is proportional to strand diameter, d_b, and the stress in the prestressing tendon immediately following release, f_{pt}. In contrast, the initial transfer length is inversely proportional to the average bond stress along this length, resulting in the proportional relationship presented as Equation 4-2.

$$l_t \propto \frac{f_{pt} d_b}{U_t} \qquad \textit{Equation 4-2}$$

where; l_t = Transfer length

d_b = Nominal strand diameter

f_{pt} = Prestress immediately following release

U_t = Average bond stress

As mentioned previously in Section 2.4.4.1, micro-cracking of the concrete in the inelastic zone creates a softened response resulting in the stiffness of the concrete being dependent on the tensile strength and elastic modulus of the concrete (Barnes et al. 2003). Since the tensile strength and elastic modulus are commonly estimated as proportional to the square root of the compressive strength of the concrete, the average bond stress can be estimated as proportional to the square root of the concrete compressive strength. It follows that the transfer length should be inversely proportional to the square root of the concrete compressive strength. Therefore, a relationship between transfer length and concrete strength may be formulated as Equation 4-3, where α is a proportionality constant that depends on other factors (Barnes et al. 2003).

$$l_t = \alpha \frac{f_{pt}}{\sqrt{f_c'}} d_b \qquad \textbf{\textit{Equation 4-3}}$$

In the aforementioned study by Swords (2005), different measures for tendon stress including the stress in the tendon before transfer (f_{pbt}), the stress in the tendon immediately following release (f_{pt}), and the effective stress (f_{pe}) as well as different measures for concrete strength (f'_c, f'_{ci}) were investigated to determine which combination produced the best correlations with the data in that study. The model which yielded the best correlation with that data was concluded to be $\frac{f_{pt}}{\sqrt{f'_{ci}}} d_b$. These parameters are also the most logical choices because they best describe the concrete strength and prestress force at the instant when equilibrium is first established along the transfer length. This conclusion is valid for both initial and four-day transfer lengths.

Using this relationship, the four-day transfer lengths were plotted against corresponding $\frac{f_{pt}}{\sqrt{f'_{ci}}} d_b$ values in units of ksi$^{-0.5}$. A linear regression analysis was performed to determine a "best-fit" line to model the data. The slope of this line is the average proportionality constant, α. Figure 4-10 depicts this relationship for dead-end transfer lengths for the sixteen flexural specimens. For dead-end transfer lengths, the average α value was found to be 0.53 ksi $^{-0.5}$ with an R^2 value equal to 0.41.

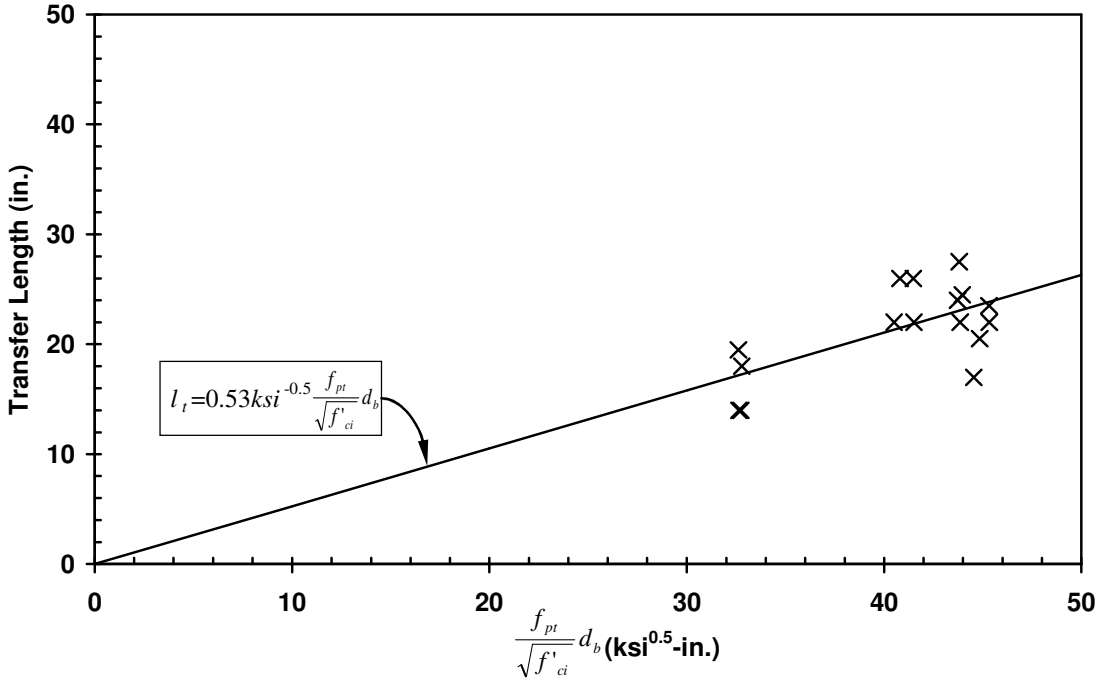

Figure 4-10: Dead-End Transfer Length as a Function of Tendon Prestress and Concrete Strength at Transfer

This model seems to work well with the data for the dead-end transfer lengths. However, much more dispersion was encountered for the live-end transfer lengths. For live-end transfer lengths, the average α value was found to be 0.71 ksi $^{-0.5}$ with an R^2

value equal to 0.39. Figure 4-11 depicts the dispersion of the live-end transfer length data as well as a best-fit line.

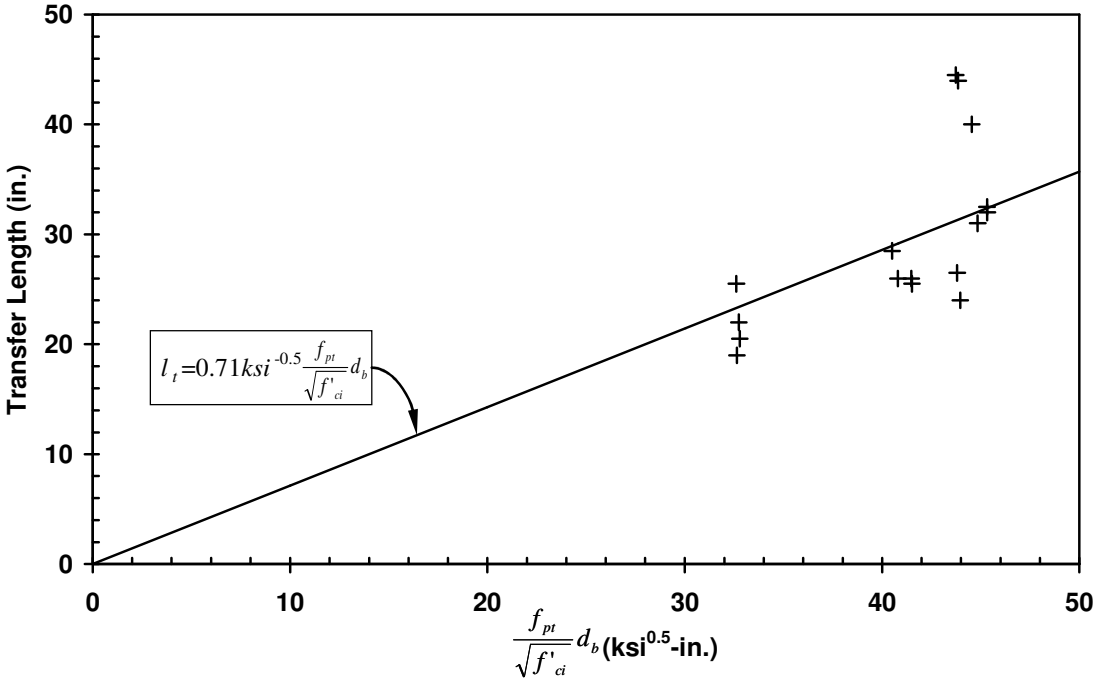

Figure 4-11: Live-End Transfer Length as a Function of Tendon Prestress and Concrete Strength at Transfer

Using the relationship in Equation 4-3, an α value can be calculated for each measured transfer length; each α value gives a measure of the relative transfer bond performance after normalization for the effects of prestress magnitude and concrete strength.

4.5.3 Comparison of Conventional and SCC Mixtures

As mentioned previously, Equation 4-3 can be used to produce normalized values of transfer length, which are useful for comparison purposes. Due to significantly different transfer lengths, dead-end and live-end transfer lengths were grouped separately for each

mixture. In order to facilitate comparison of the transfer bond performance of the various mixtures, representative α values are presented in Table 4-3. To relate SCC transfer lengths to standard mixture transfer lengths, the ratio, $\frac{\alpha}{\alpha_{STD-M}}$, was employed to make quantifiable comparisons. Four-day transfer length values were utilized for these comparisons in order to allow for later comparisons to a previous phase of this project.

Table 4-3: Comparison of Normalized α Values

Mixture	Variable	Specimen End	
		Live End	Dead End
STD-M	α	0.64	0.55
	$\frac{\alpha}{\alpha_{STD-M}}$	1.00	1.00
SCC-MA	α	0.65	0.58
	$\frac{\alpha}{\alpha_{STD-M}}$	1.00	1.07
SCC-MS	α	0.90	0.47
	$\frac{\alpha}{\alpha_{STD-M}}$	1.40	0.86
SCC-HS	α	0.67	0.50
	$\frac{\alpha}{\alpha_{STD-M}}$	1.03	0.92
All Slag	α	0.78	0.49
	$\frac{\alpha}{\alpha_{STD-M}}$	1.22	0.89
All SCC	α	0.74	0.52
	$\frac{\alpha}{\alpha_{STD-M}}$	1.15	0.95

The moderate-strength fly ash and GGBF slag dead-end transfer lengths were 7% longer and 14% shorter, respectively, than the standard mixture dead-end transfer lengths.

The high-strength GGBF slag mixture had dead-end transfer lengths which were 8% shorter than those of the standard mixture. Averaged over all SCC mixtures, the dead-end transfer lengths were 5% shorter than the dead-end transfer lengths of the standard mixture.

In terms of live-end transfer lengths, the high-strength slag mixture had 3% longer transfer lengths on average than the standard mixture. The moderate-strength fly ash mixture had comparable transfer lengths to the standard mixture. However, on the live ends, the moderate-strength GGBF slag mixture possessed transfer lengths that were 40% longer than the standard mixture transfer lengths. Averaged over all SCC mixtures, the live-end transfer lengths were 15% longer than the live-end transfer lengths of the standard mixture.

4.5.4 Effects of Time

Another important parameter affecting transfer length is the effect of time. For mixtures similar to those used in this study, Swords (2005) found less than a 2% increase in transfer length from four to forty-eight days after transfer. However, a significant growth was observed in the first few days after transfer. Due to this finding, transfer length readings were only collected immediately at transfer and four days after transfer for this study. Changes in transfer length over time were determined by comparing each initial and four-day transfer length. The results of this comparison are shown in Table 4-4, which presents average ratios of the four-day transfer length to the initial transfer length for the mixtures employed in the flexural specimens.

Table 4-4: Effect of Time on Transfer Length

	$l_{t,4}/l_{t,i}$	
SPECIMEN	**Specimen End**	
	Live	**Dead**
STD-M	1.05	1.07
SCC-MA	1.12	1.18
SCC-MS	1.05	1.02
SCC-HS	1.05	1.24

As can be seen in the above table, transfer length growth on live ends ranged from 5% to 12%. However, transfer length growth on dead ends had a much broader range from 2% to 24%. For live ends the average increase in transfer length was 5% for the standard mixture and 7% for all SCC mixtures. However, for dead ends the average increase in transfer length was 7% for the standard mixture and 15% for all SCC mixtures. These results are not similar to transfer length increases observed in Swords' (2005) study for similar mixtures. For live ends, Swords (2005) reported the average increase in transfer length over four days to be 1% for the standard mixture and 3% for all SCC mixtures. For dead ends, Swords (2005) reported the average increase in transfer length over four days to be 5% for the standard mixture and 7% for all SCC mixtures tested in that study.

Many studies have reported various increases in transfer length over time. As mentioned previously, Kaar, LaFraugh, and Mass (1963) reported an average increase in transfer length of 6 percent over a period of one year. Lane (1998) reported an increase in transfer length of 30 percent over the first twenty-eight days after release with an

additional increase of 7 percent over the next six months. Barnes et al. (2004) reported average increases in transfer lengths between 10–20 percent over the first weeks after transfer with little increase thereafter. From the results of this study and others, it is apparent that measurements of only initial transfer lengths are not adequate to assess the longer-term transfer length behavior of pretensioned members.

4.5.5 Comparison of Dead and Live Ends

Transfer lengths were observed to be significantly longer at live ends than at the dead ends of the same specimens. Using the normalized α values, transfer length comparisons between dead and live ends can be made. Table 4-4 presents average ratios of live-end to dead-end α values for all mixtures. These α values were calculated using four-day transfer length values. Each flexural specimen had one dead end and one live-end.

Table 4-5: Comparison of Normalized Dead-End and Live-End α Values

	α VALUE ($ksi^{-0.5}$)		$\frac{\alpha_{LIVE}}{\alpha_{DEAD}}$
MIXTURE	α_{LIVE}	α_{DEAD}	
STD	0.64	0.55	1.18
SCC-MA	0.65	0.58	1.10
SCC-MS	0.90	0.47	1.91
SCC-HS	0.67	0.50	1.33
All SCC	0.74	0.52	1.42
All Mixtures	0.71	0.53	1.36

As can be seen in the preceding table, transfer lengths at live ends were significantly larger than those at dead ends. For specimens cast with the standard mixture, transfer

lengths were only 18% higher on live ends than on dead ends. For all specimens, transfer lengths were 36% higher on live ends than on dead ends.

For SCC specimens, transfer lengths were 42% higher on live ends than on dead ends. This value is greatly affected by the moderate-strength slag mixture which showed live-end transfer lengths to be 91% higher than dead-end transfer lengths. This indicates that this particular mixture was greatly affected by the flame-cutting procedure used for prestress transfer. It is important to note that the GGBF slag was used in this mixture as a 50% replacement for Type III cement. The replacement amount may be significant because the extreme difference between live and dead ends was not observed for the other slag mixture, which only employed a 30% replacement. Therefore, it may be necessary to impose limitations on replacement percentages for SCC utilizing GGBF slag, or to require gradual prestress release techniques for mixtures with high slag content.

4.5.6 Effect of Cross-Section Size

As mentioned previously, in a previous phase of this project, an extensive transfer length study was conducted on smaller, concentrically prestressed specimens. The purpose of this section is to establish the effect of cross-section size, if any, on transfer length. In order to make the most direct comparison between section size and transfer length, the results from several specimens evaluated in that study (Swords 2005) will be ignored. Only results from the 4 in. x 6 in. specimens prestressed with two strands will be considered. In addition, data from specimens constructed with mixtures not used in this study will not be considered. Therefore, only two-strand specimens constructed with the

same mixtures used in this study will be evaluated. The cross section of those specimens is geometrically equivalent to the bottom 4 in. of the cross section of the flexural specimens of this phase of the study. This selection process yields 16 dead-end transfer zones and 8 live-end transfer zones for comparison with the eccentrically prestressed flexural specimens.

Unless otherwise noted, the transfer lengths presented in this section for concentrically prestressed specimens represent seven-day transfer lengths. In that study, readings were not taken at consistent times for all mixtures before seven days. Readings were taken at three or four days after transfer. There was no significant difference between the three or four-day readings and the seven-day readings. Therefore, seven - day transfer length readings from the concentrically prestressed specimens were used for comparison to the four-day transfer length readings from the T-beam specimens.

Swords (2005) used the relationship, $\frac{f_{pt}}{\sqrt{f'_{ci}}} d_b$, to establish α values for all mixes used in that study. Considering only the relevant specimens, an average α value of 0.65 ksi $^{-0.5}$ was found for dead-end transfer lengths of the smaller specimens. This value is shown on Figure 4-12, plotted with both the data and average α value for dead-end transfer lengths for this study. The small-specimen α value is 24% higher than the average α value from this study for dead-end transfer lengths.

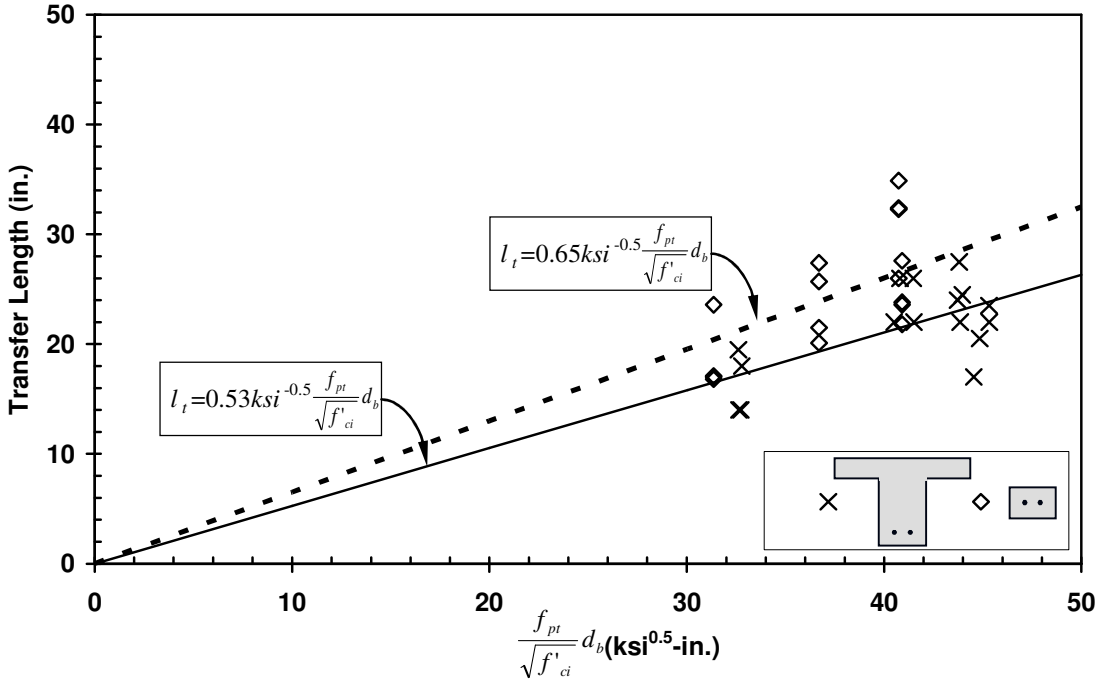

Figure 4-12: Effect of Cross-Section Size on Dead-End Transfer Length

For live-end transfer lengths, an average α value of 1.00 ksi $^{-0.5}$ was found for the smaller specimens. This value is shown on Figure 4-13, plotted with both the data and average α value for live-end transfer lengths for this study. The small-specimen value is 40% higher than the average α value from this study for live-end transfer lengths.

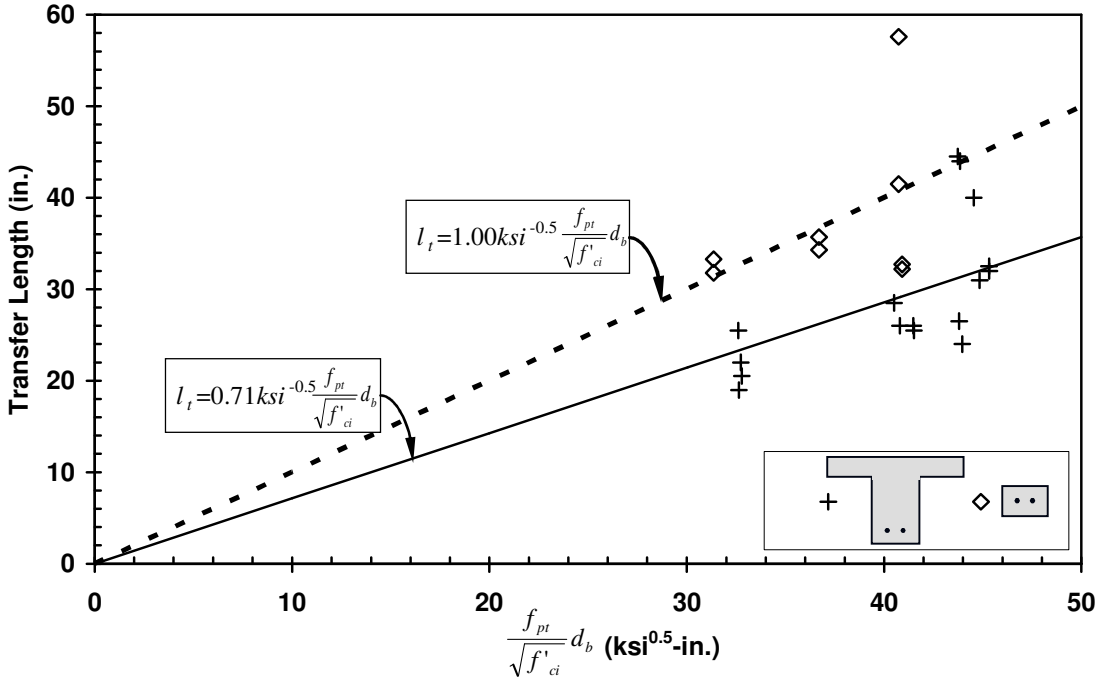

Figure 4-13: Effect of Cross-Section Size on Live-End Transfer Length

Figure 4-12 and 4-13 show that for both the live-end and dead-end transfer lengths, the α values for the smaller, concentrically prestressed specimens are higher. This shows some indication that—after normalization of the influence of strand stress and concrete strength—transfer length decreases with increasing cross-section size. This effect is more pronounced for live ends—almost twice as large in this study—than for dead ends.

The effect of SCC on transfer length for both cross sections can be evaluated in Table 4-6. As discussed in Section 4.5.3, the ratio, $\frac{\alpha}{\alpha_{STD-M}}$, can be used to demonstrate the difference between any set of specimens and the standard mixture specimens. Table 4-6 presents this ratio to compare all SCC mixtures to the standard mixture for both cross-sections.

Table 4-6: Comparison of Normalized α Values for Both Cross-Sections

		Specimen End	
		Live End	**Dead End**
$\frac{\alpha_{SCC}}{\alpha_{STD-M}}$	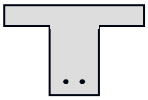	1.15	0.95
		1.35	1.13

As can be seen in Table 4-6, dead-end transfer lengths were 5% shorter in the larger specimens and 13% longer in the smaller specimens for SCC specimens compared to standard mixture specimens. Live-end transfer lengths were 15% longer in the larger specimens and 35% longer in the smaller specimens for SCC specimens compared to standard mixture specimens.

The data for the concentrically prestressed specimens and T-beams may also be compared in terms of live and dead ends. Table 4-7 presents the ratio of live-end α to dead-end α values for both the relevant concentrically prestressed and T-beam specimens.

Table 4-7: Ratio of Normalized Dead-End and Live-End α Values for Concentrically Prestressed and T-Beam Specimens

MIXTURE	$\frac{\alpha_{LIVE}}{\alpha_{DEAD}}$	
	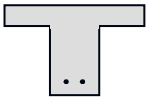	
STD	1.18	1.34
SCC-MA	1.10	1.48
SCC-MS	1.91	1.58
SCC-HS	1.33	1.75
All Slag	1.62	1.66
All SCC	1.42	1.60
All Mixtures	1.36	1.54

As discussed previously, one of the most notable values on this table is the ratio of live to dead ends for the moderate-strength slag mixture, SCC-MS. This shows that for SCC-MS, transfer lengths on live ends were 91% higher than on dead ends. Swords (2005) also found a large discrepancy between live and dead end transfer lengths for SCC-MS, reporting a 58% increase on the live ends. However, the largest increase found by Swords was for SCC-HS which showed live-end transfer lengths to be 75% longer than dead-end transfer lengths. Thus, for this project, it has been repeatedly observed that for specimens cast with GGBF slag, flame-cutting significantly affects transfer length.

In terms of cross section size, Table 4-7 also provides evidence that transfer length is affected by specimen size. Considering all mixtures, for the smaller specimens, transfer lengths were 54% longer on live ends than on dead ends. However, for the larger

specimens, transfer lengths were only 36% longer on live ends than on dead ends. Live-end transfer lengths were longer by a greater percentage on all concentrically prestressed specimens as opposed to the T-beam specimens for all mixtures except SCC-MS.

The comparisons presented in this section seem to point toward the conclusion that transfer length is affected by specimen size. This theory is supported by a study by Russell and Burns (1993) which included tests on a variety of different cross section shapes with varying strand patterns. The results of that study showed that test specimens with larger cross sections possess shorter transfer lengths than smaller specimens (Russell and Burns 1993). This may be due to the hypothesis that larger cross sections with greater mass can absorb more energy than smaller sections, and will therefore exhibit greater transfer bond (Russell and Burns 1993).

4.6 DESIGN IMPLICATIONS

In the preceding section, several parameters were considered for making comparisons and draw conclusions from the data obtained from transfer length testing. Based on these conclusions, a set of design expressions was formulated and is presented in this section.

Considering all specimens, an average α value can be calculated to represent the entire data set. For strength design purposes, an upper-bound value which exceeds 95% of the data would be appropriate to use as a model for the data. This upper-bound was calculated by fitting a line which would encompass at least 95% of the data. For strength design, overestimating the transfer length leads to conservative underestimations of the flexural strength and shear strength. Figure 4-14 below shows the average α value for all

transfer lengths and a 95% upper-bound for these values. This plot does not discriminate between the methods of prestress transfer for each transfer zone.

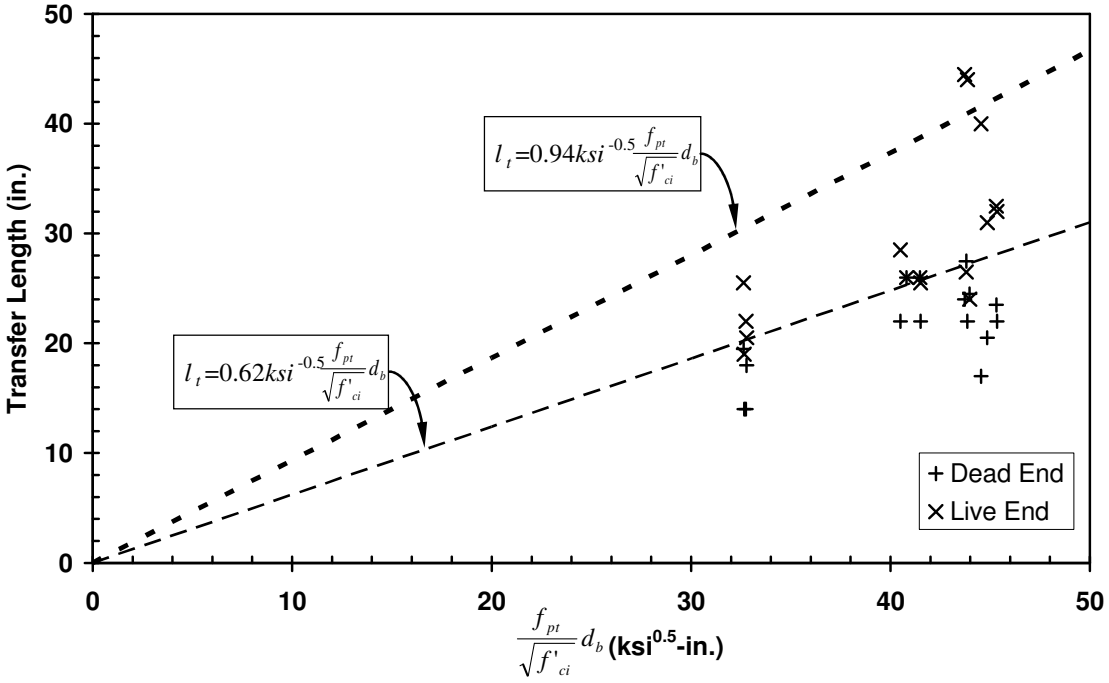

Figure 4-14: Transfer Length as a Function of Tendon Prestress and Concrete Strength at Transfer with 95% Upper Bound

Looking at the above figure, it is clear that discriminating between live and dead ends would yield more effective prediction models. When separated, the average α value is 0.53 ksi $^{-0.5}$ for dead-end transfer lengths and 0.71 ksi $^{-0.5}$ for live-end transfer lengths. For design purposes, upper-bound α values for dead-end and live-end transfer lengths were determined to be 0.64 and 1.02 ksi $^{-0.5}$, respectively. These values can be seen on Figures 4-15 and 4-16.

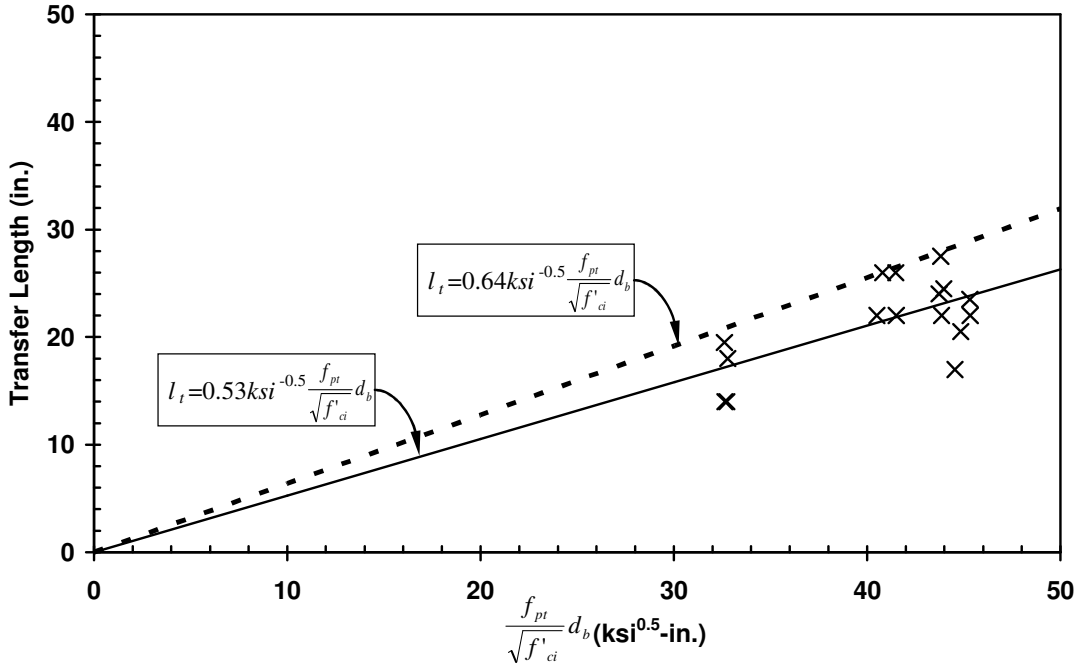

Figure 4-15: Dead-End Transfer Length as a Function of Tendon Prestress and Concrete Strength at Transfer with 95% Upper Bound

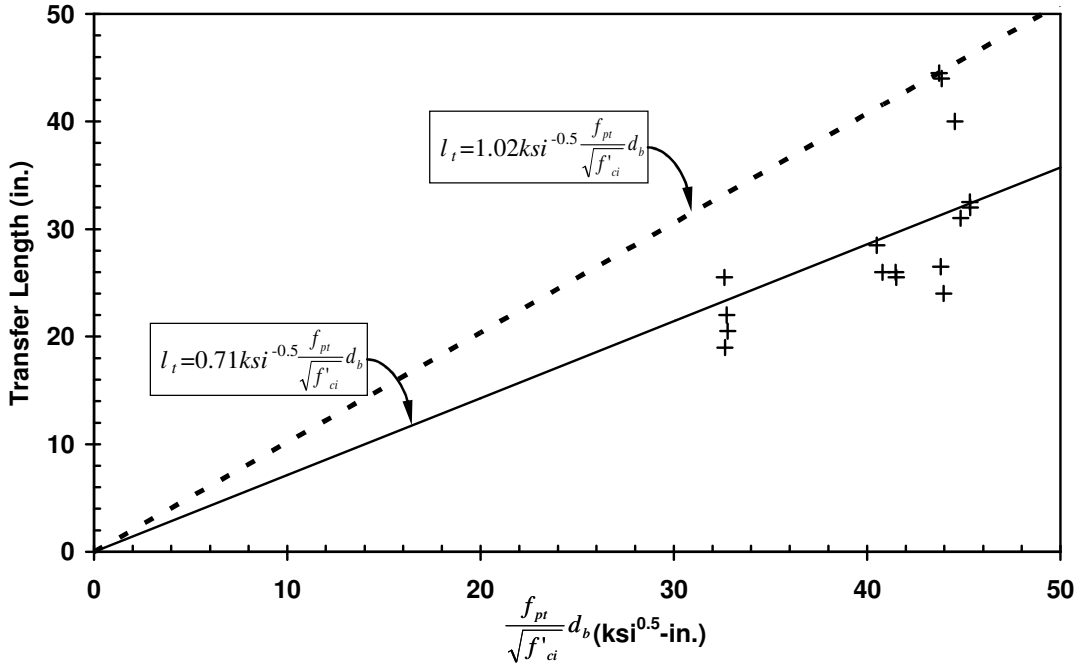

Figure 4-16: Live-End Transfer Length as a Function of Tendon Prestress and Concrete Strength at Transfer with 95% Upper Bound

In the case for which the above models would be used, if flame-cutting were permitted, the designer would have to specify the worst case as the model indicated for live ends. However, if flame-cutting was not permitted, the dead-end model could be employed for all transfer lengths.

Taking a closer look at the live-end transfer lengths, it is clear that the wide scatter of the points causes the 95% upper bound to be much higher than the average value. It is therefore important that the data be investigated further. The longest transfer lengths were for the moderate-strength slag mixture, SCC-MS. Also, all normalized live-end transfer lengths were longer for SCC specimens than STD-M specimens. Therefore, it may be necessary to have separate prediction models for SCC and standard concrete mixtures. Figure 4-17 depicts the scatter of live-end transfer lengths and categorizes the data by mixture.

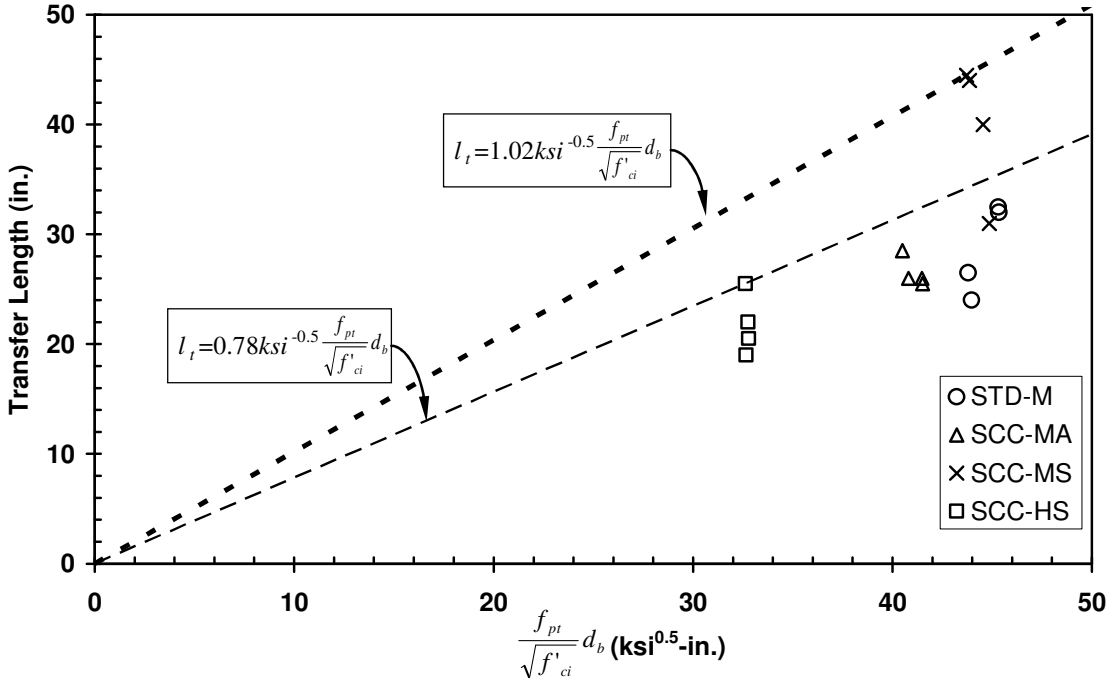

Figure 4-17: Live-End Transfer Length as a Function of Tendon Prestress and Concrete Strength at Transfer with 95% Upper Bound for SCC

Looking at Figure 4-17, it is evident that the live-end transfer lengths for the moderate-strength slag mixture, SCC-MS, are quite a bit longer than the transfer lengths for all other mixtures. This mixture had a 50% GGBF slag replacement, whereas the high-strength slag mixture, SCC-HS, had only a 30% replacement. Therefore, as discussed in Section 4.5.5., it may be necessary to impose slag limitations for use in SCC mixtures.

Expressions with and without slag limitations were formulated based on the 95% upper-bound values shown in Figure 4-17. The 95% upper bound value, shown on Figure 4-17, for standard mixtures and SCC mixtures with slag limitations when considering live-end transfer lengths is 0.78 ksi $^{-0.5}$. Whereas, the 95% upper bound value, also shown on Figure 4-17, for SCC mixtures without slag limitations when

considering live-end transfer lengths is 1.02 ksi $^{-0.5}$. However, the problem with GGBF slag only seems to manifest itself on live-end transfer lengths. Therefore, the distinction between SCC with and without slag limitations would only be necessary for specimens for which flame-cutting is the method of prestress transfer. Therefore, the following set of equations to model transfer length can be defined by the equations given in Table 4-8.

Table 4-8: Transfer Length Models Recommended for Design

Prestress Release Method	**Concrete Type**	**Transfer Length**
Gradual	Standard & All SCC	$l_t = 0.64 ksi^{-0.5} \frac{f_{pt}}{\sqrt{f'_{ci}}} d_b$
Sudden	Standard & SCC with Slag Limitation	$l_t = 0.78 ksi^{-0.5} \frac{f_{pt}}{\sqrt{f'_{ci}}} d_b$
	SCC without Slag Limitation	$l_t = 1.02 ksi^{-0.5} \frac{f_{pt}}{\sqrt{f'_{ci}}} d_b$

It is important to note that the 95% upper-bound values are conservative design expressions for strength design purposes. However, this is not the case for checking allowable stress limits under service loads, for which overestimating the transfer length at prestress transfer is not conservative. Because slight underestimation of stresses at transfer or under service loads is not likely to lead to collapse of a prestressed member, computation of the transfer length based on an average α value is reasonable when computing stresses for service limit state design. Although not presented in graphical form, the average α value for standard mixtures and SCC mixtures with slag limitations when considering live-end transfer lengths is 0.65 ksi $^{-0.5}$. Recommendations for allowable stress design are presented in Table 4-9.

Table 4-9: Transfer Length Models Recommended for Use in Checking Concrete Stresses at Transfer

Release Method	Concrete Type	Transfer Length
Gradual	Standard & All SCC	$l_t = 0.53ksi^{-0.5} \frac{f_{pt}}{\sqrt{f'_{ci}}} d_b$
Sudden	Standard & SCC with Slag Limitation	$l_t = 0.65ksi^{-0.5} \frac{f_{pt}}{\sqrt{f'_{ci}}} d_b$
	SCC without Slag Limitation	$l_t = 0.71ksi^{-0.5} \frac{f_{pt}}{\sqrt{f'_{ci}}} d_b$

4.7 COMPARISON OF TEST DATA WITH DESIGN EXPRESSIONS

As discussed in Chapter 2, there are several design expressions for transfer length. The purpose of this section is compare the test data gathered in this study with these design expressions and the design expressions recommended in Section 4.6.

4.7.1 RECOMMENDED EXPRESSIONS FROM THIS STUDY

The first comparison made here is with the recommended expressions presented in the preceding section. Predicted values from expressions given in Table 4-8 are plotted against corresponding measured transfer length values in Figure 4-18. The predicted values are a result of applying the recommended expression for each data point. All dead-end transfer lengths were predicted using the expression, $l_t = 0.64ksi^{-0.5} \frac{f_{pt}}{\sqrt{f'_{ci}}} d_b$.

The live-end transfer lengths were predicted using the expression, $l_t = 0.78ksi^{-0.5} \frac{f_{pt}}{\sqrt{f'_{ci}}} d_b$ for transfer lengths from mixtures with a slag contents less than 50% (STD-M, SCC-MA,

and SCC-HS) and $l_t = 1.02ksi^{-0.5} \frac{f_{pt}}{\sqrt{f'_{ci}}} d_b$ for transfer lengths from the mixture without a slag limitation (SCC-MS). The line of equality represents the points where the predicted transfer length equals the measured transfer length. Any data points which fall below this line indicate situations where the measured transfer length exceeded the predicted transfer length. This would be unconservative for shear strength and development length prediction. When applying the expressions recommended in the previous section, it can be seen in Figure 4-18 that at least 95% of the data falls on or above the line.

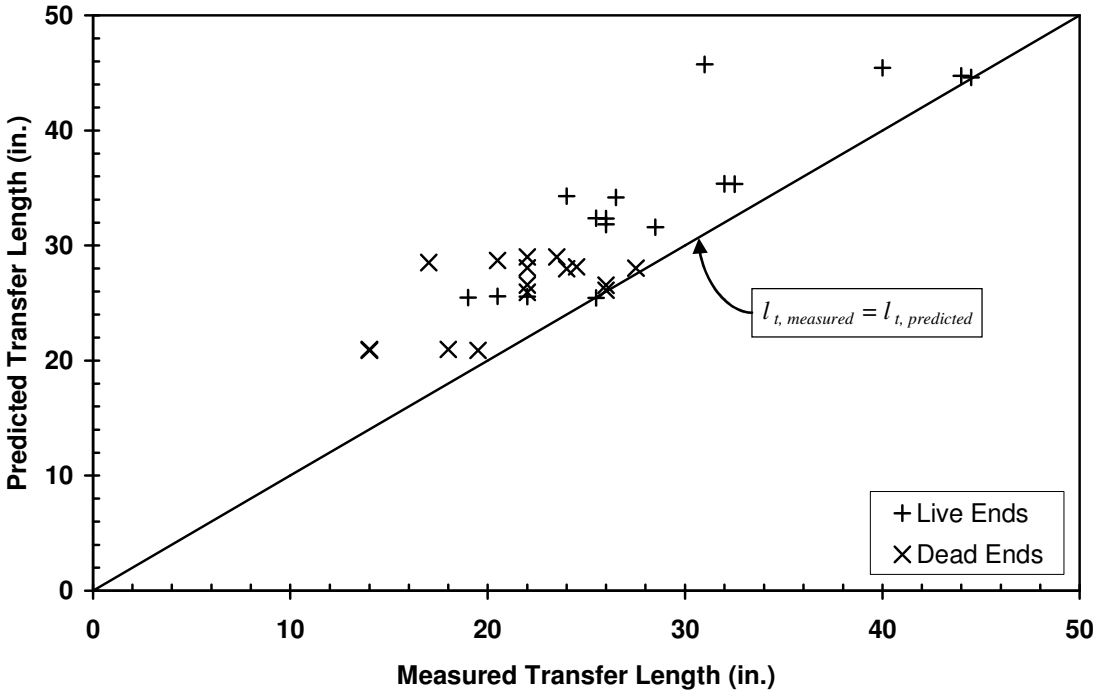

Figure 4-18: Comparison of 95% Upper-Bound Relationships to Measured Transfer Lengths

In order to further investigate the accuracy of the recommended expression, Figure 4-19 depicts a frequency distribution of the predictions as well as the performance of the

prediction across a range of concrete strengths. The histogram, shown by Figure 4-19 (a), reinforces Figure 4-18 by showing the distribution of the ratio, $\frac{l_{t,meas}}{l_{t,pred}}$. The bars on the graph show the frequency of occurrence of this ratio and the line shows the cumulative frequency of all the data. Also shown on this plot are the mean, standard deviation, the coefficient of variance, the 95% fractile and the 5% fractile values. Fractile values were established based on the actual cumulative frequency distribution rather than assuming a normal frequency distribution. Figure 4-19 (a) shows that transfer lengths were, on average, 17% shorter than predicted by the model. The spread of the data was relatively small, with a standard deviation, *s*, of 0.11. It can also be seen that the recommended expression is conservative for more than 95% of the data.

Figure 4-19 (b) depicts $\frac{l_{t,meas}}{l_{t,pred}}$ across a range of concrete strengths. This plot shows the effectiveness of the model relative to the concrete strength of the mixture. For this prediction model, 95% of the measured values should fall below the line of equality, shown as the horizontal line where $\frac{l_{t,meas}}{l_{t,pred}}$=1.0. Figure 4-19 shows that as concrete strength increases, the points remain evenly spread under the line of equality. Looking at the figure, the model seems to effectively predict transfer lengths for a variety of concrete strengths.

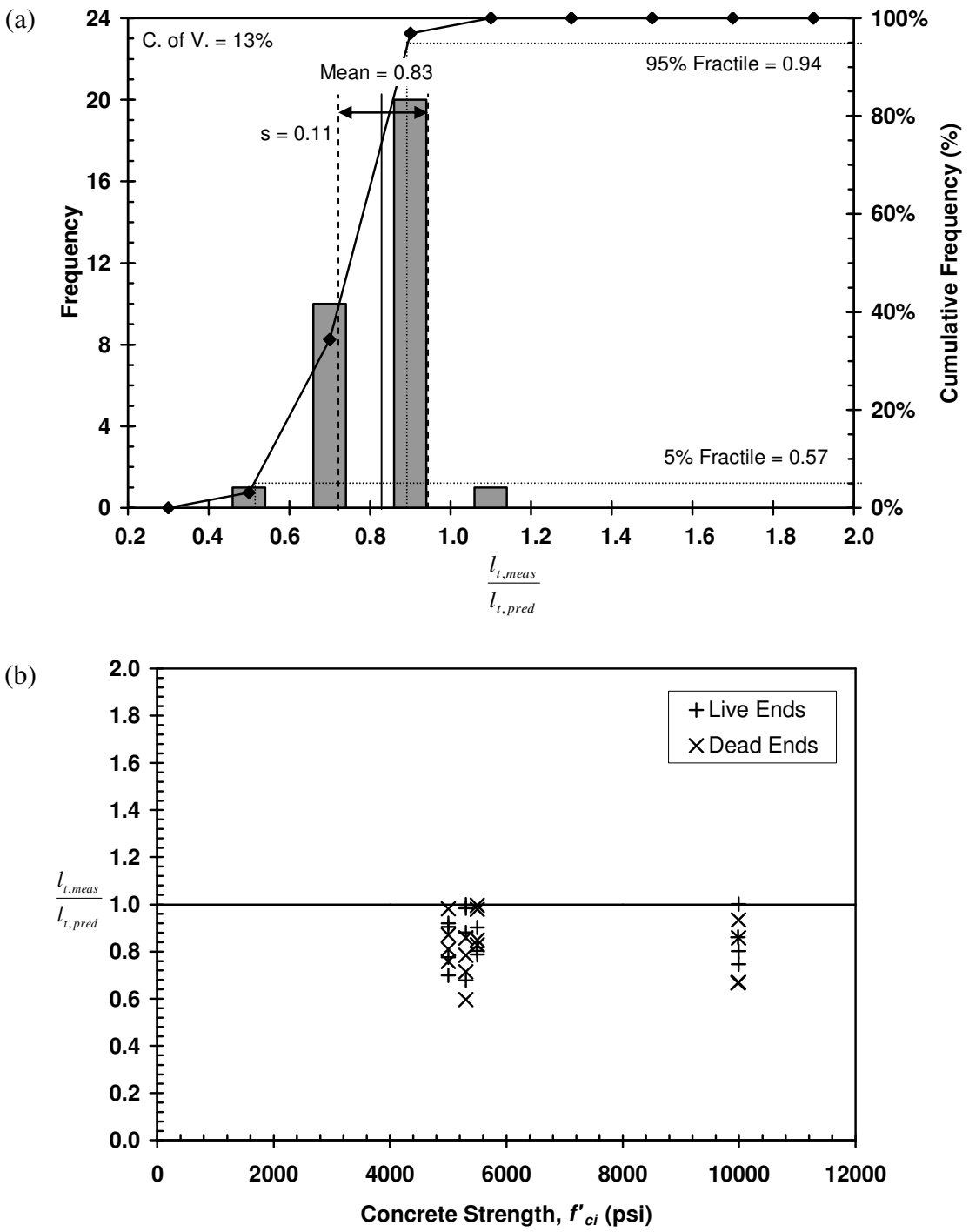

Figure 4-19: Accuracy of Recommended Transfer Length Expressions (a) Frequency Distribution (b) Performance across Range of Concrete Strengths

4.7.2 ACI 318-05 EXPRESSION

Article 12.9.1 of the ACI *Standard Building Code Requirements for Reinforced Concrete* suggests the expression, $l_t = \left(\frac{f_{pe}}{3000}\right) d_b$, as a model for transfer length (ACI 318-05). A comparison of transfer lengths predicted by this expression versus measured transfer lengths is depicted by Figure 4-20. The figure shows that the data does not follow the line of equality in any way. Also, the expression is unconservative for live-end transfer lengths, with three data points falling below the line of equality. The data points which fall below the line imply that this expression is unsafe for shear and flexural strength design. In addition, several dead-end transfer length data points are very far from the line of equality. This is indicative of the ineffectiveness of this expression for predicting transfer length.

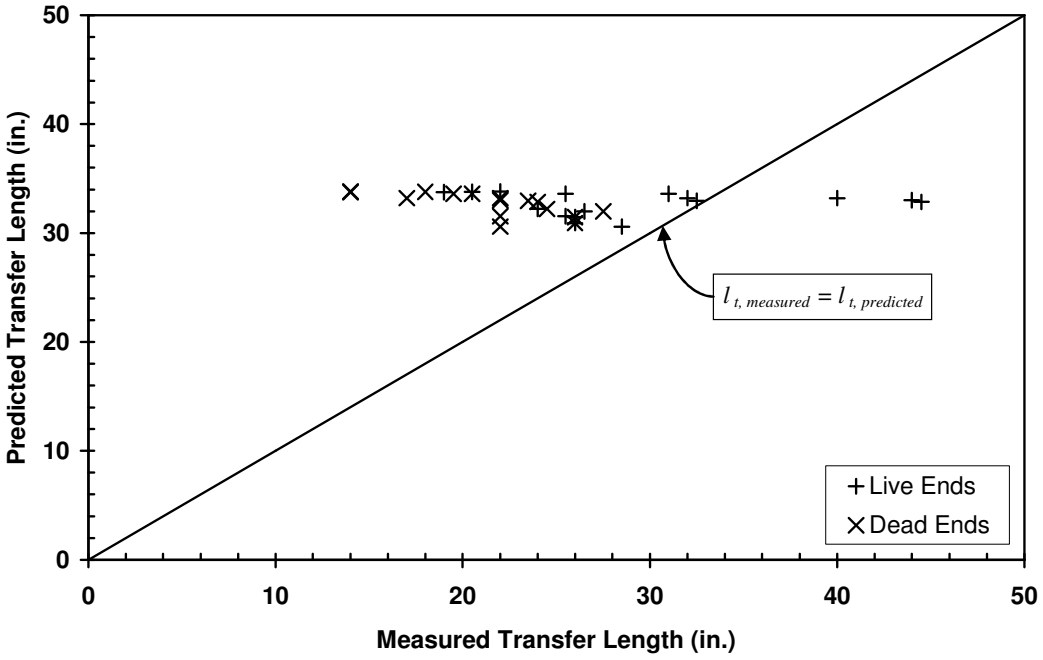

Figure 4-20: Comparison of ACI 318-12.9 Values to Measured Transfer Lengths

The wide scatter of the data shown in Figure 4-20 can also be seen by the frequency distribution shown in Figure 4-21(a). Although the dead and live ends cannot be discerned on this graph, it is evident that this expression underestimates transfer length. Figure 4-21(a) shows that transfer lengths were, on average, 22% shorter than predicted by the model. The spread of the data are larger than the previous model, with a standard deviation of 0.22. It can also be seen that the recommended expression is conservative for 90% of the data. Therefore, 10% of the data are underestimated by this expression. This is could be unsafe for shear and flexural strength design. Also, the 95% fractile is 1.19; thus 5% of the data are underestimated by 19% or more.

Figure 4-19 (b) shows the same three data points above the line of equality. These three points all correspond to moderate-strength concrete mixtures. It also shows that the data at higher strengths are further away from the line of equality, suggesting that this model is less effective for higher-strength concretes. However, this figure does show that the model is conservative, although not accurate, for higher-strength concrete mixtures, yet unconservative for lower strength concrete mixtures. Based on the trend evident in this figure, it could be hypothesized that this expression becomes significantly unconservative for sudden-release prestressing when concrete compressive strengths are less than 5000 psi at prestress transfer.

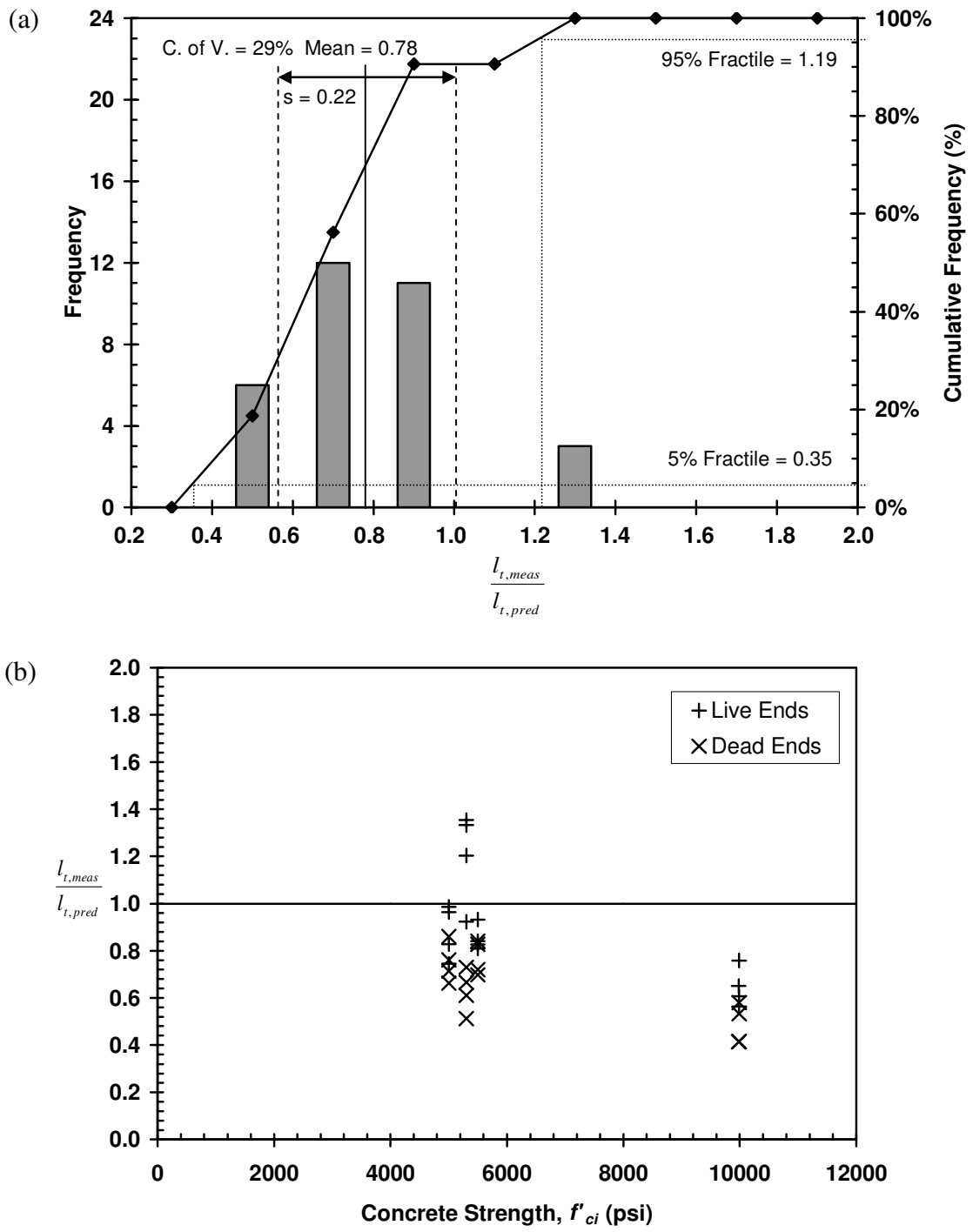

Figure 4-21: Accuracy of ACI 318-05 Transfer Length Expressions (a) Frequency Distribution (b) Performance across Range of Concrete Strengths

4.7.3 ACI 318-05 SHEAR PROVISIONS EXPRESSION

The next recommended expression for transfer length, $l_t = 50d_b$, can be found in the shear strength design provisions of ACI 318-05. Figures 4-22 depicts the use of this model to predict transfer length of the specimens in this study. As can be seen, this model predicts a constant transfer length for this data set. This model does not accurately predict transfer length for this data, as the data does not follow the line of equality in any way. It is unconservative for much of the data, especially for live-end transfer lengths. Also, there are several points on either side which are very far away from the line equality. This figure shows the model to be inaccurate and unsafe when predicting transfer length for this data set.

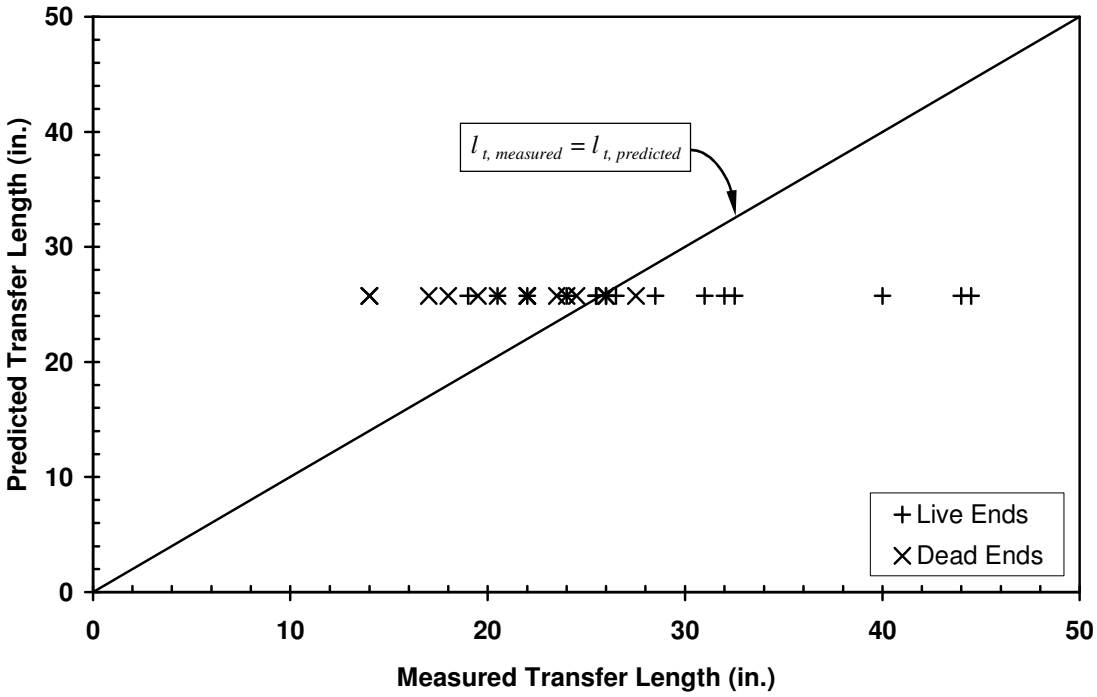

Figure 4-22: Comparison of ACI 318 Shear Provisions to Measured Transfer Lengths

The wide scatter of the data shown in Figure 4-22 can also be seen by the frequency distribution shown in Figure 4-23(a). Although the dead and live ends cannot be discerned on this graph, it is evident that this expression underestimates transfer length. Figure 4-23(a) shows that transfer lengths were, on average, 2% shorter than predicted by the model. This indicates that much of the data was underestimated by this expression. The spread of the prediction accuracy is larger than with the previous model, with a standard deviation of 0.28. It can also be seen that the recommended expression is conservative for only 70% of the data. Therefore, 30% of the data are underestimated by this expression. This is very unsafe for shear and flexural strength design. Also, the 95% fractile is 1.54; thus 5% of the data are underestimated by 54% or more.

Figure 4-23(b) shows several data points above the line of equality. All data points that are underestimated by this model correspond to moderate-strength concrete mixtures. However, this figure does show that the model is conservative, although not accurate, for higher-strength concrete mixtures, yet very unconservative for lower strength concrete mixtures.

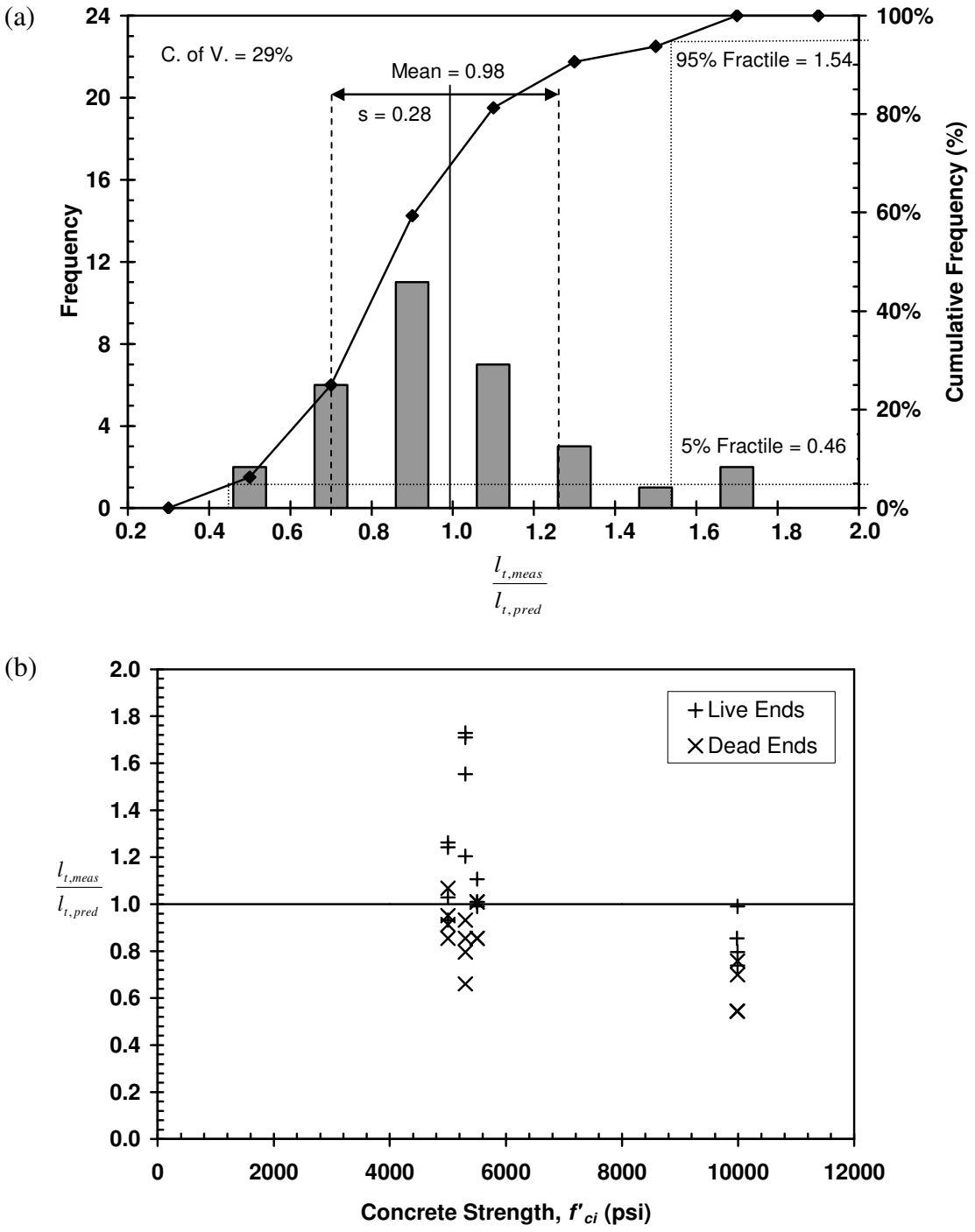

Figure 4-23: Accuracy of ACI 318 Shear Provisions Transfer Length Expressions (a) Frequency Distribution (b) Performance across Range of Concrete Strengths

4.7.4 AASHTO LRFD SPECIFICATIONS

The design expression of the AASHTO LRFD Specifications, $l_t = 60d_b$, also proves to be unconservative for some of the results from this study. Figures 4-24 depicts the use of this model to predict transfer length. As can be seen, this model predicts a constant transfer length for this data set. This model does not accurately predict transfer length for this data, as the data does not follow the line of equality in any way. Although the model is safe for dead-end transfer lengths, there are several points which are very far from the line, proving the model to be quite inaccurate. It is unconservative for live-end transfer lengths. Although this model is more conservative than the previous expression due to a larger multiplier, this figure shows the model to be inaccurate and unsafe when predicting transfer length for this data set.

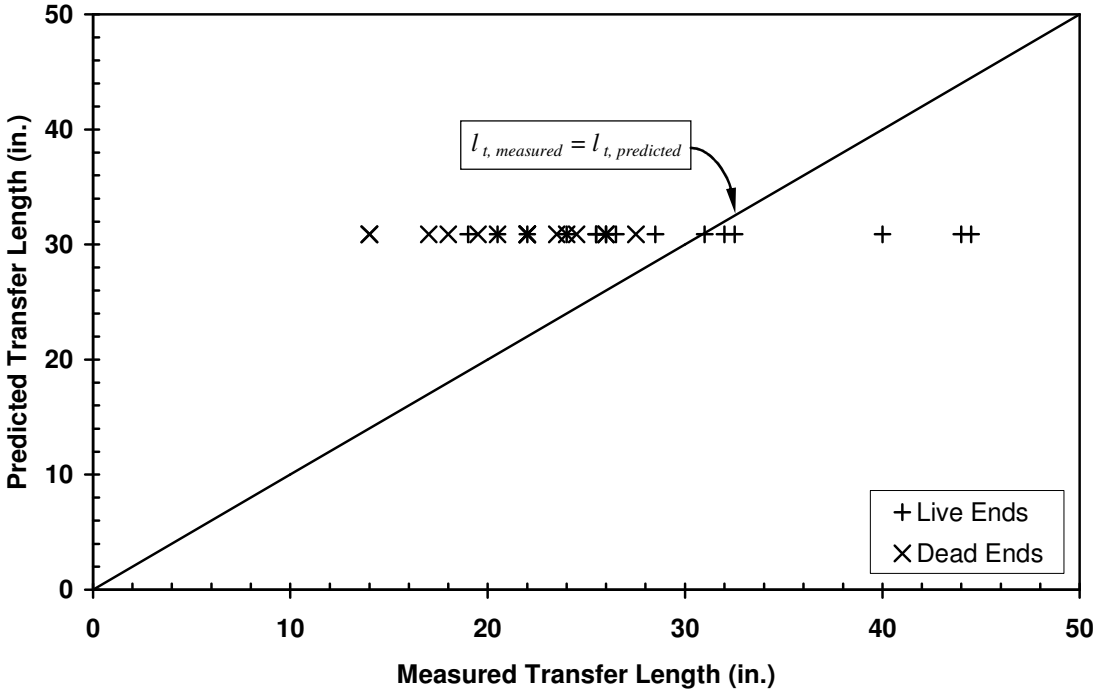

Figure 4-24: Comparison of AASHTO LRFD Provisions to Measured Transfer Lengths

The wide scatter of the data shown in Figure 4-24 can also be seen by the frequency distribution shown in Figure 4-25(a). Although the dead and live ends cannot be discerned on this graph, it is evident that this expression underestimates transfer length. Figure 4-25(a) shows that transfer lengths were, on average, 18% shorter than predicted by the model. This indicates that much of the data was underestimated by this expression. The spread of the data are smaller than the previous model, with a standard deviation of 0.24. It can also be seen that the recommended expression is conservative for only 85% of the data. Therefore, 15% of the data are underestimated by this expression. This is very unsafe for shear and flexural strength design. Also, the 95% fractile is 1.34; thus 5% of the data are underestimated by 34% or more.

Figure 4-25(b) shows several data points above the line of equality. All data points that are underestimated by this model correspond to moderate-strength concrete mixtures. However, this figure does show that the model is conservative, although not accurate, for higher-strength concrete mixtures, yet increasingly unconservative for lower strength concrete mixtures.

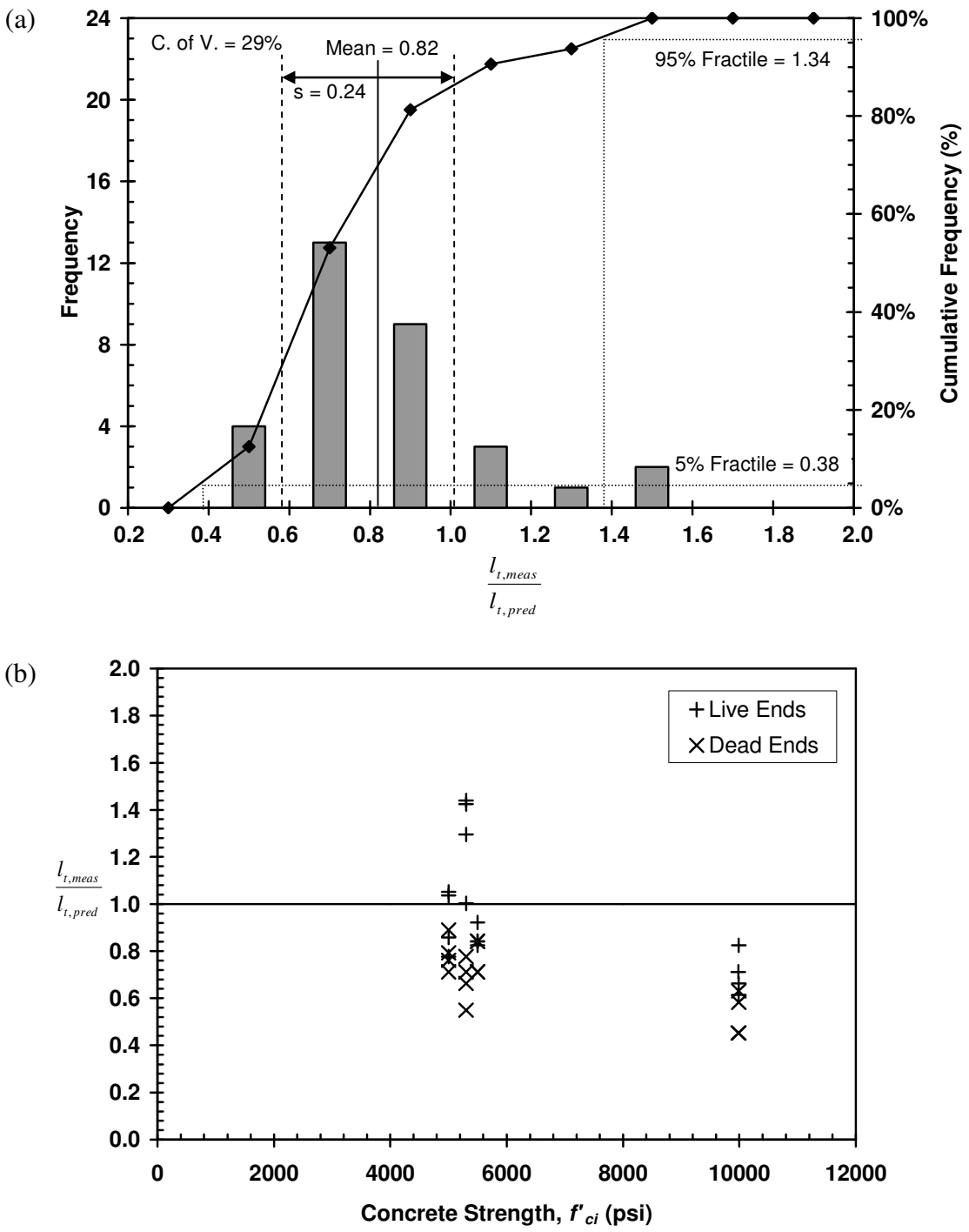

Figure 4-25: Accuracy of AASHTO LRFD Transfer Length Expressions (a) Frequency Distribution (b) Performance across Range of Concrete Strengths

4.8 SUMMARY AND CONCLUSIONS

Transfer length testing was performed on sixteen specimens. Each of the specimens had two transfer zones, one at each end, resulting in a total of thirty-two transfer zones. Concrete surface strains were measured using mechanical strain gauges immediately after transfer as well as four days after transfer. The 95% AMS method was used to establish transfer lengths from surface compressive strain profiles. After the determination of transfer lengths, the results were analyzed and compared to the results of previous studies.

Several conclusions regarding transfer length were reached for this study:

- On average, specimens constructed with higher compressive strengths at transfer had shorter transfer lengths than specimens which were constructed with lower concrete strengths at transfer.
- The decrease in transfer length with increasing concrete strength could be accurately estimated by assuming the transfer length is inversely proportional to $\sqrt{f'_{ci}}$. This relationship provides a simple yet accurate method of describing this trend over a wide range of concrete strengths.
- When normalized against strand stress and concrete strength, the moderate-strength fly ash mixture had dead-end transfer lengths slightly higher (7%) than the standard mixture.
- When normalized against strand stress and concrete strength, the GGBF slag mixture had dead-end transfer lengths approximately 10% shorter than the standard mixture.

- When normalized against strand stress and concrete strength, the moderate-strength fly ash mixture had live-end transfer lengths approximately the same as the standard mixture.
- When normalized against strand stress and concrete strength, the moderate-strength slag mixture had live-end transfer lengths significantly longer (40%) than the standard mixture.
- When normalized against strand stress and concrete strength, the high-strength slag mixture had live-end transfer lengths approximately the same as the standard mixture.
- In general, SCC transfer behavior only differed significantly from the standard mixture at cut ends of the moderate-strength mixture with a 50% replacement of GGBF slag.
- Reliable estimates of long-term transfer lengths are difficult to obtain solely on measurements of initial transfer lengths.
- Dead-end transfer lengths of some SCC specimens increased as much as 25% in the first four days after prestress transfer.
- On average, live-end transfer lengths were 18% longer than dead-end transfer lengths for the standard mixture.
- Live-end transfer lengths for the moderate-strength fly ash mixture were 10% longer than the dead-end transfer lengths.
- The effect of the method of release was more pronounced for slag mixtures.

- Live-end transfer lengths for the moderate-strength GGBF slag mixture were 90% longer than the dead-end transfer lengths and live-end transfer lengths for the high-strength GGBF slag mixture were 33% longer than the dead-end transfer lengths.
- There appears to be a trend concerning the increase of the percent GGBF slag replacement with the increase in transfer length on live-ends.
- When normalized against strand stress and concrete strength, transfer length decreases with increasing cross-section size. This effect is more pronounced at live ends than at dead ends.
- Differences in transfer length behavior between SCC and the standard mixture decrease with increasing section size.
- With the exception of the moderate-strength GGBF slag mix (50% replacement), the disparities between transfer length behaviors at live and dead ends decrease with increasing cross-section size.
- Cross-sectional size is a critical parameter in determining transfer lengths, particularly for specimen ends adjacent to flame-cutting of the strands.
- The ACI 318 12.9 expression for transfer length is unconservative for live-end transfer lengths. This expression does not reflect the influence of concrete strength; and, it is more unconservative at lower strength levels.
- The ACI 318 shear provision expression for transfer length is unconservative for one third of specimen ends, particularly for flame-cut strands at moderate-strength levels.

- AASHTO LRFD specifications are unconservative for approximately 15% of flame-cut ends of moderate strength mixtures. This unconservatism increases with decreasing compressive strength.
- To predict transfer length with more uniform levels of safety across the full range of practical concrete strengths, it is necessary to include the concrete strength parameter in the relevant design expressions.
- If flame-cutting of strands is allowed, transfer length design expressions must result in much higher estimates of transfer length than would be the case if only gradual release is allowed.
- A distinction between SCC and standard concrete in transfer length design provisions is only necessary for cases where flame-cutting of strands is **combined** with a relatively high proportion of GGBF slag.
- If gradual release is to be used, only one equation is necessary to model SCC and standard concrete.
- If sudden release is to be used or if there is no slag limitation, other expressions are necessary to predict transfer length for design.

- To check allowable stresses at transfer:

Table 4-10: Transfer Length Models Recommended for Use in Checking Concrete Stresses at Transfer

Release Method	Concrete Type	Transfer Length
Gradual	Standard & All SCC	$l_t = 0.53ksi^{-0.5} \frac{f_{pt}}{\sqrt{f'_{ci}}} d_b$
Sudden	Standard & SCC with Slag Limitation	$l_t = 0.65ksi^{-0.5} \frac{f_{pt}}{\sqrt{f'_{ci}}} d_b$
	SCC without Slag Limitation	$l_t = 0.71ksi^{-0.5} \frac{f_{pt}}{\sqrt{f'_{ci}}} d_b$

- For strength design and design for service loads:

Table 4-11: Transfer Length Models Recommended for Design

Prestress Release Method	Concrete Type	Transfer Length
Gradual	Standard & All SCC	$l_t = 0.64ksi^{-0.5} \frac{f_{pt}}{\sqrt{f'_{ci}}} d_b$
Sudden	Standard & SCC with Slag Limitation	$l_t = 0.78ksi^{-0.5} \frac{f_{pt}}{\sqrt{f'_{ci}}} d_b$
	SCC without Slag Limitation	$l_t = 1.02ksi^{-0.5} \frac{f_{pt}}{\sqrt{f'_{ci}}} d_b$

CHAPTER 5

DEVELOPMENT LENGTH TEST PROGRAM

5.1 INTRODUCTION

The development length test program was characterized by flexural tests of all sixteen T-beam specimens. Four beams of varying length were cast for each of the four mixes, and each beam was tested once in flexure for this test program. Preparation for development length testing began after two sets of specimens had been cast. Testing began for each set of specimens after at least 28 days of curing. This chapter provides details on development length testing configuration, instrumentation, procedure, and results.

5.2 TEST APPROACH

As discussed in Section 2.2.3, the development length in a prestressed member is the bonded tendon length required to develop the full resistance of the tendons, f_{ps}, at the nominal strength of the member. Unfortunately, determining this tendon length cannot be achieved within the bounds of a single experiment. Therefore, a more indirect method by trial and error was employed to quantify the development length.

For this test program, four specimens of varying lengths were cast for each mix. The lengths of the beams were varied to create different embedment lengths for each of the beams in order to determine the necessary bonded length to ensure a favorable flexural failure. As discussed in Section 2.2.4, embedment length, l_e, can be defined as the

bonded length of tendon from the beginning of bond of the tendon to the cross section for which strength capacity is being assessed. The critical section of the member is usually taken as the cross section closest to the beginning of bond at which the member needs to develop its full flexural resistance. If the embedment length at a cross section is shorter than the development length, a bond failure will occur before the section can develop its full flexural capacity. Design of such cross sections should reflect the reduced strand stress achievable prior to bond failure.

Each beam was loaded to failure and then evaluated based on failure type. Three distinct failure modes were identified: flexural, flexural with moderate strand slip, and bond failure. The failure type indicated whether the bonded length of strand was adequate to fully develop the resistance of the tendons necessary to achieve full flexural strength of the member at the critical section.

Thus the tendon behavior and magnitude of the ultimate bending moment indicated whether the embedment length provided exceeded or fell short of the development length. If the embedment length was shorter than the development length, either a bond failure or strand slip occurred. Thus through a series of tests involving a variety of embedment lengths, the development length was identified to be within certain bounds.

5.3 TEST CONFIGURATION

Based on the aforementioned test approach, a testing configuration was employed for all flexural tests to achieve a variety of failure modes. The flexural test setup and methodology used to determine specimen geometry are presented in this section.

5.3.1 DETERMINATION OF SPECIMEN LENGTH

The individual beam lengths were dependent upon several geometrical parameters of the flexural test setup. The flexural test setup, depicted by Figure 5-1, consisted of a simply supported beam loaded by two equal concentrated loads. The concentrated loads, centered about midspan, were separated by a distance of three feet.

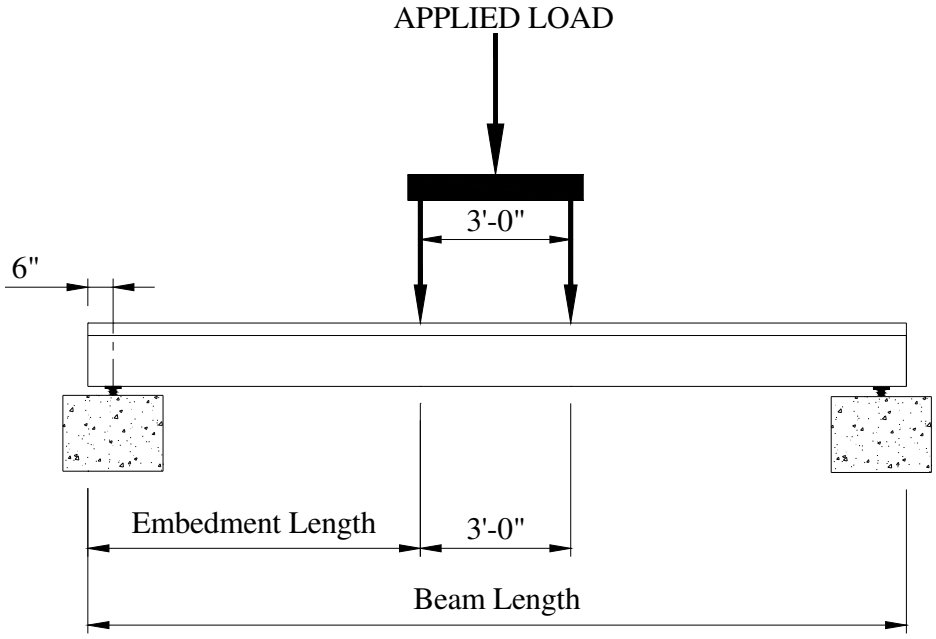

Figure 5-1: Load Test Setup

The four beam lengths were based on fractions of the required embedment length as recommended by ACI and AASHTO. Using the expression for development length, previously described as Equation 2-1, the estimated development length, $l_{d,est}$, of the beams was approximated by using a nominal strand diameter of 0.515 in., an f_{ps} value of 270 ksi, and an f_{pe} value of 165 ksi. Using these values, it was determined that the approximate code-required development length for these test specimens was 80 in.

In order to test the effectiveness of the prediction model, four fractions of this approximate ACI development length were tested to estimate the actual dvelopment length. The embedment lengths, l_e, tested were 150%, 100%, 75%, and 50% of the estimated development length, $l_{d,AASHTO.}$. Each specimen length was determined by providing the desired embedment length on each end of the simply supported beam and allowing for a constant 3-ft spacing between the applied loads. Simple supports were located 6 in. from each beam end. Therefore, the shear span for each specimen was equal to the embedment length minus 6 in. The embedment and beam length matrix is presented in Table 5-1.

Table 5-1: Flexural Specimen Embedment and Beam Length Matrix

Embedment Length		Beam Length	Beam ID
150% $l_{d,AASHTO}$	120 in.	276 in. (23'-0")	A
100% $l_{d,AASHTO}$	80 in.	196 in. (16'-4")	B
75% $l_{d,AASHTO}$	60 in.	156 in. (13'-0")	C
50% $l_{d,AASHTO}$	40 in.	116 in. (9'-8")	D

5.3.2 SHEAR REINFORCEMENT

Minimum shear reinforcement was provided to provide adequate shear capacity for each specimen to reach its full flexural capacity under applied test loads. Appendix B contains details of the stirrup spacing for each specimen group. For all specimen groups other than the D group (50% $l_{d,AASHTO}$), only minimum transverse reinforcement (maximum stirrup spacing) was required. Stirrup spacing was halved in some portions of the shear spans for the D specimens so that a shear failure would not occur prior to a flexure or

bond failure. As will be seen, no web-shear cracking was observed in any of the flexural tests.

5.3.3 Flexural Test Setup

As mentioned previously, the flexural test setup consisted of a simply supported beam loaded by two concentrated loads at the critical section. Steel supports located at 6 in. rested on steel plates embedded in reinforced concrete blocks to elevate and support the specimens during testing. These supports can be seen in Figure 5-2.

Figure 5-2: Steel Supports for Flexural Testing

Loading was applied by displacement of a hydraulic actuator attached to a reaction frame. The reaction frame and hydraulic actuator may be seen in Figure 5-3. Load was transferred from the actuator to the specimen by means of a spreader beam resting on two steel rollers spaced three feet apart. Thus, a 3-ft length of uniform bending moment due to applied loads was induced in the middle of the beam span. The rollers transferred the load to steel plates mounted to the beam at the critical sections. Figure 5-4 depicts these

load application components. Table 5-2 presents the casting and flexural testing dates for all specimens.

Figure 5-3: Reaction Frame and Hydraulic Actuator

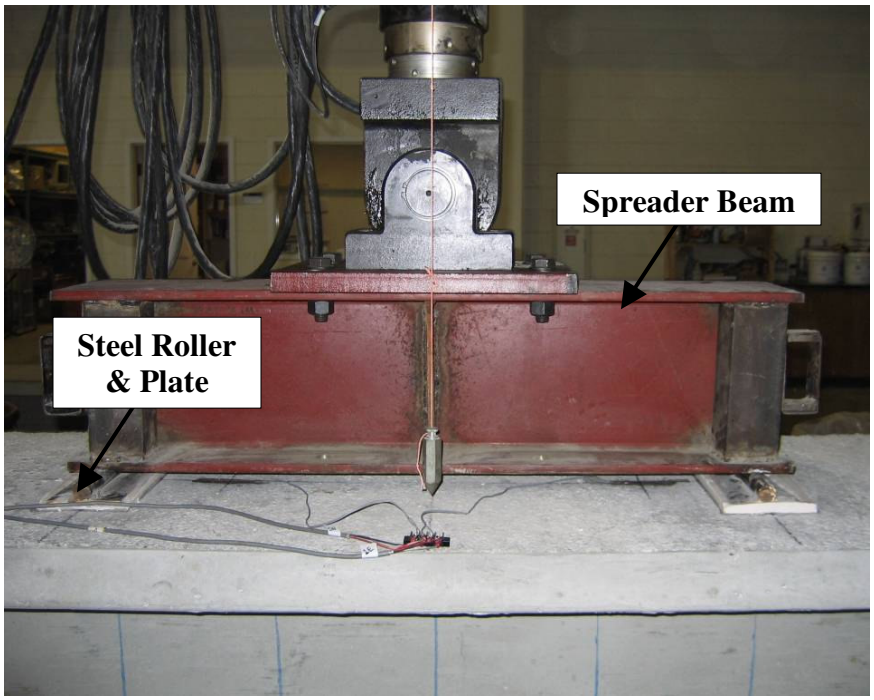

Figure 5-4: Load Application Components

Table 5-2: Specimen Ages at Flexural Testing

Specimen	Casting Date	Prestress Transfer Date	Flexural Test Date	Concrete Age at Test (days)
STD-M-A	11/14/2005	11/17/2005	5/19/2006	186
STD-M-B	11/14/2005	11/17/2005	6/5/2006	203
STD-M-C	11/14/2005	11/17/2005	6/8/2006	206
STD-M-D	11/14/2005	11/17/2005	6/21/2006	219
SCC-MA-A	12/13/2005	12/14/2005	7/27/2006	226
SCC-MA-B	12/13/2005	12/14/2005	7/20/2006	219
SCC-MA-C	12/13/2005	12/14/2005	7/18/2006	217
SCC-MA-D	12/13/2005	12/14/2005	7/6/2006	205
SCC-MS-A	6/26/2006	6/29/2006	8/31/2006	66
SCC-MS-B	6/26/2006	6/29/2006	9/7/2006	73
SCC-MS-C	6/26/2006	6/29/2006	9/12/2006	78
SCC-MS-D	6/26/2006	6/29/2006	9/21/2006	87
SCC-HS-A	8/21/2006	8/22/2006	10/5/2006	45
SCC-HS-B	8/21/2006	8/22/2006	10/3/2006	43
SCC-HS-C	8/21/2006	8/22/2006	9/28/2006	38
SCC-HS-D	8/21/2006	8/22/2006	9/26/2006	36

5.4 INSTRUMENTATION

Several instruments were used to monitor the performance of each specimen during flexural testing. A description of the instruments used during the development length test program to monitor specimen response is presented in this section.

5.4.1 MEASUREMENT OF APPLIED LOAD

The applied load was measured by a built-in force transducer (load cell) between the hydraulic actuator and the spreader beam. Each of the two load cells in the test program was calibrated over its full scale prior to beginning the testing.

5.4.2 MEASUREMENT OF DISPLACEMENTS

Linear potentiometers were used to measure all displacements. Potentiometers were used to measure vertical deflection relative to the floor under each of the load points as well as directly under midspan. Potentiometers were also placed under the flange overhang on each face at each support cross section to measure any support deflections throughout each test. These potentiometers were also used as a safety measure to monitor any possible rocking of the beam while undergoing deflection. The actual displacement of the beam relative to its supports was calculated using the output of these potentiometers. To eliminate reading inaccuracies due to surface imperfections, 2 in. x 2 in. glass microscope slides were glued to the surface of the beam at the point of contact for each potentiometer. Figures 5-5, 5-6 and 5-7 show the use of 4-in. linear potentiometers to monitor displacement.

Figure 5-5: Linear Potentiometers Used to Monitor Beam Deflection

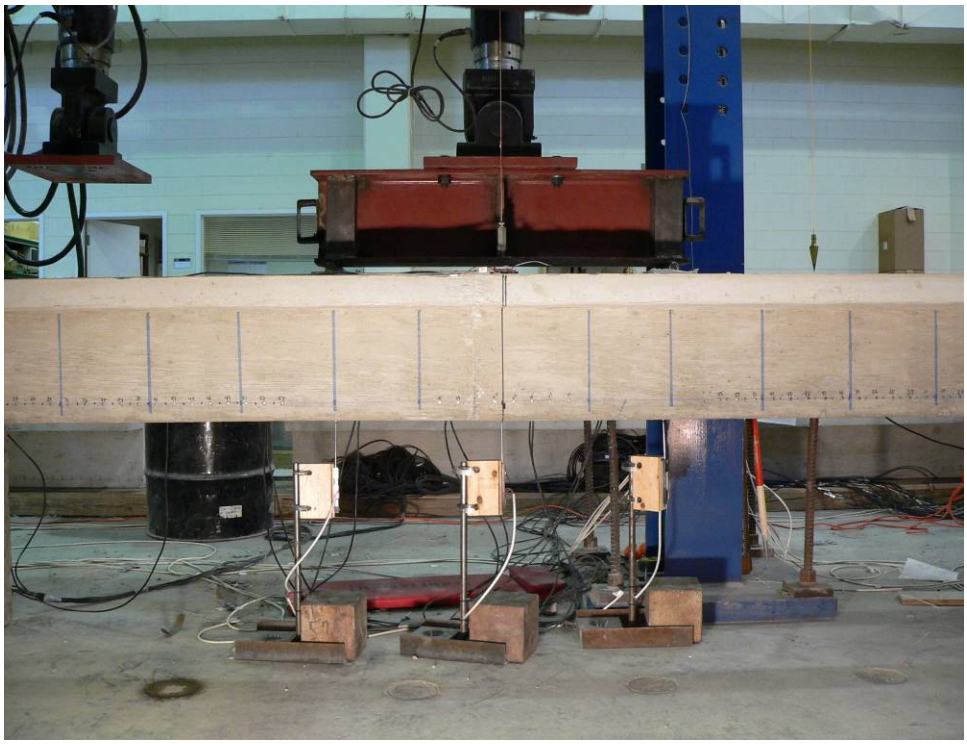

Figure 5-6: Linear Potentiometer Setup

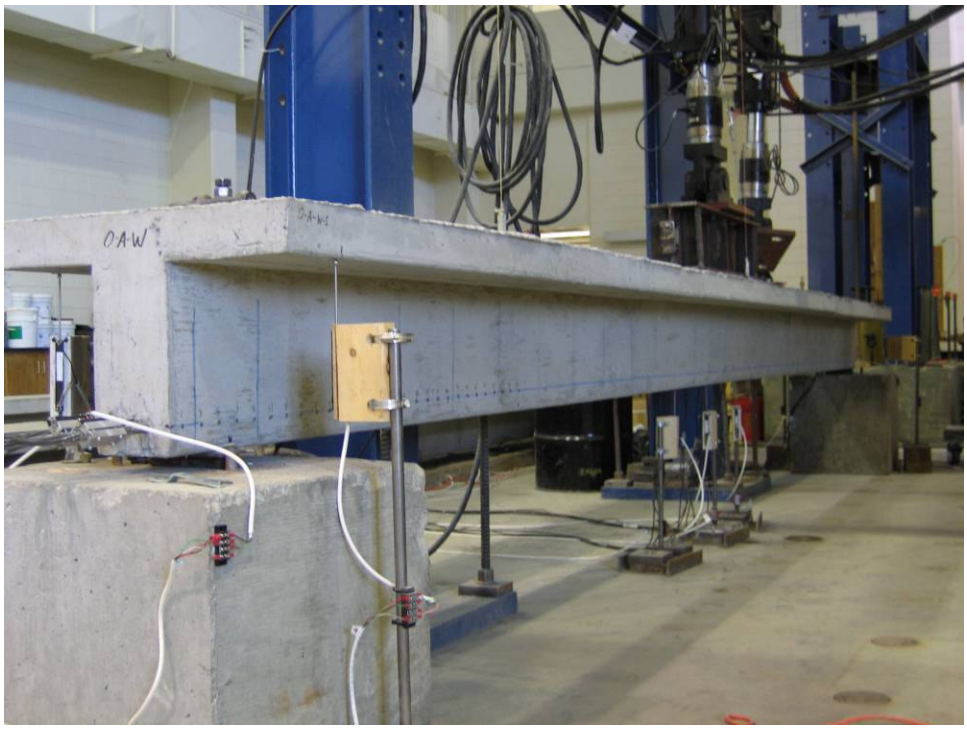

Figure 5-7: Linear Potentiometer Used to Monitor Support Deflection

5.4.3 Measurement of Strand Slip

Linear potentiometers attached to each strand at the end of the beam were used to measure strand slip during flexural load testing. All strand movement was measured relative to the end of the beam. The potentiometers were mounted onto brackets which were then attached to the strands. Figure 5-8 shows the 2-in. linear potentiometers used to measure strand slip.

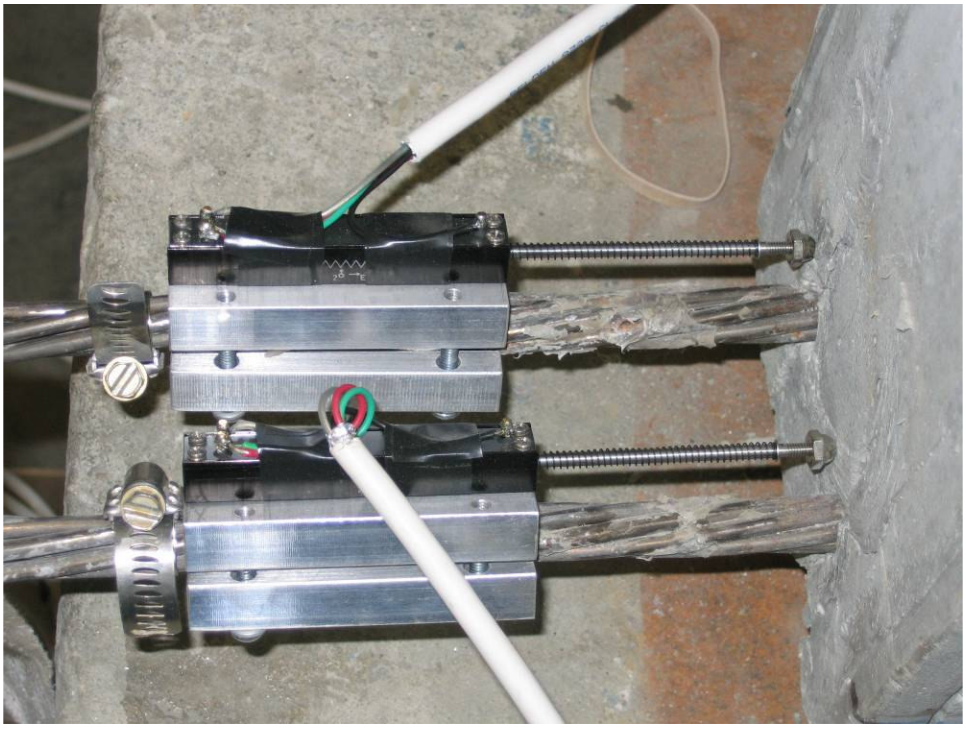

Figure 5-8: Linear Potentiometers Used to Measure Strand Slip

5.4.4 Measurement of Strains at Extreme Compression Fiber

Flexural compressive strains at the top surface of the beam in the uniform moment region were monitored during flexural testing using two Electrical Resistance Strain Gauges (ERSGs) with a 60 mm gauge length. For the test on the first specimen (STD-M-A), the strain gauges were located 12 in. on each side of the midspan section along the centerline of the beam. However, for all other tests, the strain gauges were placed at 9 in. on each

side of midspan. At this location, the strain gauges fell directly over a stirrup, and thus an eventual cracked cross section, for all tests. Figure 5-9 shows the use of ERSGs to measure strains at the extreme compression fiber.

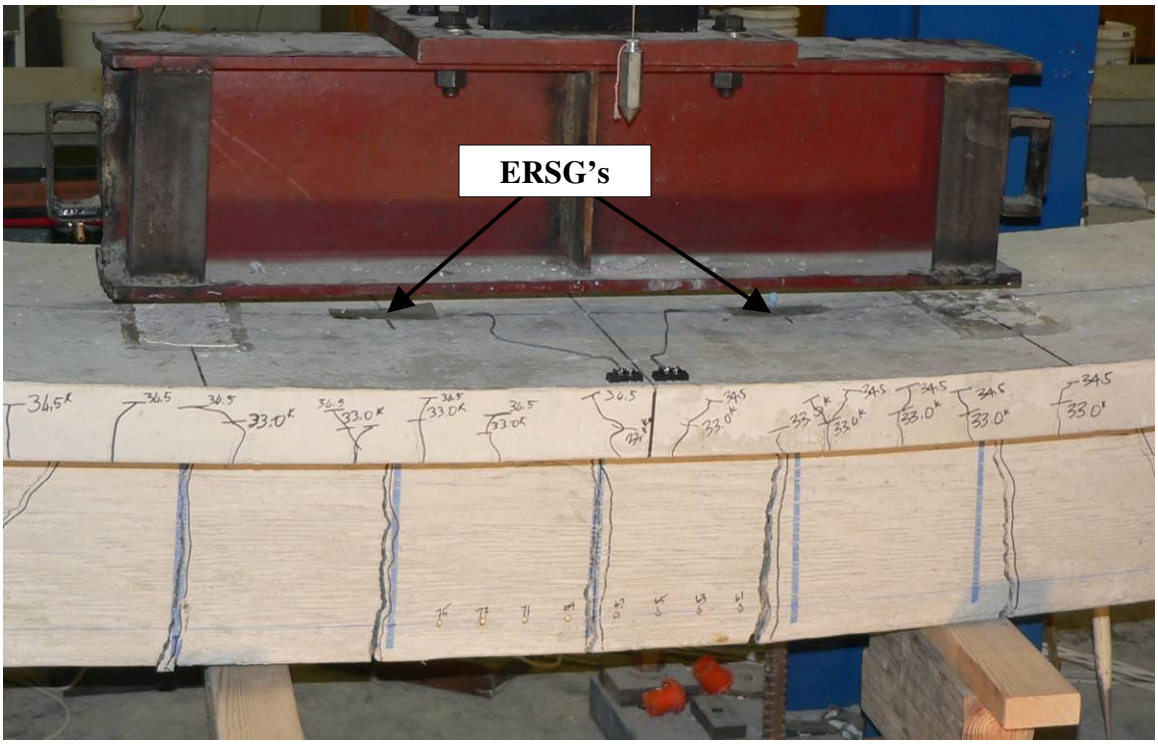

Figure 5-9: Strain Gauges Used to Measure Extreme Compression Fiber Strains

5.4.5 DATA ACQUISITION

All instrumentation signals were read at 0.5-sec intervals by an Optim MEGADAC Data Acquisition/Signal Conditioning Unit and then transferred to a laptop computer where all data were recorded and stored. Deflections and strain readings were monitored during the course of each test and hand recorded at critical loading steps in a test log as a backup. The data acquisition system used for flexural testing is shown in Figure 5-10.

Figure 5-10: Data Acquisition System

5.5 TEST PROCEDURE

While undergoing flexural testing, all specimens were subjected to acoustic emissions (AE) monitoring as well as part of a collaborative effort between researchers at Auburn University. The results of AE monitoring are not presented within the body of this thesis; however, due to AE monitoring, a specific loading scheme was devised and followed for all flexural tests.

All loads were applied via manual displacement control using a closed-loop MTS hydraulic testing system. The loading pattern contained five pairs of load cycles, resulting in a total of 10 loading cycles. Figure 5-11 depicts the 10 load cycles versus time. All levels of applied loading used in the load cycles were functions of four load values determined prior to the flexural testing of each specimen. The first of these three loads, P_{min}, was the minimum load, 500 lbs, which was maintained after the start of the

test. The next of the three loads, P_s, was the service-level design load for Alabama Department of Transportation (ALDOT) bridge girders. This load was the applied load computed to cause zero stress in the bottom fiber of the beam at the critical sections.

The next load value which was critical to the loading cycles was the flexural cracking load, P_{cr}. This load value, unlike the other three, was not determined before the test. During the 5th load cycle, the load was applied at a rate of approximately 0.1 kips/sec until the cracking load was reached. Achievement of the cracking load was signaled by a slight drop in load accompanied by visible cracking. Although a calculated cracking load, $P_{cr,calc}$, was calculated prior to the test using the assumption that cracking would coincide with a bottom-fiber tensile stress equal to $7.5\sqrt{f'_c}$, the actual cracking load, P_{cr}, was used to determine the load value for the 6th cycle.

Finally, the last of the three load values determined prior to testing, P_n, was the load computed to cause a bending moment equal to the nominal moment capacity, M_n, at the critical section. The nominal moment was computed using AASHTO LRFD procedures. For the determination of $M_{n,AASHTO}$, an f_{pu} value of 270 ksi was used along with an f'_c value equal to the 28-day cylinder compressive strength. In addition, $f_{ps,AASHTO}$, was calculated in accordance with Article 5.7.3.1.1 of AASHTO LRFD. Since the non-prestressed top-flange reinforcement was estimated to be in tension when subjected to $M_{n,AASHTO}$, but not necessarily beyond the yield strain, a strain compatibility analysis was employed to determine f_{ps} and $M_{n,AASHTO}$.

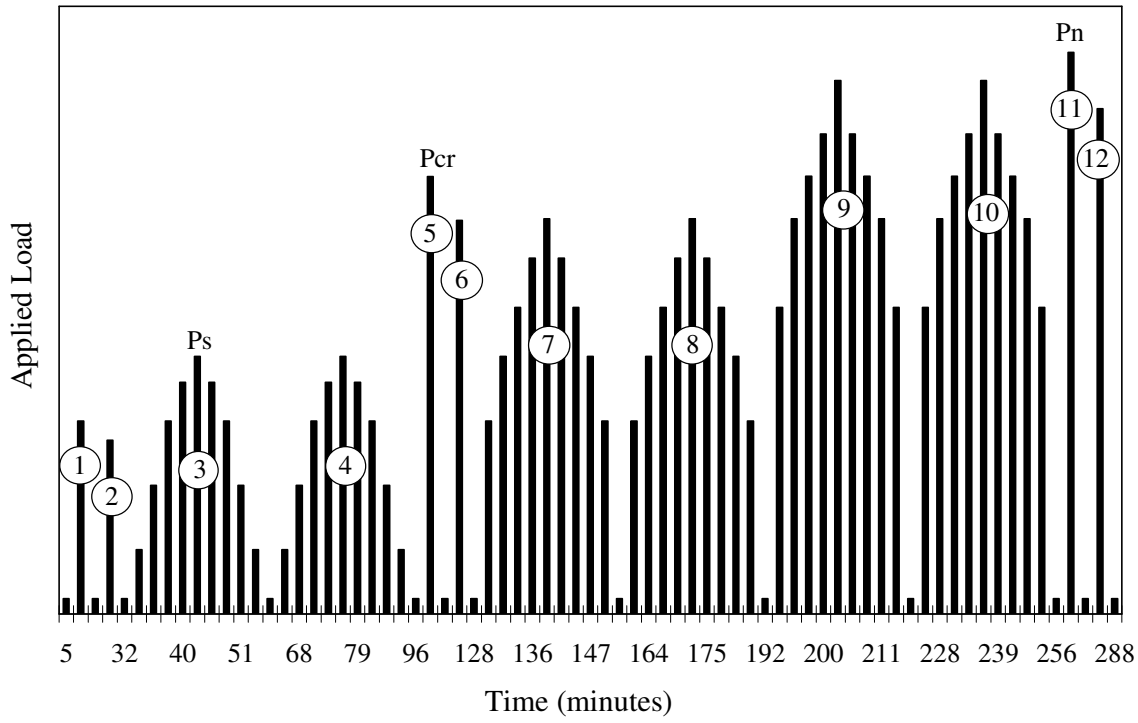

Figure 5-11: Development Length Testing Load Cycles

At the end of the AE monitoring cycles, cracks were marked with the corresponding causative load level for the majority of the tests. However, AE monitoring was paused during a few of the tests to mark cracks. In all cases, crack patterns were recorded throughout the entire loading process.

At the end of AE monitoring load cycles, all AE sensors were removed from the beam, and then loading resumed beyond the nominal flexural capacity of the beam. At this point, beam displacement was applied at a rate of approximately 0.1 in. per minute. In most cases, testing ceased after rupturing of the prestressing tendons. In a few cases, testing ceased after concrete crushing at the extreme compression fiber. Specific details of each flexural test are given in Section 5.8.

5.6 ANALYSIS PROCEDURES

Two types of flexural analysis procedures were used for this study including a procedure based upon AASHTO LRFD recommendations and another based upon strain compatibility and nonlinear material properties. The AASHTO procedure used for the determination was outlined in the previous section. The strain compatibility procedure is presented in this section. The analysis procedures used for this study were based upon the same procedures described in Barnes et al. (1999). Therefore, the description of these procedures is very similar to the description presented within that report.

Stresses and strains in the specimens prior to flexural testing were computed based upon a time-dependent linear elastic, uncracked response. Transformed properties were used instead of gross section properties. Stress-strain relationships for the concrete were based upon strength and stiffness results of tests conducted on representative test cylinders. Stress-strain relationships for the prestressed and non-prestressed steel were based upon results of tests conducted by the manufacturer of each material. Complete stress-strain responses for the concrete and steel were modeled according to relationships presented by Collins and Mitchell (1991) using the strength and stiffness parameters obtained from tests. Relaxation of the prestressing steel was modeled as described by Collins and Mitchell (1991) for low-relaxation strand. Creep and shrinkage deformations were calculated according to the relevant provisions of the AASHTO LRFD (2004) specifications. The stresses and strains in the concrete and steel were calculated for each specimen at five time events including immediately prior to transfer, immediately after

transfer, four days after transfer, after the movement of supports, and immediately prior to flexural testing.

Using the layer-by-layer approach described by Collins and Mitchell (1991), stress and moment-curvature analysis of each specimen during flexural testing was performed. The beam cross section was discretized into several thin layers, which were each analyzed as an individual member subjected to axial loading. The relative deformations of these layers were constrained by the "plane sections remain plane" hypothesis. Each beam section was subdivided into forty-one layers of unequal thickness. Thinner concrete layers were used in the flange of the beam, where nonlinear behavior of concrete was expected, while thicker layers were used to section the stem of the section. The rows of mild steel reinforcement and prestressing strand represented an additional two layers. The layers for each beam are depicted by Figure 5-12. The elastic uncracked analysis described previously was used to determine initial stresses and strains for each layer.

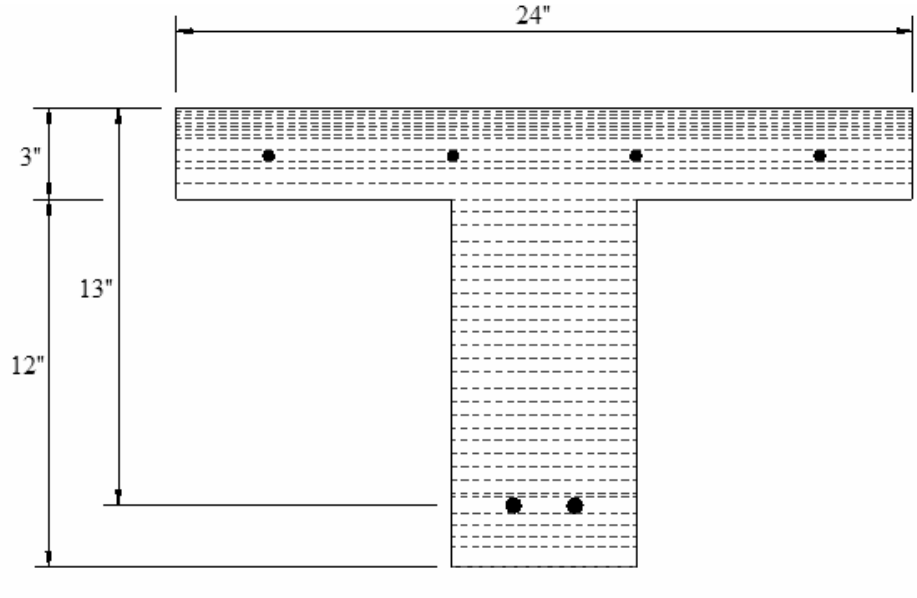

Figure 5-12: Discretized Layers for Section Analysis

For each value of top fiber strain, an iterative approach was used to solve for the neutral axis position (and resulting curvature) that satisfied force equilibrium on the cross section (sum of all layer forces equal to zero). Once the neutral axis was located for a given extreme fiber strain, the corresponding bending moment was calculated by summing the individual moments resulting from the layer axial forces. Repetition of this process for several top fiber strains resulted in the full cracked-section moment-curvature response. For the cracked-section response, concrete layers were modeled as resisting tensile stresses up to the modulus of rupture; layers with larger strains carried no tensile stress.

Tension stiffening was considered in the prediction of the load-deflection response for each specimen based upon the procedure described by Collins and Mitchell (1991). After cracking, concrete fibers located within 7.5 bar or strand diameters of reinforcement were assigned average tensile stresses according to the relationship described by Collins and Mitchell (1991). Figure 5-13 depicts the zones of concrete fibers affected by tension stiffening. The tension-stiffened model was only used to compute the beam deformations up to the ultimate load. The calculated load-displacement relationships for each flexural specimen are presented with the actual test values in Appendix H. The ultimate load was determined based on the unstiffened response of the cracked section only.

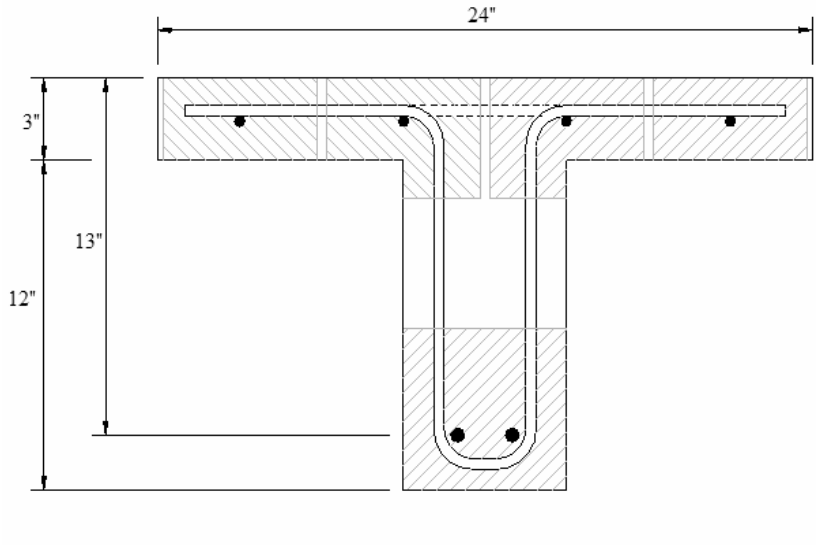

Figure 5-13: Concrete Fibers affected by Tension Stiffening

This analysis was conducted before development length testing for all specimens. The nominal moment according to the AASHTO procedure, $M_{n,AASHTO}$, and according to strain compatibility, $M_{n,calc}$, were calculated prior to testing. A precise ACI/AASHTO development length, $l_{d,AASHTO}$, for each specimen was also determined using the calculated effective stress in the strands at the critical section immediately prior to development length testing, $f_{pe,test}$. This value of effective prestress was computed using the linear elastic, uncracked, time-dependent procedure described above. Using the strain compatibility flexural analysis procedure, the strain at the strand level at the nominal resistance of the member, $\varepsilon_{max,calc}$, was calculated as an indication of the strand strain necessary to achieve the full flexural capacity of the member. Also using the strain compatibility flexural analysis procedure, the stress in prestressed reinforcement at the estimated nominal strength, $f_{ps,calc}$, was also calculated. In addition, $f_{ps,AASHTO}$, which was discussed in Section 5.5, was calculated in accordance with Article 5.7.3.1.1 of AASHTO LRFD. These values are all presented in Table 5-3.

Table 5-3: Variables Calculated from Analysis Procedures

Test Specimen	l_e (in.)	$l_{d,AASHTO}$ (in.)	$f_{pe,test}$ (kips)	$f_{ps,AASHTO}$ (kips)	$M_{n,AASHTO}$ (kip-ft)	$f_{ps,calc}$ ksi	$M_{n,calc}$ (kip-ft)	$\varepsilon_{max,calc}$ (in./in.)
STD-M-A	120	75	178	264	92.5	276	96.0	0.0593
SCC-MA-A	120	78	170	265	93.7	287	100.6	0.0684
SCC-MS-A	120	72	188	265	96.7	285	100.6	0.0625
SCC-HS-A	120	71	192	266	98.7	301	107.4	0.0847
STD-M-B	80	78	169	264	92.5	277	96.0	0.0522
SCC-MA-B	80	80	165	265	93.7	287	100.6	0.0655
SCC-MS-B	80	74	183	265	96.7	284	100.6	0.0614
SCC-HS-B	80	71	192	266	98.7	300	107.4	0.0874
STD-M-C	60	78	168	264	92.5	277	96.0	0.0513
SCC-MA-C	60	80	165	265	93.7	288	100.6	0.0661
SCC-MS-C	60	76	182	265	96.7	285	100.6	0.0623
SCC-HS-C	60	71	192	266	98.7	302	107.4	0.0875
STD-M-D	40	76	174	264	92.5	276	96.0	0.0503
SCC-MA-D	40	79	168	265	93.7	287	100.6	0.0650
SCC-MS-D	40	73	184	265	96.7	284	100.6	0.0627
SCC-HS-D	40	71	192	266	98.7	302	107.4	0.0871

5.7 FAILURE MODES

As mentioned previously, the predicted nominal moment capacity was calculated by two methods: AASHTO LRFD and strain compatibility. For the purposes of notation the nominal moment computed from AASHTO LRFD recommendations shall be $M_{n,AASHTO}$ and the nominal moment computed by strain compatibility analysis shall be $M_{n,calc}$. Each specimen's ability to achieve and maintain the nominal moment capacity as predicted by these methods influenced the failure mode it was assigned. Three failure modes were observed during development length testing: flexural failure, flexural with slip failure, and bond failure. These failure modes are discussed in this section.

5.7.1 FLEXURAL FAILURE MODE

The flexural failure mode was characterized by a pure flexural failure. For a flexural failure, the nominal moment capacity was exceeded for both AASHTO and strain compatibility prediction models. In addition, no end slip was measured throughout the entire loading process. The first cracks were observed at or between the load points. The crack pattern was generally symmetric for this failure mode. For all flexural failures, both strands ruptured at a stress beyond their predicted ultimate capacity. Strand rupture occurred at or between the load points for all flexural failures. Failure was also accompanied by crushing of the concrete in the compression flange between the load points. Figure 5-14 depicts the typical crack pattern observed for a flexural failure.

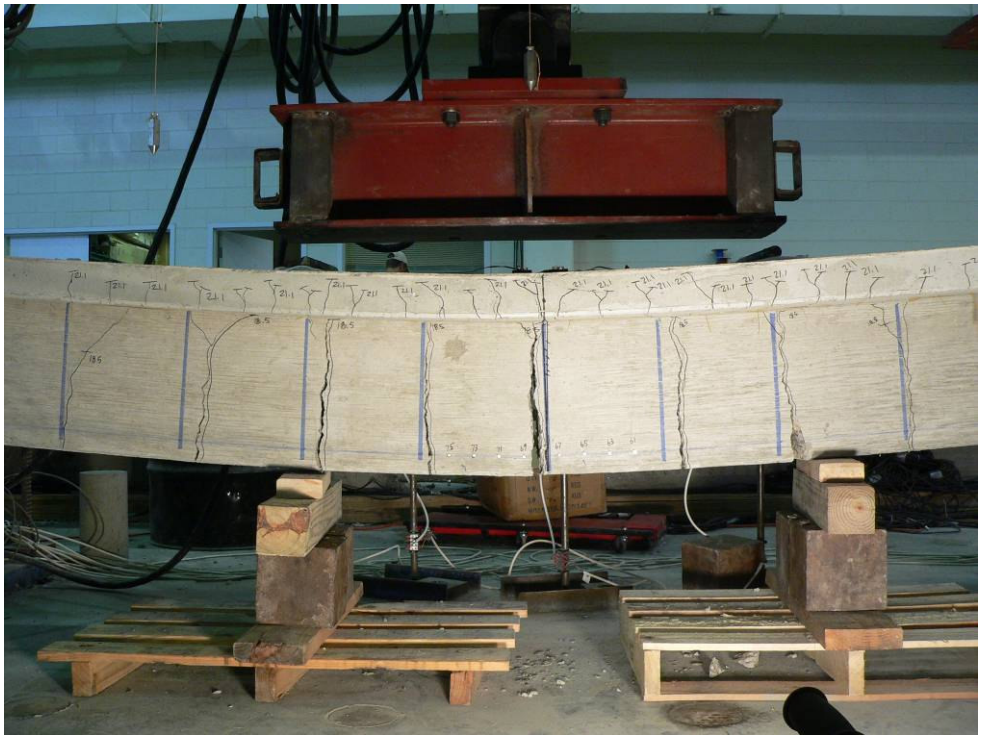

Figure 5-14: Flexural Failure Mode

5.7.2 FLEXURAL FAILURE WITH STRAND SLIP

The flexural with strand slip failure mode was characterized by flexural failure with moderate strand slip. For a flexural failure with slip, the nominal moment capacity was exceeded for both AASHTO and strain compatibility prediction models. The cracking patterns varied among different specimens more for this type of failure than for pure flexural failures. Also, for each of these failures, it was determined that the strand slip did not significantly affect the failure load of the beam. Concrete crushing of the extreme compression fiber was experienced by all specimens exhibiting this failure mode. For specimens satisfying this failure mode, the only case in which the strands did not rupture was in the case of Specimen SCC-MA-D. In that case, the load required to cause failure of the beam, exceeded the maximum load capacity for the actuator. Figure 5-15 depicts the typical crack pattern observed for a flexural-slip failure.

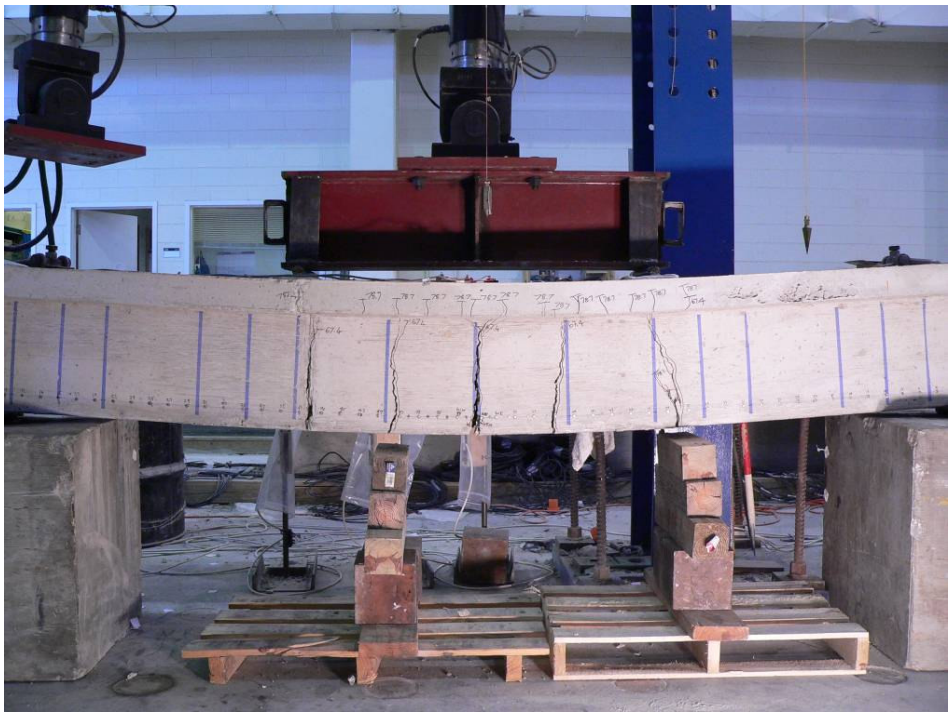

Figure 5-15: Flexural-Slip Failure Mode

5.7.3 BOND FAILURE

This failure mode was characterized by extreme strand slip leading to a premature shear failure. For the bond failure mode, the nominal flexural capacity of the section was not achieved. This failure began with a large strand slip at one end of the beam, resulting in a dramatic loss of load-carrying capacity of the section. Also, the crack pattern was asymmetric with a large crack forming just within the transfer length of the end of the beam which experienced strand slip. The stress in the strand at failure was much lower than its ultimate strength and strand rupture was not achieved. The bond failure mode was only observed in STD-M-D. Figure 5-16 depicts the crack pattern observed for the bond failure.

Figure 5-16: Bond Failure Mode (STD-M-D)

5.8 PRESENTATION OF TEST RESULTS

The results of the sixteen development length tests performed for this study are presented in this section. The load-deflection plot for each specimen can be found in Appendix H of this thesis. The results have been categorized into four groups, sectioned by embedment length. All moments reported in this section include the applied loads and self-weight of the girder. All deflections reported in this section are midspan deflections. A brief description of each test is included in this section as well as a presentation of significant load, deflection, strain, and strand slip magnitudes recorded during each test.

5.8.1 SPECIMENS WITH 120-IN. EMBEDMENT LENGTHS

For these tests, the embedment length, l_e, was targeted to be approximately 150% of the development length, $l_{d,\ AASHTO}$, calculated by the ACI/AASHTO expression. These beams were designed to have a 120-in. embedment length and given the designation, "A". Each specimen in this group was 23'-0" long. Flexural tests for these beams used the setup depicted in Figure 5-17. The load-deflection relationships for all four of these tests are shown in Figure 5-18. As would be expected because the embedment length significantly exceeded $l_{d,\ AASHTO}$, all of these specimens experienced flexural failure modes.

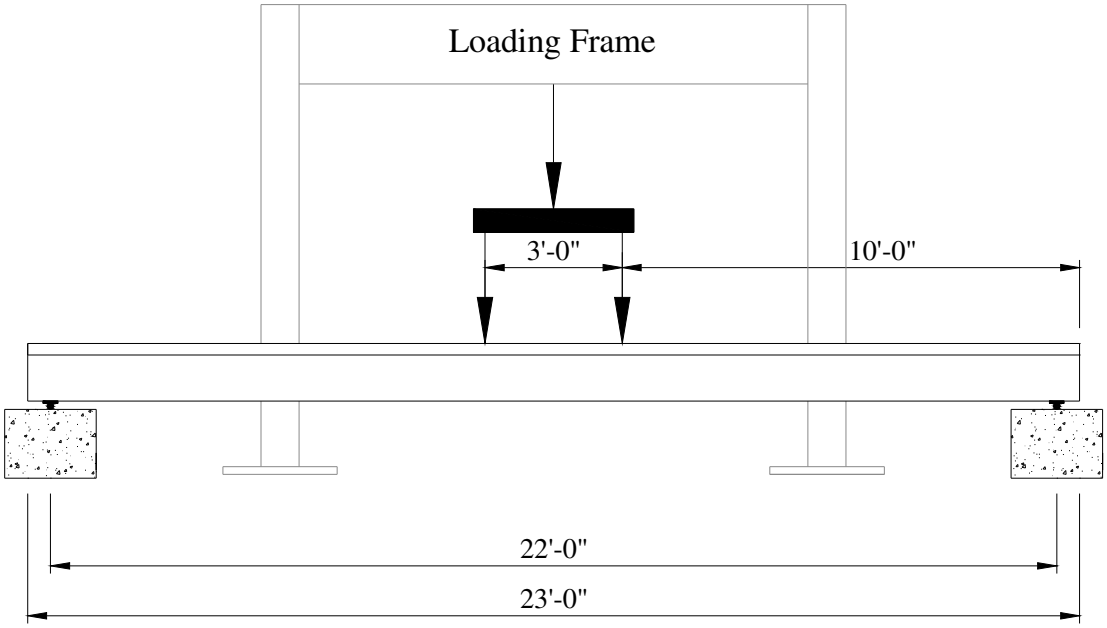

Figure 5-17: Test Setup for Specimens with l_e = 120 in.

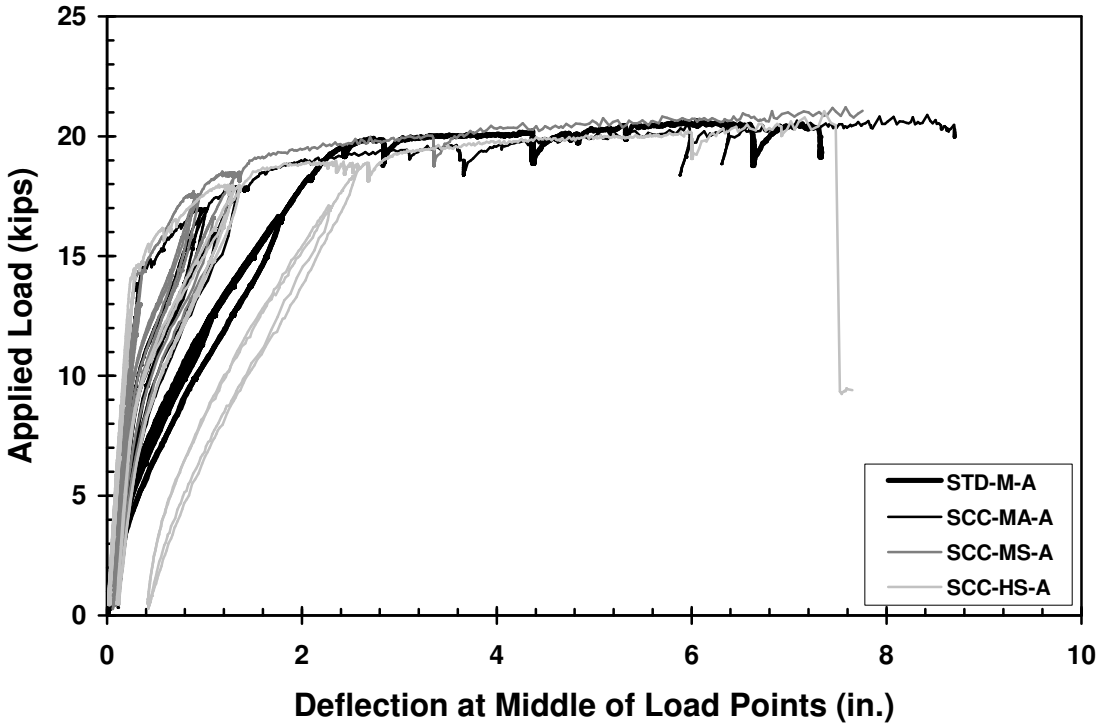

Figure 5-18: Load-Deflection Relationship for Specimens with l_e = 120 in.

5.8.1.1 STD-M-A

This was the first specimen tested for the development length test program. Before the beginning of the development length test, this specimen was prematurely loaded beyond its cracking load. Due to this error, the cracking load and moment as well as the deflections at cracking are unknown. Therefore, the load-deflection diagram shown in Figure 5-18 and given in Appendix H shows the beam to be much less stiff than would be expected if it was initially uncracked.

The specimen failed in a flexural manner. No strand end slip was detected during the test. The maximum load reached for this specimen was 20.5 kips at a maximum deflection of 7.4 in. The maximum moment resisted by this beam, M_{max}, was 11% greater than $M_{n,calc}$ and 15% greater than $M_{n,AASHTO}$. The stress in the strands at the actual maximum moment was estimated to be 306 ksi. The beam lost its load-carrying capacity due to strand rupture. No web-shear cracking was observed in this specimen. The crack pattern corresponding to the maximum load for this beam is depicted in Figure 5-19. The transfer lengths, l_t, measured on each of the beam are shown in all the crack pattern figures.

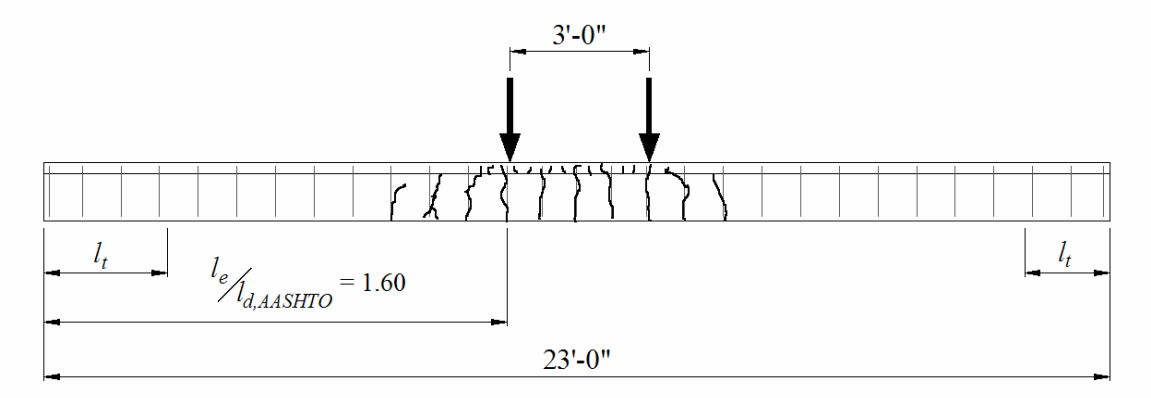

Figure 5-19: Crack Pattern for STD-M-A at Failure

5.8.1.2 SCC-MA-A

This specimen failed in a flexural manner. No strand end slip was detected during the test. The first flexural cracking was observed at a load of 13.8 kips, corresponding to a deflection of 0.33 in. The cracking moment, M_{cr}, for this specimen was 12% greater than the calculated cracking moment, $M_{cr,calc.}$ The maximum load reached for this specimen was 20.6 kips, corresponding to a deflection of 8.7 in. The maximum moment resisted by this beam, M_{max}, was 6% greater than $M_{n,calc}$ and 14% greater than $M_{n,AASHTO.}$ The stress in the strands at the actual maximum moment was estimated to be 304 ksi. The beam lost its load-carrying capacity due to strand rupture. No web-shear cracking was observed in this specimen. The crack pattern corresponding to the maximum load for this beam is depicted in Figure 5-20.

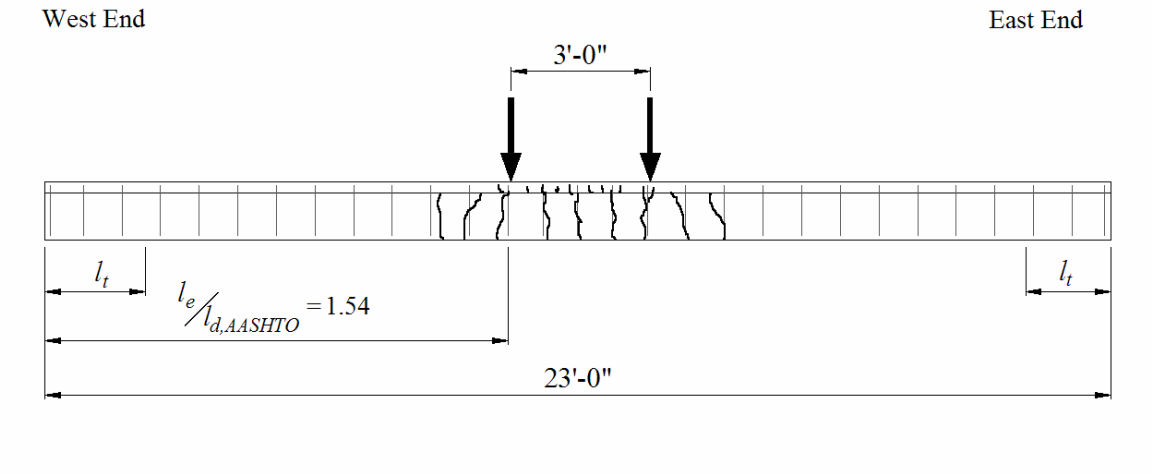

Figure 5-20: Crack Pattern for SCC-MA-A at Failure

5.8.1.3 SCC-MS-A

This specimen failed in a flexural manner. No strand end slip was detected during the test. The first flexural cracking was observed at a load of 14.4 kips, corresponding to a deflection of 0.36 in. The cracking moment, M_{cr}, for this specimen was 9% greater than the calculated cracking moment, $M_{cr,calc.}$ The maximum load reached for this specimen was 21.1 kips, corresponding to a deflection of 7.8 in. The maximum moment resisted by this beam, M_{max}, was 8% greater than $M_{n,calc}$ and 13% greater than $M_{n,AASHTO.}$ The stress in the strands at the actual maximum moment was estimated to be 309 ksi. The beam lost its load-carrying capacity due to strand rupture. No web-shear cracking was observed in this specimen. The crack pattern corresponding to the maximum load for this beam is depicted in Figure 5-21.

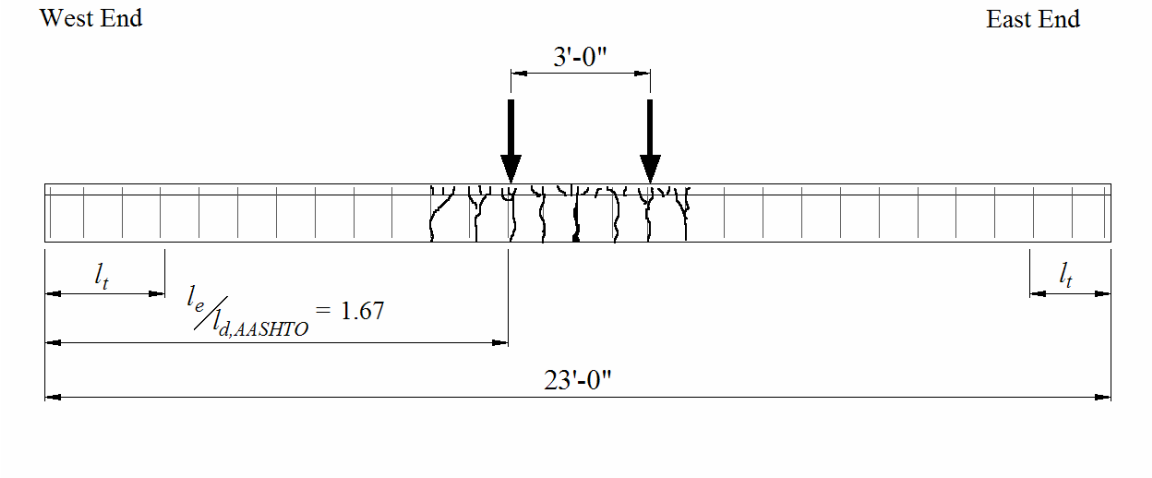

Figure 5-21: Crack Pattern for SCC-MS-A at Failure

5.8.1.4 SCC-HS-A

This specimen failed in a flexural manner. No strand end slip was detected during the test. The first flexural cracking was observed at a load of 14.1 kips, corresponding to a deflection of 0.27 in. The cracking moment, M_{cr}, for this specimen was 1% lower than the calculated cracking moment, $M_{cr,calc.}$ The maximum load reached for this specimen was 21.0 kips, corresponding to a deflection of 7.7 in. The maximum moment resisted by this beam, M_{max}, was 1% greater than $M_{n,calc}$ and 10% greater than $M_{n,AASHTO.}$ The stress in the strands at the actual maximum moment was estimated to be 304 ksi. The beam lost its load-carrying capacity due to strand rupture. No web-shear cracking was observed in this specimen. The crack pattern corresponding to the maximum load for this beam is depicted in Figure 5-22.

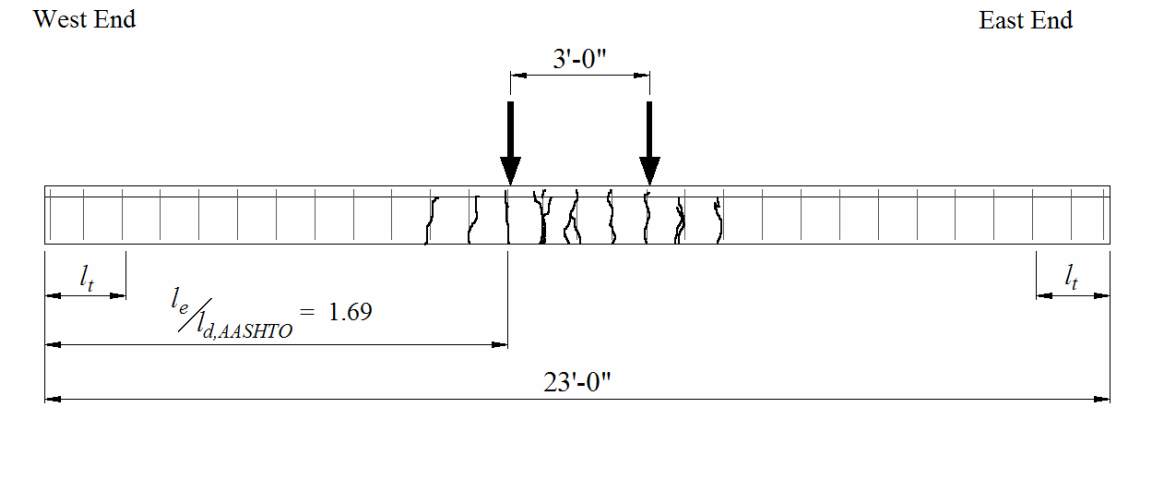

Figure 5-22: Crack Pattern for SCC-HS-A at Failure

5.8.2 SPECIMENS WITH 80-IN. EMBEDMENT LENGTHS

For these tests, the embedment length, l_e, was targeted to be equivalent to the development length, $l_{d,\ AASHTO}$, calculated by the ACI/AASHTO expression. These beams were designed to have an 80-in. embedment length and given the designation "B". Each specimen in this group was 16'-4" long. Flexural tests for these beams used the setup depicted in Figure 5-23. The load-deflection relationships for all four of these tests are shown in Figure 5-24. All of these specimens experienced flexural failure modes.

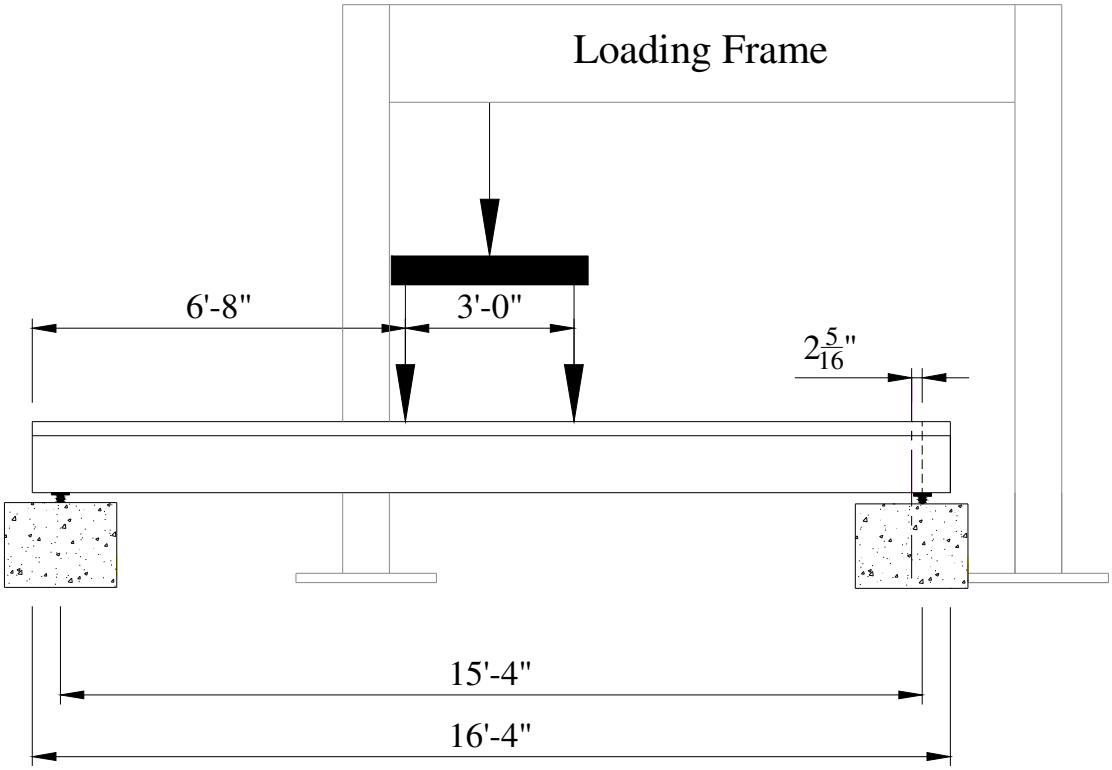

Figure 5-23: Test Setup for Specimens with l_e = 80 in.

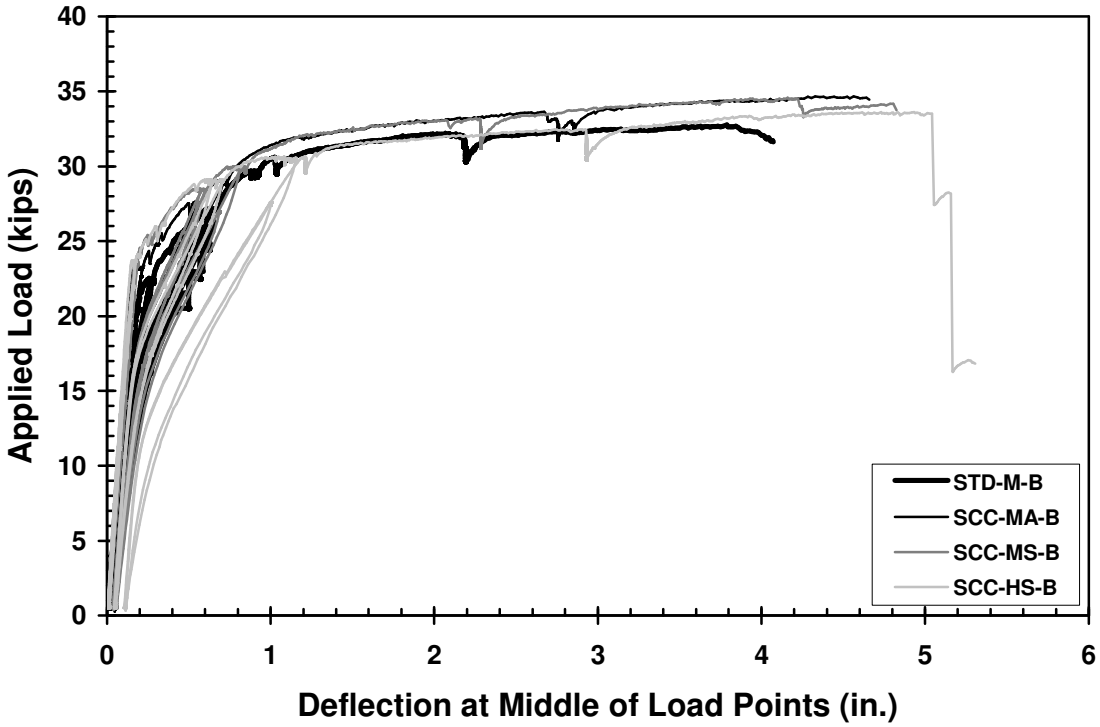

Figure 5-24: Load-Deflection Relationship for Specimens with l_e = 80 in.

5.8.2.1 STD-M-B

This specimen failed in a flexural manner. No strand end slip was detected during this test. The first flexural cracking was observed at a load of 21.5 kips, corresponding to a deflection of 0.22 in. The cracking moment, M_{cr}, for this specimen was 10% greater than the calculated cracking moment, $M_{cr,calc.}$ The maximum load reached for this specimen was 31.7 kips, corresponding to a deflection of 4.0 in. The maximum moment resisted by this beam, M_{max}, was 6% greater than $M_{n,calc}$ and 10% greater than $M_{n,AASHTO.}$ The stress in the strands at the actual maximum moment was estimated to be 294 ksi. The beam lost its load-carrying capacity due to strand rupture. No web-shear cracking was observed in this specimen. The crack pattern corresponding to the maximum load for this beam is depicted in Figure 5-25.

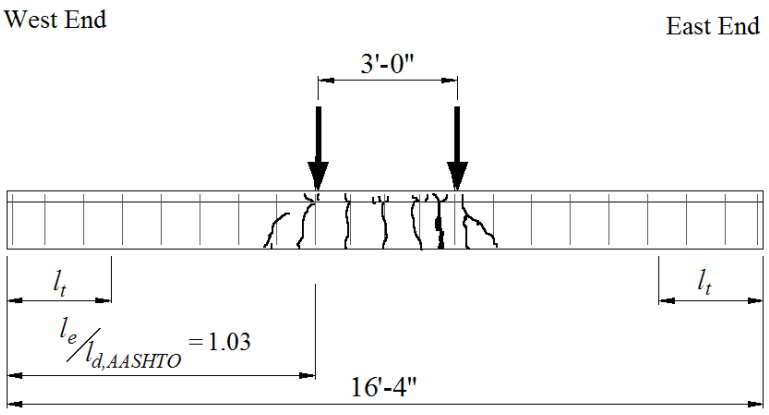

Figure 5-25: Crack Pattern for STD-M-B at Failure

5.8.2.2 SCC-MA-B

This specimen failed in a flexural manner. No strand end slip was detected during this test. The first flexural cracking was observed at a load of 23.2kips, corresponding to a deflection of 0.21 in. The cracking moment, M_{cr}, for this specimen was 16% greater than the calculated cracking moment, $M_{cr,calc.}$ The maximum load reached for this specimen was 34.6 kips, corresponding to a deflection of 4.7 in. The maximum moment resisted by this beam, M_{max}, was 10% greater than $M_{n,calc}$ and 18% greater than $M_{n,AASHTO.}$ The stress in the strands at the actual maximum moment was estimated to be 316 ksi. The beam lost its load-carrying capacity due to strand rupture. No web-shear cracking was observed in this specimen. The crack pattern corresponding to the maximum load for this beam is depicted in Figure 5-26.

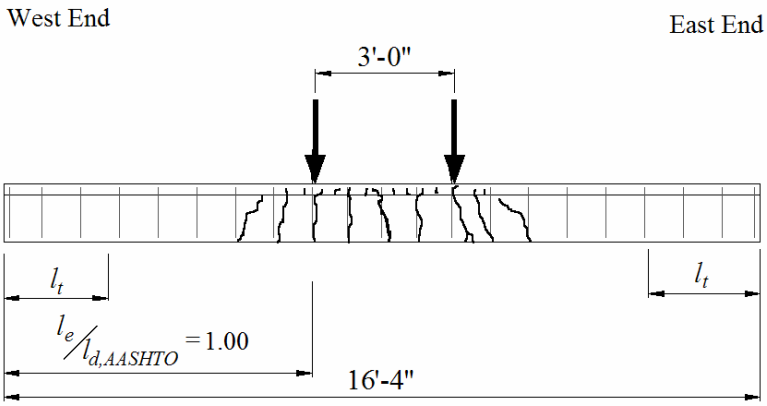

Figure 5-26: Crack Pattern for SCC-MA-B at Failure

5.8.2.3 SCC-MS-B

This specimen failed in a flexural manner. No strand end slip was detected during this test. The first flexural cracking was observed at a load of 23.6 kips, corresponding to a deflection of 0.19 in. The cracking moment, M_{cr}, for this specimen was 10% greater than the calculated cracking moment, $M_{cr,calc.}$ The maximum load reached for this specimen was 33.0 kips, corresponding to a deflection of 5.3 in. The maximum moment resisted by this beam, M_{max}, was 5% greater than $M_{n,calc}$ and 10% greater than $M_{n,AASHTO.}$ The stress in the strands at the actual maximum moment was estimated to be 299 ksi. The beam lost its load-carrying capacity due to strand rupture. No web-shear cracking was observed in this specimen. The crack pattern corresponding to the maximum load for this beam is depicted in Figure 5-27.

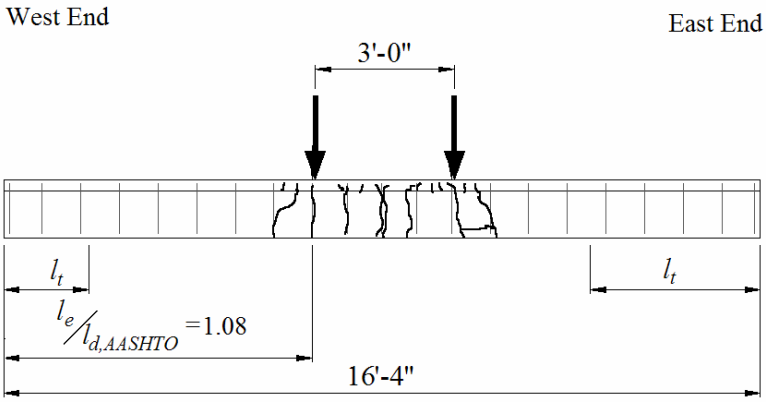

Figure 5-27: Crack Pattern for SCC-MS-B at Failure

5.8.2.4 SCC-HS-B

This specimen failed in a flexural manner. No strand end slip was detected during this test. The first flexural cracking was observed at a load of 23.7 kips, corresponding to a deflection of 0.17 in. The cracking moment, M_{cr}, for this specimen was 1% greater than the calculated cracking moment, $M_{cr,calc.}$ The maximum load reached for this specimen was 33.6 kips, corresponding to a deflection of 5.3 in. The maximum moment resisted by this beam, M_{max}, was equivalent to $M_{n,calc}$ and 9% greater than $M_{n,AASHTO.}$ The stress in the strands at the actual maximum moment was estimated to be 301 ksi. The beam lost its load-carrying capacity due to strand rupture. No web-shear cracking was observed in this specimen. The crack pattern corresponding to the maximum load for this beam is depicted in Figure 5-28.

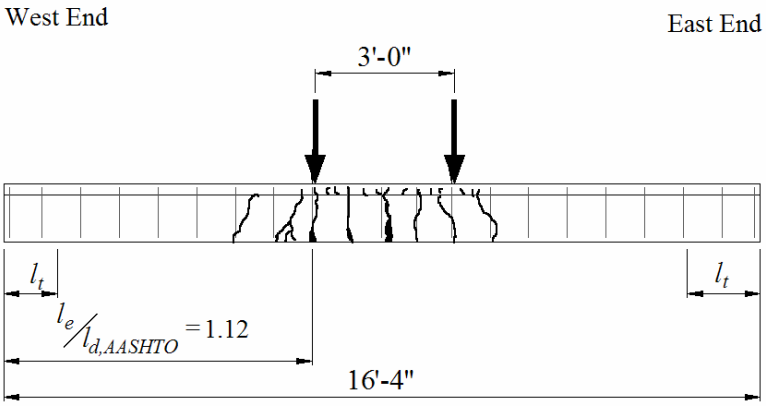

Figure 5-28: Crack Pattern for SCC-HS-B at Failure

5.8.3 SPECIMENS WITH 60-IN. EMBEDMENT LENGTHS

For these tests, the embedment length, l_e, was targeted to represent 75% of the development length, $l_{d,\ AASHTO}$, calculated by the ACI/AASHTO expression. These beams were designed to have a 60-in. embedment length and given the designation "C". Each specimen in this group was 13'-0" long. Flexural tests for these beams used the setup depicted in Figure 5-29. The load-deflection relationships for all four of these tests are shown in Figure 5-30. Despite the fact that this embedment length was significantly less than $l_{d,\ AASHTO}$, the three SCC specimens experienced flexural failure modes and the specimen constructed with standard concrete experienced a flexural-slip failure.

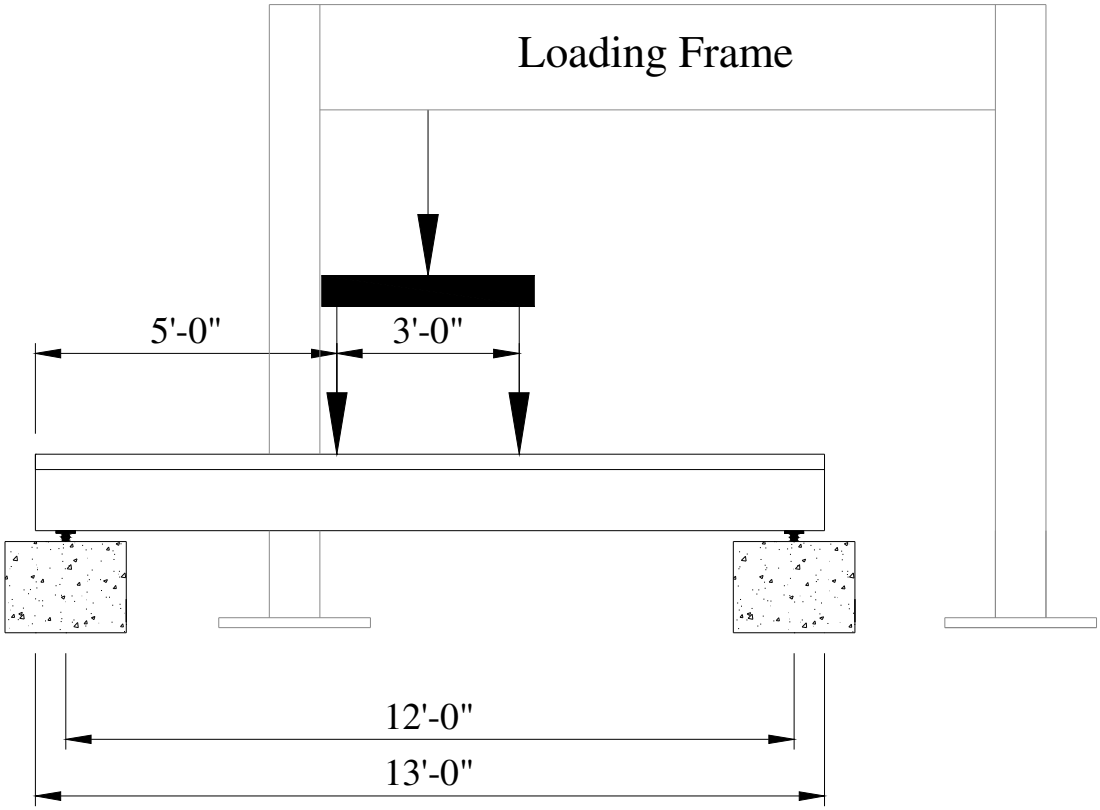

Figure 5-29: Test Setup for Specimens with l_e = 60 in.

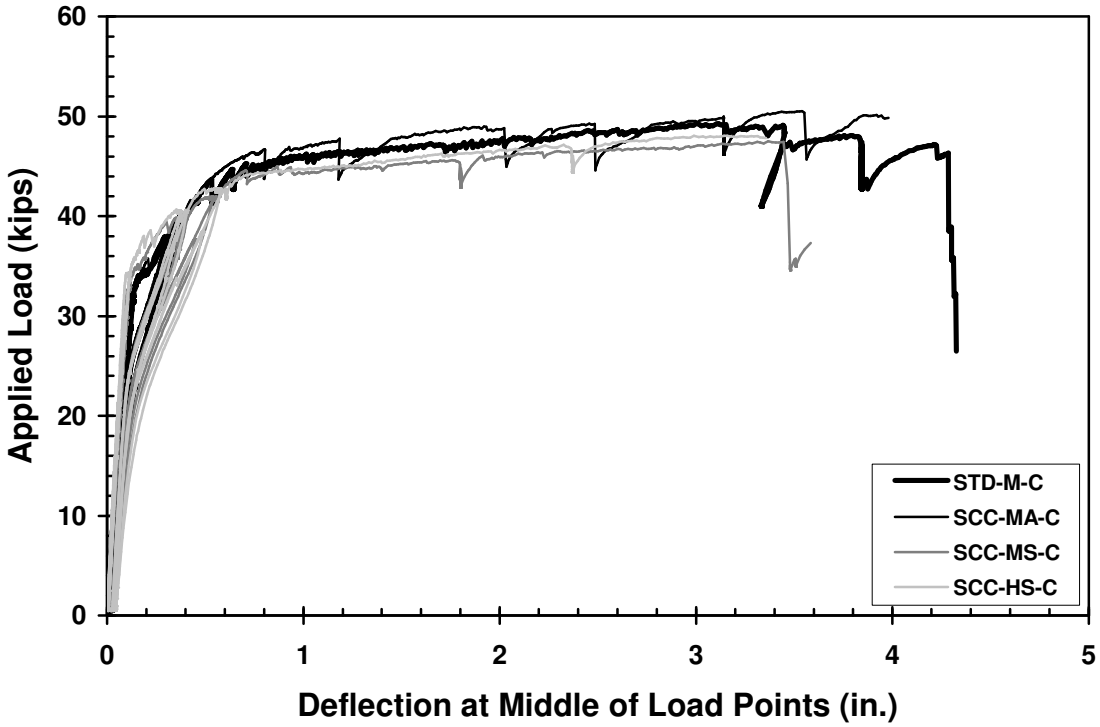

Figure 5-30: Load-Deflection Relationship for Specimens with l_e = 60 in.

5.8.3.1 STD-M-C

This specimen failed in a flexural manner with moderate strand slip. The first flexural cracking was observed at a load of 32.0 kips, corresponding to a deflection of 0.14 in. The cracking moment, M_{cr}, for this specimen was 16% greater than the calculated cracking moment, $M_{cr,calc.}$

A diagram relating strand slip and applied load to the deflection at the middle of the load points is depicted in Figure 5-31. At a load of 49.1 kips, corresponding to a deflection of 3.3 in. and well beyond the calculated load-carrying capacity of the specimen, the south strand began to slip at the east end of the beam. The stress in the prestressing strand at the first slip was estimated to be 325 ksi. After this slip, the peak load was not regained for the remainder of the test, but the loading remained constant just below the peak load. At the time of this initial slip, loading of the beam was paused for a short period of time. Upon restart of the loading, the north strand began to slip at the east end of the beam. At a load of 45 kips, corresponding to a deflection of 3.8 in., noticeable additional slip occurred in both strands at the east end of the beam. This slip was accompanied by a sudden decrease of load resistance on the magnitude of 4 kips. At that time, the slip in the south strand was 0.27 in. and the slip in the north strand was 0.15 in. At a load of 46 kips, corresponding to a deflection of 4.3 in., the north strand ruptured, having experienced a maximum slip of 0.22 in. When the north strand ruptured, the slip in the south strand was 0.34 in. Loading continued until the south strand ruptured at a load of 19.8 kips, corresponding to a deflection of 4.4 in. The maximum slip for the south strand was 0.49 in. at the time of rupture.

The maximum load reached for this specimen was 49.1 kips, corresponding to a deflection of 3.4 in. The strand end slip experienced by the specimen at the peak load was 0.1 in. The maximum moment resisted by this beam, M_{max}, was 18% greater than $M_{n,calc}$ and 22% greater than $M_{n,AASHTO.}$ The stress in the strands at the actual maximum moment was estimated to be 325 ksi. The beam lost its load-carrying capacity due to strand rupture. No web-shear cracking was observed in this specimen. The crack pattern corresponding to the maximum load for this beam is depicted in Figure 5-32.

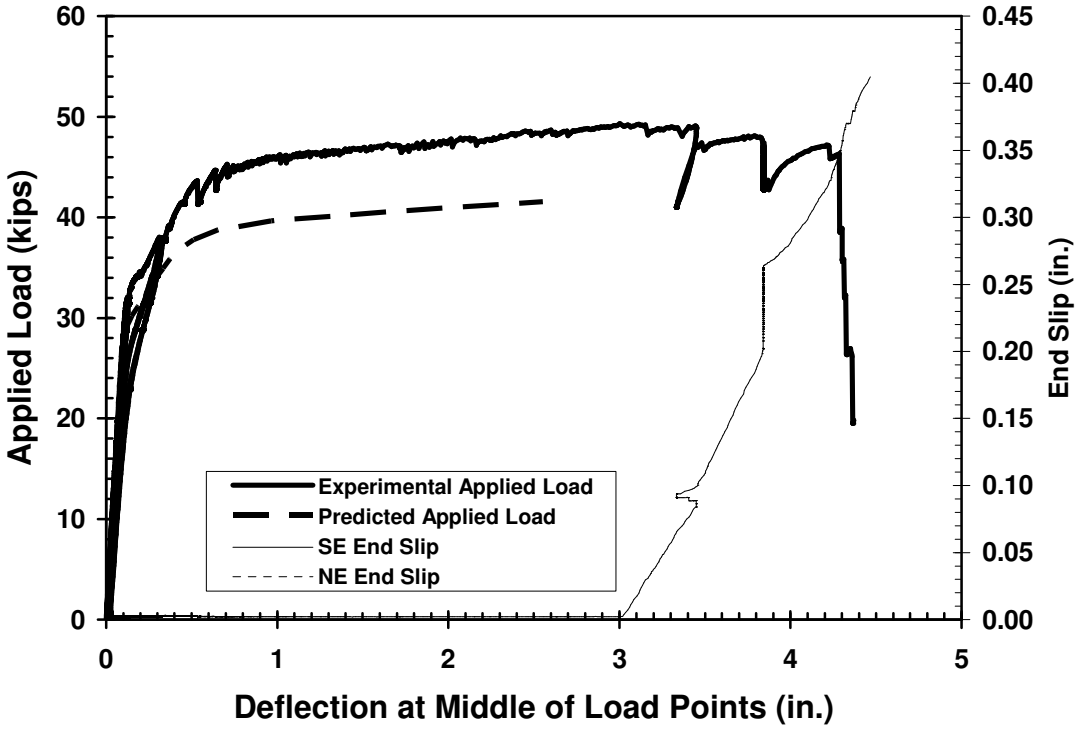

Figure 5-31: End Slip and Applied Load versus Deflection for STD-M-C

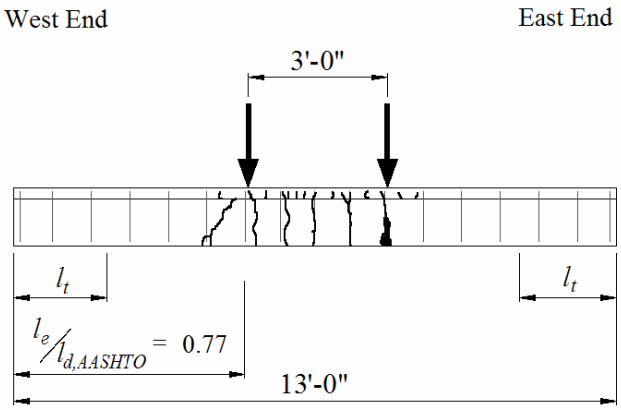

Figure 5-32: Crack Pattern for STD-M-C at Failure

5.8.3.2 SCC-MA-C

This specimen failed in a flexural manner. No strand end slip was detected during this test. The first flexural cracking was observed at a load of 31.8 kips, corresponding to a deflection of 0.12 in. The cracking moment, M_{cr}, for this specimen was 14% greater than the calculated cracking moment, $M_{cr,calc.}$ The maximum load reached for this specimen was 50.4 kips, corresponding to a deflection of 3.5 in. The maximum moment resisted by this beam, M_{max}, was 15% greater than $M_{n,calc}$ and 24% greater than $M_{n,AASHTO.}$ The stress in the strands at the actual maximum moment was estimated to be 332 ksi. The beam lost its load-carrying capacity due to strand rupture. No web-shear cracking was observed in this specimen. The crack pattern corresponding to the maximum load for this beam is depicted in Figure 5-33.

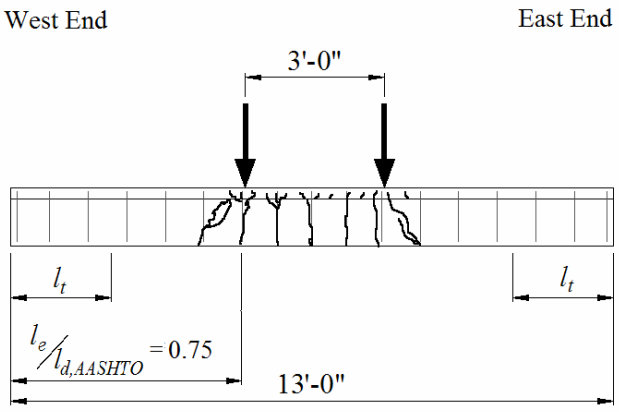

Figure 5-33: Crack Pattern for SCC-MA-C at Failure

5.8.3.3 SCC-MS-C

This specimen failed in a flexural manner. No strand end slip was detected during this test. The first flexural cracking was observed at a load of 32.6 kips, corresponding to a deflection of 0.12 in. The cracking moment, M_{cr}, for this specimen was 9% greater than the calculated cracking moment, $M_{cr,calc.}$ The maximum load reached for this specimen was 47.5 kips, corresponding to a deflection of 3.4 in. The maximum moment resisted by this beam, M_{max}, was 9% greater than $M_{n,calc}$ and 13% greater than $M_{n,AASHTO.}$ The stress in the strands at the actual maximum moment was estimated to be 310 ksi. The beam lost its load-carrying capacity due to strand rupture. No web-shear cracking was observed in this specimen. The crack pattern corresponding to the maximum load for this beam is depicted in Figure 5-34.

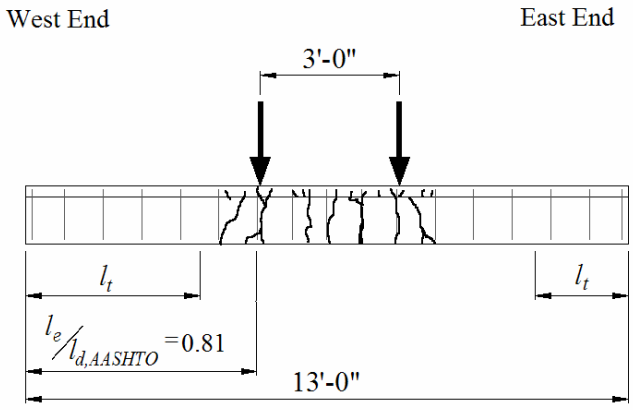

Figure 5-34: Crack Pattern for SCC-MS-C at Failure

5.8.3.4 SCC-HS-C

This specimen failed in a flexural manner. No strand end slip was detected during this test. The first flexural cracking was observed at a load of 32.6 kips, corresponding to a deflection of 0.10 in. The cracking moment, M_{cr}, for this specimen was 5% greater than the calculated cracking moment, $M_{cr,calc.}$ The maximum load reached for this specimen was 48.0 kips, corresponding to a deflection of 3.3 in. The maximum moment resisted by this beam, M_{max}, was 3% greater than $M_{n,calc}$ and 12% greater than $M_{n,AASHTO.}$ The stress in the strands at the actual maximum moment was estimated to be 311 ksi. The beam lost its load-carrying capacity due to strand rupture. No web-shear cracking was observed in this specimen. The crack pattern corresponding to the maximum load for this beam is depicted in Figure 5-35.

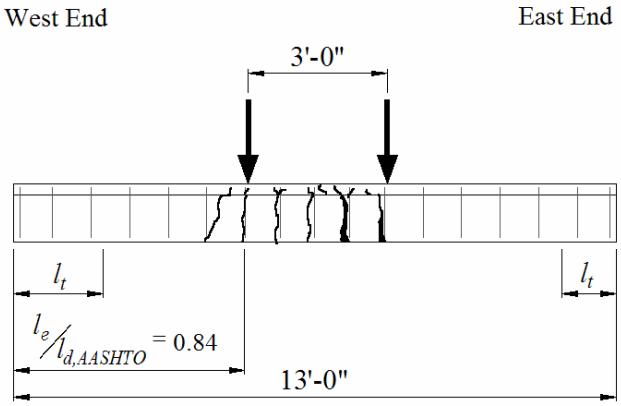

Figure 5-35: Crack Pattern for SCC-HS-C at Failure

5.8.4 SPECIMENS WITH 40-IN. EMBEDMENT LENGTHS

For these tests, the embedment length, l_e, was targeted to be 50% of the development length, $l_{d,\ AASHTO}$, calculated by the ACI/AASHTO expression. These beams were designed to have a 40-in. embedment length and given the designation "D". Each specimen in this group was 9'-8" long. Flexural tests for these beams used the setup depicted in Figure 5-36. The load-deflection relationships for all four of these tests are shown in Figure 5-37. The three SCC specimens experienced flexural-slip failure modes and the specimen constructed with standard concrete experienced a bond failure.

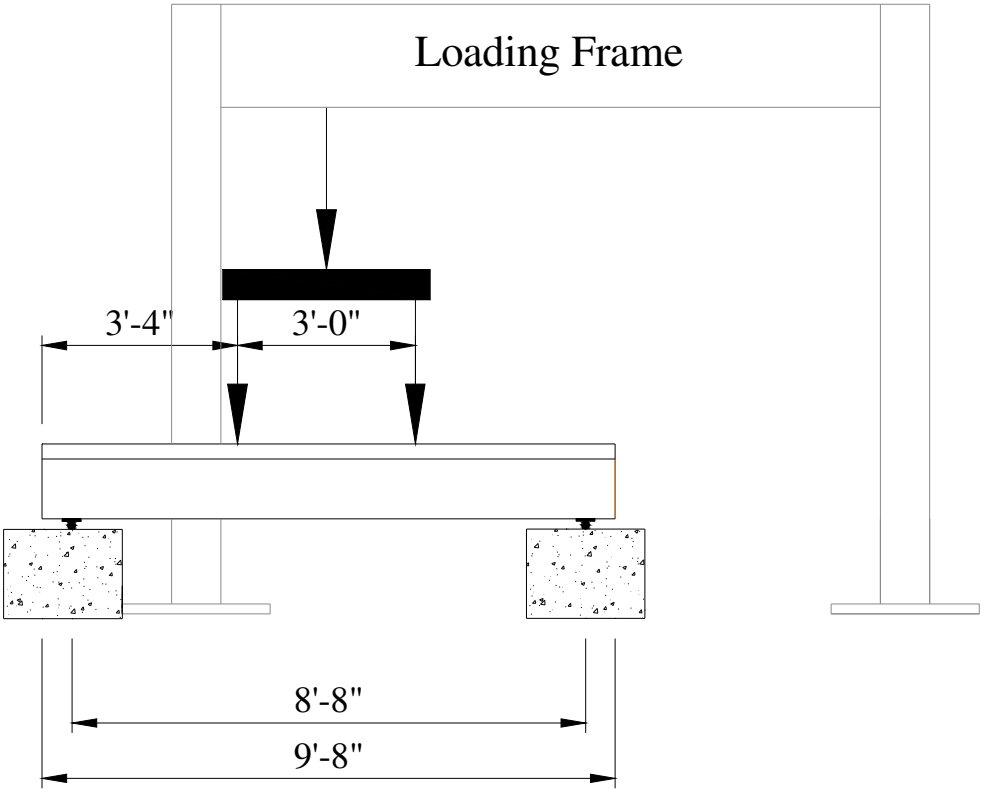

Figure 5-36: Test Setup for Specimens with l_e = 40 in.

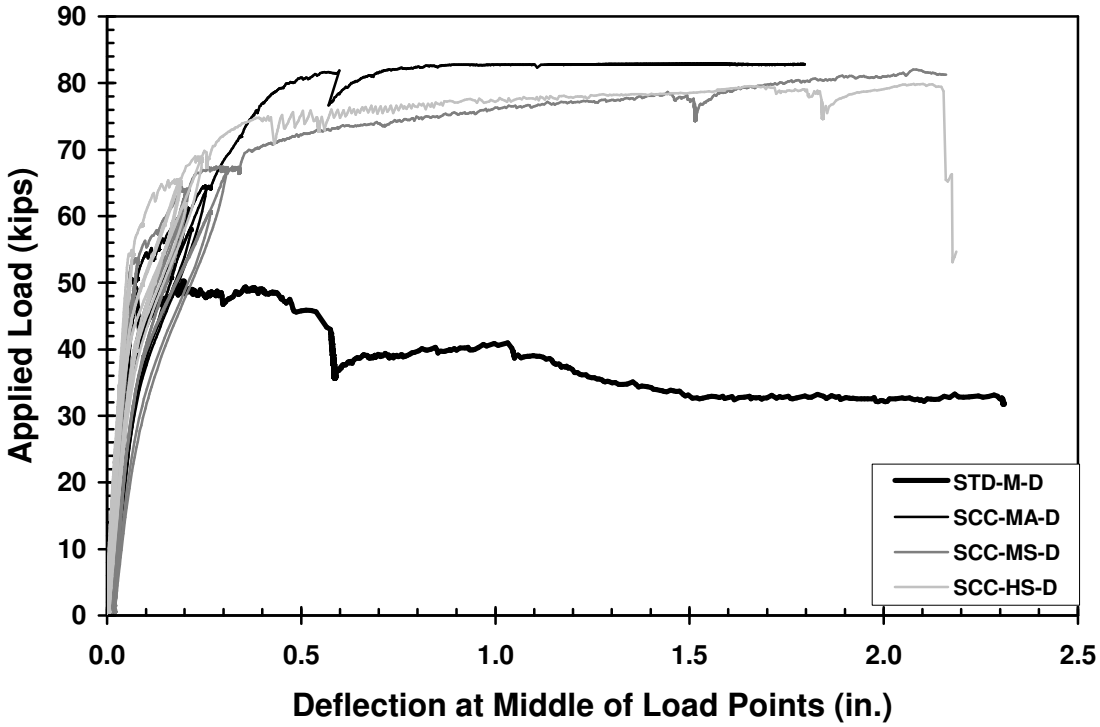

Figure 5-37: Load-Deflection Relationship for Specimens with l_e = 40 in.

5.8.4.1 STD-M-D

This specimen failed as a result of bond failure. The first flexural cracking was observed at a load of 49.1 kips, corresponding to a deflection of 0.07 in. The cracking moment, M_{cr}, for this specimen was 8% greater than the calculated cracking moment, $M_{cr,calc.}$

A diagram relating strand slip and applied load to the deflection at the middle of the load points is depicted in Figure 5-38. When the beam was initially loaded to the cracking load of 49.1 kips, corresponding to a deflection of 0.074, a large crack opened on the east end of the beam within the transfer length. The opening of this crack initiated a midspan displacement of 0.02 in. along with the slip of the north strand at the east end of the beam. The stress in the prestressing strand based on moment-curvature analysis at the first slip was 204 ksi. Once displacement application resumed, the south strand slipped on the east end of the beam at a load of 41.9 kips, corresponding to a displacement of 0.088 in. Figure 5-40 depicts the specimen shortly after initial slip and cracking. As displacement application continued, the peak load of 50.2 kips was reached at a deflection of 0.2 in. However, with continued displacement application, the strands continued to slip and the concrete crushed at a load of 41.9 kips, corresponding to a deflection of 0.57 in. Both strands continued to slip as displacement was increased, reaching a maximum slip in each strand of 1.4 in. Displacement application ceased at a final displacement of 2.3 in. at a load of 31.7 kips. Figure 5-41 depicts the specimen at the end of the test.

The maximum load reached for this specimen was 50.2 kips, corresponding to a deflection of 0.2 in. The strand end slip experienced by the specimen at the peak load was 0.1 in. The maximum moment resisted by this beam, M_{max}, was 75% of $M_{n,calc}$ and

77% of $M_{n,AASHTO.}$ The stress in the strands at the actual maximum moment was estimated to be 206 ksi. The beam lost its load-carrying capacity due to concrete crushing after significant strand slip. The crack pattern corresponding to the maximum load for this beam is depicted in Figure 5-39.

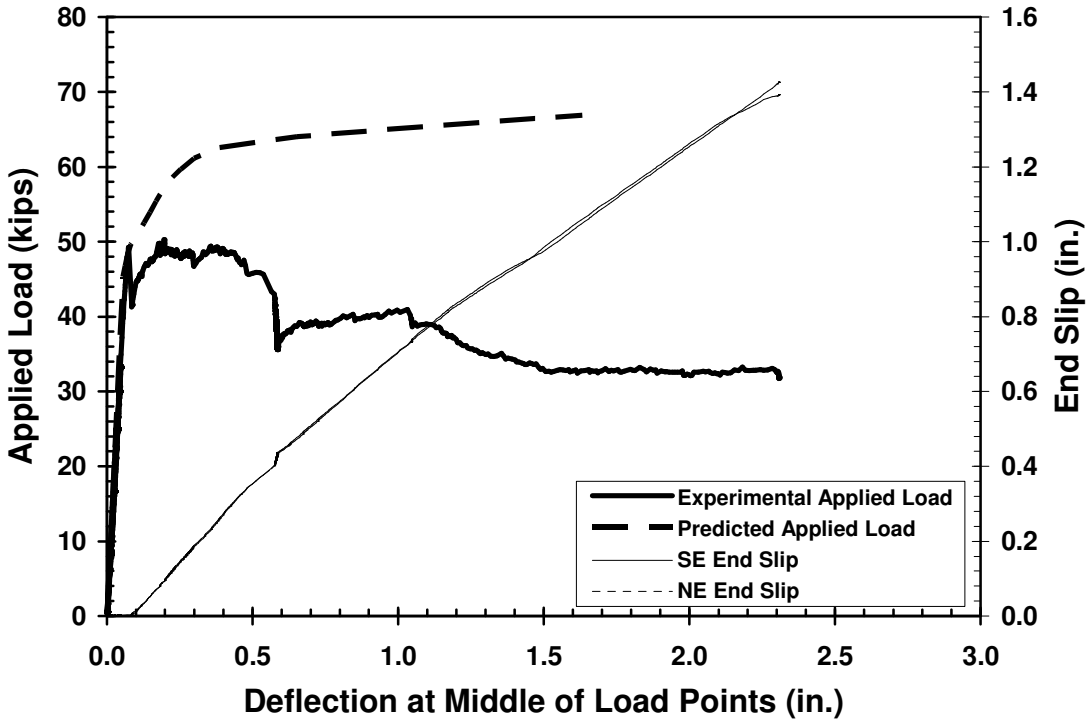

Figure 5-38: End Slip and Applied Load versus Deflection for STD-M-D

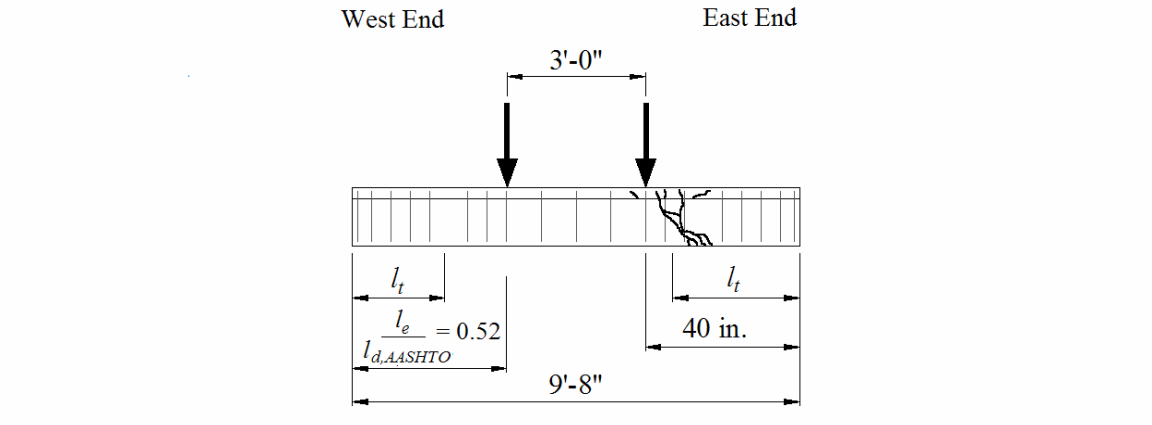

Figure 5-39: Crack Pattern for STD-M-D at Failure

Figure 5-40: STD-M-D at Initial Strand Slip

Figure 5-41: STD-M-D at a Deflection of 2.3 in.

5.8.4.2 SCC-MA-D

This specimen failed in a flexural manner with moderate strand slip. The first flexural cracking was observed at a load of 49.8 kips, corresponding to a deflection of 0.09 in. The cracking moment, M_{cr}, for this specimen was 8% greater than the calculated cracking moment, $M_{cr,calc.}$

A diagram relating strand slip and applied load to the deflection at the middle of the load points is depicted in Figure 5-42. At a load of 64.1 kips, corresponding to a deflection of 0.26 in., the south strand began to slip at the west end of the beam. The stress in the prestressing strand at the first slip was estimated to be 262 ksi from moment-curvature analysis. As loading continued, the north strand began to slip at a load of 69.8 kips corresponding to a deflection of 0.32 in. at the east end of the beam. At a load of 74.7 kips, corresponding to a deflection of 0.37 in., the south strand began to slip at the east end of the beam and the north strand began to slip at the west end of the beam. Loading continued until the actuator reached a capacity of 82 kips, causing the pump to shut off. Upon restart, a noticeable slip was seen in both strands at all ends. The maximum load reached for this beam was 82.8 kips corresponding to a deflection of 1.8 in. At the maximum load, the strand slips in the south strand at the west and east ends were 0.18 and 0.21 in., respectively and the strand slips in the north strand at the west and east ends were 0.13 and 0.24 in., respectively. The load required to rupture the strands in this specimen exceeded the capacity of the actuator. Therefore, the strands were not ruptured in this specimen.

The maximum load reached for this specimen was 82.8 kips, corresponding to a deflection of 1.8 in. All of the displacement beyond approximately 0.8 in. resulted from

holding of the load at the closed-loop system peak capacity while the strands slowly slipped and the flange concrete softened inelastically under very high compressive stresses. The strand end slip experienced by the specimen at the peak load was 0.24 in. The maximum moment resisted by this beam, M_{max}, was 18% greater than $M_{n,calc}$ and 26% greater than $M_{n,AASHTO.}$ The stress in the strands at the actual maximum moment was estimated to be 338 ksi. No web-shear cracking was observed in this specimen. The crack pattern corresponding to the maximum load for this beam is depicted in Figure 5-43.

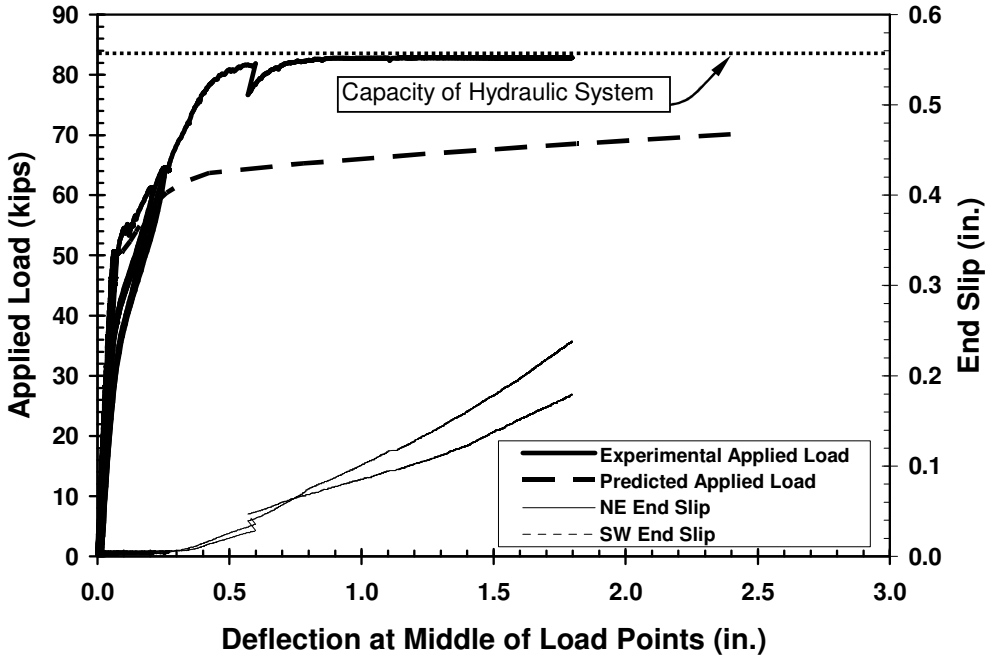

Figure 5-42: End Slip and Applied Load versus Deflection for SCC-MA-D

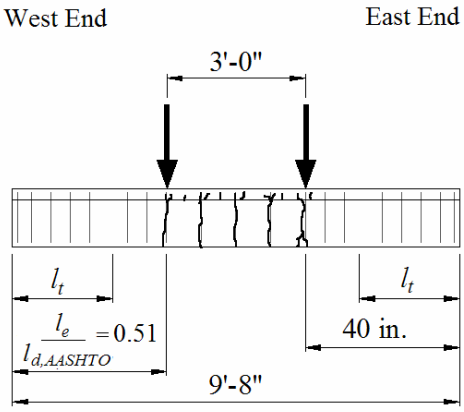

Figure 5-43: Crack Pattern for SCC-MA-D at Failure

5.8.4.3 SCC-MS-D

This specimen failed in a flexural manner with moderate strand slip. The first flexural cracking was observed at a load of 53.5 kips, corresponding to a deflection of 0.08 in. The cracking moment, M_{cr}, for this specimen was 9% greater than the calculated cracking moment, $M_{cr,calc.}$

A diagram relating strand slip and applied load to the deflection at the middle of the load points is depicted in Figure 5-44. At a load of 74.0 kips, corresponding to a deflection of 0.7 in., the south strand began to slip at the east end of the beam. The stress in the prestressing strand at the first slip was estimated as 299 ksi based in moment-curvature analysis. The south strand continued to slip gradually as the beam was loaded to 76.9 kips corresponding to a deflection of 1.5 in., when both strands experienced noticeable slip. At that time, the slip in the south strand was 0.034 in. and the slip in the north strand was 0.001 in. Both strands continued to slip gradually under sustained loading until both strands ruptured simultaneously at a load of 81.3 kips corresponding to a deflection of 2.2 in. When the strands ruptured, the south strand had slipped 0.06 in. and the north strand had slipped 0.017 in.

The maximum load reached for this specimen was 81.9 kips, corresponding to a deflection of 2.2 in. The strand end slip experienced by the specimen at the peak load was 0.06 in. The maximum moment resisted by this beam, M_{max}, was 17% greater than $M_{n,calc}$ and 21% greater than $M_{n,AASHTO.}$ The stress in the strands at the actual maximum moment was estimated to be 331 ksi. The beam lost its load-carrying capacity due to strand rupture. No web-shear cracking was observed in this specimen. The crack pattern corresponding to the maximum load for this beam is depicted in Figure 5-45. Note that

the maximum moment region for this specimen is immediately adjacent to the end of the 4-day measured transfer length on the east end of the specimen. As would be expected in this case, there was slip of the strands at that end; however, there was enough post-slip bond strength to develop the full capacity of the strands.

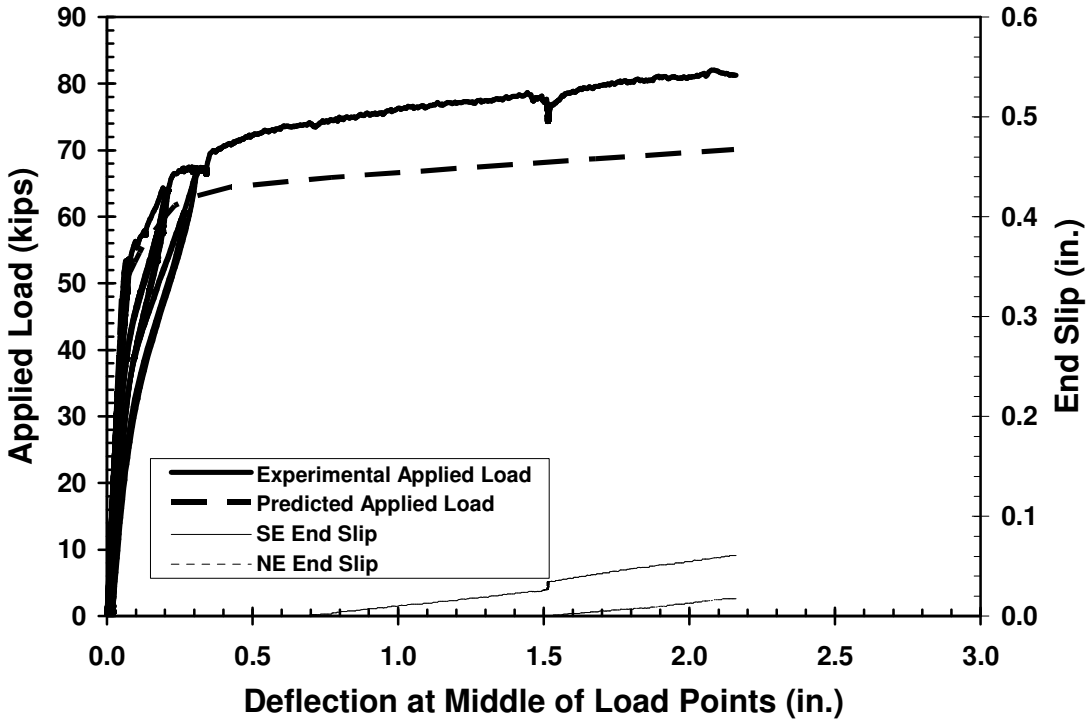

Figure 5-44: End Slip and Applied Load versus Deflection for SCC-MS-D

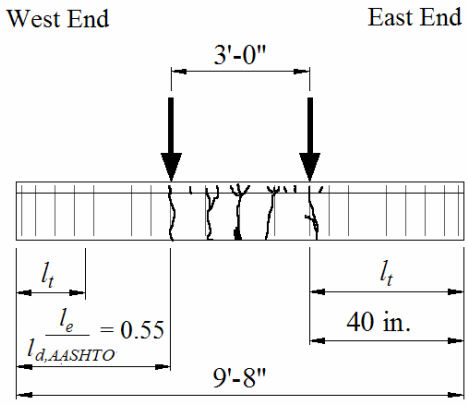

Figure 5-45: Crack Pattern for SCC-MS-D at Failure

5.8.4.4 SCC-HS-D

This specimen failed in a flexural manner. No strand end slip was detected during this test. The first flexural cracking was observed at a load of 54.3 kips, corresponding to a deflection of 0.07 in. The cracking moment, M_{cr}, for this specimen was 3% greater than the calculated cracking moment, $M_{cr,calc.}$ The maximum load reached for this specimen was 79.9 kips, corresponding to a deflection of 2.2 in. The maximum moment resisted by this beam, M_{max}, was 7% greater than $M_{n,calc}$ and 16% greater than $M_{n,AASHTO.}$ The stress in the strands at the actual maximum moment was estimated to be 322 ksi. The beam lost its load-carrying capacity due to strand rupture. No web-shear cracking was observed in this specimen. The crack pattern corresponding to the maximum load for this beam is depicted in Figure 5-46.

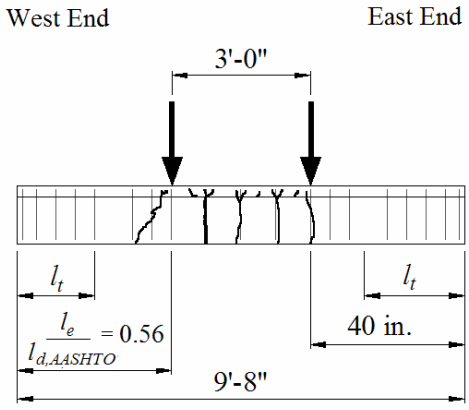

Figure 5-46: Crack Pattern for SCC-HS-D at Failure

5.9 DISCUSSION OF TEST RESULTS

A summary of results from the development length test program and a discussion of the flexural bond performance of all specimens are presented in this section.

5.9.1 SUMMARY OF TEST RESULTS

Table 5-4 presents a summary of the results from the development length test program. Fifteen of sixteen specimens exhibited a flexural failure, with only three of these being accompanied by moderate bond slip. One specimen, STD-M-D, experienced a bond failure.

Table 5-4: Summary of Development Length Testing Results

Test Specimen	$\frac{l_e}{l_{d,AASHTO}}$	$\frac{M_{cr}}{M_{cr,calc}}$	$\frac{M_{\max}}{M_{n,calc}}$	$\frac{M_{\max}}{M_{n,AASHTO}}$	Failure Type	ε_{max} (in./in.)	Max. Slip (in.)
STD-M-A	1.60	-	1.11	1.15	Flexural	-0.0019[a]	-
SCC-MA-A	1.54	1.12	1.06	1.14	Flexural	-0.0034	-
SCC-MS-A	1.67	1.09	1.08	1.13	Flexural	-0.0029	-
SCC-HS-A	1.69	0.99	1.01	1.10	Flexural	-0.0024	-
STD-M-B	1.03	1.10	1.06	1.10	Flexural	-0.0034	-
SCC-MA-B	1.00	1.16	1.10	1.18	Flexural	-0.0025	-
SCC-MS-B	1.08	1.10	1.05	1.10	Flexural	-0.0038	-
SCC-HS-B	1.12	1.01	1.00	1.09	Flexural	-0.0028	-
STD-M-C	0.77	1.16	1.18	1.22	Flex. w/Slip	-0.0020	0.10
SCC-MA-C	0.75	1.14	1.15	1.24	Flexural	-0.0033	-
SCC-MS-C	0.81	1.09	1.09	1.13	Flexural	-0.0026	-
SCC-HS-C	0.84	1.05	1.03	1.12	Flexural	-0.0027	-
STD-M-D	0.52	1.08	0.75	0.77	Bond	-0.0004	1.4
SCC-MA-D	0.51	1.08	1.18	1.26	Flex. w/Slip	-0.0024	0.24
SCC-MS-D	0.55	1.09	1.17	1.21	Flex. w/Slip	-0.0029	0.06
SCC-HS-D	0.56	1.03	1.07	1.16	Flexural	-0.0027	-

NOTE: [a] Strain gauges located between cracked sections for STD-M-A

Table 5-4 indicates that the service and ultimate load behavior was well predicted. The ultimate and cracking moment were well predicted by strain compatibility. The ultimate moment was also conservatively predicted using AASHTO formulations when the prestressing steel was fully developed. For all specimens except the specimen which experienced a bond failure, the maximum moment achieved by the specimens during flexural testing exceeded the predicted moment. This even occurred in seven specimens that had embedment lengths shorter than the ACI/AASHTO development length. In many cases, the maximum moment achieved during testing was much higher than predicted. One possible reason for this phenomenon may be attributed to the strand being significantly stronger than anticipated. It is possible that the ultimate strength of the strands used in this study greatly exceeded 270 ksi. In addition, a significant axial force due to frictional restraint of support translation at high deformation levels may have enhanced the moment capacity of the specimens by reducing the demand on the prestressing steel. However, this thrust would only have been present at extreme deformation levels.

Table 5-4 also indicates that SCC specimens performed at least as well as specimens constructed with a conventional or standard concrete mixture. For specimens in which l_e was approximately 75% of $l_{d,\ AASHTO}$, the only specimen to experience general bond slip was STD-M-C, which was constructed with a standard concrete mixture. Likewise, for specimens in which l_e was approximately 50% of $l_{d,\ AASHTO}$, the only specimen to experience a bond failure was STD-M-D, which was constructed with a standard concrete mixture. Therefore, it can be concluded that SCC mixture proportioning did not have an

adverse effect on the overall flexural bond performance of these specimens—either with respect to current design procedures or with respect to a comparable non-SCC mixture.

5.9.2 FLEXURAL BOND PERFORMANCE

In order to assess the flexural bond performance of each specimen, the flexural bond lengths for each test specimen was compared to the flexural bond length predicted by the ACI/AASHTO equation. The flexural bond length was predicted by isolating the flexural bond portion of the development length equation. Figures 5-47 and 5-48 depict the flexural bond performance of the specimens with respect to the ACI/AASHTO equation. Figure 5-47 depicts the flexural bond performance in specimens that experienced a general bond slip.

The ordinate of each point represents $\frac{f_{p,slip} - f_{pe,test}}{f_{ps,calc} - f_{pe,test}}$. The numerator of this expression represents the change in the stress from the calculated effective stress in the strands at the beginning of the test, $f_{pe,test}$, to the calculated stress in the strands at the time slip occurred, $f_{p,slip}$. In order the normalize the numerator for all specimens, the expression is then divided by the difference between the predicted ultimate stress in the strands, $f_{ps,calc}$, and and the $f_{pe,test}$. Thus, the ordinate represents the portion of the total flexural bond stress achieved prior to slip *relative to* the flexural bond stress required for development of full flexural capacity. The abscissa of each point represents $\frac{l_e - l_t}{l_{fb,ACI}}$. The numerator in this expression, which represents the available flexural bond length, is the difference between the embedment length, l_e, and the measured transfer length, l_t, at that end of the specimen. This expression is then normalized for all specimens by dividing

the numerator by the flexural bond length predicted by the ACI/AASHTO expression. Thus, the abscissa represents the actual flexural bond length *relative to* the flexural bond length required by ACI/AASHTO to develop the full flexural capacity.

The solid line shown on the plot represents the flexural bond length expression from ACI 318, $l_e - l_t = (f_{p,slip} - f_{pe,test})d_b$, as discussed in Chapter 2 of this thesis, with the performance criterion being general bond slip. Therefore, the data that fall above or to the left of this solid line indicate that the expression is conservative at predicting the flexural bond length required to prevent slip for these data points.

Figure 5-47 depicts the flexural bond performance in specimens which experienced a general bond slip. Bond slip was only experienced in four specimens. In all but one of these specimens, bond slip was only experienced on one end of the beam. This figure indicates that the expression is generally conservative with respect to bond slip. The one point which falls below this line represents the only specimen in which a bond failure occurred (STD-M-D). Thus, the current expression is therefore mildly unconservative for predicting strand slip in that specimen. However, it is difficult to draw any conclusions from one specimen test. In contrast, the flexural bond length portion of the current development length equation appears to be conservative for precluding strand slip for all of the SCC mixtures tested in this phase of the study.

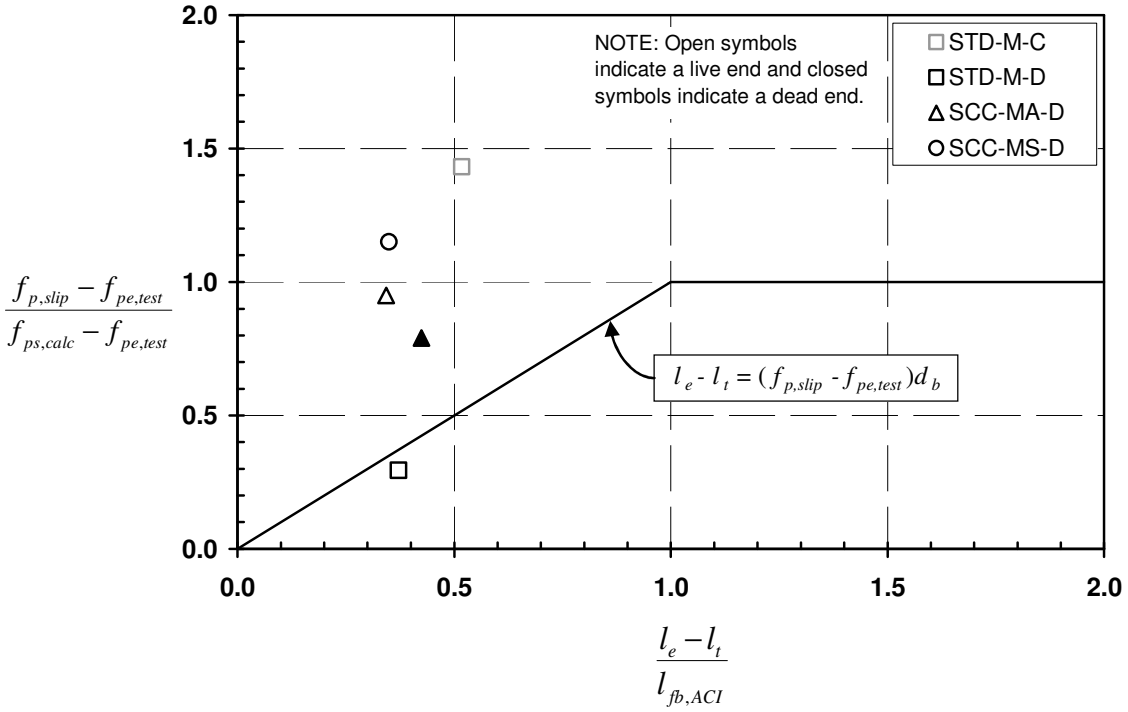

Figure 5-47: Flexural Bond Performance—Normalized Flexural Strand Stress at Slip vs. Normalized Flexural Bond Length Provided

Similarly, Figure 5-48 depicts the flexural bond performance with respect to strand stress development at ultimate strength in all specimens. For this graph, the ordinate of each point represents, $\frac{f_{p,\max} - f_{pe,test}}{f_{ps,calc} - f_{pe,test}}$. The numerator of this expression represents the change in the stress from the calculated effective stress in the strands at the beginning of the test, $f_{pe,test}$, to the stress in the strands at the peak load, $f_{p,max}$. The abscissa is defined the same way as in the previous figure. The solid line shown on the plot represents the flexural bond length expression, $l_e - l_t = (f_{p,slip} - f_{pe,test})d_b$ from ACI 318. The graph indicates that the expression for flexural bond length is conservative with respect to strength predictions (regardless of slip) for all SCC specimens as well as for three standard concrete specimens. The one point which falls below the line corresponds to the

specimen in which a bond failure occurred, STD-M-D; this specimen was constructed with the standard concrete mixture. Although this point illustrates some unconservatism in the flexural bond equation, there is not enough evidence to claim that a change should be made to current design expressions. In addition, the point is not very far removed from the line, indicating that the current expression yields only slightly unconservative results for this specimen.

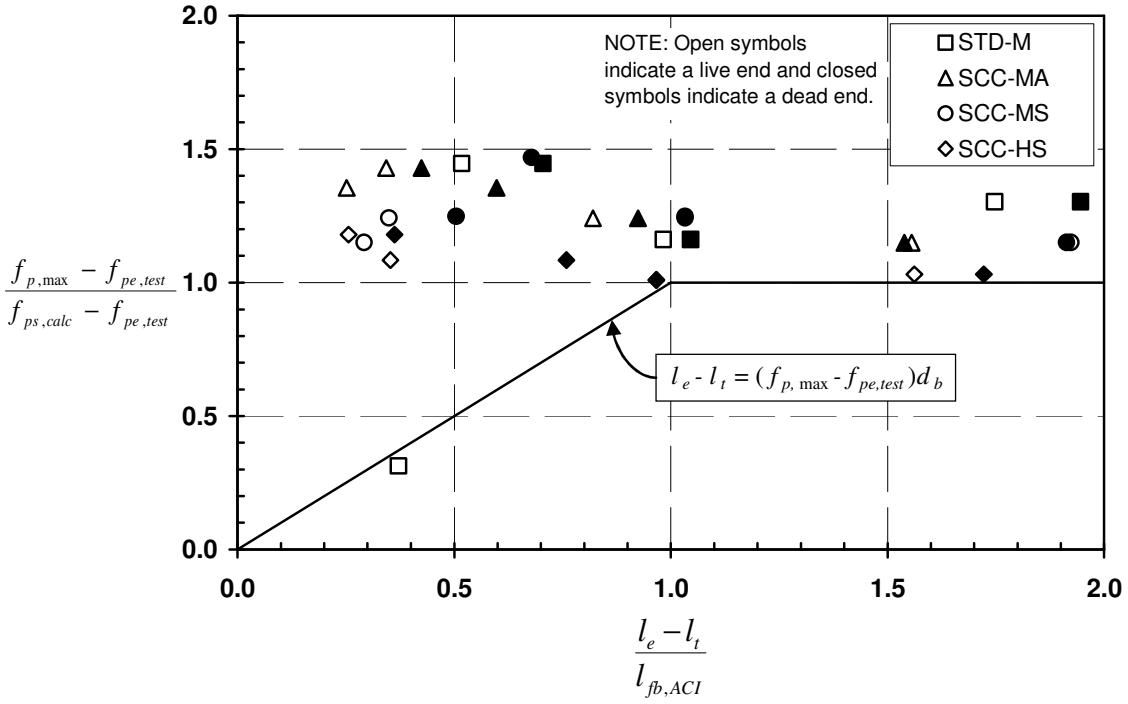

Figure 5-48: Flexural Bond Performance—Normalized Flexural Strand Stress at Maximum Moment vs. Normalized Flexural Bond Length Provided

5.10 DESIGN IMPLICATIONS

The flexural bond length predicted by the ACI/AASHTO expression proved to be conservative for all SCC specimens. The results of this study do not indicate a need to alter the expression for flexural bond length from the current expression. There was only

one specimen for which the current equation was not conservative. Therefore, there is not enough evidence that a change to the current flexural bond expression should be made.

By combining the current flexural bond length portion of the development length code equation with the expressions suggested in Chapter 4 for transfer length, a set of expressions to model development length are suggested in Table 5-5.

Table 5-5: Development Length Models Recommended for Design

Release Method	Concrete Type	Development Length
Gradual	Standard & All SCC	$l_d = 0.64ksi^{-0.5}\frac{f_{pt}}{\sqrt{f'_{ci}}}d_b + (f_{ps} - f_{pe})d_b$
Sudden	Standard & SCC with Slag Limitation	$l_d = 0.78ksi^{-0.5}\frac{f_{pt}}{\sqrt{f'_{ci}}}d_b + (f_{ps} - f_{pe})d_b$
	SCC without Slag Limitation	$l_d = 1.02ksi^{-0.5}\frac{f_{pt}}{\sqrt{f'_{ci}}}d_b + (f_{ps} - f_{pe})d_b$

5.11 CONCLUSIONS

Flexural testing was conducted on sixteen specimens for the development length test program. Fifteen of these specimens failed in a flexural manner and achieved maximum moments that exceeded the predicted nominal moment capacity. Seven of these specimens possessed embedment lengths shorter than the required development length suggested by the ACI/AASHTO expression. Only one of the sixteen specimens—none of the twelve SCC specimens—failed below its predicted nominal moment capacity as a result of a general bond failure. The embedment length in this specimen was 52% of the

required development length specified by the ACI/AASHTO expression. The available flexural bond length was less than 40% of the flexural bond length portion of the ACI/AASHTO development length expression.

Flexural testing results indicated that SCC specimens performed at least as well as specimens constructed with standard concrete. Therefore, it can be concluded that SCC mixture proportioning did not have an adverse effect on the overall flexural bond performance of these specimens.

There was not substantial evidence that the flexural bond portion of the current design equations for development length need to be changed. Therefore, the development length equations presented in Table 5-5 result from combination of the transfer length recommendations of Chapter 4 with the existing flexural bond length expression.

CHAPTER 6

SUMMARY AND CONCLUSIONS

6.1 SUMMARY

Due to the recent advent of self-consolidating concrete (SCC) research ventures by the precast, prestressed concrete industry have been undertaken to investigate the possible use of this material for use in prestressed applications. Currently, very limited test data is available concerning the bond interaction of prestressing strand with SCC. If approved for use in prestressed concrete applications, SCC could increase productivity and worker safety, lower labor costs, improve product quality, and provide innumerable design possibilities for the prestressed concrete industry.

This study consisted of an investigation into the bond behavior of the prestressed reinforcement in a total of sixteen beams with a T-shaped cross section. Twelve of these T-beams were constructed with SCC. The remaining four beams were constructed with a concrete mixture similar to that used in precast, prestressed ALDOT girders in which proper consolidation is obtained using internal vibration. All specimens in this study were pretensioned with 0.5-in. "oversized" prestressing strand—the most frequently used strand size in ALDOT prestressed girders. This strand size also provides a more critical force versus circumference ratio relative to a standard 0.5-in strand. Strand embedment lengths were varied to assess the bonded length necessary to ensure a desirable flexural

failure type. The mixing, fabrication, measurement, and flexural testing were performed in the Structural Engineering Laboratory of the Auburn University Department of Civil Engineering. All concrete was mixed in a ready-mix concrete truck in 3.5 cubic yard batch sizes.

One conventional mixture and three SCC mixtures were used to construct the beams. For each mixture, four beams of varying lengths were constructed. The conventional, or standard, mixture was a moderate-strength mixture with a compressive strength at prestress transfer of 5,000 psi. Three SCC mixtures were utilized to construct the remaining twelve beams, including two moderate-strength mixtures and one high-strength mixture. Type III cement, no. 78 crushed dolomitic limestone, and natural river sand was used for all mixtures. The sand-aggregate ratio (by volume) for all the SCC mixtures was 0.46. The sand-aggregate ratio for the standard concrete mixture was 0.37. The first moderate-strength SCC mixture constructed utilized Class C fly ash as an SCM and had a compressive strength at transfer of 5,500 psi. The next moderate-strength SCC mixture constructed utilized ground-granulated blast-furnace (GGBF) slag as an SCM and had a compressive strength at transfer of 5,300 psi. The high-strength SCC mixture utilized GGBF slag as an SCM and had a compressive strength at transfer of 9,900 psi.

Transfer length testing was performed on sixteen specimens. Each of the specimens had two transfer zones, one at each end, resulting in a total of thirty-two transfer zones. Concrete surface strains were measured using mechanical strain gauges immediately after transfer as well as four days after transfer. The 95% AMS method was used to establish transfer lengths from surface compressive strain profiles. After the determination of

transfer lengths, the results were analyzed and compared to the results of previous studies.

The development length test program was characterized by flexural tests of all sixteen T-beam specimens. Preparation for development length testing began after two sets of specimens had been cast. Testing began for each set of specimens after at least 28 days of curing. Loading was applied by displacement of a hydraulic actuator attached to a reaction frame. Linear potentiometers were used to measure all displacements and were also attached to each strand at the end of the beam were used to measure strand slip during flexural load testing. Two types of flexural analysis procedures were used for this study including a procedure based upon AASHTO LRFD recommendations and another based upon strain compatibility and nonlinear material properties.

While undergoing flexural testing, all specimens were subjected to acoustic emissions (AE) monitoring as part of a collaborative effort between researchers at Auburn University. Due to AE monitoring, a specific loading scheme was devised and followed for all flexural tests. At the end of AE monitoring load cycles, all AE sensors were removed from the beam, and then loading resumed beyond the nominal flexural capacity of the beam. Details and results of the AE monitoring are not reported in this thesis.

Three failure modes were observed during development length testing: flexural failure, flexural with slip failure, and bond failure. Each specimen's ability to achieve and maintain the nominal moment capacity as predicted by these methods influenced the failure mode it was assigned.

6.2 TRANSFER LENGTH TESTING RESULTS

Several conclusions regarding transfer length were reached for this study:

- On average, specimens constructed with higher compressive strengths at transfer had shorter transfer lengths than specimens that were constructed with lower concrete strengths at transfer.
- The average decrease in transfer length with increasing concrete strength could be accurately estimated by assuming the transfer length is inversely proportional to $\sqrt{f'_{ci}}$. This relationship provides a simple yet accurate method of describing this trend over a wide range of concrete strengths.
- In general, SCC transfer behavior only differed significantly from the standard mixture at flame-cut ends of the moderate-strength mixture with a 50% replacement of GGBF slag.
- Dead-end transfer lengths of some SCC specimens increased as much as 30% in the first four days after prestress transfer.
- On average, cut-end transfer lengths were 18% longer than dead-end transfer lengths for the standard mixture.
- Cut-end transfer lengths for the moderate-strength GGBF slag mixture were 90% longer than the dead-end transfer lengths and cut-end transfer lengths for the high-strength GGBF slag mixture were 33% longer than the dead-end transfer lengths.
- There appears to be a trend concerning the increase of the percent GGBF slag replacement with the increase in transfer length at cut ends.
- Cross-sectional size of the beam is a critical parameter in determining transfer lengths, particularly for specimen ends adjacent to flame-cutting of the strands.

- The ACI 318-05 12.9 expression for transfer length is unconservative for cut-end transfer lengths. This expression does not reflect the influence of concrete strength; therefore, it is more unconservative at lower concrete strength levels.
- ACI 318 (2005) shear transfer-length provisions are unconservative for one third of specimen ends, particularly for flame-cut strands at moderate strength levels.
- AASHTO LRFD (2006) specifications are unconservative for approximately 15% of flame-cut ends of moderate-strength mixtures. This unconservatism increases with decreasing compressive strength.
- To predict transfer length with more uniform levels of safety across the full range of practical concrete strengths, it is necessary to include concrete compressive strength as a parameter in the relevant design expressions.
- A distinction between SCC and standard concrete in transfer length design provisions is only necessary for cases where flame-cutting of strands is **combined** with a 50% proportion of GGBF slag replacement of cement.

Several equations are recommended for design as a result of this study. If gradual release is to be used, only one equation is necessary to model SCC and standard concrete. If sudden release is to be used or if there is no GGBF slag limitation, other expressions are necessary to predict transfer length for design.

- Table 6-1 lists recommended expressions for checking allowable stresses at transfer and estimating time-dependent deformations:

Table 6-1: Transfer Length Models Recommended for Use in Checking Concrete Stresses at Transfer

Release Method	Concrete Type	Transfer Length
Gradual	Standard & All SCC	$l_t = 0.53ksi^{-0.5} \frac{f_{pt}}{\sqrt{f'_{ci}}} d_b$
Sudden	Standard & SCC with Slag Limitation	$l_t = 0.65ksi^{-0.5} \frac{f_{pt}}{\sqrt{f'_{ci}}} d_b$
	SCC without Slag Limitation	$l_t = 0.71ksi^{-0.5} \frac{f_{pt}}{\sqrt{f'_{ci}}} d_b$

- Table 6-2 lists recommended expressions for strength design and checking stress limits under full service loads:

Table 6-2: Transfer Length Models Recommended for Design

Prestress Release Method	Concrete Type	Transfer Length
Gradual	Standard & All SCC	$l_t = 0.64ksi^{-0.5} \frac{f_{pt}}{\sqrt{f'_{ci}}} d_b$
Sudden	Standard & SCC with Slag Limitation	$l_t = 0.78ksi^{-0.5} \frac{f_{pt}}{\sqrt{f'_{ci}}} d_b$
	SCC without Slag Limitation	$l_t = 1.02ksi^{-0.5} \frac{f_{pt}}{\sqrt{f'_{ci}}} d_b$

6.3 DEVELOPMENT LENGTH TESTING RESULTS

Fifteen of sixteen specimens exhibited a flexural failure; only three of these were accompanied by moderate bond slip. One specimen of the conventional-slump concrete, STD-M-D, experienced a bond failure. The ultimate and cracking moment were well predicted by strain compatibility. The moment capacity was also well predicted using AASHTO formulations. For all specimens except the specimen that experienced a bond failure, the maximum moment achieved during flexural testing exceeded the predicted moment capacity.

SCC specimens performed at least as well as specimens constructed with a conventional, or standard, concrete mixture. For specimens in which l_e was approximately 75% of $l_{d,\ AASHTO}$, the only specimen to experience general bond slip was STD-M-C, which was constructed with a standard concrete mixture. Likewise, for specimens in which l_e was approximately 50% of $l_{d,\ AASHTO}$, the only specimen to experience a bond failure was STD-M-D, which was constructed with a standard concrete mixture. Thus, flexural testing results indicated that SCC specimens performed at least as well as specimens constructed with standard concrete. Therefore, it can be concluded that SCC mixture proportioning did not have an adverse effect on the overall flexural bond performance of these specimens—either with respect to current design procedures or with respect to a comparable non-SCC mixture.

The flexural bond length predicted by the ACI/AASHTO expression proved to be conservative for all SCC specimens. The results of this study do not indicate a need to alter the expression for flexural bond length from the current expression. There was only one beam end for which the current equation was slightly unconservative. There was not

substantial evidence that the flexural bond portion of the current design equations for development length need to be changed. Therefore, the equations presented in Table 5-6 are recommended for design.

Table 6-3: Development Length Models Recommended for Design

Release Method	Concrete Type	Development Length
Gradual	Standard & All SCC	$l_d = 0.64ksi^{-0.5}\frac{f_{pt}}{\sqrt{f'_{ci}}}d_b + (f_{ps} - f_{pe})d_b$
Sudden	Standard & SCC with Slag Limitation	$l_d = 0.78ksi^{-0.5}\frac{f_{pt}}{\sqrt{f'_{ci}}}d_b + (f_{ps} - f_{pe})d_b$
	SCC without Slag Limitation	$l_d = 1.02ksi^{-0.5}\frac{f_{pt}}{\sqrt{f'_{ci}}}d_b + (f_{ps} - f_{pe})d_b$

6.4 RECOMMENDATIONS FOR FUTURE STUDY

The scope of this study was limited to small-scale, prestressed specimens. As the results of this study indicate that transfer length is affected by member size, it is necessary to conduct similar tests on full-scale specimens. It is also necessary to calibrate the recommendations for design presented within this thesis with transfer and development length testing of full-scale specimens.

REFERENCES

AASHTO. 2006. *AASHTO LRFD Bridge Design Specifications: Customary U.S. Units*. 3rd ed. Washington D.C.: American Association of State Highway and Transportation Officials (AASHTO).

AASHTO. 2005. *AASHTO LRFD Bridge Design Specifications: Customary U.S. Units*. 3rd ed. Washington D.C.: American Association of State Highway and Transportation Officials (AASHTO).

AASHTO. 2002. *Standard Specifications for Highway Bridges*. 16th ed. Washington D.C.: American Association of State Highway and Transportation Officials (AASHTO).

ACI 318. 2005. "Building Code Requirements for Structural Concrete (ACI 318-05) and Commentary (ACI 318R-05)." Farmington Hills, Michigan: American Concrete Institute (ACI).

ASTM C 39. 1998. "Standard Test Method for Compressive Strength of Cylindrical Concrete Specimens". *ASTM International*. West Conshohocken, Pennsylvania.

ASTM C 138. 1998. "Standard Test Method for Unit Weight, Yield, and Air Content". *ASTM International*. West Conshohocken, Pennsylvania.

ASTM C 192. 1998. “Standard Practice for Making and Curing Concrete Test Specimens in the Laboratory”. *ASTM International*. West Conshohocken, Pennsylvania.

ASTM C 469. 1998. “Standard Test Method for Static Modulus of Elasticity and Poisson’s Ratio Strength of Concrete in Compression.” *ASTM International*. West Conshohocken, Pennsylvania.

ASTM C 1611. 2006. “Standard Test Method for Slump Flow of Self-Consolidating Concrete”. *ASTM International*. West Conshohocken, Pennsylvania.

ASTM C 1621. 2006. “Standard Test Method for Passing Ability of Self-Consolidating Concrete by J-Ring.” *ASTM International*. West Conshohocken, Pennsylvania.

Barnes, R. W., N. H. Burns, and M. E. Kreger. 1999. “Development Length of 0.6-Inch Prestressing Strand in Standard I-Shaped Pretensioned Concrete Beams.” *Research Report No. 1388-1*. Austin: Center for Transportation Research, The University of Texas at Austin.

Barnes, R. W., J. W. Grove, and N. H. Burns. 2003. Experimental Assessment of Factors Affecting Transfer Length. *ACI Structural Journal* 100, no. 6: 740–748.

Buckner, C. Dale. 2005. A Review of Strand Development Length of Pretensioned Concrete Members. *PCI Journal* 40, no. 2: 84–105.

Burgueño, R., and M. Haq. 2005. Development Length of Prestressing Strands in Precast/Prestressed Girders using Self Compacting Concrete. 2005 ASCE Structures Congress, New York, NY.

Cousins, T., D. Johnston, and P. Zia. 1990. Transfer and Development Length of Epoxy Coated Prestressing Strand. *PCI Journal* 35, no. 4: 92–103.

Deatherage, J. H., Burdette, E. G., and Chew, C. K. 1994. Development Length and Lateral Spacing Requirements of Prestressing Strand for Prestressed Concrete Bridge Girders. *PCI Journal* 39, no. 1: 70–83.

FHWA. 1988. Prestressing Strand for Pretension Applications–Development Length Revisited. Memorandum, Chief, Bridge Division, Washington, D.C.

Hamilton, H. R., T. Labonte, and M.H. Ansley. 2005. "Behavior of Pretensioned Type II AASHTO Girders Constructed with Self-Consolidating Concrete". In *Ned H Burns Symposium on Historic Innovations in Prestressed Concrete*, ed. B.W. Russell and S. P. Gross. Farmington Hills, Michigan: American Concrete Institute: 252–270.

Hanson, Norman W. 1969. Influence of Surface Roughness of Prestressing Strand on Bond Performance. *PCI Journal* 14, no. 1: 32–45.

Hanson, N.W. and P. H. Kaar. 1959. Flexural Bond Tests of Pretensioned Prestressed Beams. *ACI Journal. Proceedings* 55, no. 7: 783–802.

Haq, M. 2005. Effect of Self Consolidating Concrete Mix Proportioning on Transfer and Development Length of Prestressing Strands. M.S. Thesis, Michigan State University.

Janney, J. R. 1954. Nature of Bond in Pre-Tensioned Prestressed Concrete. *ACI Journal. Proceedings* 50, no. 9: 717–736.

Kaar, P. H., R. W. LaFraugh, and M. A. Mass. 1963. Influence of Concrete Strength on Strand Transfer Length. *PCI Journal* 8, no. 5: 47–67.

Kaar, P. H. and D. D. Magura. 1965. Effect of Strand Blanketing on Performance of Pretensioned Girders. *PCI Journal* 10, no. 6: 20–34.

Khayat, K. H., N. Petrov, E. K. Attiogbe, and H. T. See. 2003. "Uniformity of Bond Strength of Prestressing Strands in Conventional Flowable and Self-Consolidating Concrete Mixtures". In *Self-Compacting Concrete*: *Proceedings of the Third International RILEM Symposium,* ed. O. Wallevik and I. Nielsson. Bagneux, France: RILEM Publications, 703–709.

Lane, S. N. 1998. "A New Development Length Equation For Pretensioned Strands in Bridge Beams and Piles." In *Report No. FHWRA-RD-98-116*. McLean, Virginia: Federal Highway Administration.

Logan, Donald R. 1997. Acceptance Criteria for Bond Quality of Strand for Pretensioned Prestressed Concrete Applications. *PCI Journal* 42, no. 2: 52–90.

MacGregor, J. G., and J. K. Wight. 2005. Reinforced Concrete: Mechanics and Design. 4th Edition. Prentice Hall.

Mitchell, D., W. D. Cook, A. A. Kahn, and T. Tham. 1993. Influence of High-Strength Concrete on Transfer and Development Length of Pretensioning Strand. *PCI Journal* 38, no. 3: 52–66

Naito, Clay., G. Parent, and G. Brunn. 2006. Performance of Bulb-Tee Girders Made with Self Consolidating Concrete. *PCI Journal* 51, no. 6: 72–85.

Okamura, H. and M. Ouchi. 1999. "Self-Compacting Concrete. Development, Present Use and Future". In *Self-Compacting Concrete*: *Proceedings of the First International RILEM Symposium,* ed. A. Skarendahl and O. Petersson. Cachan Cedex, France: RILEM Publications, 3-14.

Precast/Prestressed Concrete Institute (PCI). 2003. *Interim Guidelines for the Use of Self-Consolidating Concrete in Precast/Prestressed Concrete Institute Member Plants*, 1st edition. Chicago Illinois: Precast/Prestressed Concrete Institute.

Roberts, James. 2005. Evaluation of Self-Consolidating Concrete for Use in Prestressed Girder Applications. M.S. Thesis, Auburn University.

Russell, B. W. and N. H. Burns. 1997. Measurement of Transfer Lengths on Pretensioned Concrete Elements. *Journal of Structural Engineering* 123, no. 5: 541–549.

Russell, Bruce W., and Ned H. Burns. 1993. Design Guidelines for Transfer, Development and Debonding of Large Diameter Seven Wire Strands in Pretensioned Concrete Girders. Research Report 1210-5F. Austin: Center for Transportation Research, The University of Texas at Austin.

Schindler, A., R.W. Barnes, J.B. Roberts, and S. Rodriguez, 2007. Properties of Self-Consolidating Concrete for Prestressed Members. *ACI Materials Journal* 104, no. 1: 54-61.

Shahawy, Mohsen. 2001. A Critical Evaluation of the AASHTO Provisions for Strand Development Length of Prestressed Concrete Members. *PCI Journal* 46, no.4: 94–116.

Swords, Shane. 2005. Transfer Length in Prestressed Self-Consolidating Concrete. M.S. Thesis, Auburn University.

Tabatabai, H. and T. J. Dickson. 1993. The History of Prestressing Strand Development Length Equation. *PCI Journal* 38, no. 6: 64–75.

Zia, P. and T. Mostafa. 1978. Development Length of Prestressing Strands. *PCI Journal* 22, no. 5: 54–65.

Zia, P., R.A. Nunez, L.A. Mata, and H.M. Dwairi. 2005. "Implementation of Self-Consolidating Concrete for Prestressed Girders". In *Seventh International Symposium on Utilization of High-Strength/ High Performance Concrete*, ed. H.G. Russell. Farmington Hills, Michigan: American Concrete Institute: 297–314.

APPENDIX A

NOTATION

Report (AASHTO LRFD)	AASHTO Standard	ACI 318-05	Description
A_{ps}	A_s*	A_{ps}	area of prestressing steel
d_b	D	d_b	nominal diameter of reinforcement
E_p	—	—	modulus of elasticity of prestressing reinforcement
$\varepsilon_{max,calc}$	—	—	strain at the strand level at the nominal resistance of the member
ε_p	—	—	strain in prestressing reinforcement
f'_c	f'_c	f'_c	specified compressive strength of concrete
f'_{ci}	f'_{ci}	f'_{ci}	specified compressive strength of concrete at transfer of prestress force
$f'_{c,28}$	—	—	specified compressive strength of concrete at 28 days
f_p	—	—	stress in prestressing reinforcement (not in AASHTO LRFD)
f_{pe}	f_{se}	f_{se}	effective stress in prestressed reinforcement after losses
$f_{pe,test}$	f_{se}	f_{se}	effective stress in prestressed reinforcement after losses immediately prior to flexural testing
f_{pbt}	—	—	stress in prestressing reinforcement immediately prior to transfer
f_{ps}	f^*_{su}	f_{ps}	stress in prestressed reinforcement at the estimated nominal strength
$f_{ps,AASHTO}$	—	—	stress in prestressed reinforcement at the estimated nominal strength estimated by AASHTO prior to flexural testing

$f_{ps,calc}$	—	—	stress in prestressed reinforcement at the estimated nominal strength calculated by strain compatibility
$f_{ps,max}$	—	—	stress in prestressed reinforcement calculated by strain compatibility at the nominal strength of the specimen experienced during flexural testing
$f_{p,slip}$	—	—	stress in prestressed reinforcement calculated by strain compatibility at the first slip of the prestressing strand in the specimen during flexural testing
f_{pt}	—	—	stress in prestressed reinforcement immediately after transfer
f_{pu}	f'_s	f_{pu}	specified tensile strength of prestressing reinforcement
f_r	—	f_r	modulus of rupture
f_t	—	—	splitting tensile strength
f_y	—	—	yield stress of steel reinforcement
κ	κ	—	multiplier used in Section 5.11.4 of AASHTO LRFD
l_d	l_d	l_d	development length (only refers to nonprestressed reinforcement in AASHTO Standard and ACI 318)
$l_{d,est}$	—	—	development length estimated by ACI/AASHTO with estimated properties
$l_{d,AASHTO}$	—	—	development length estimated by ACI/AASHTO with calculated properties
l_e	—	—	embedment length
M_{cr}	—	—	actual cracking moment achieved by specimen during flexural testing
$M_{cr,calc}$	—	—	predicted cracking moment according to strain compatibility
M_{max}	—	—	maximum moment achieved by specimen during flexural testing
M_n	—	—	predicted nominal moment capacity
$M_{n,AASHTO}$	—	—	predicted nominal moment capacity according to AASHTO LRFD specifications

$M_{n,calc}$	—	—	predicted nominal moment capacity according to strain compatibility
$\sum o$	—	—	strand perimeter
P_{min}	—	—	minimum load used for AE load cycles
P_{cr}	—	—	cracking load experienced during flexural load testing
$P_{cr,calc}$	—	—	cracking load calculated using strain compatibility prior to flexural load testing
P_n	—	—	ultimate load predicted prior to flexural load testing
n	—	n	modular ratio
T_e	—	—	average concrete temperature during time interval
T_r	—	—	reference curing temperature
t_e	—	—	equivalent age
Δt	—	—	time interval used in Arrhenius equation
ω_c	—	—	unit weight of concrete

APPENDIX B

SHEAR REINFORCEMENT DETAILS

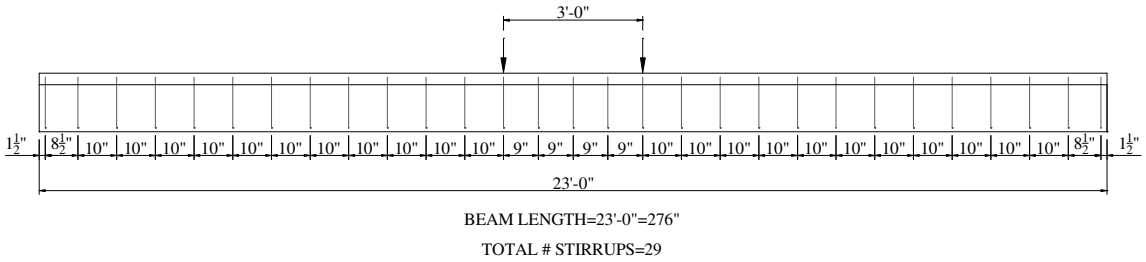

Figure B-1: Stirrup Spacing for "A" Specimens

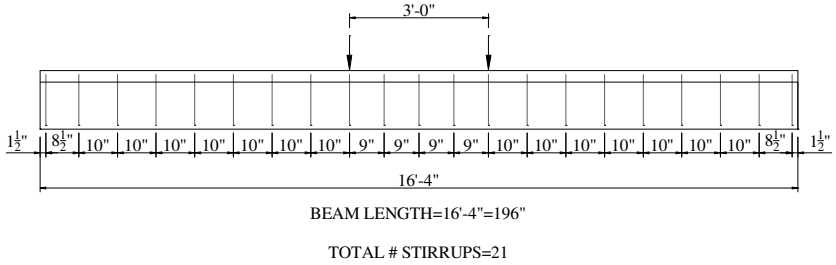

Figure B-2: Stirrup Spacing for "B" Specimens

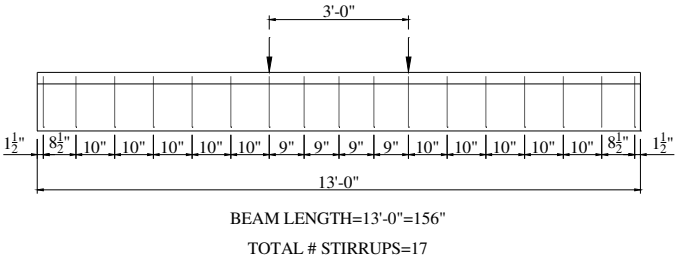

Figure B-3: Stirrup Spacing for "C" Specimens

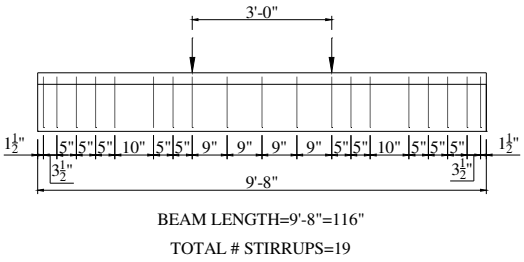

Figure B-4: Stirrup Spacing for "D" Specimens

APPENDIX C

FRESH CONCRETE PROPERTIES

Table C-1: Fresh Property Testing Results

FRESH PROPERTIES	MIXTURES							
	STD-M		SCC-MA		SCC-MS		SCC-HS	
	Start	End	Start	End	Start	End	Start	End
Slump Flow (in.)	9.5	9.5	29	27	28.5	28	26	20
Unit Weight (lb/ft^3)	142.2	140.8	151.8	152.1	148.4	147.2	155.2	153.2
Air (%)	11.0	9.0	2.0	1.8	5.0	4.3	3.0	3.2
VSI	-	-	1.0	1.0	1.0	1.0	1.0	0.5
T-50 (sec.)	-	-	2.47	2.53	1.54	1.34	3.75	12.22
J-ring (Value @ Slump Flow)	-		25.5 @ 27		26.5 @ 28.5		23 @ 25.5	
L-Box (H_2/H_1)	-		0.84		0.92		0.63	
Temperature (°F)	82	74	62	63	89	88	95	96

Table C-2: Summary of Fresh Property Testing Results

FRESH PROPERTIES	MIXTURES			
	STD-M	SCC-MA	SCC-MS	SCC-HS
Slump Flow (in.)	9.5	29	28.5	26
Unit Weight (lb/ft^3)	142.2	151.8	148.4	155.2
Air (%)	11.0	2.0	5.0	3.0
VSI	-	1.0	1.0	1.0
T-50 (sec.)	-	2.47	1.54	3.75
J-ring (Difference in in.)	-	1.5	2	2.5
L-Box (H_2/H_1)	-	0.84	0.92	0.63
Temperature (°F)	82	62	89	95

APPENDIX D

STRENGTH-MATURITY RELATIONSHIP CURVES

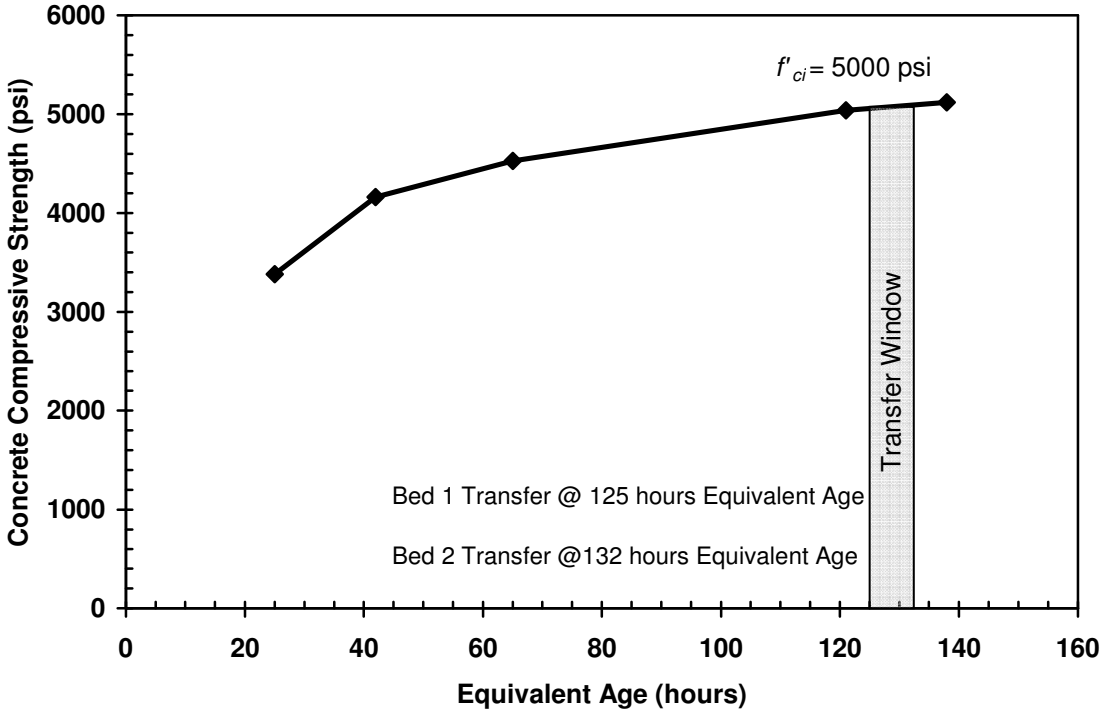

Figure D-1: Strength-Maturity Relationship Curve for STD-M

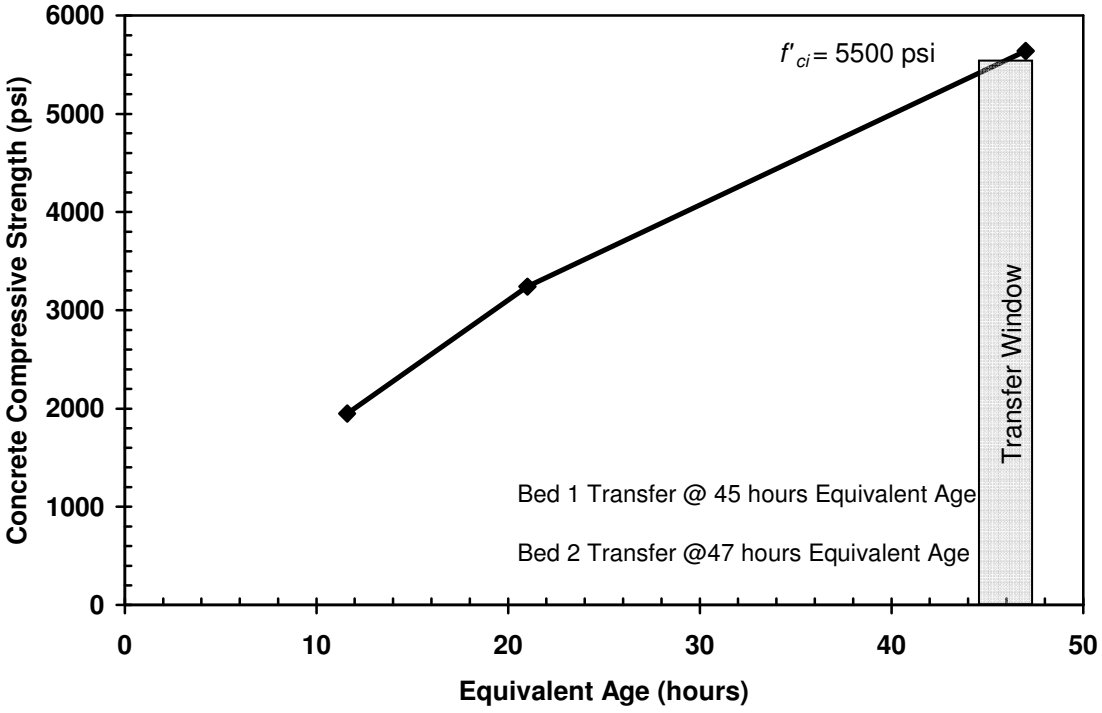

Figure D-2: Strength-Maturity Relationship Curve for SCC-MA

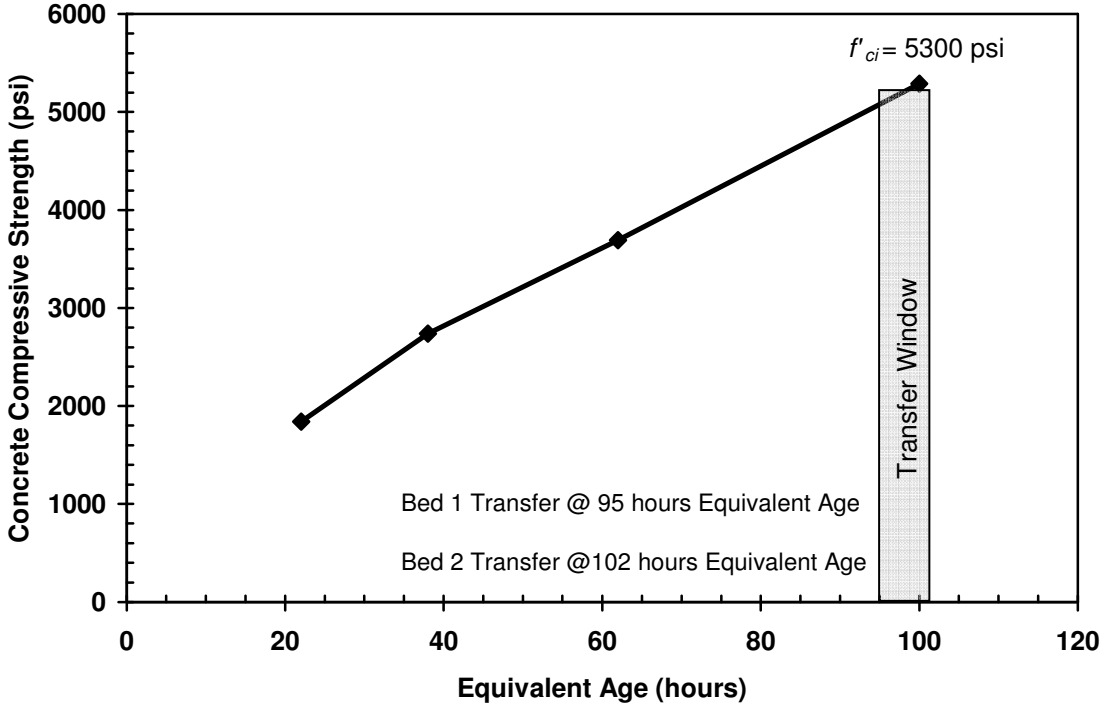

Figure D-3: Strength-Maturity Relationship Curve for SCC-MS

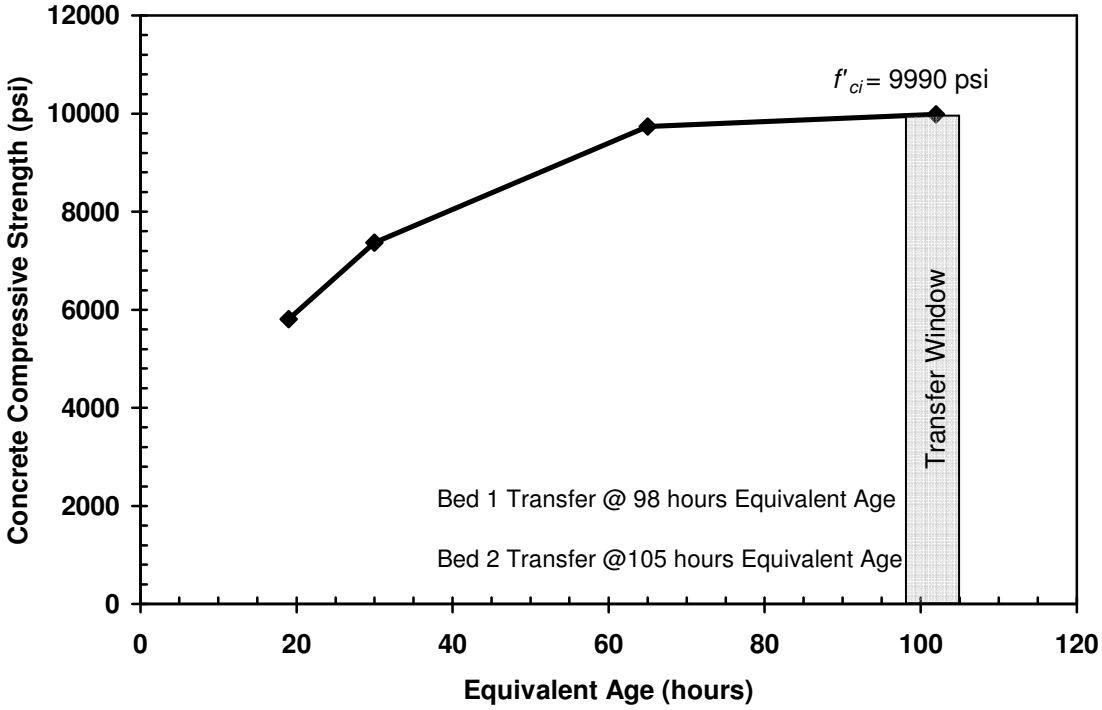

Figure D-4: Strength-Maturity Relationship Curve for SCC-HS

APPENDIX E

HARDENED CONCRETE PROPERTIES

Table E-1: Summary of Results for Hardened Concrete Property Testing

HARDENED PROPERTIES		MIXTURES							
		STD-M		SCC-MA		SCC-MS		SCC-HS	
Compressive Strength		f'_c (psi)	E_c (ksi)	f'_c (psi)	E_c (ksi)	f'_c (psi)	E_c (ksi)	f'_c (psi)	E_c (ksi)
Match Cured	Transfer	-	-	5540	-	-	-	9760	6350
	Post-Test	6410	4950	9360	5450	10480	6100	13890	7100
Air Cured	1	3380	-	1950	-	1840	3300	5810	4800
	2	4160	4350	3240	4000	2740	3800	7370	5400
	3	4530	4500	-	-	3690	4250	9740	5800
	Transfer	5040	5000	5640	5000	5290	4950	9990	6050
	7	5120	5050	7670	5450	7140	5400	11780	6450
	28	6320	5150	8540	5400	9170	6150	13380	7050
	Post-Test	6210	4900	8290	5650	9190	6350	13380	6950
ASTM 6x12	28	5990	-	8840	-	9640	-	13150	-
Splitting Tensile Strength		f_{ct} (psi)		f_{ct} (psi)		f_{ct} (psi)		f_{ct} (psi)	
Air-Cured	28	560		760		840		830	
	Post-Test	590		740		810		780	
Modulus of Rupture		f_r (psi)		f_r (psi)		f_r (psi)		f_r (psi)	
Air-Cured	Post-Test	1050		1250		1280		1520	
ASTM	Post-Test	875		1215		1400		1760	

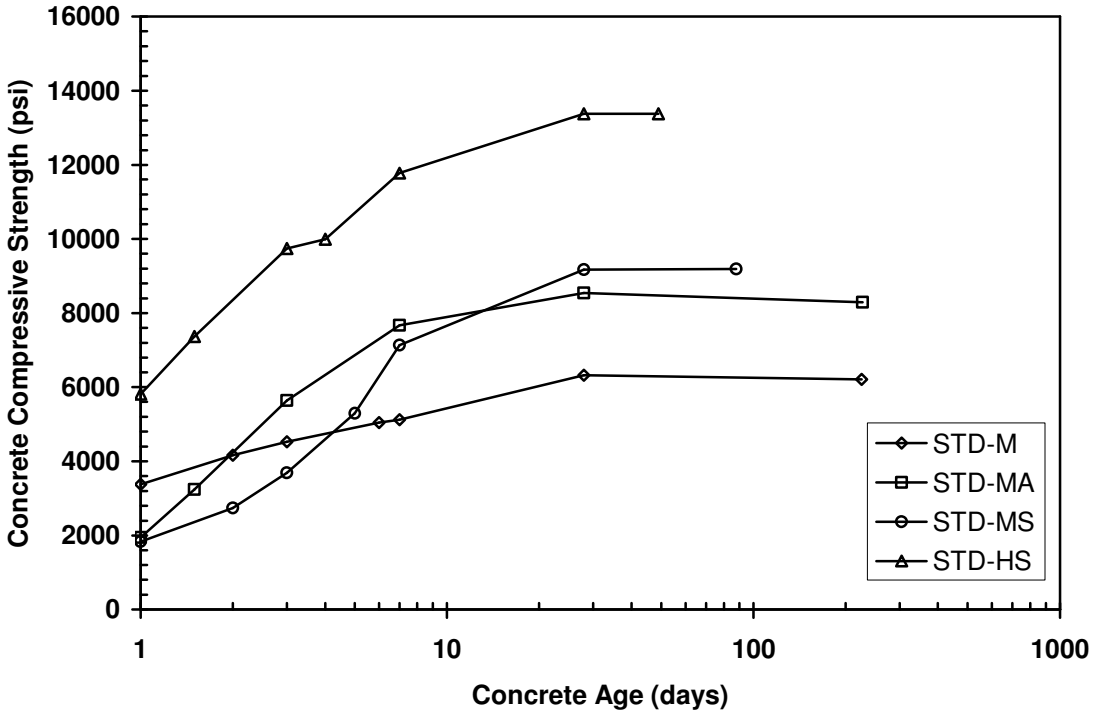

Figure E-1: Air-Cured 4 x 8 in. Cylinder Compressive Strength vs. Concrete Age

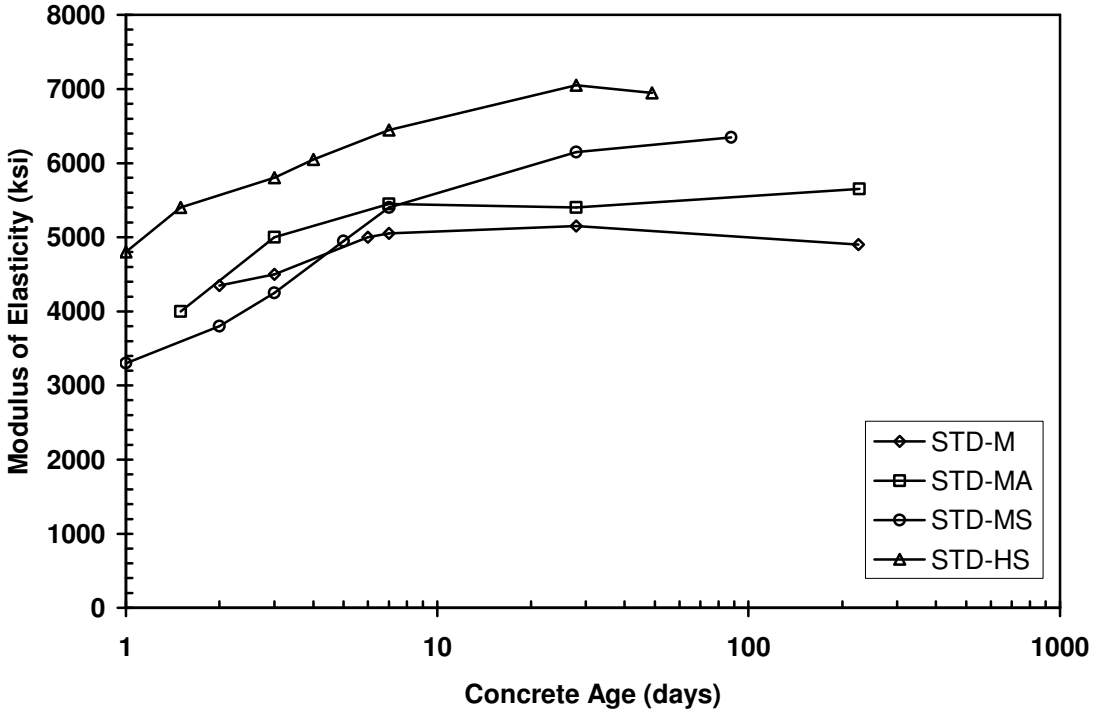

Figure E-2: Air-Cured 4 x 8 in. Cylinder Elastic Modulus vs. Concrete Age

APPENDIX F

CONCRETE STRAIN PROFILES

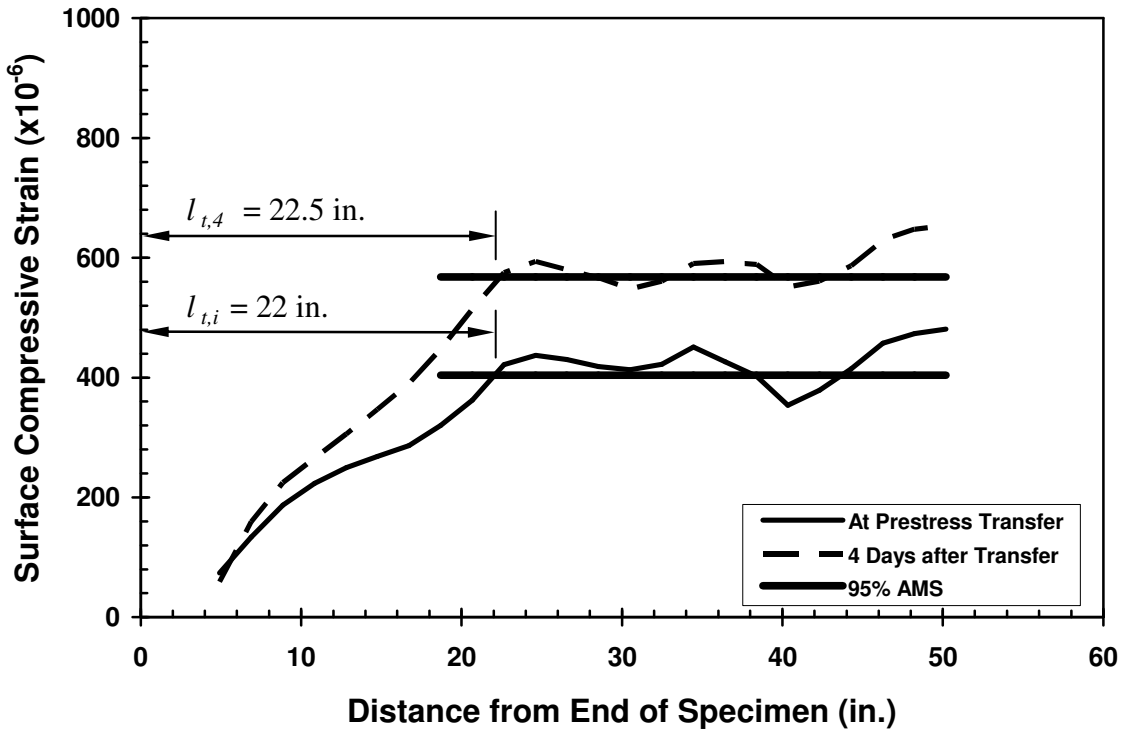

Figure F-1: Initial and Four-Day Transfer Lengths for STD-M-AE

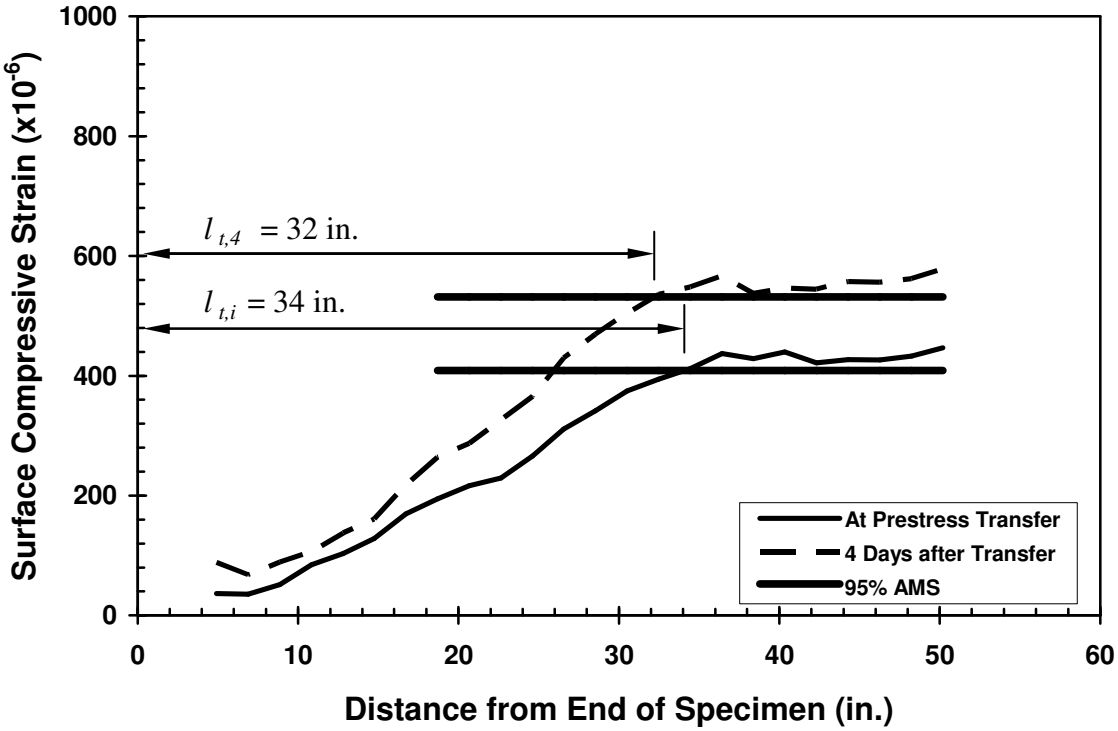

Figure F-2: Initial and Four-Day Transfer Lengths for STD-M-AW

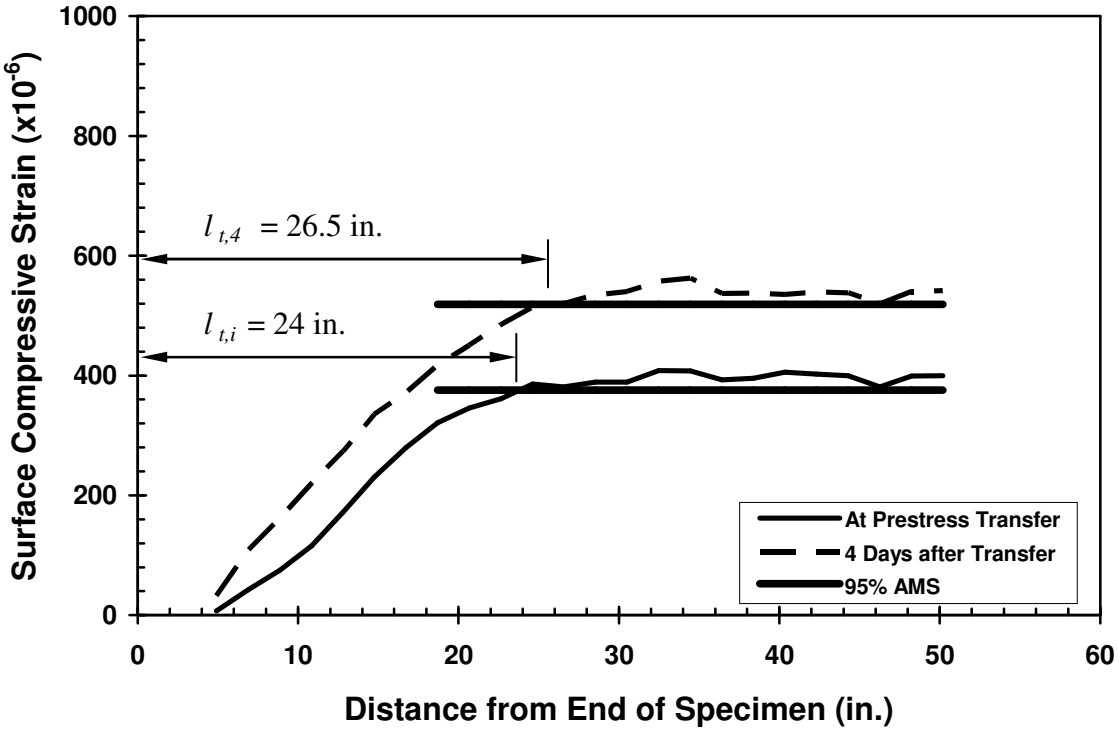

Figure F-3: Initial and Four-Day Transfer Lengths for STD-M-BE

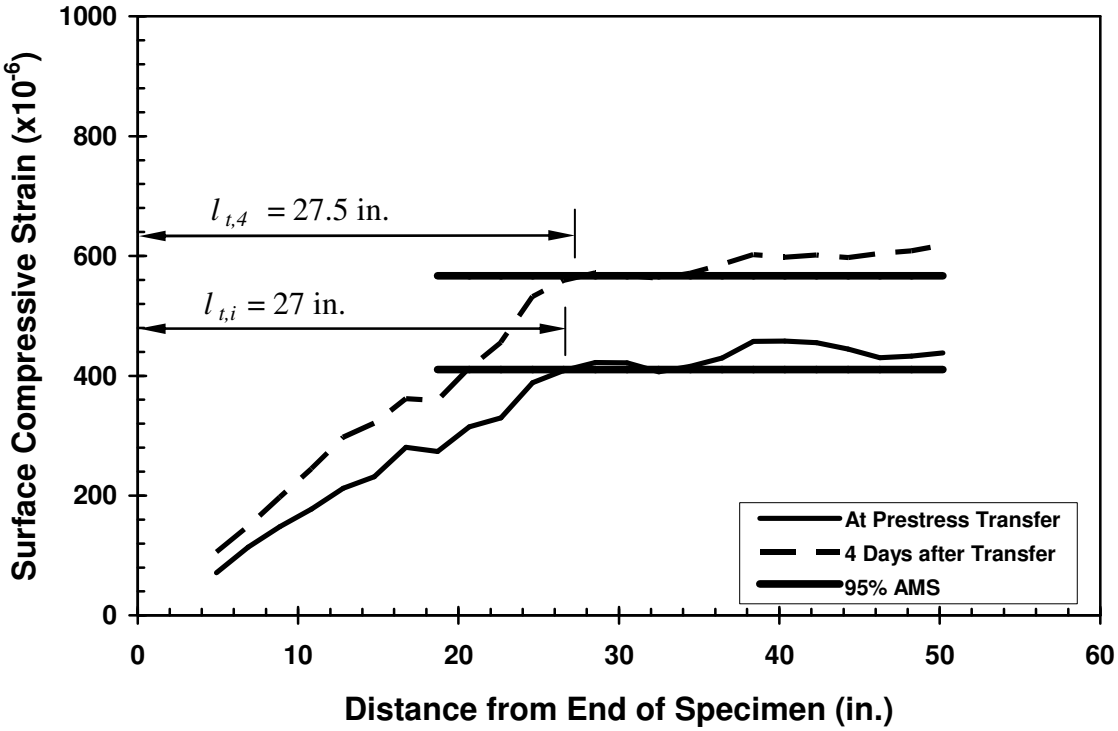

Figure F-4: Initial and Four-Day Transfer Lengths for STD-M-BW

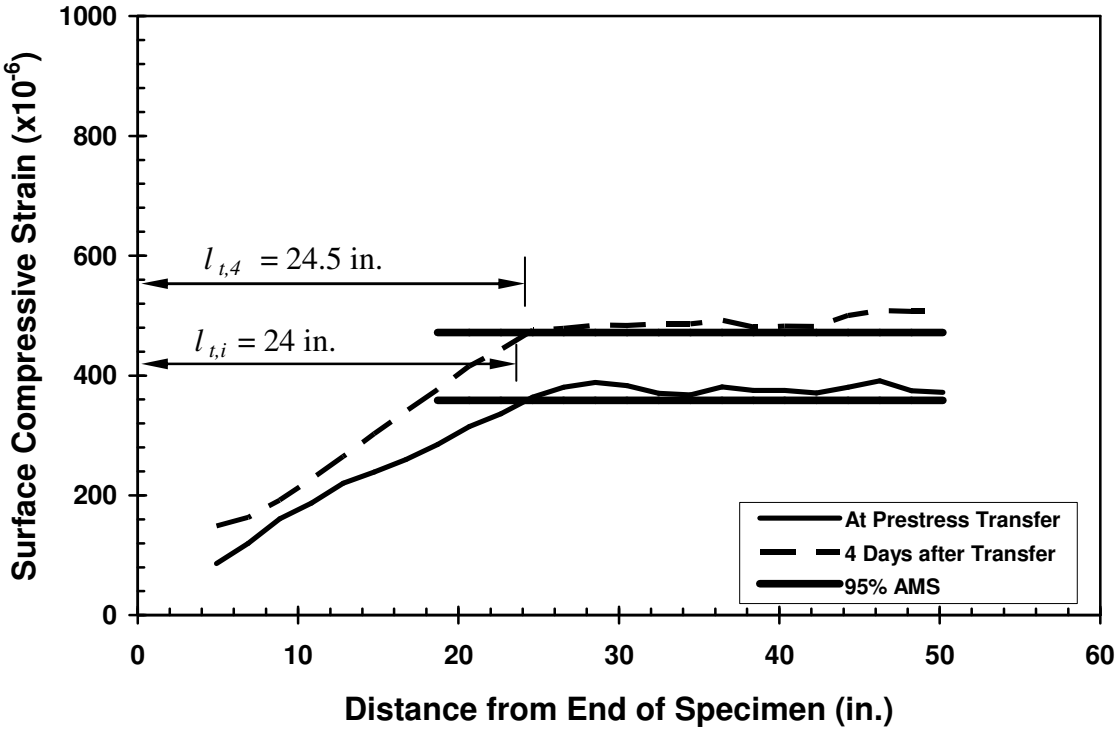

Figure F-5: Initial and Four-Day Transfer Lengths for STD-M-CE

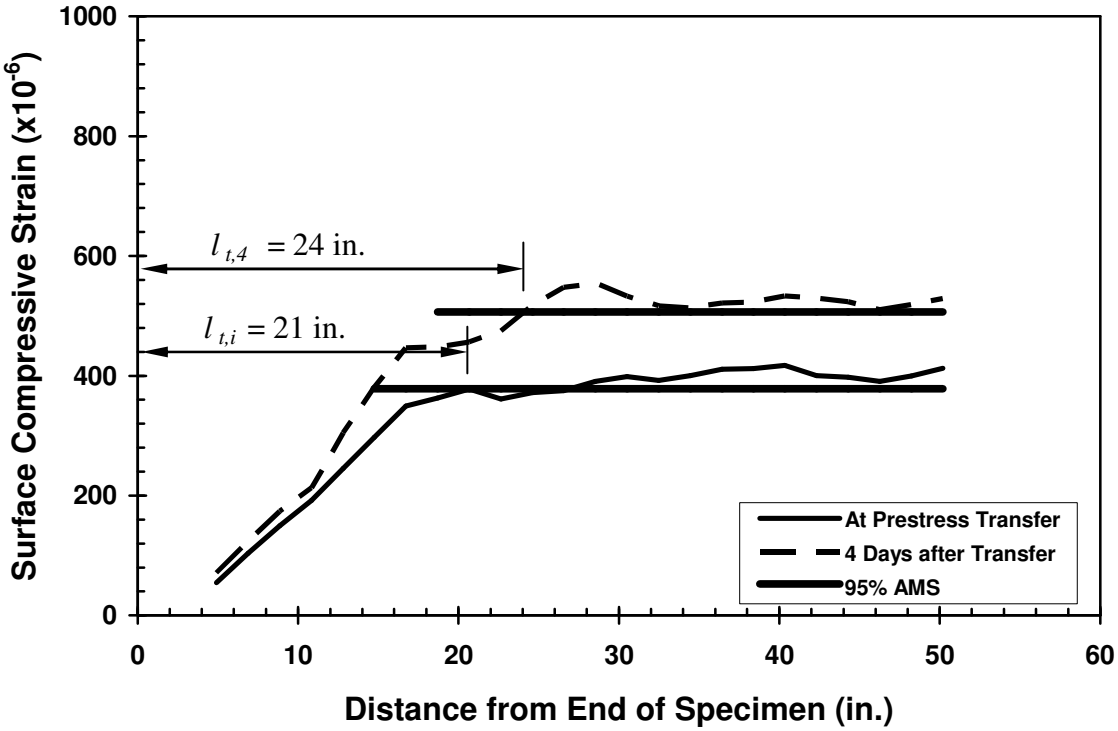

Figure F-6: Initial and Four-Day Transfer Lengths for STD-M-CW

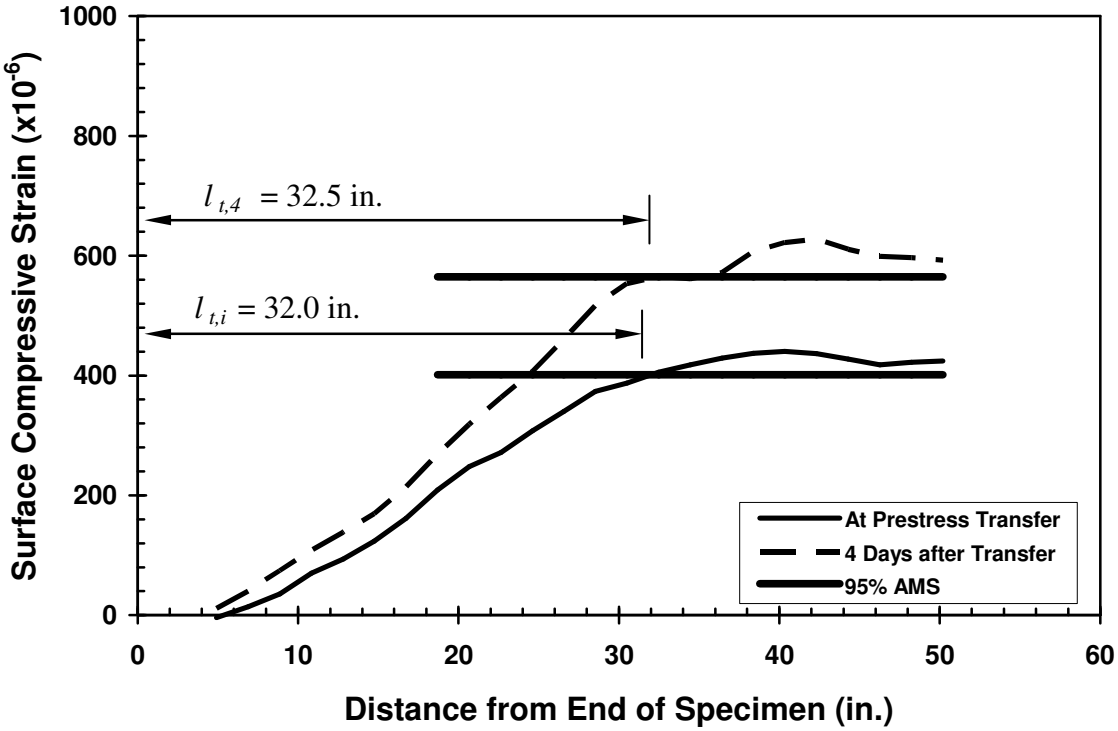

Figure F-7: Initial and Four-Day Transfer Lengths for STD-M-DE

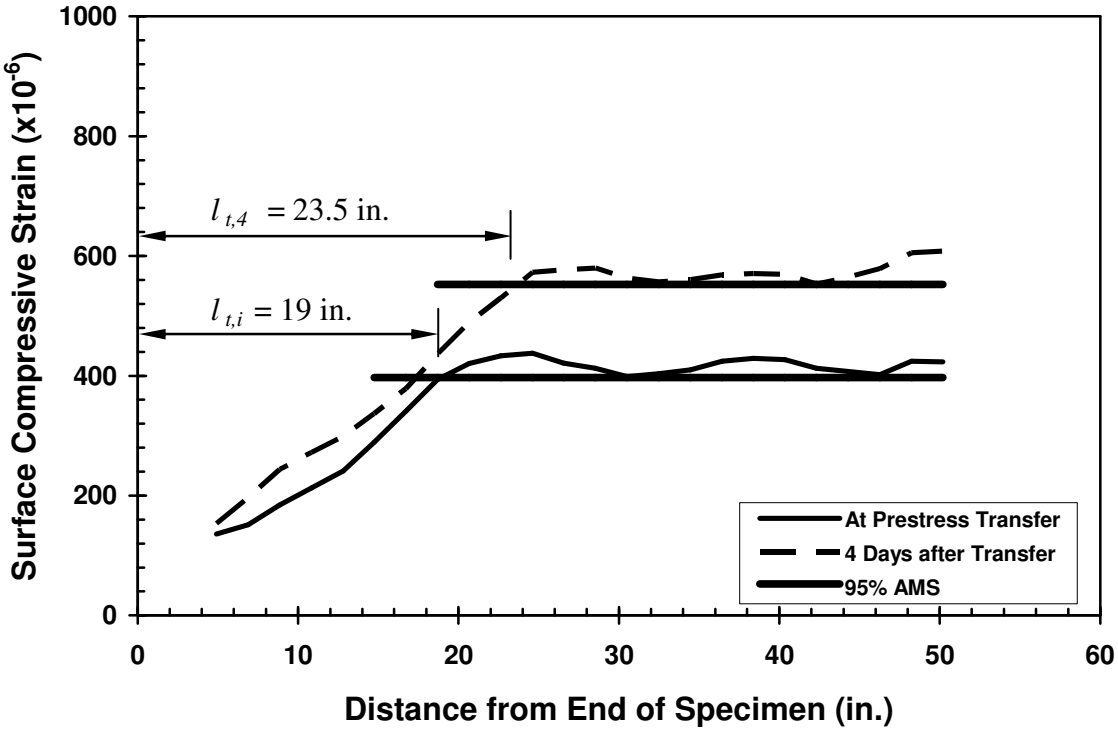

Figure F-8: Initial and Four-Day Transfer Lengths for STD-M-DW

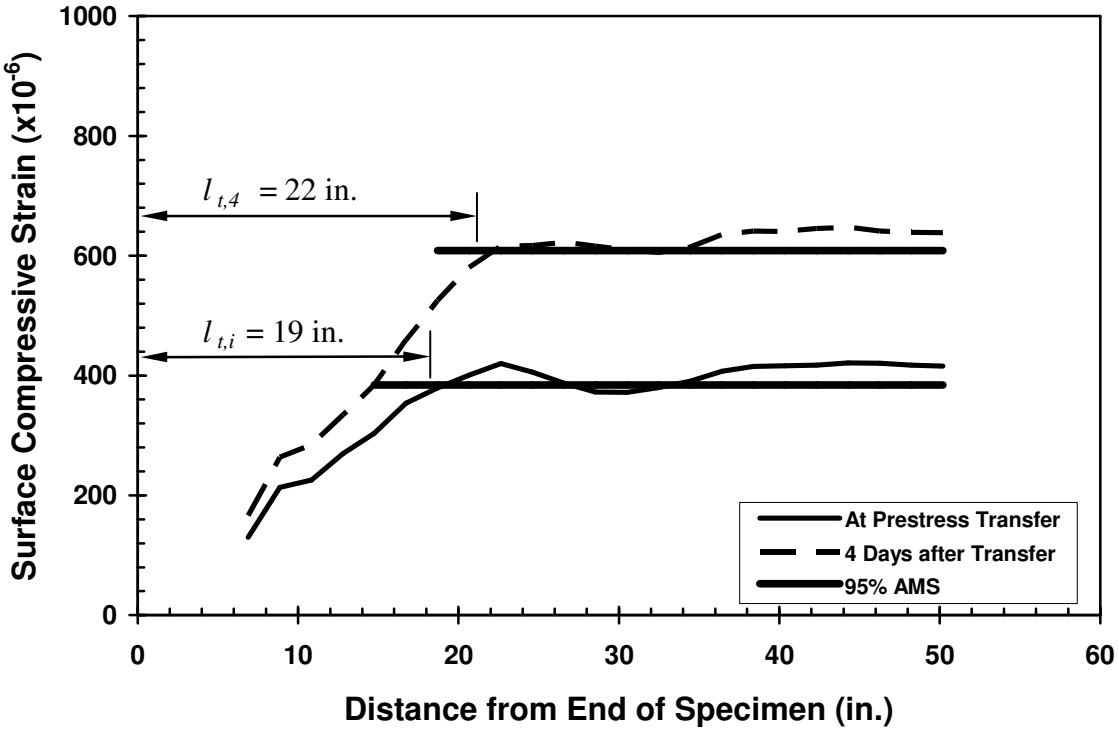

Figure F-9: Initial and Four-Day Transfer Lengths for SCC-MA-AE

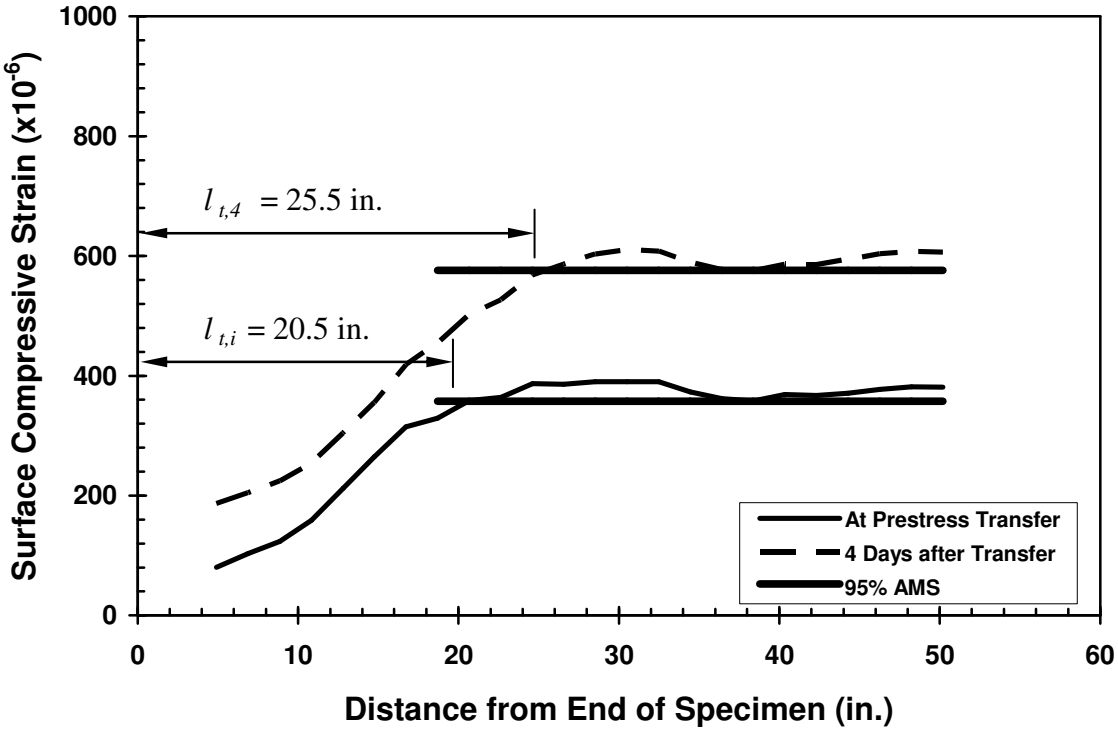

Figure F-10: Initial and Four-Day Transfer Lengths for SCC-MA-AW

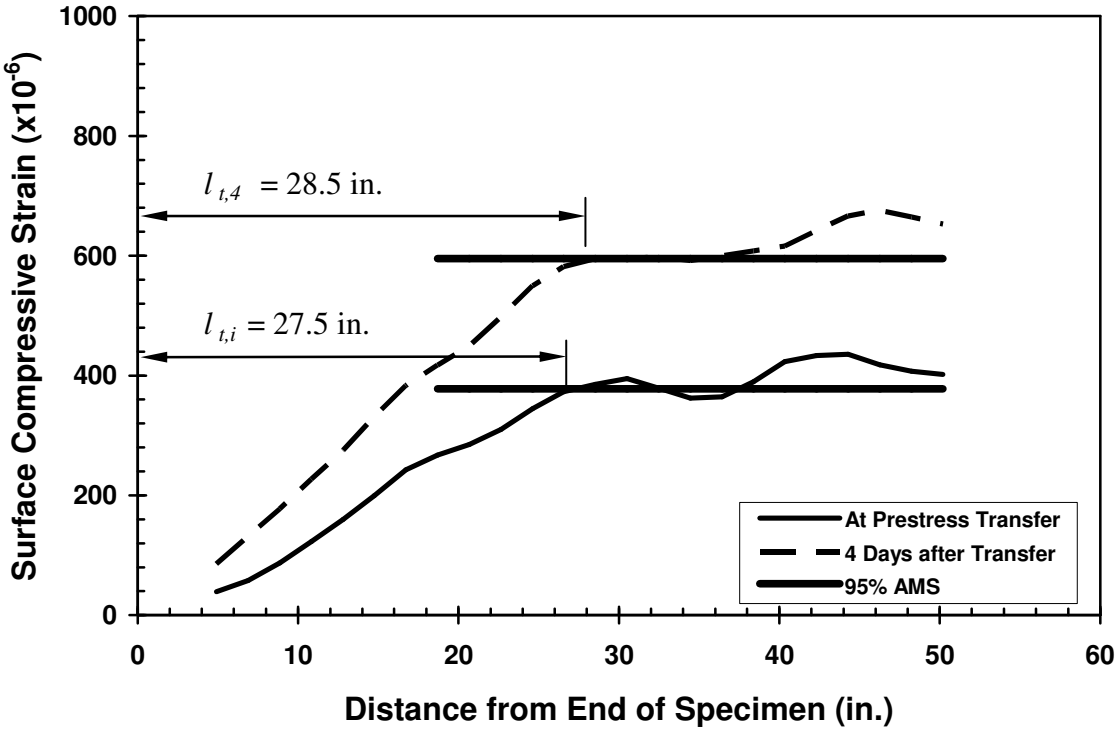

Figure F-11: Initial and Four-Day Transfer Lengths for SCC-MA-BE

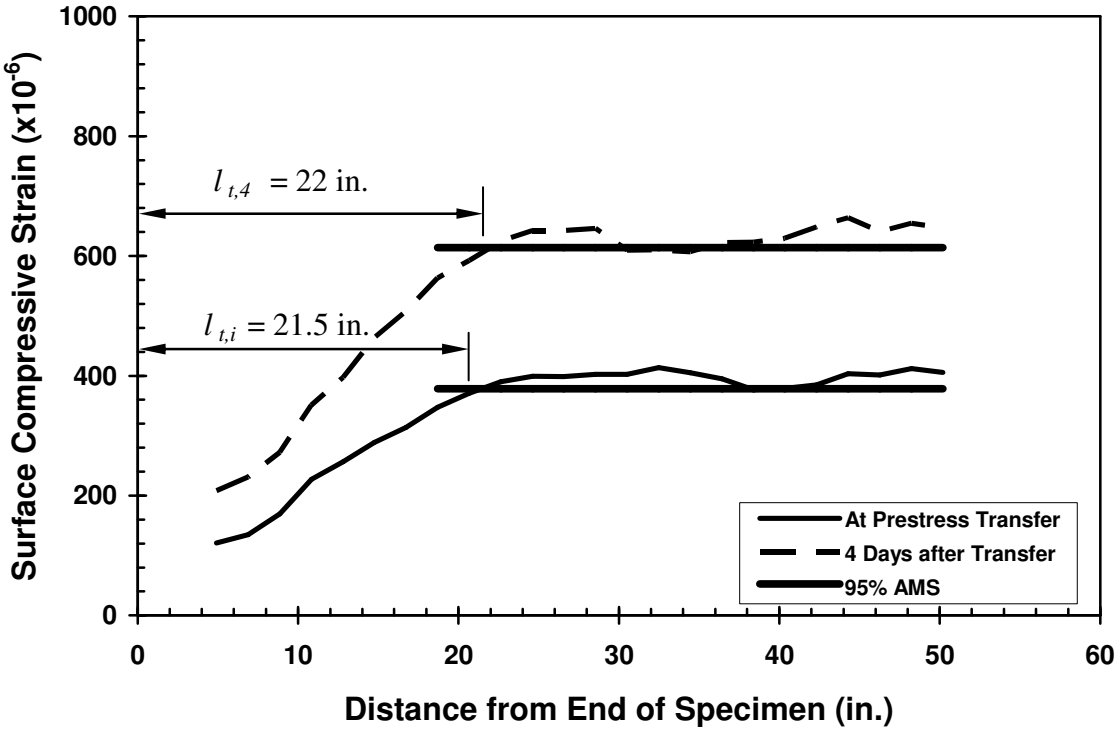

Figure F-12: Initial and Four-Day Transfer Lengths for SCC-MA-BW

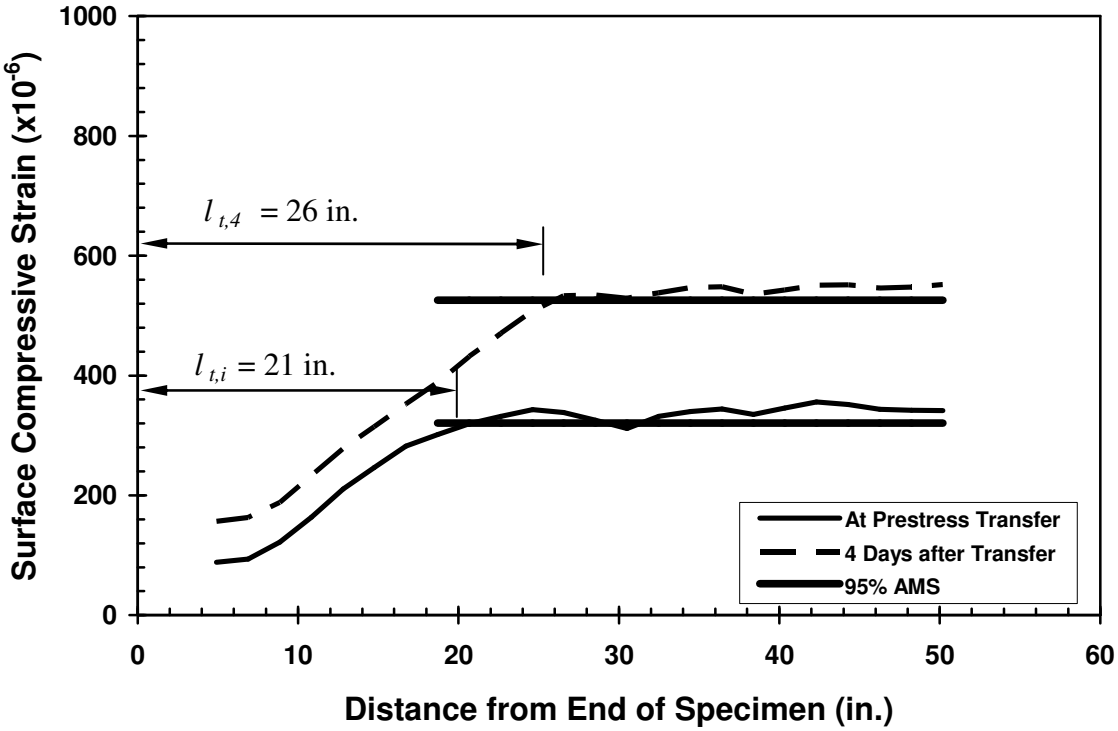

Figure F-13: Initial and Four-Day Transfer Lengths for SCC-MA-CE

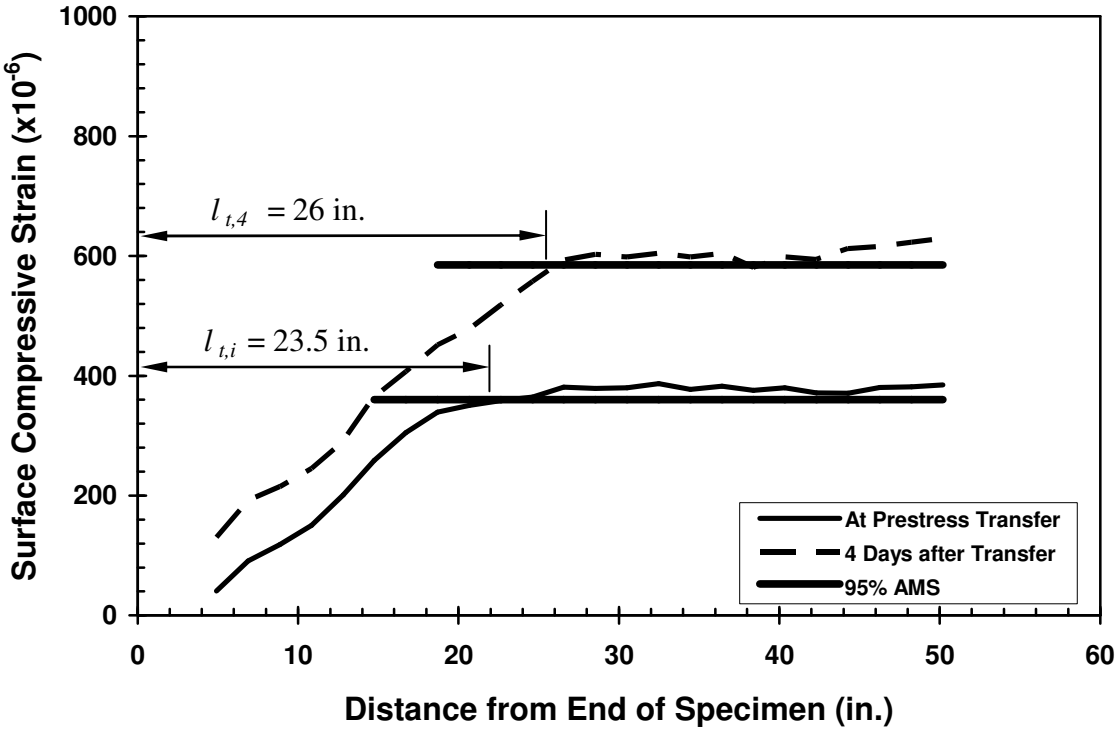

Figure F-14: Initial and Four-Day Transfer Lengths for SCC-MA-CW

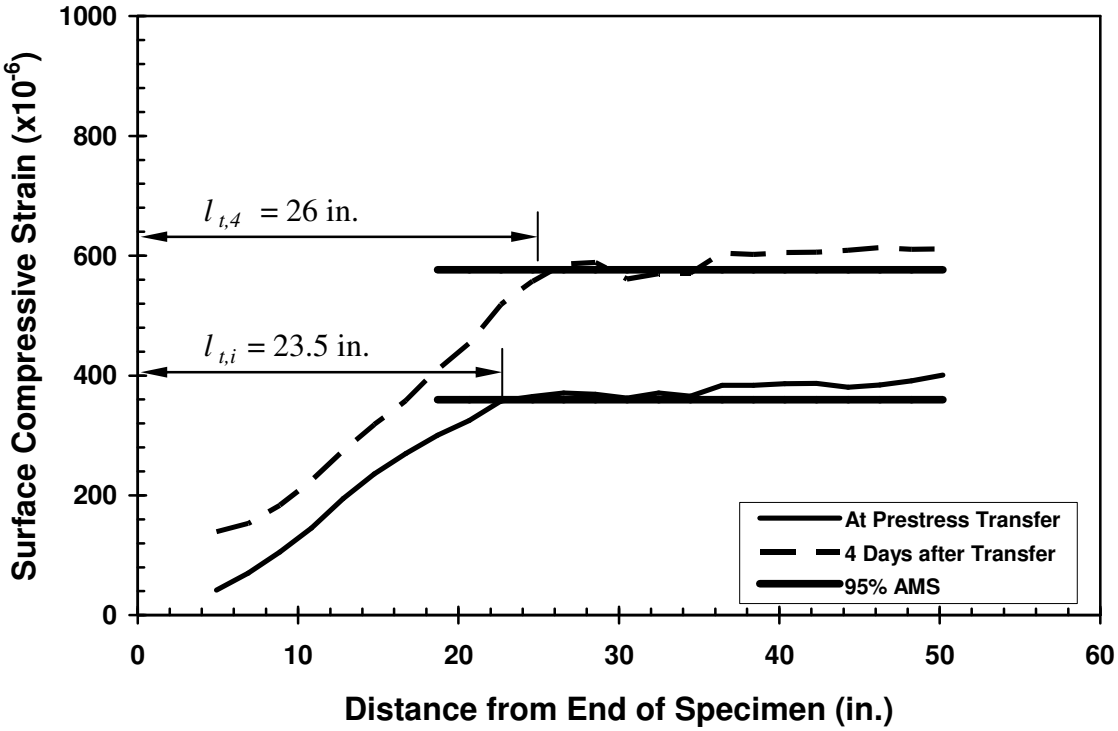

Figure F-15: Initial and Four-Day Transfer Lengths for SCC-MA-DE

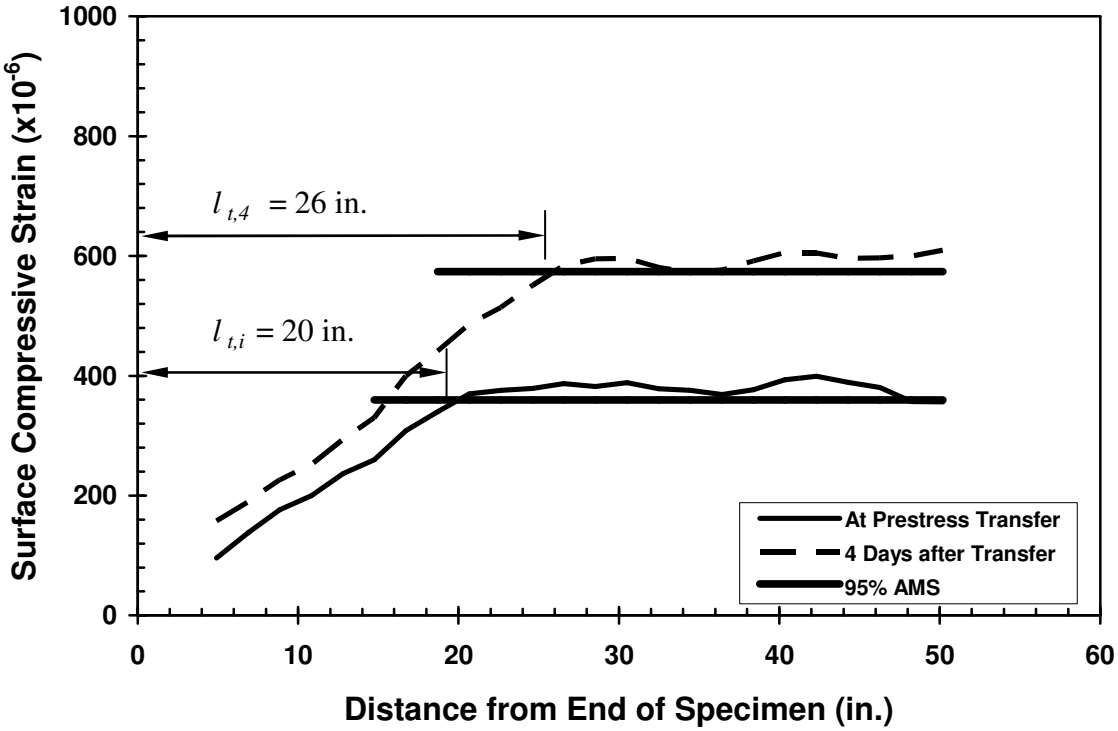

Figure F-16: Initial and Four-Day Transfer Lengths for SCC-MA-DW

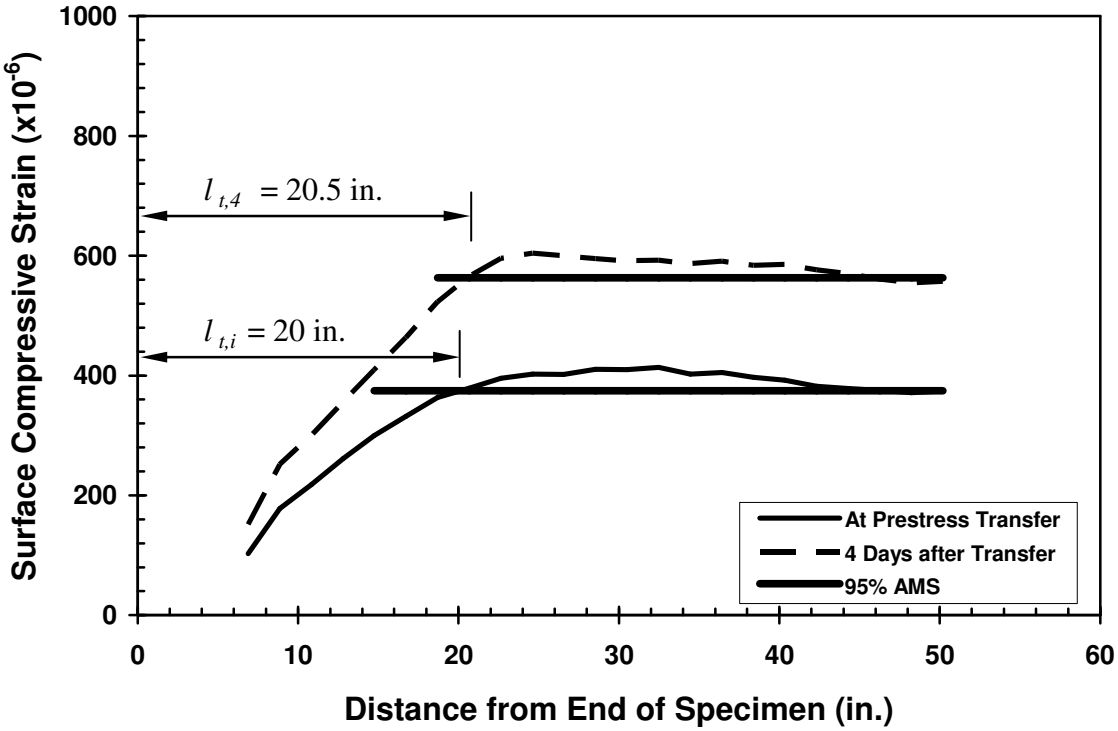

Figure F-17: Initial and Four-Day Transfer Lengths for SCC-MS-AE

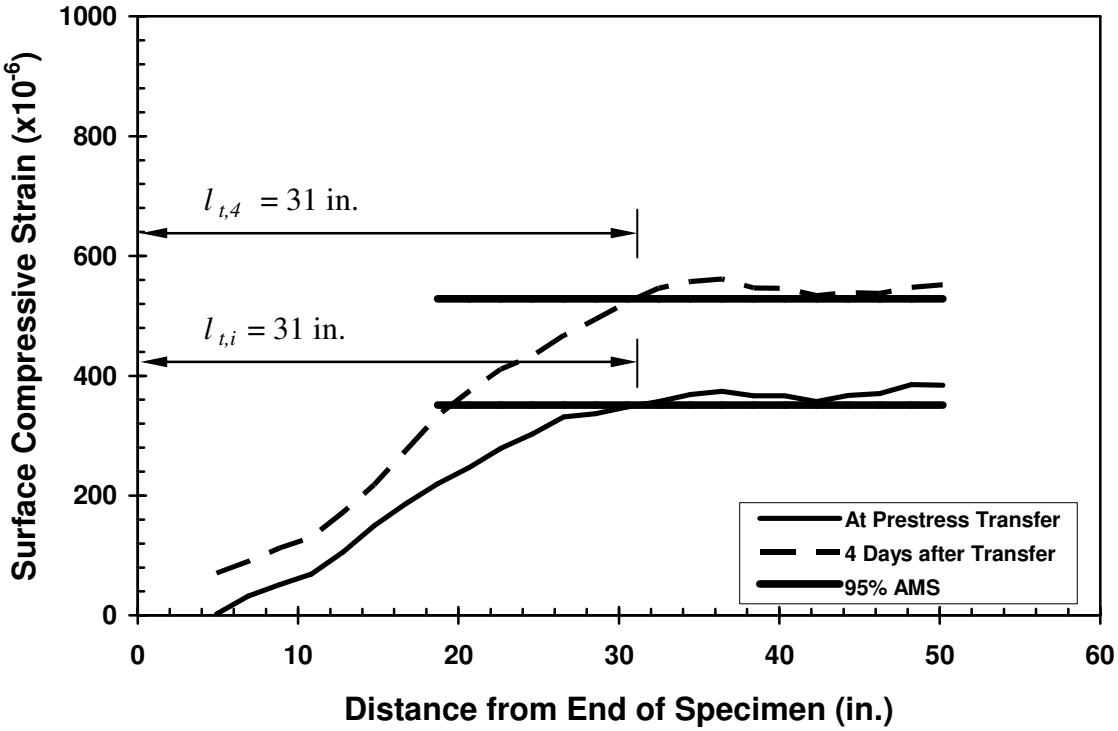

Figure F-18: Initial and Four-Day Transfer Lengths for SCC-MS-AW

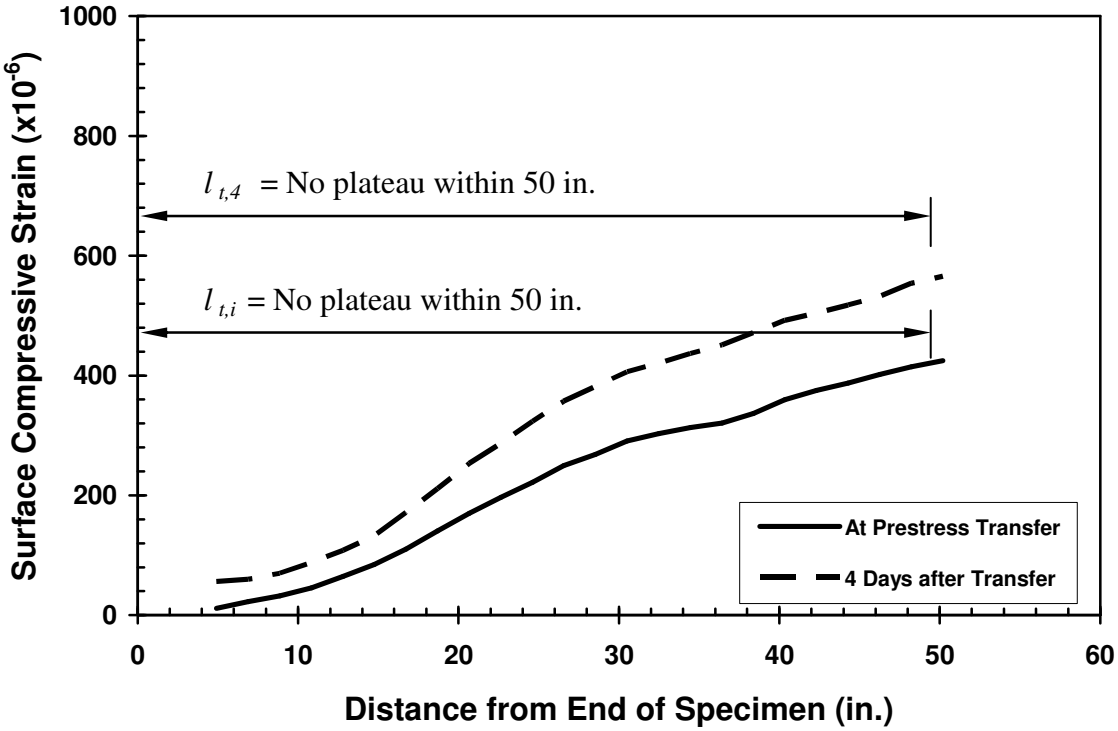

Figure F-19: Initial and Four-Day Transfer Lengths for SCC-MS-BE

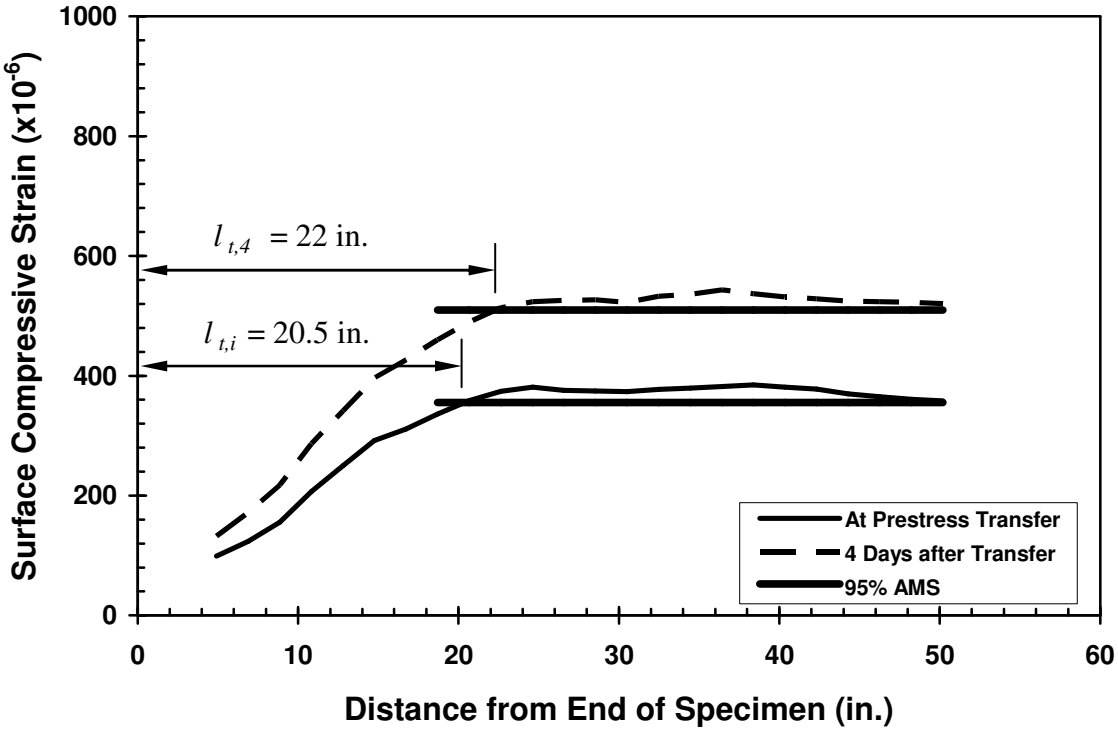

Figure F-20: Initial and Four-Day Transfer Lengths for SCC-MS-BW

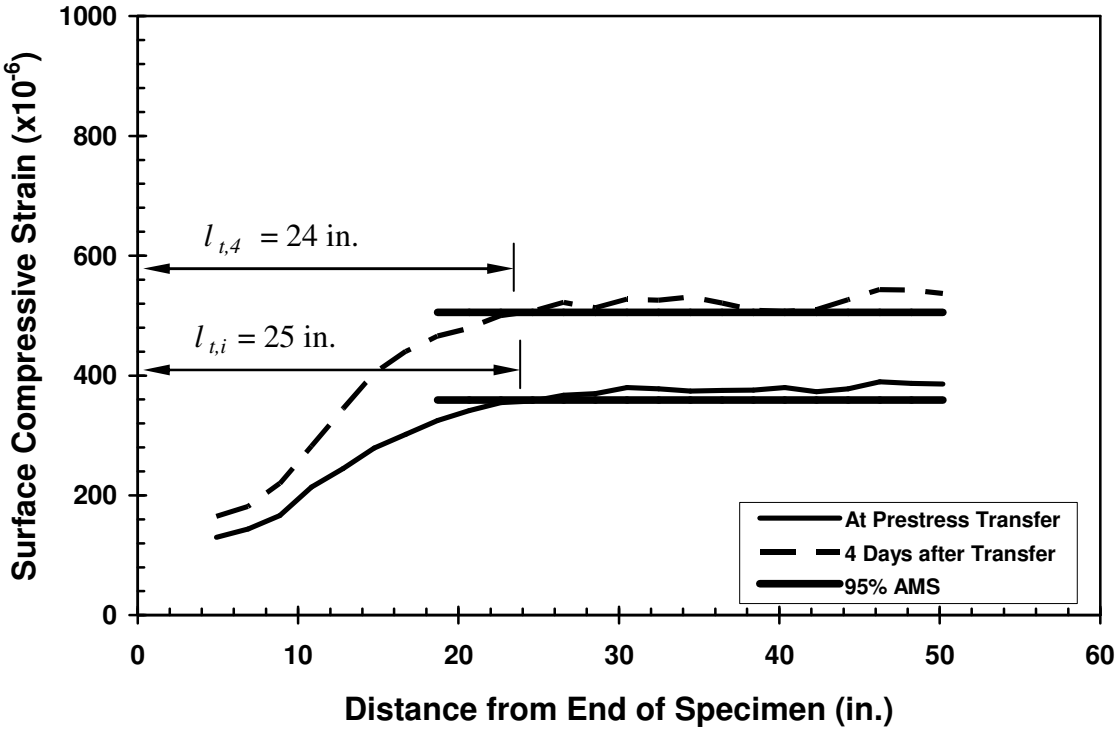

Figure F-21: Initial and Four-Day Transfer Lengths for SCC-MS-CE

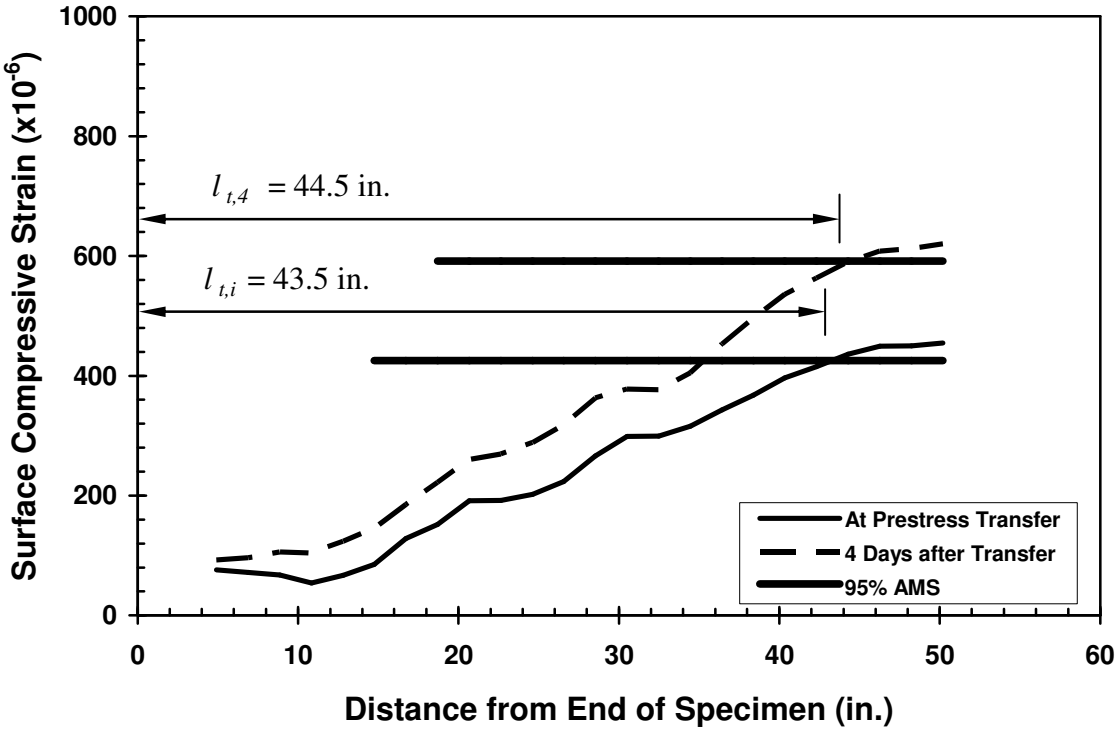

Figure F-22: Initial and Four-Day Transfer Lengths for SCC-MS-CW

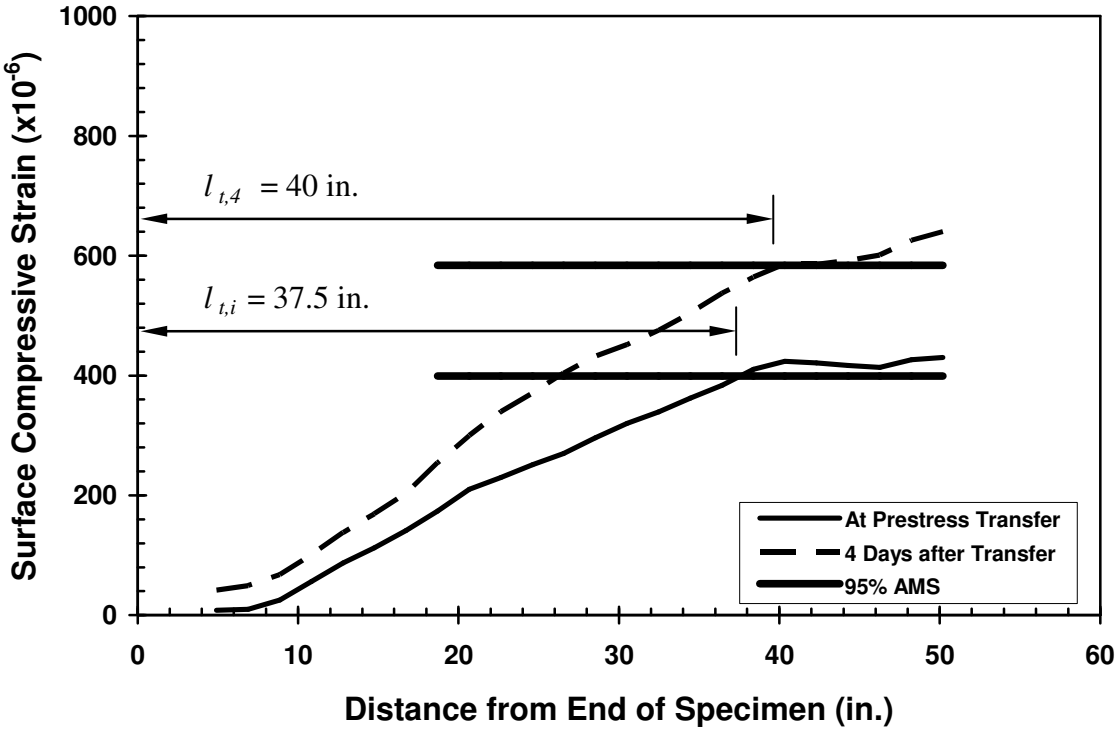

Figure F-23: Initial and Four-Day Transfer Lengths for SCC-MS-DE

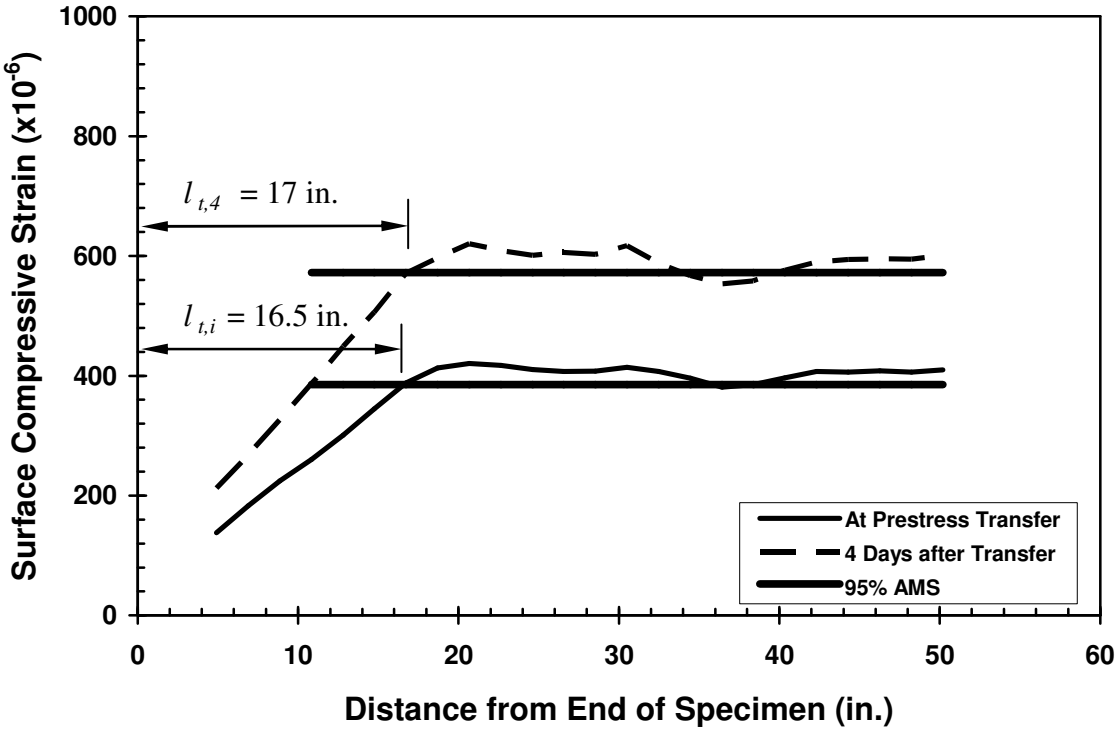

Figure F-24: Initial and Four-Day Transfer Lengths for SCC-MS-DW

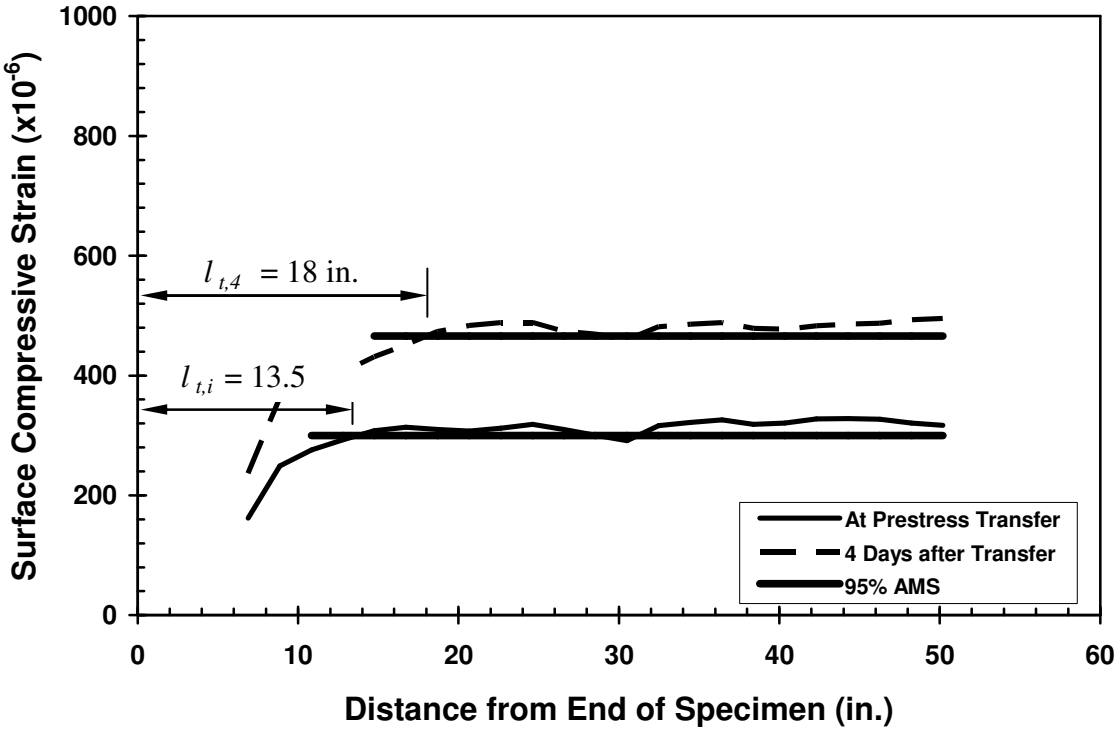

Figure F-25: Initial and Four-Day Transfer Lengths for SCC-HS-AE

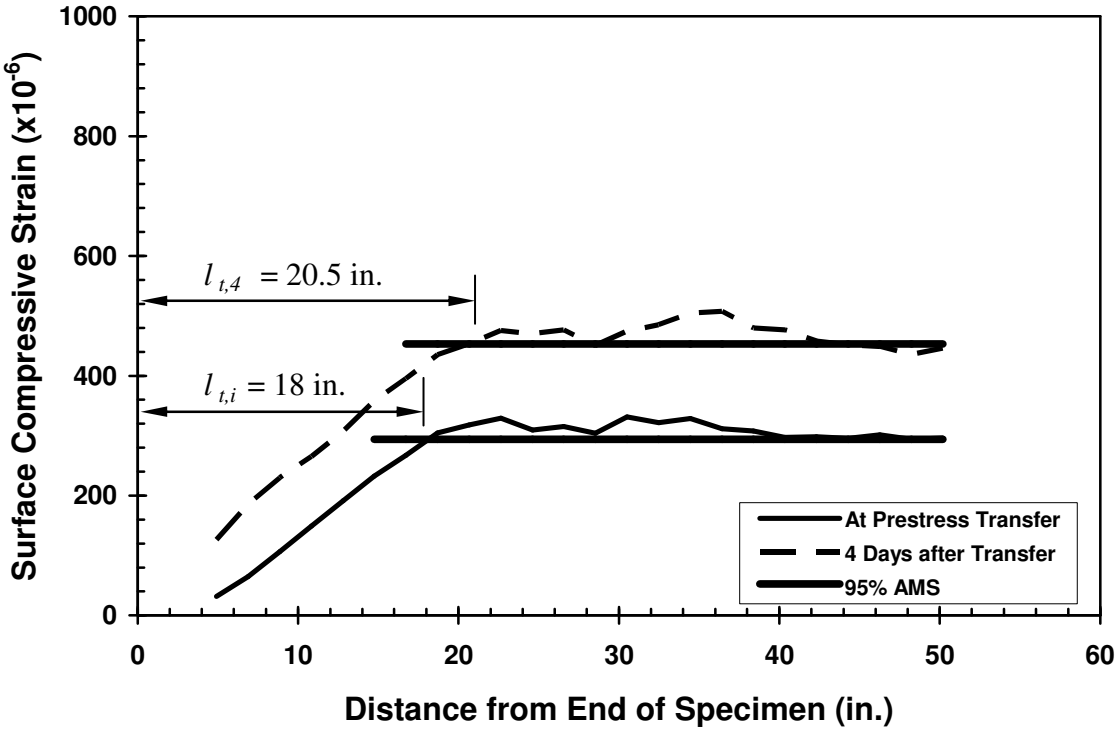

Figure F-26: Initial and Four-Day Transfer Lengths for SCC-HS-AW

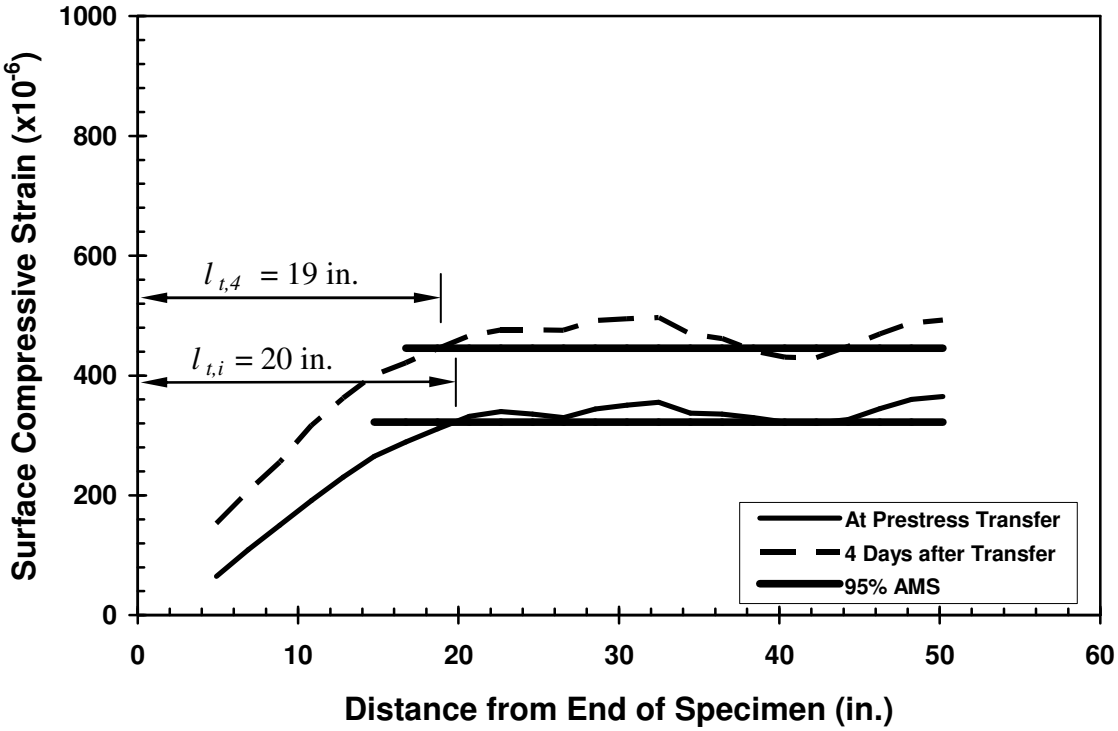

Figure F-27: Initial and Four-Day Transfer Lengths for SCC-HS-BE

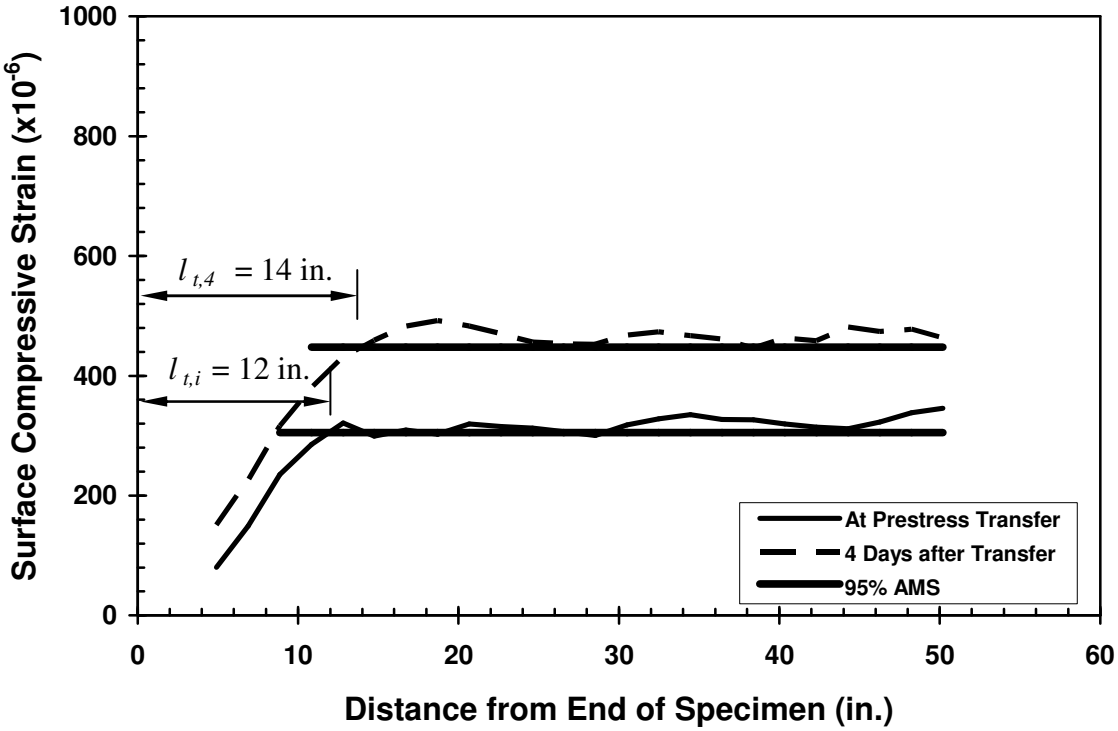

Figure F-28: Initial and Four-Day Transfer Lengths for SCC-HS-BW

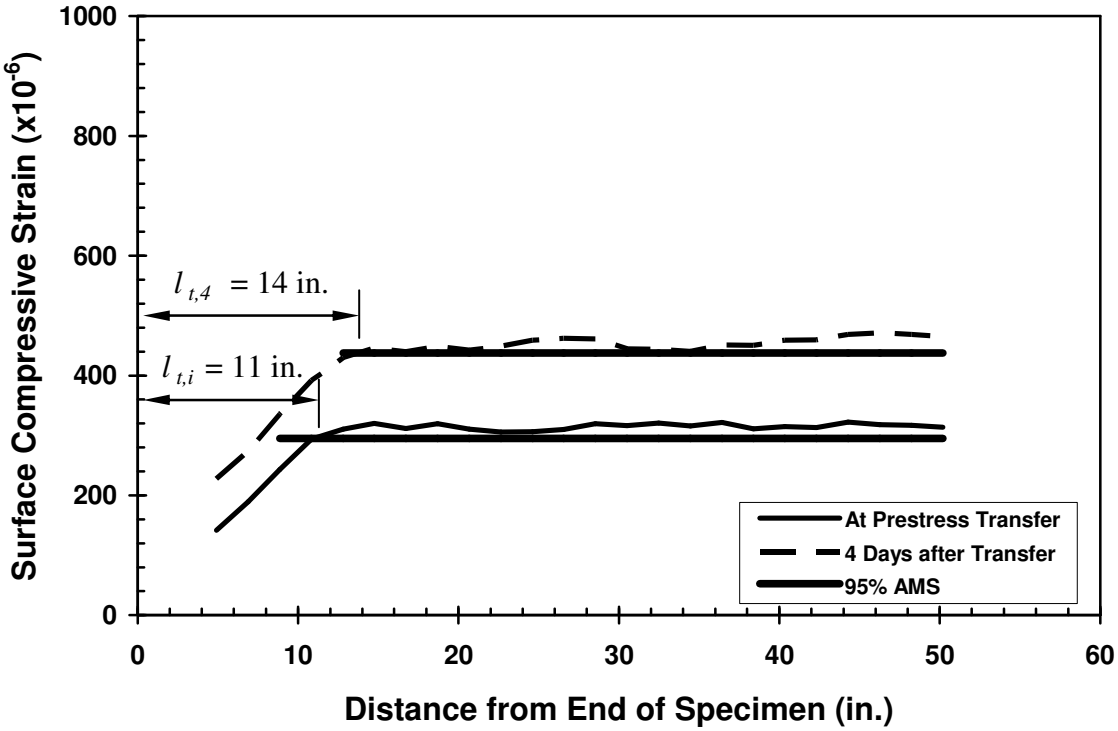

Figure F-29: Initial and Four-Day Transfer Lengths for SCC-HS-CE

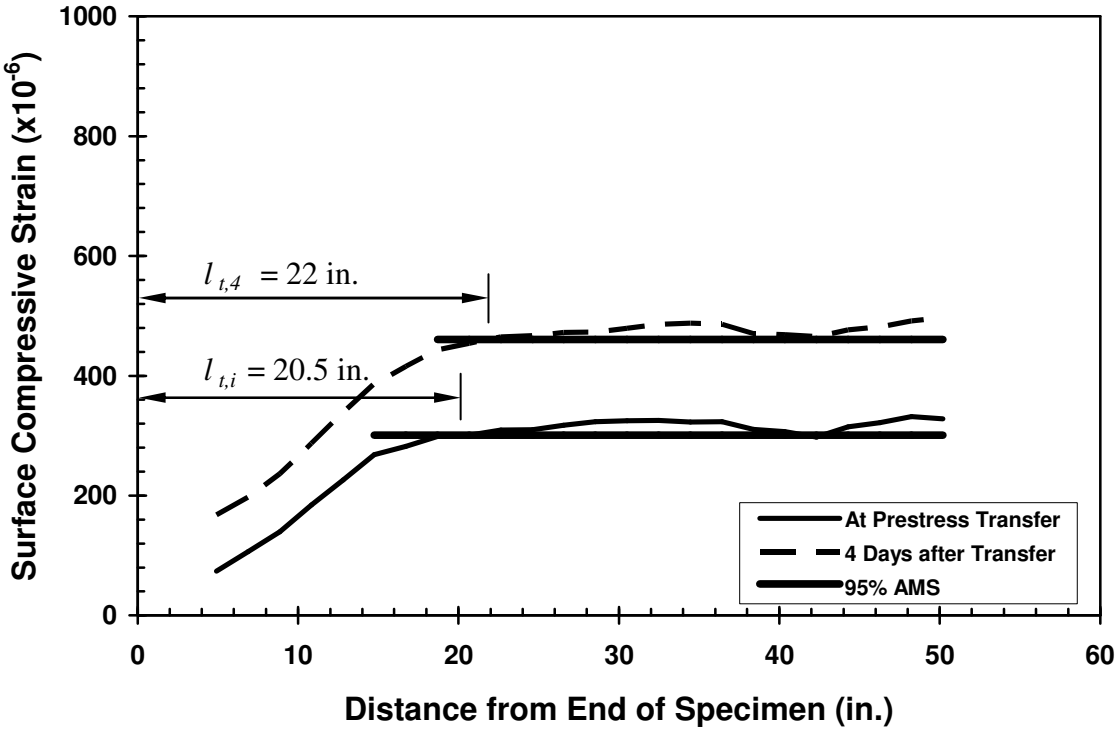

Figure F-30: Initial and Four-Day Transfer Lengths for SCC-HS-CW

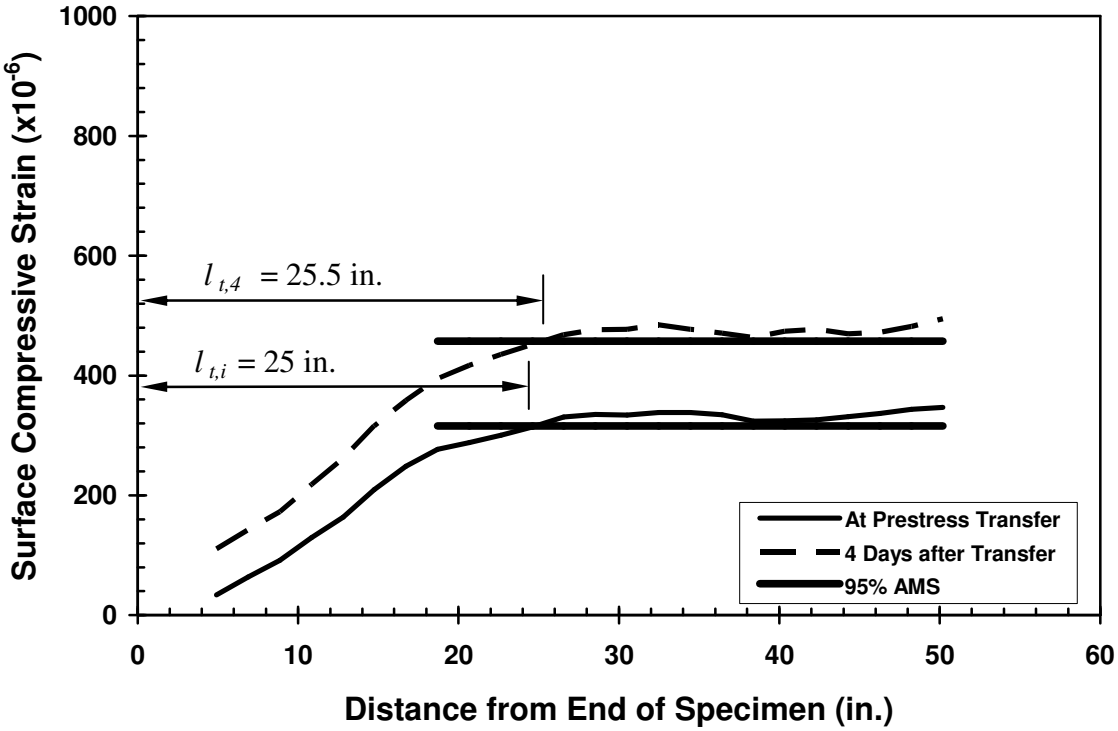

Figure F-31: Initial and Four-Day Transfer Lengths for SCC-HS-DE

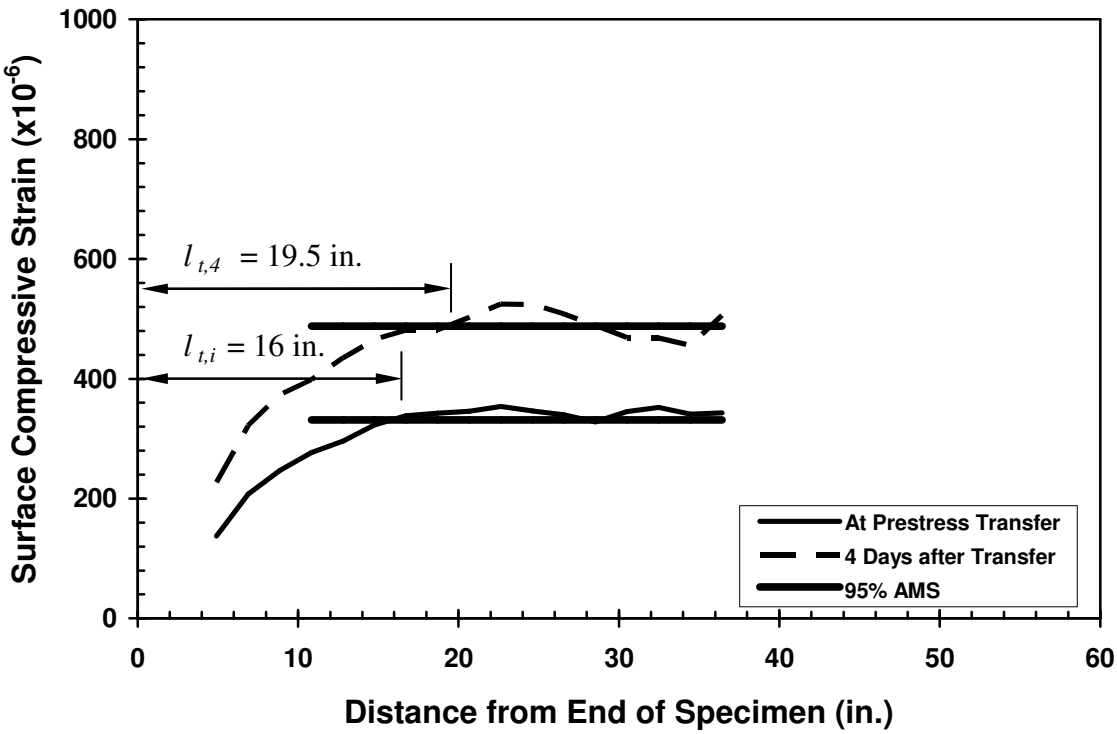

Figure F-32: Initial and Four-Day Transfer Lengths for SCC-HS-DW

APPENDIX G

TRANSFER LENGTH GRAPHS

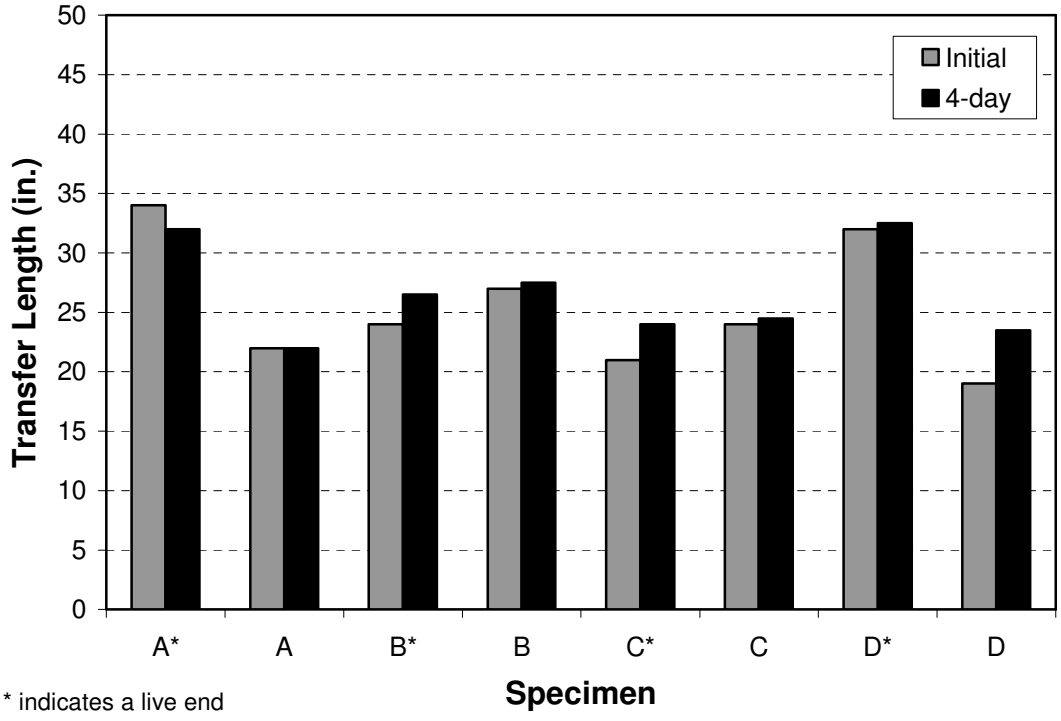

Figure G-1: Transfer Lengths for STD-M

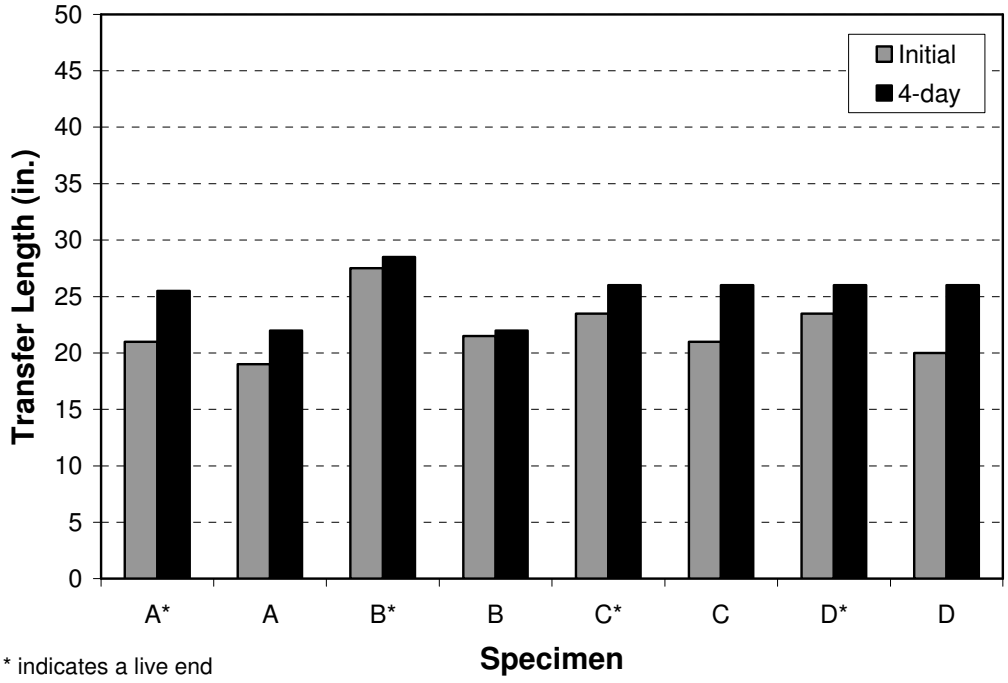

Figure G-2: Transfer Lengths for SCC-MA

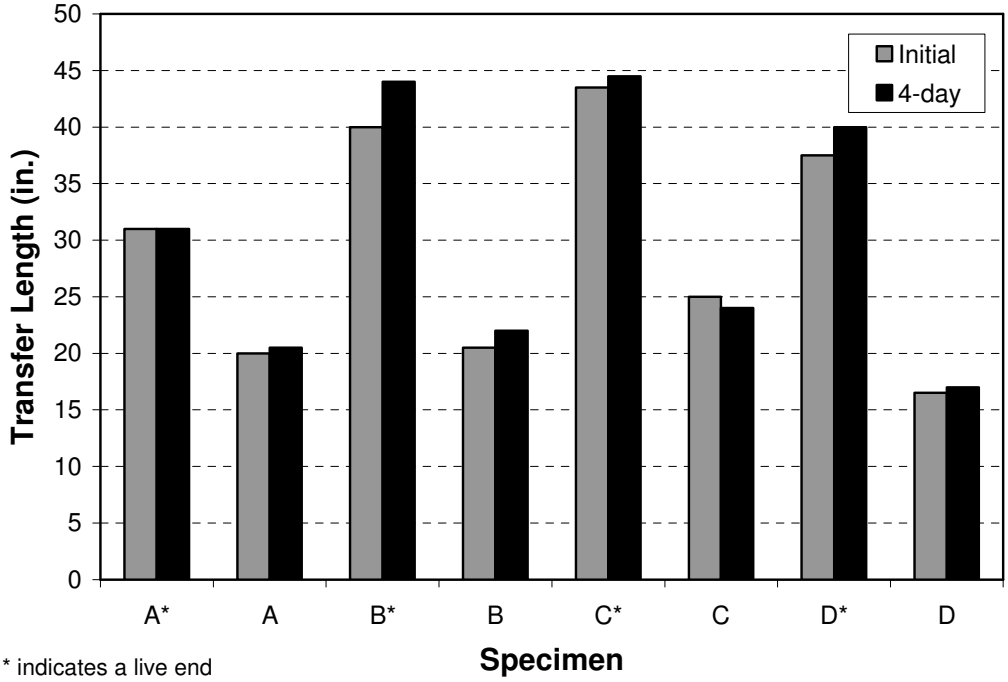

Figure G-3: Transfer Lengths for SCC-MS

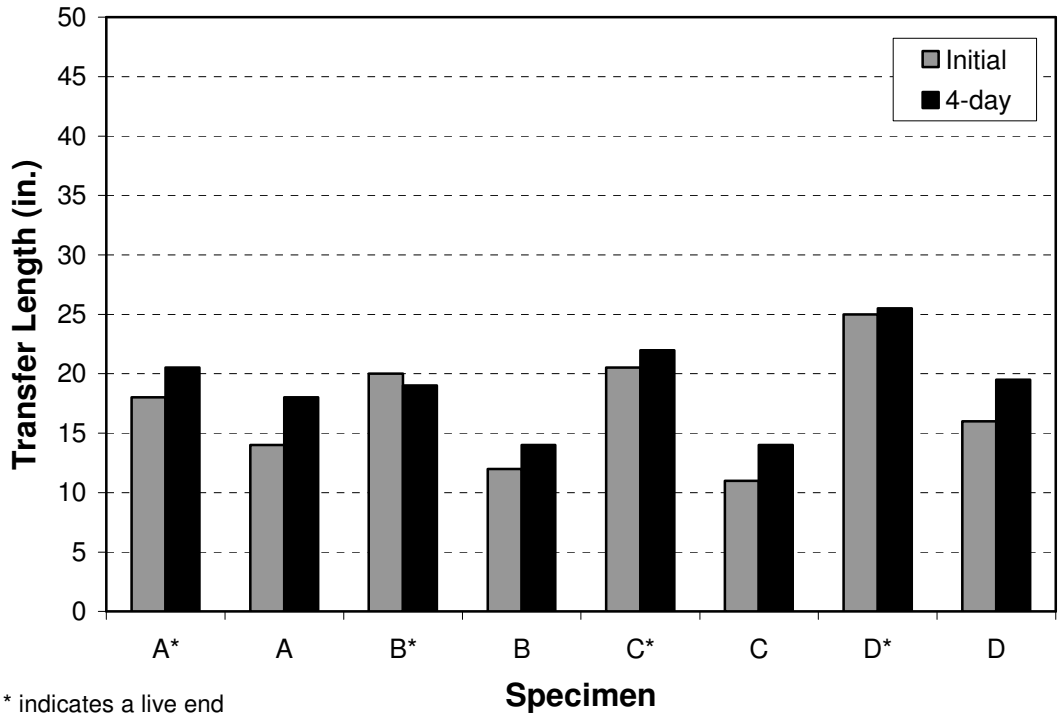

Figure G-4: Transfer Lengths for SCC-HS

APPENDIX H

LOAD VERSUS DISPLACEMENT DIAGRAMS

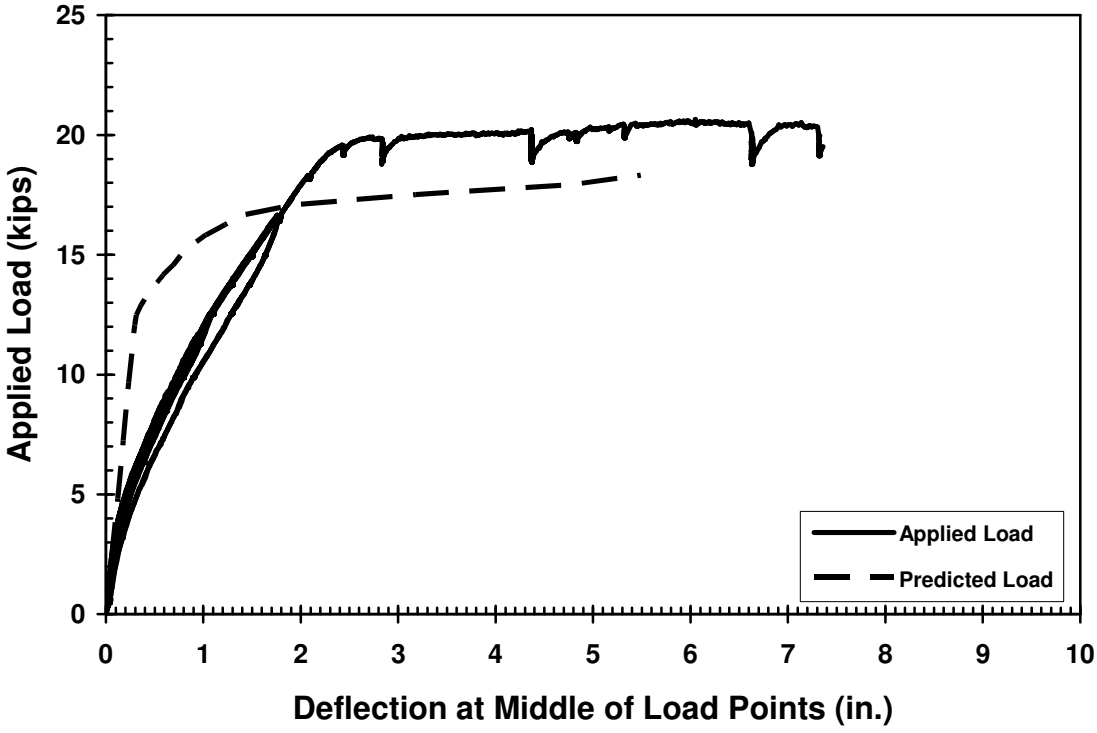

Figure H-1: Load vs. Displacement for STD-M-A

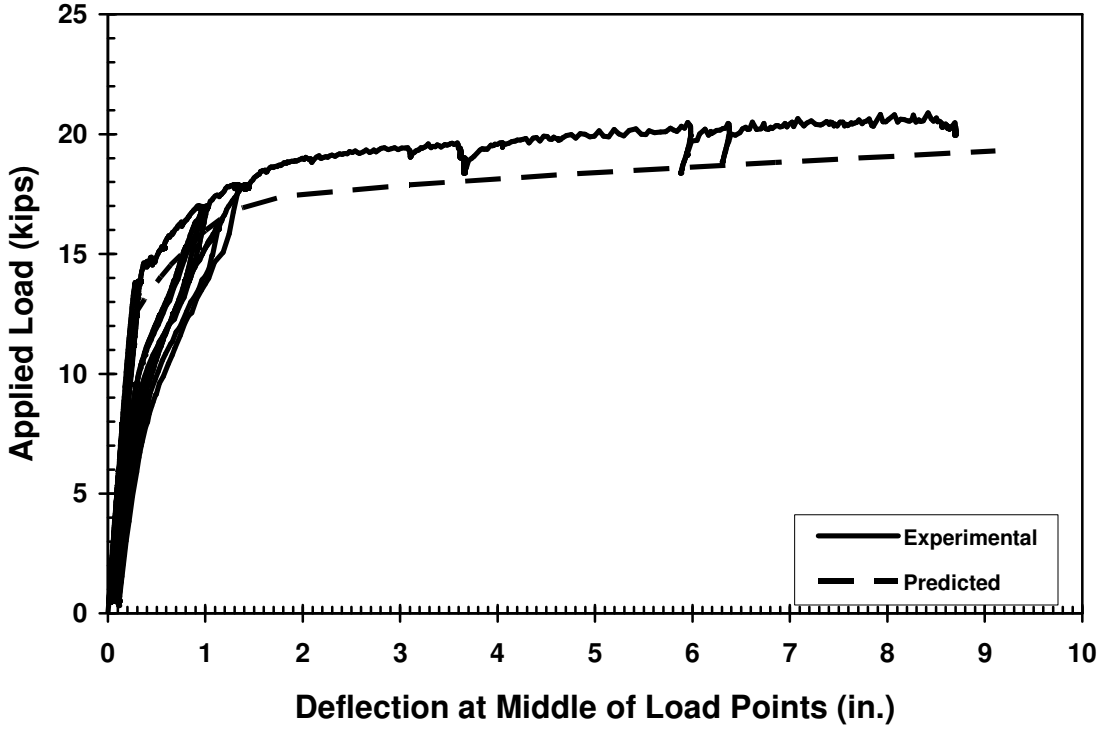

Figure H-2: Load vs. Displacement for SCC-MA-A

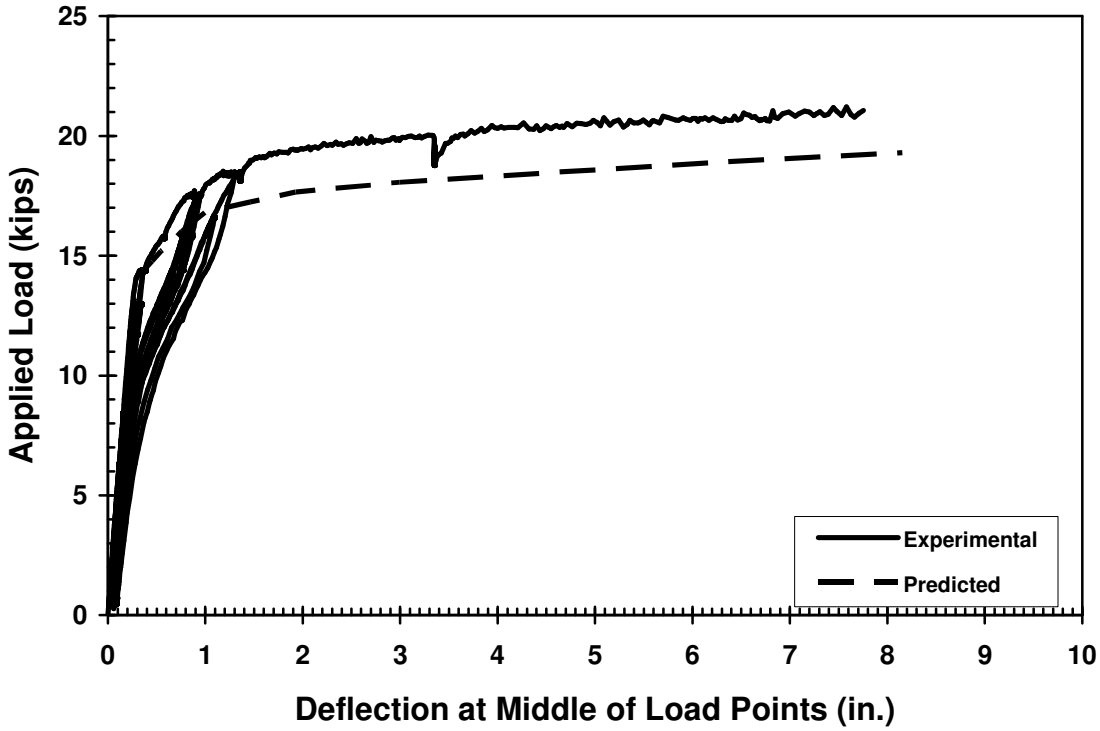

Figure H-3: Load vs. Displacement for SCC-MS-A

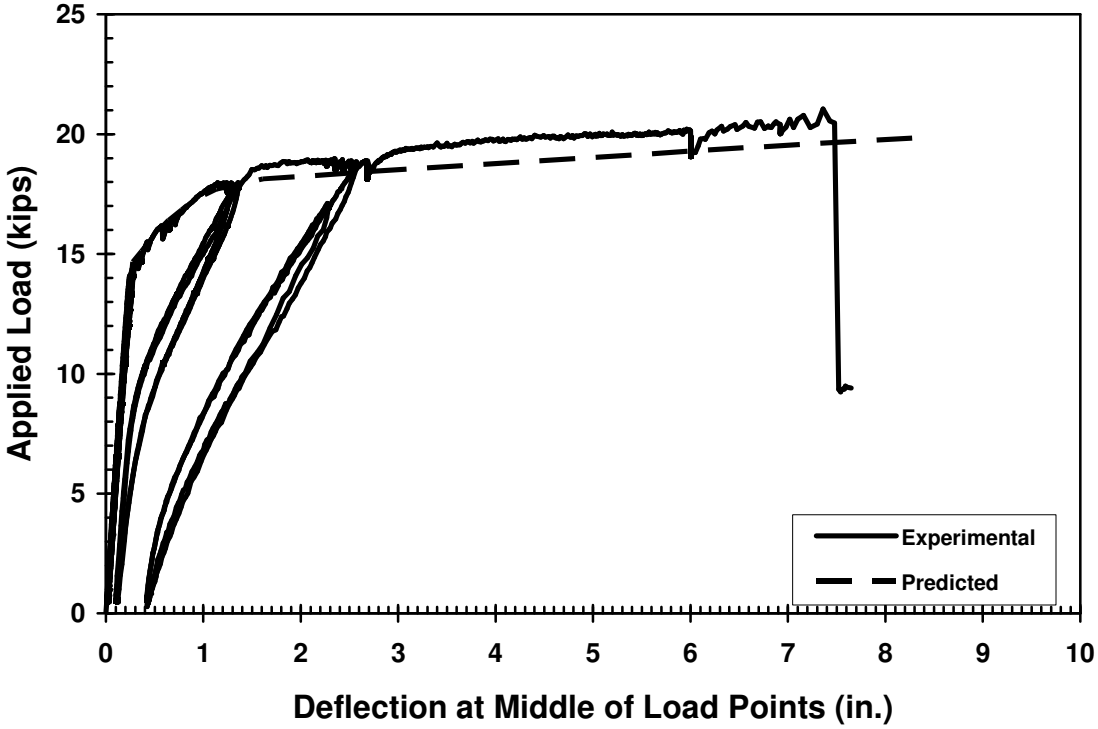

Figure H-4: Load vs. Displacement for SCC-HS-A

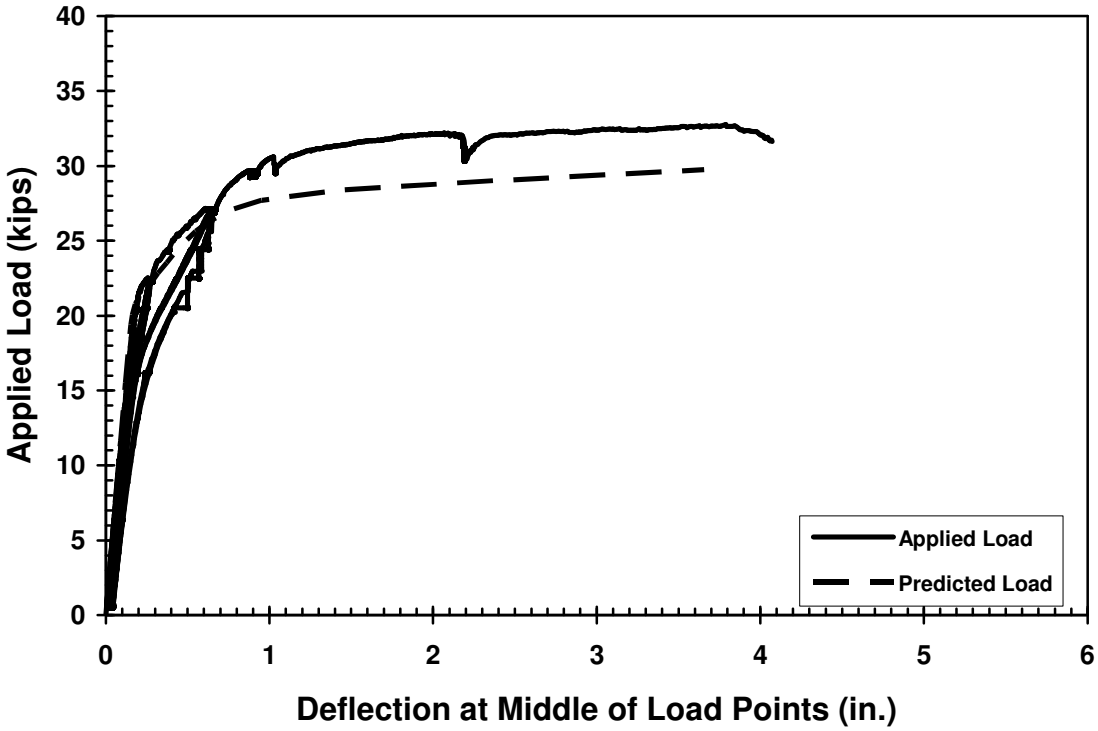

Figure H-5: Load vs. Displacement for STD-M-B

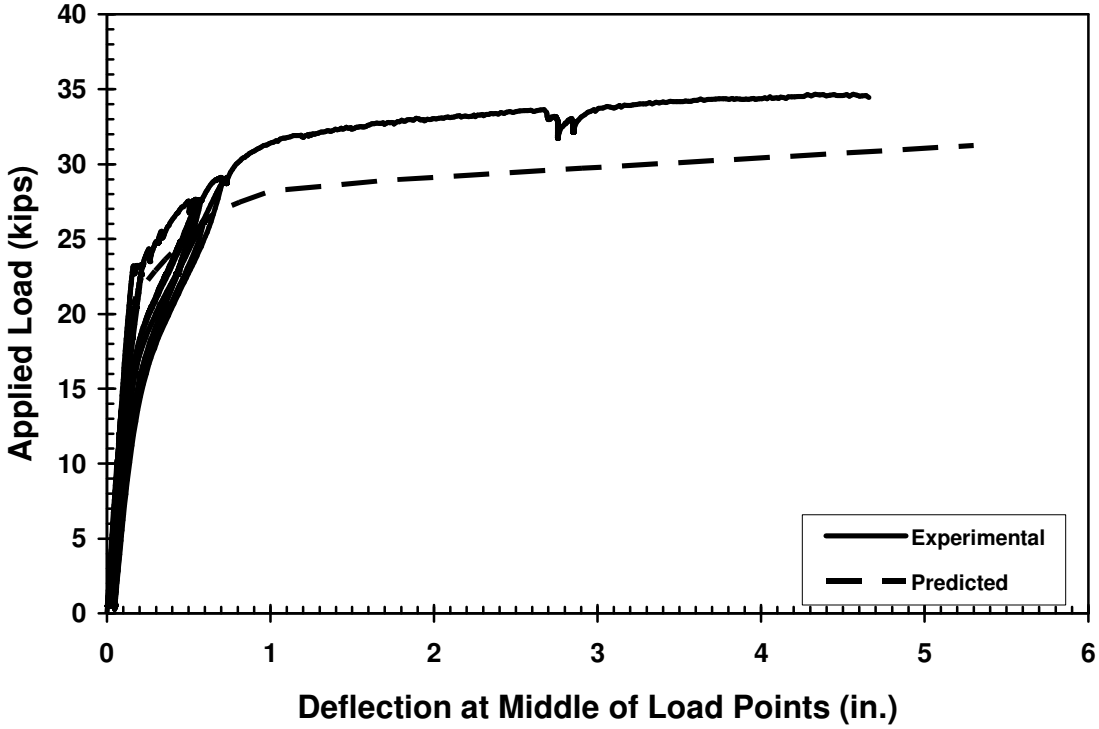

Figure H-6: Load vs. Displacement for SCC-MA-B

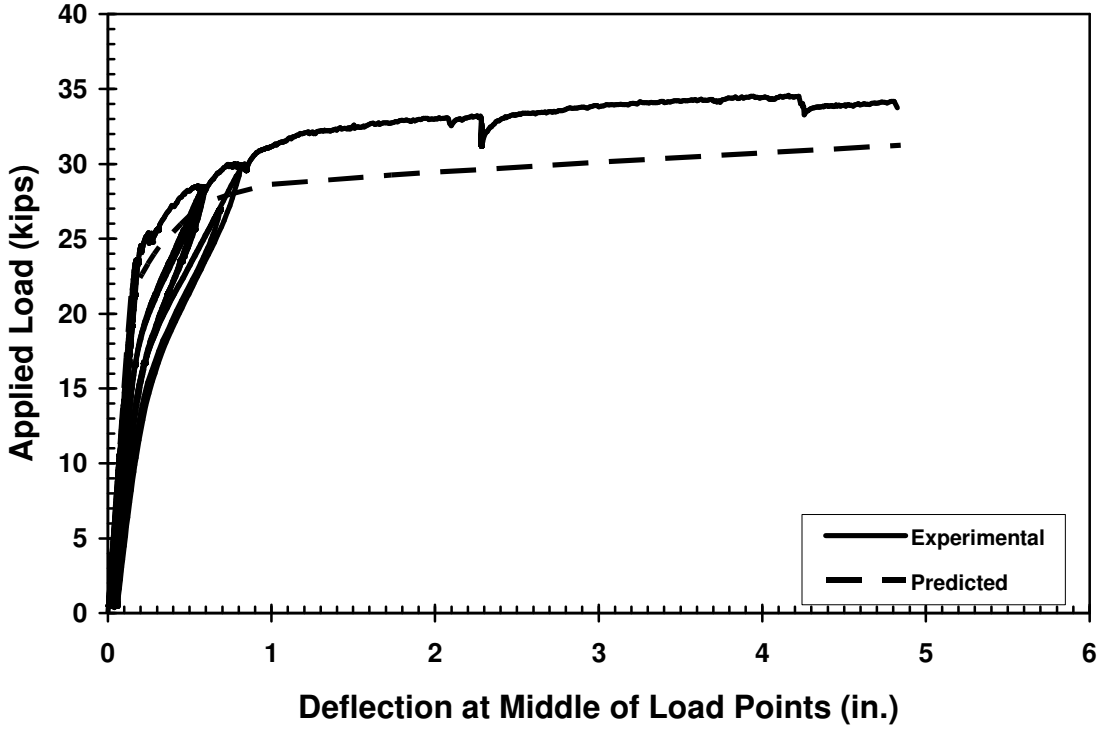

Figure H-7: Load vs. Displacement for SCC-MS-B

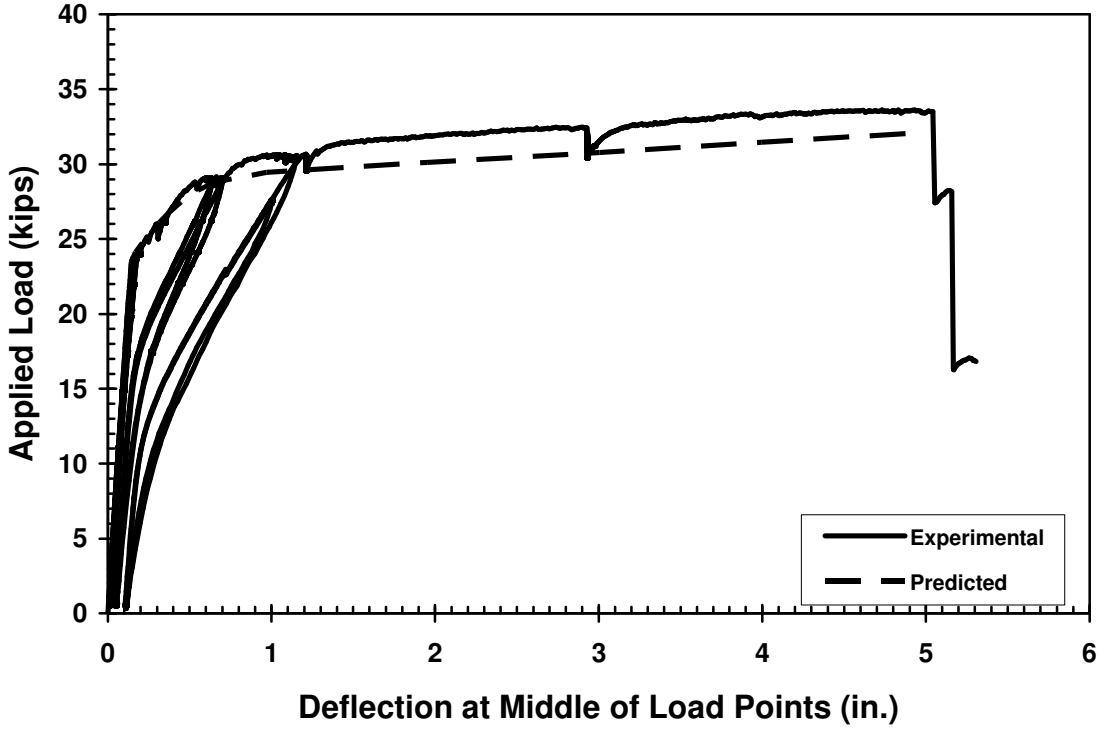

Figure H-8: Load vs. Displacement for SCC-HS-B

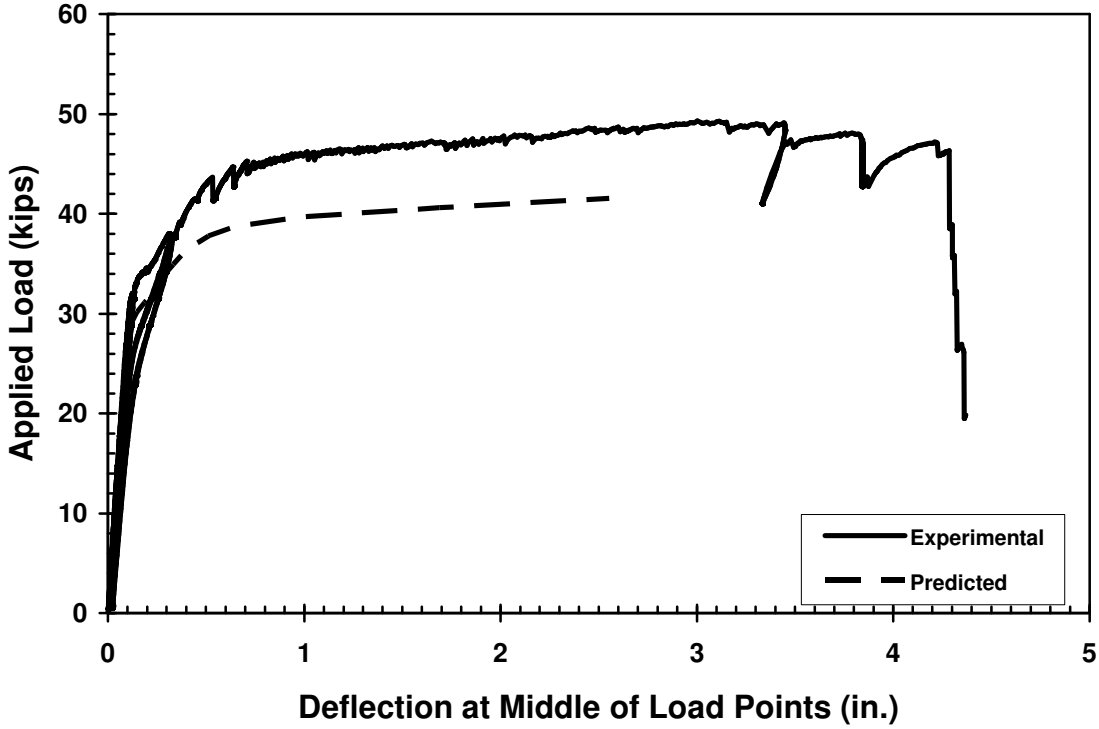

Figure H-9: Load vs. Displacement for STD-M-C

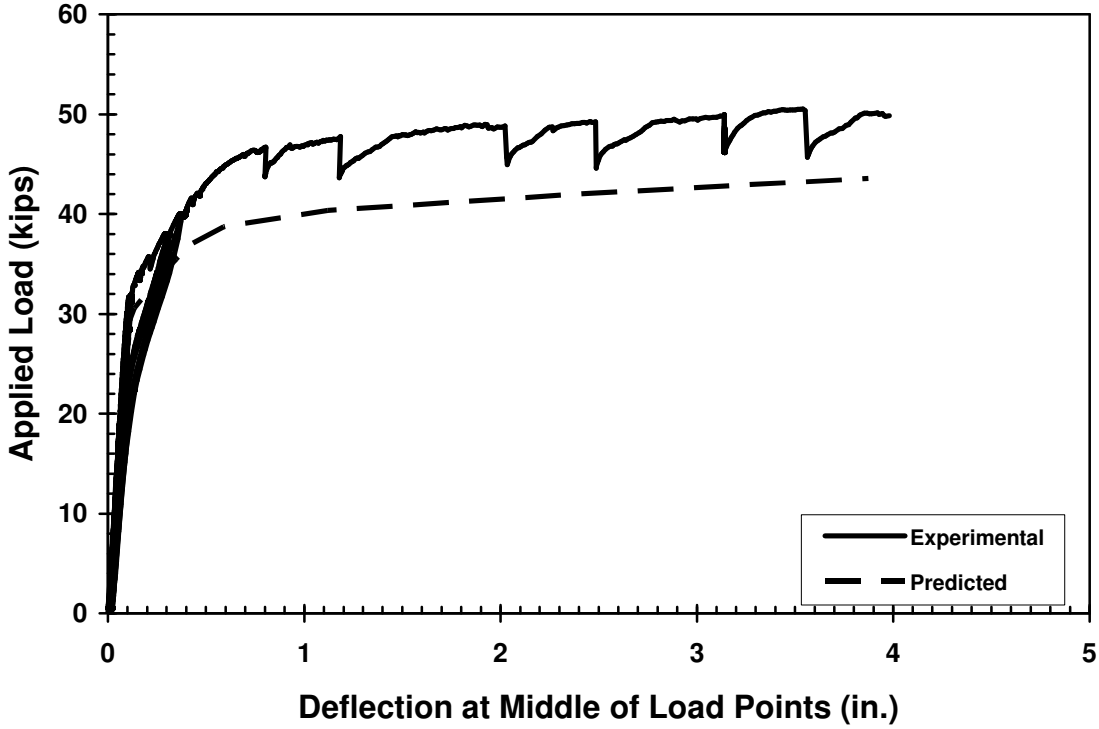

Figure H-10: Load vs. Displacement for SCC-MA-C

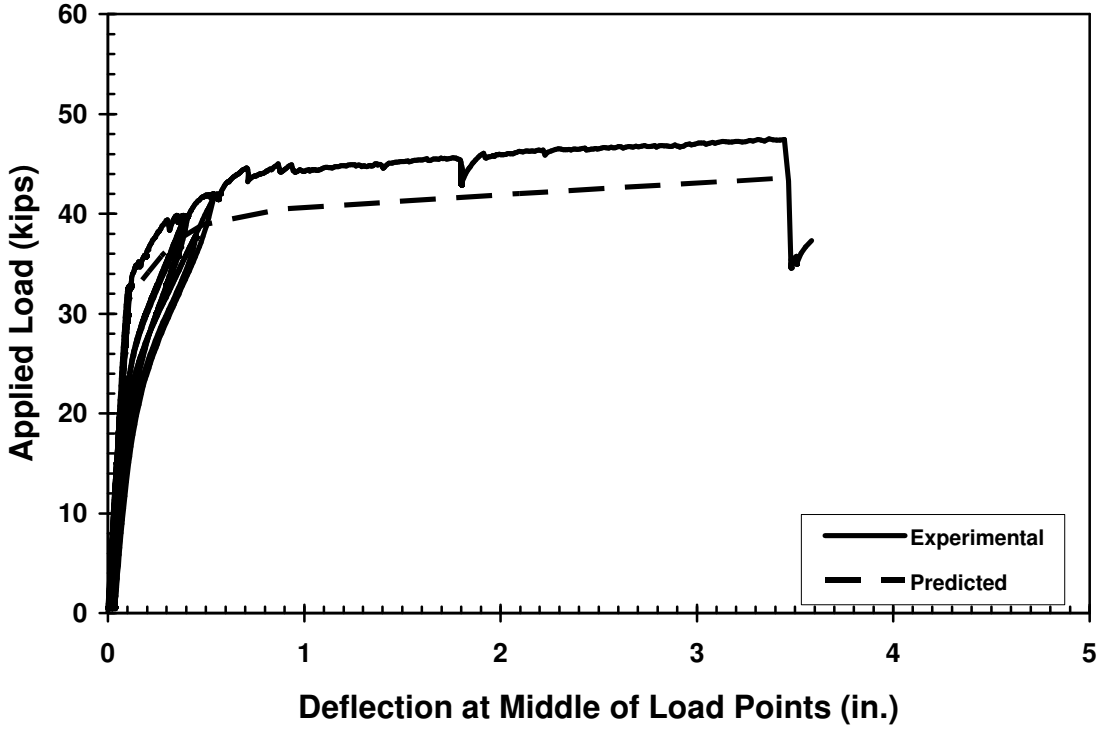

Figure H-11: Load vs. Displacement for SCC-MS-C

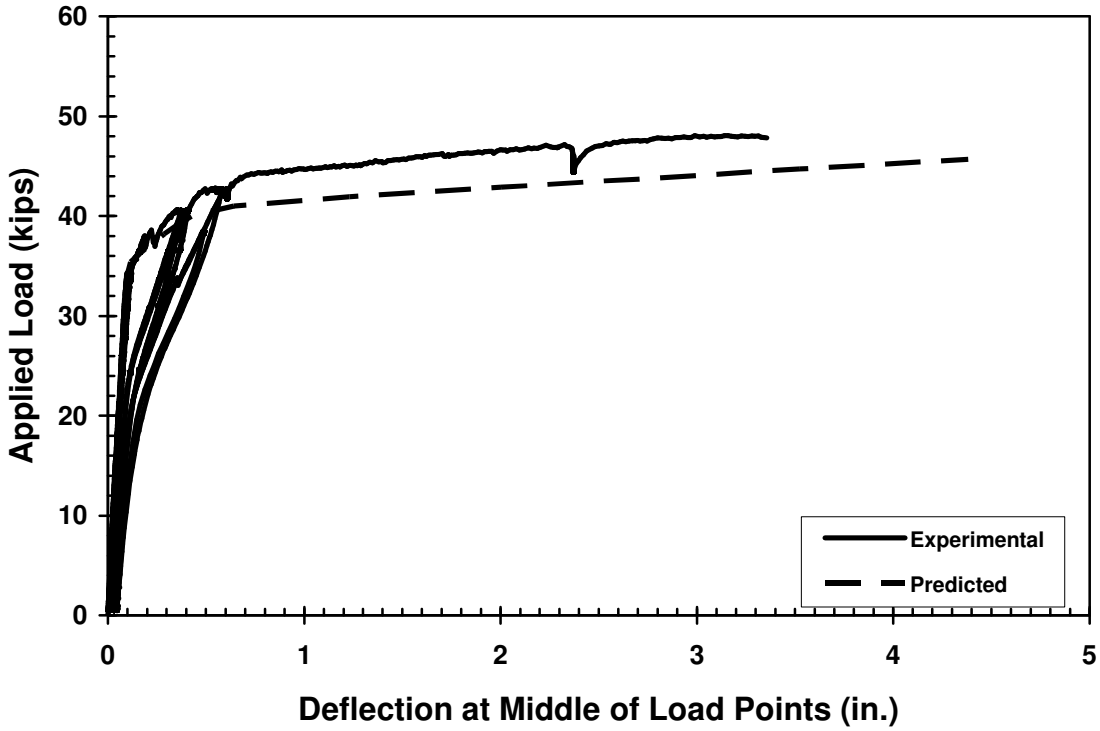

Figure H-12: Load vs. Displacement for SCC-HS-C

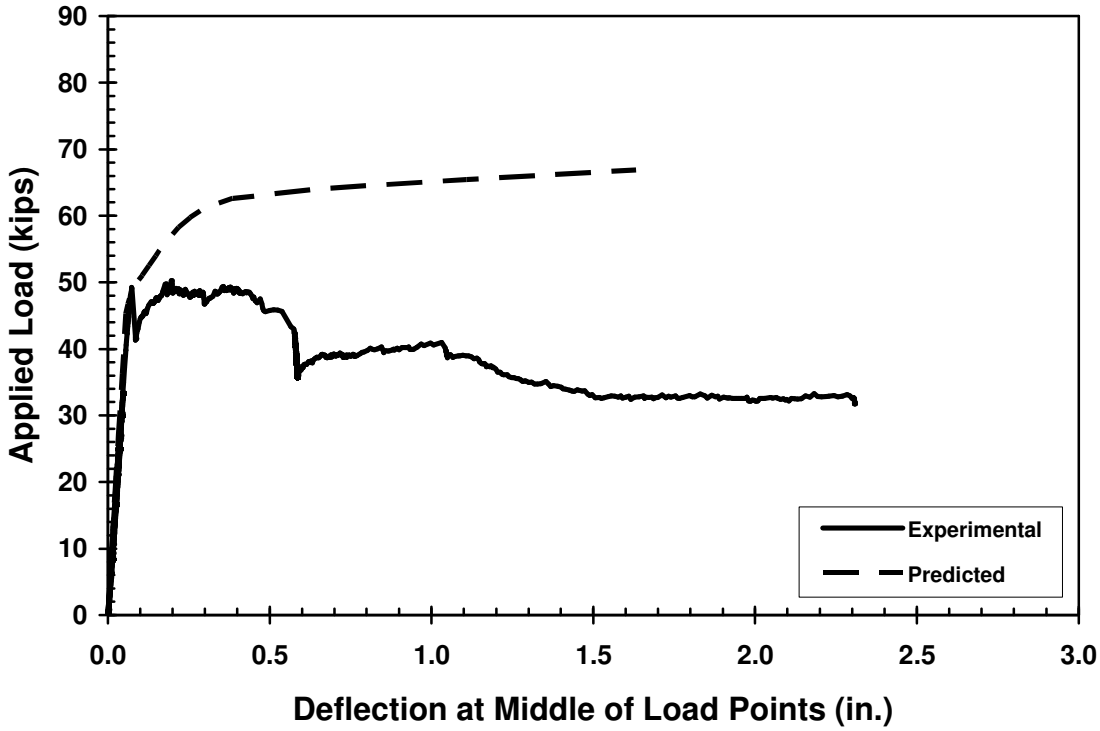

Figure H-13: Load vs. Displacement for STD-M-D

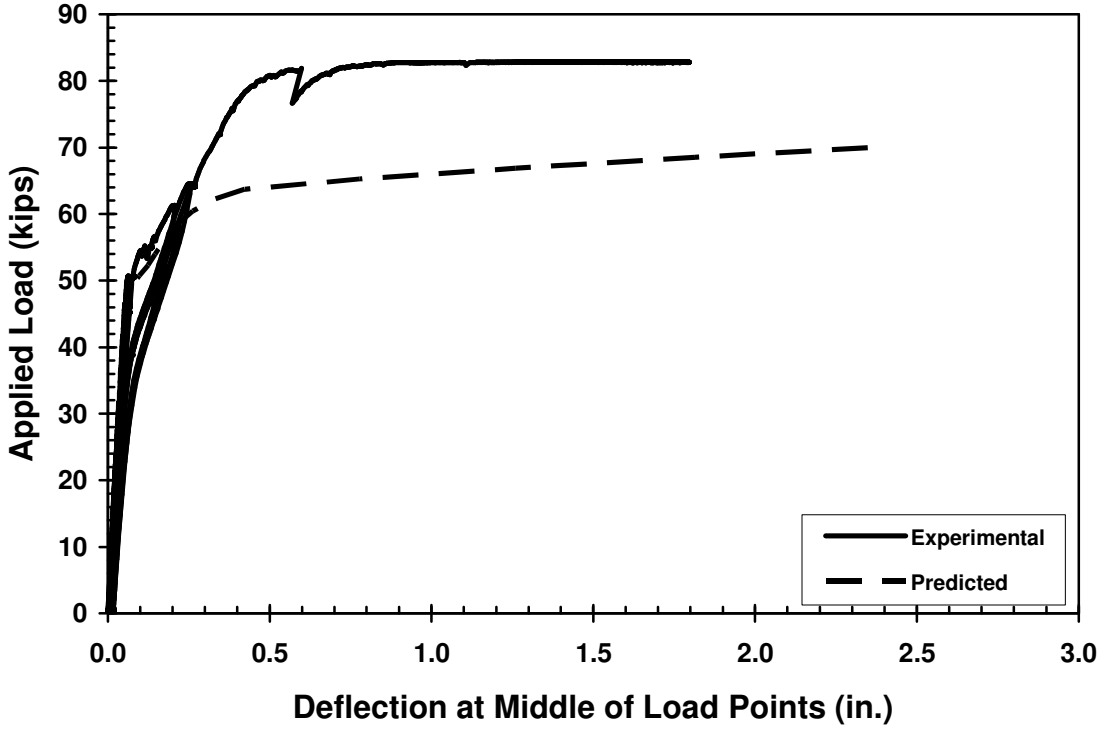

Figure H-14: Load vs. Displacement for SCC-MA-D

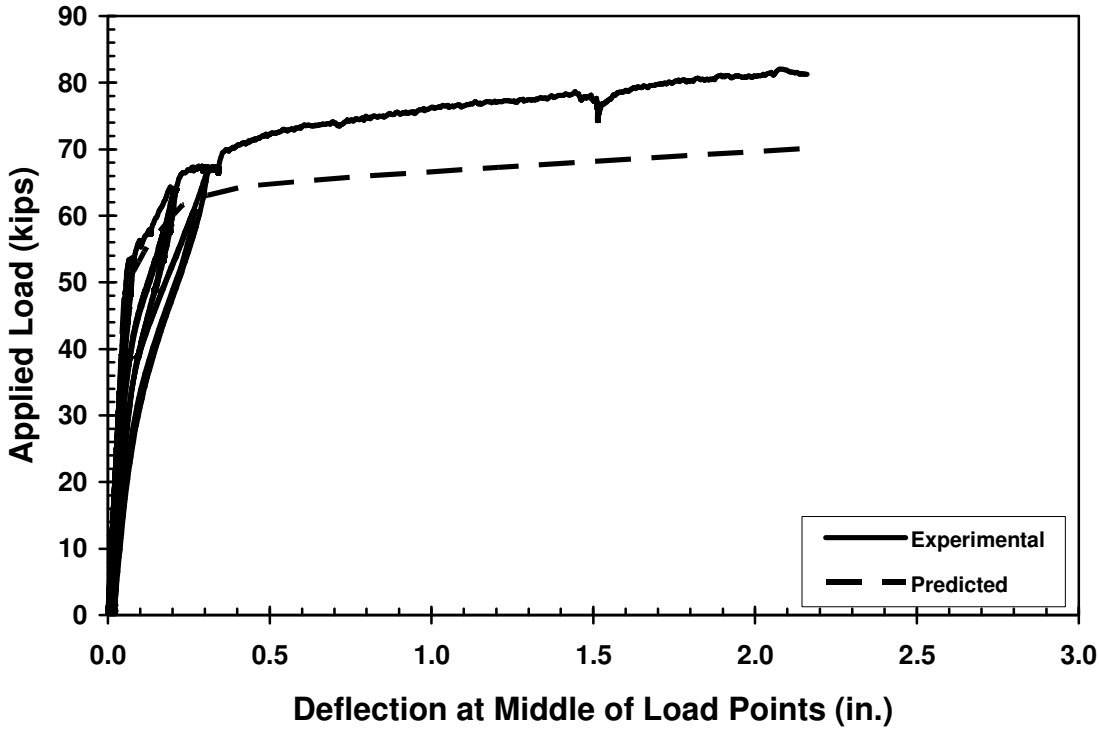

Figure H-15: Load vs. Displacement for SCC-MS-D

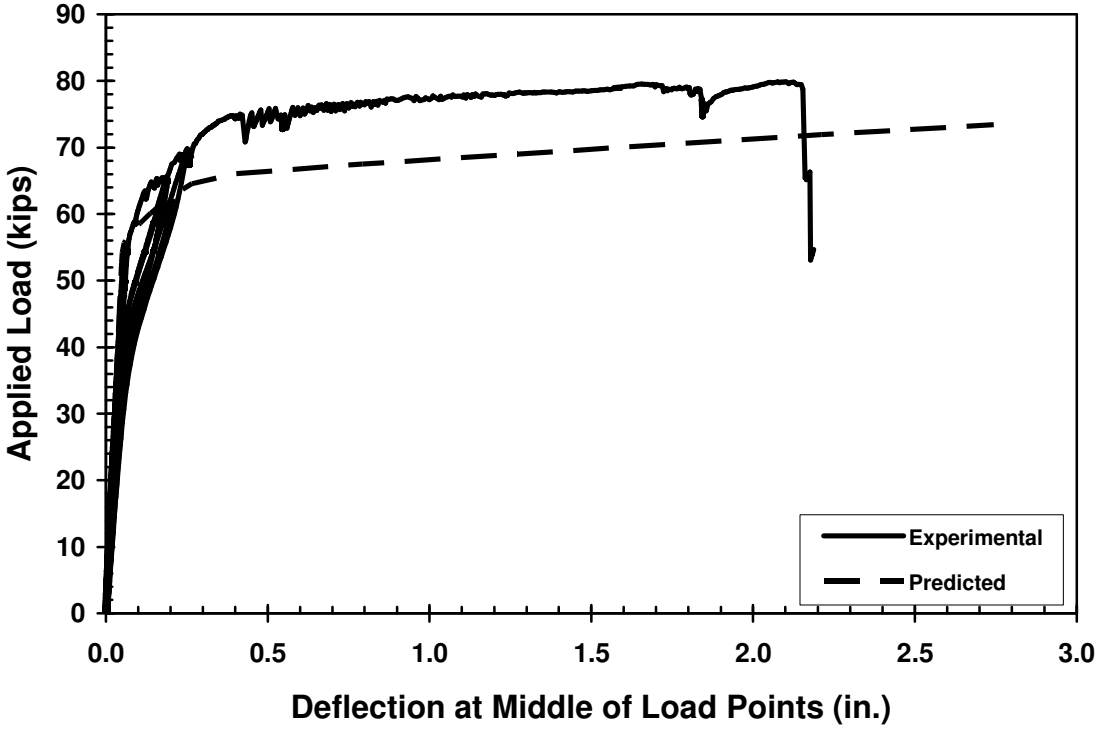

Figure H-16: Load vs. Displacement for SCC-HS-D